DOCTOR OF PHILOSOPHY

Identification and Characterisation of Novel Cancer-Testis Genes in Human Cancer Cell Lines

Anderson, Rebecca

Award date:
2013

Awarding institution:
Bangor University

Bangor University

Identification and Characterisation of Novel Cancer-Testis Genes in Human Cancer Cell Lines

Ph.D. Thesis 2013

Rebecca Anderson

Abstract

Cancer-testis (CT) antigen genes display a highly tissue-restricted expression profile; the genes encoding CT antigens are normally expressed in the testes of adult males, but are aberrantly expressed in various types of cancer. The testes confer a site of immune privilege therefore CT antigens represent attractive and potentially important therapeutic and/or diagnostic targets. Sexual reproduction in eukaryotes requires the creation of haploid gametes via a specialised process called meiosis. Meiosis is restricted to germ cells and several meiotic proteins have previously been identified as CT antigens, therefore we hypothesised that meiosis-specific genes may provide a good source from which to identify novel CT genes.

Meiotic genes were identified from the literature and a bioinformatics pipeline. RT-PCR was used to validate the meiotic genes in a wide range of normal human tissues and those genes found to display testis-associated expression profiles in the normal tissues were screened for expression in a range of cancer cells. The RT-PCR results identified five genes as novel CT genes, out of the 37 genes screened. Biochemical analysis was also carried out on the product of *NUT*, a novel meiCT gene identified by the CT gene screen.

Surprisingly a significant portion of the purported meiosis-specific genes displayed expression in a wide range of normal human tissues, including *REC8* and *STAG3*. The meiosis-specificity of REC8, and its orthologues, has been reported to be widely conserved from yeast to humans. Biochemical analysis results showed that REC8 appears to localise to the nucleus of five human cancer cell lines and fibroblast cells. Here we present evidence to suggest that REC8 displays strong chromatin association in mitotically dividing cells and is involved in a large protein complex. However, REC8 knockdown in cancer cell lines was unsuccessful and therefore a potential functional role for REC8 could not be established in human mitotic cells.

The results from this study identified five of the meiotic genes as novel CT genes thus supporting the original hypothesis. They also provide evidence to suggest that there are greater differences, than previously proposed, in the control and regulation of meiotic genes and/or proteins within different species.

Acknowledgements

I would like to take this opportunity to thank Ramsay McFarlane for all his advice and guidance throughout all aspects of my project, and Jane Wakeman for all her help. I would also like to thank Prof. Alistair Goldman and Dr. Helen Bryant for the HeLa T-REx cancer cell line and giving me the opportunity to work in the Institute for Cancer Studies, University of Sheffield. A special thanks to Helen for all the guidance and support when I was working in Sheffield.

I would also like to acknowledge that this project was funded by a Knowledge Economy Skills Scholarship (Welsh Government's European Science Foundation convergence programme)/UK NHS.

Thank you to Dave for always being around with a friendly smile and chocolate. Thanks also to Rolf and Natalia for their help and support. Thanks to all the members of the D7 lab, for being helpful and supportive and making my time in the lab enjoyable, and in particular Ibrahim for being my second pair of eyes. Thanks also to Heledd, Alessa and Jana for your friendship and always being understanding.

I am so grateful to my mom for all the late night phone calls and for always encouraging and inspiring me to do the best I can do. And last but not least I would like to thank my husband Ed, for all his love, support and patience (and all the cups of tea).

Abbreviations

ABC	ATPase bind cassette
AE	axial element
AEBSF	4-(2-Aminoethyl) benzenesulfonyl fluoride hydrochloride
ANN	artificial neural network
APC/C	anaphase promoting complex/cyclosome
ATP	adenosine-5'-triphosphate
ATR	ataxia telangiectasia and Rad3-related protein
BBB	blood-brain barrier
BCA	bicinchoninic acid
BGH	bovine growth hormone
bp	base pair
BSA	bovine serum albumin
BTB	blood-testis barrier
C	cytoplasmic
CDK	cyclin dependent kinase
CdLS	Cornelia de Lange syndrome
cDNA	Complementary DNA
CE	central element
Ch	Chromatin
CNS	central nervous system
CO	crossover
CpG	-cytosine-phosphate-guanine-
Cq	quantification cycle
CT	cancer-testis
DAPI	4'-6-diamidino-2-phylindole
DDR	DNA damage response
DEPC	diethylpyrocarbonate
dHJ	double Holliday junction
D-loop	dissociation loop
DMEM	Dulbecco's modified Eagles medium
DMSO	dimethyl sulfoxide
DNA	deoxyribonucleic acid
DSB	double strand break

DSR	determinant of selective removal
DTT	1,4-dithio-DL-threitol
ECL	electrochemiluminescence
EDTA	ethylenediaminetetraacetic acid
EST	expressed sequence tag
FBS	foetal bovine serum
G_0	quiescent phase of the cell cycle
G_1	Gap-1 phase
G_2	Gap-2 phase
HAT	histone acetyltransferase
HJ	Holliday junction
HMM	Hidden Markov Model
HMW	high molecular weight
HR	homologous recombination
HRP	horseradish peroxidase
hrs	hours
HSC	Haematopoietic stem cell
IF	Immunofluorescent staining
IR	ionising radiation
LE	lateral element
M	Mitosis phase
MHC	major histocompatibility complex
min	minute
MRN	Mre11-Rad50-Nbs1
mRNA	messenger RNA
MRX	Mre11-Rad50-Xrs2
MSCI	meiotic sex chromosome inactivation
N	nuclear
NCO	non-crossover
NES	nuclear export sequence
NHDF	normal human dermal fibroblasts
NHEJ	non-homologous end-joining
NLS	nuclear localization sequence
NMC	NUT midline carcinoma

NRT	no reverse transcriptase
NTC	no template control
PBS	phosphate buffered saline
PCR	polymerase chain reaction
PMSF	phenylmethylsulfonyl fluoride
PVDF	polyvinylidene difluoride
qRT-PCR	quantitative, real time PCR
RNA	ribonucleic acid
RNAi	RNA interference
RPMI	Roswell Park Memorial Institute 1640 medium
RT-PCR	reverse transcription PCR
S	Synthesis-phase
s	seconds
SAC	spindle assembly checkpoint
SC	synaptonemal complex
SDS-PAGE	sodium dodecyl sulphate polyacrylamide gel electrophoresis
SEC	size exclusion chromatography
SEI	strand exchange intermediate
SIC	synapsis initiation complex
siRNA	small interfering RNA
SMC	structural maintenance of chromosomes
ssDNA	single strand DNA
TBS	tris buffered saline
TF	transverse filament
T-REx	tetracycline regulated expression
TSA	Trichostatin A
TSS	transcription start site
WB	western blot
WCE	whole cell extract

List of Contents

List of Figures

Chapter 1.0

Chapter 3.0

Chapter 4.0

Chapter 5.0

Chapter 6.0

Chapter 7.0

List of Tables

Chapter 1.0

Chapter 2.0

Chapter 3.0

Chapter 4.0

Chapter 7.0

1.0 Introduction

1.1 Cell Division

Two processes of cell division exist in eukaryotic cells; mitosis and meiosis. Mitosis occurs as part of the normal cell cycle and maintains the chromosome complement, whereas meiosis reduces the diploid complement by half. Mitotic and meiotic cell division involves DNA replication followed by chromosome segregation events, which enables the intact genome to be maintained from one generation to the next. These two processes are tightly regulated and require the action of a wide and diverse array of proteins (Clift and Marston, 2011; Silkworth and Cimini, 2012).

1.1.1 The mitotic cell cycle

In eukaryotes, the mitotic cell cycle involves one round of DNA replication followed by one round of chromosome segregation. Two identical daughter cells are produced, each containing a diploid number of chromosomes, from a single parental cell (Silkworth and Cimini, 2012). The majority of cells in an adult metazoan lie in a quiescent state, also known as G_0 phase (O'Farrell, 2011). Mitotic cell division is required for tissue homeostasis and regeneration of damaged tissues, in adults. Mitogenic signals cause quiescent cells to enter mitosis, however oncogenic changes may also disrupt quiescence, and thus initiate cell proliferation. Aberrant cell proliferation may lead to the formation of neoplasms or tumours, therefore cell growth and division is highly regulated and strictly controlled (O'Farrell, 2011; Silkworth and Cimini, 2012).

1.1.2 The sub-stages of mitosis

The cell cycle is divided into four main stages known as; Gap-1 (G_1), Synthesis (S)-phase, Gap-2 (G_2) and Mitosis (M), of which the G_1, S and G_2 phases collectively known as interphase. Preparation for cell division occurs in interphase, during which the cell grows in size and the chromosomal DNA is replicated. Cell progression through mitosis is controlled by a series of checkpoints, surveillance mechanisms and the cellular abundance of cyclin dependent kinases (CDKs), and their respective activators (cyclins) (reviewed in Kronja and Orr-Weaver, 2011; Uhlmann *et al.*, 2011). For example, checkpoints within M-phase prevent the cell from completing cell division if a single chromosome is not correctly

bioriented on the mitotic spindle; this checkpoint is essential for faithful chromosome segregation. M-phase is divided into five distinct stages, known as; prophase, prometaphase, metaphase, anaphase and telophase (Figure 1.1).

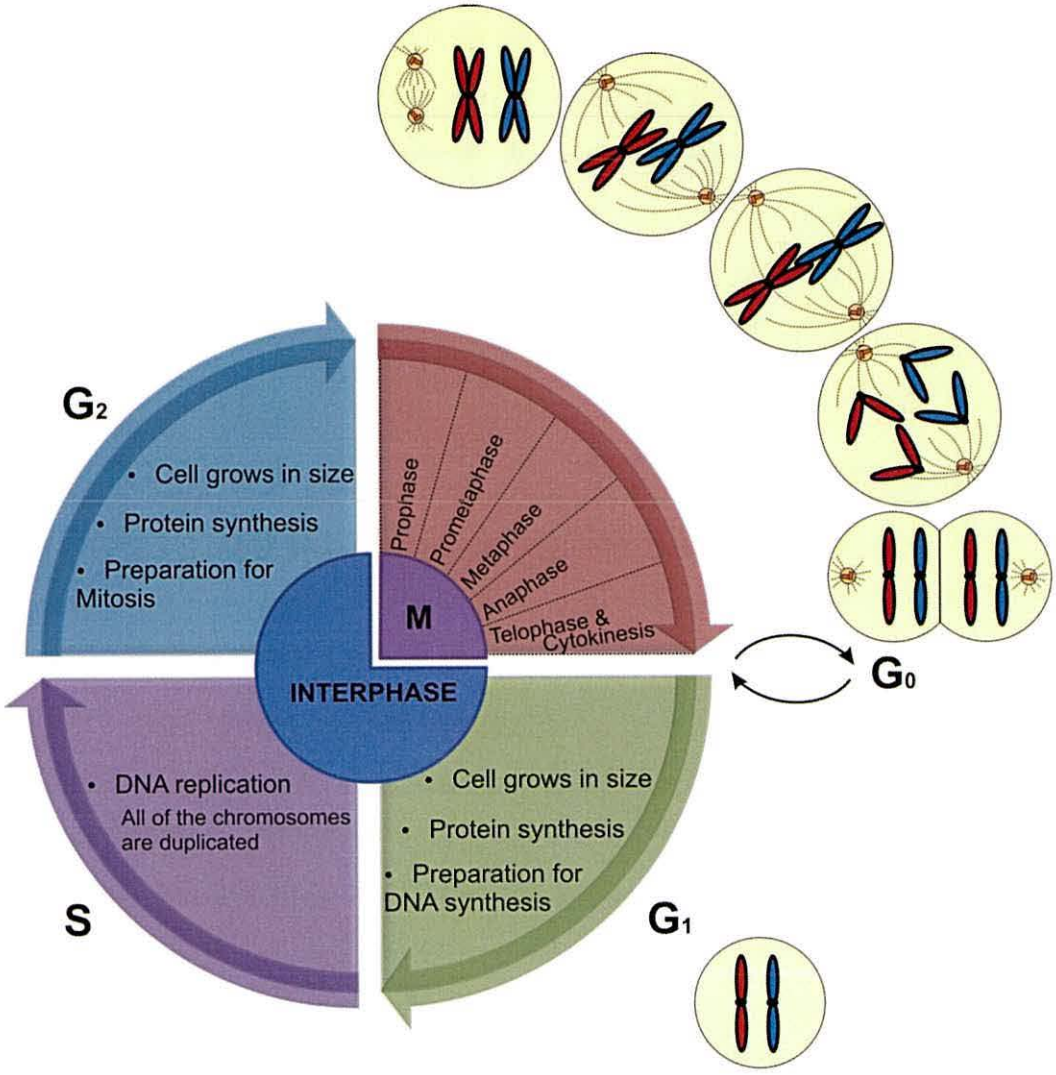

Figure 1.1. Diagrammatic representation of the mitotic cell cycle. The cell cycle is divided into two main stages; interphase and mitosis (M) phase, with G_0 representing cells in a quiescent state between cell cycles. Interphase is comprised of the Gap-1 (G_1), Synthesis (S) and Gap-2 (G_2) phases. During G_1 the cell grows in size and prepares to enter S-phase, which involves the synthesis of the proteins required for DNA replication. DNA replication occurs during S phase, and during G_2 the cell prepares to enter M-phase, which involves the synthesis of proteins required for mitosis. M-phase is subdivided into five stages; prophase, prometaphase, metaphase, anaphase and telophase. The chromatin condenses into chromosomes and the spindle apparatus forms during prophase. The centrosomes move to opposite poles of the cells, driven by the polar microtubules. During prometaphase, the nuclear membrane breaks down thus allowing kinetochore microtubules to invade the nuclear space and attach to the kinetochores. Bioriented chromosomes align along the metaphase plate in metaphase and the sister chromatids are pulled to opposite poles during anaphase. Telophase takes place in conjunction with cytokinesis, wherein nuclear membranes reform around each set of chromatids producing two genetically identical daughter cells with a haploid number of chromosomes. The chromatids then unwind.

Cell division is a complex process which requires the cell to undergo some major structural changes in a relatively short period of time, such as cytoskeletal rearrangement and nuclear membrane breakdown (Silkworth and Cimini, 2012). Major cytoskeletal re-arrangement drives mitotic cell rounding and cortical stiffening, which then functions as a foundation for spindle assembly and aids spindle orientation (Kunda and Baum, 2009). Breakdown of the nuclear membrane is an essential process during mitosis in higher eukaryotes, which allows microtubule attachment to the sister chromatid kinetochores (De Souza and Osmani, 2007; Lippincott-Schwartz, 2002). A model has been suggested wherein nuclear membrane breakdown takes place via a force driven tearing process and is facilitated by the microtubules. Spindle microtubules attachment to the nuclear membrane gives rise to microtubule-dependent changes in the nuclear envelope structure which induces the localised disassembly of nuclear pores and creates an epicentre for tearing. Pieces of the nuclear envelope, attached to the endoplasmic reticulum, are then transported along the microtubules and away from the chromosomes (Beaudouin *et al.*, 2002; Salina *et al.*, 2002). Beaudouin *et al.*, (2002) also suggested that the influx of cytoplasmic molecules may facilitate mitotic processes such as chromosome condensation and spindle formation.

Microtubules originating from opposite poles of the cell attach to the kinetochores of the sister chromatids after nuclear membrane breakdown in prometaphase. Metaphase is achieved when the chromosomes align on the metaphase plate and display bipolar attachment. The spindle assembly checkpoint (SAC) delays metaphase-anaphase transition until all the chromosomes are correctly attached to the mitotic spindle in a bipolar orientation (Malmanche *et al.*, 2006). The sister chromatids are then pulled to opposite poles during anaphase and the cell divides in two, forming nuclear membranes around each set of chromatids during telophase (reviewed in Silkworth and Cimini, 2012).

1.1.3 The meiotic cell cycle

In contrast, meiosis is a highly specialised process of chromosomal segregation which results in the production of four genetically different daughter cells, each containing a haploid number of chromosomes (Petronczki *et al.*, 2003). The process of meiosis involves one round of DNA replication followed by two rounds of chromosome segregation; first, reductional chromosome segregation (meiosis I) and second, equational chromosome segregation (meiosis II) (Marston and Amon, 2004). Gamete fusion during sexual

reproduction restores the diploid number of chromosomes, thus maintaining ploidy from one generation to the next (Holt and Jones, 2009). The meiotic products are highly specialised cells (sperm and egg in higher eukaryotes); therefore entry into meiosis is strictly regulated. Mammalian germ cells are surrounded by specialised somatic cells which influence their homeostasis and meiotic status by producing signals which can initiate meiosis (Handel and Schimenti, 2010).

The chromosomes are replicated during an extended pre-meiotic S-phase, which is thought to be required to establish the inter-homologue interactions which are required for meiotic recombination and segregation of homologous chromosomes (Lee and Amon, 2001). Similar to mitosis, meiosis I and II take place in a series of distinct stages, with each involving prophase, metaphase, anaphase and telophase phases. Homologous pairing and alignment takes place during prophase I, and thus allowing crossover events to occur. Homologous chromosomes align on the metaphase plate during metaphase I and are pulled to opposite poles during anaphase I. The cell divides in two during telophase I at the end of meiosis I, which is followed by the second meiotic division with no intervening DNA replication. Meiosis II involves a mitosis-like chromosome segregation, wherein chromosomes align along the metaphase plate during metaphase II and sister chromatids are pulled to opposite poles during anaphase II. With the sister chromatids at opposite poles, the cells divide in two during telophase II and thus produces four genetically unique haploid gamete cells (Page and Hawley, 2004; Zickler and Kleckner, 1998). The key stages of meiotic cell division are shown in Figure 1.2.

This highly complex process is essential for establishing genetic diversity whilst maintaining chromosome fidelity. Genetic diversity is created during meiosis I through the independent assortment of chromosomes and crossover events between homologous chromosomes. During metaphase I the homologous chromosomes align along the metaphase plate in a random order, with the maternal and paternal chromosomes in a bipolar orientation. This stage alone produces a great potential number of genetically diverse outcomes. Homologous recombination of the maternal and paternal chromosomes involves the swapping of genetic material and thus creates new combinations of maternal and paternal alleles (Gerton and Hawley, 2005; Longhese *et al.*, 2008).

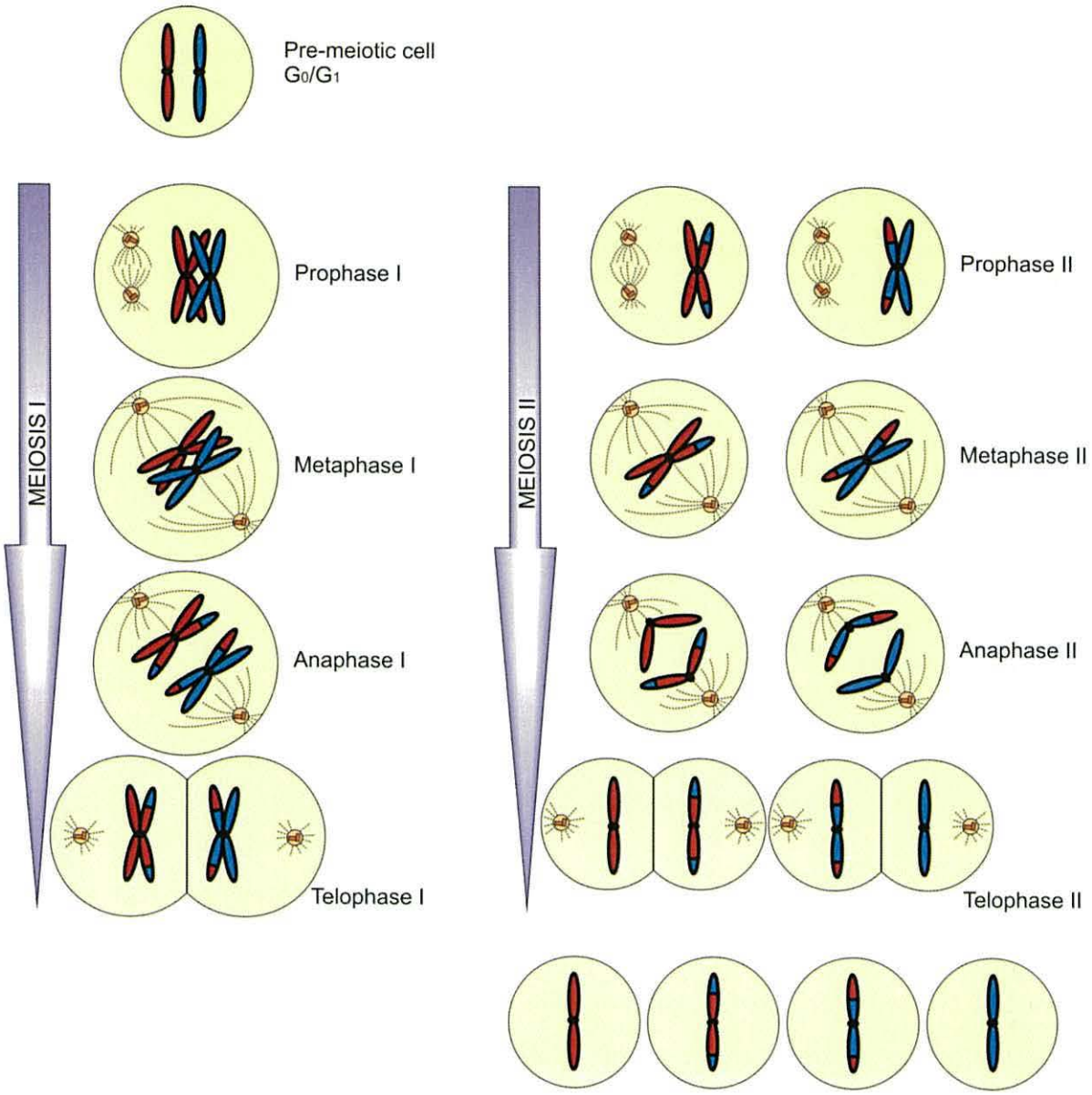

Figure 1.2. Diagrammatic representation of meiotic cell division. Meiosis involves two rounds of chromosomal segregation; reductional segregation (meiosis I) and equational segregation (meiosis II), which follows one round of DNA replication that occurs during the extended pre-meiotic S-phase. The red chromosome represents the maternal chromosome and the blue chromosome represents the paternal chromosome. Meiosis I consists of four main stages; prophase I, metaphase I, anaphase I and telophase I. During prophase I spindle formation occurs, the nuclear envelope breaks down and the homologous chromosomes align, allowing crossover formation to take place. Chiasmata are resolved by the end of prophase I. The homologous chromosomes align on the metaphase plate in metaphase I and are pulled to opposite poles during anaphase I. During telophase I, the homologues are at the opposite poles of the cell and the cell divides into two. Meiosis II follows meiosis I and similarly consists of four stages; prophase II, metaphase II, anaphase II and telophase II. The nuclear envelope breaks down and the spindle apparatus forms during prophase II. Chromosomes align along the metaphase plate (as in mitosis) during metaphase II and sister chromatids are pulled to opposite poles in anaphase II. With the sister chromatids at opposite poles, the cells divide in two; thus producing four genetically unique haploid daughter cells.

1.1.4 The sub-stages of meiotic prophase

The key defining events which differentiate the process of meiosis from that of mitosis occur during prophase I. Prophase I is highly regulated and is divided into five cytological substages; leptonema, zygonema, pachynema, diplonema and diakinesis; which are identified by changes in chromosome morphology (described in Table 1.1).

Table 1.1. Summary of the sub-stages in prophase I

Sub-stage	Description of the key meiotic events
Lepotene	The replicated chromosomes condense and become visible. Homologous chromosomes pair.
Zygotene	The homologous chromosomes begin to synapse. Synapsis occurs, in most organisms, through the formation of a large proteinacious structure called the synaptonemal complex (SC).
Pachytene	The homologous chromosomes are fully synapsed. The chromosomes crossover at distinct recombination nodules (chiasmata).
Diplotene	The SC begins to disassemble, which coincides with chromosome de-condensation. Homologues remain physically linked by chiasmata.
Diakinesis	The SC has completely dissociated. Homologous chromosomes condense prior to the onset of metaphase I, but remain physically linked via chiasmata.

(Zickler and Kleckner, 1999).

No homologous alignment is observed in the early stages of leptotene but high levels of pairing are achieved in a relatively short period of time, as all of the homologues are fully aligned by late leptotene/early zygotene (Page and Hawley, 2004). Homologous pairing is facilitated by the polarised chromosome arrangement, known as the bouquet formation, which arises from a clustering of telomeres on the inner nuclear envelope. This chromosomal arrangement is highly conserved and has been observed in most eukaryotes. The bouquet formation is thought to aid homologous recognition and alignment by concentrating the chromosomes within a limited region within the nucleus (Zickler and Kleckner, 1998). However, in some organisms the bouquet formation is not a prerequisite to homologous pairing. For example, the bouquet arrangement follows chromosome pairing in the fungus, *Sordaria macrospora* (Storlazzi *et al.*, 2003), and follows synaptic initiation in female mice (Tankimanova *et al.*, 2004). Conservation of the bouquet structure may suggest a conserved function, therefore it has been suggested that these chromosomal movements may promote the destabilisation of inappropriate chromosomal interactions and/or entanglements (Koszul and Kleckner, 2009).

1.1.5 Differences in male and female meiosis

Although the process of meiosis is essentially the same in males and females, there are some fundamental differences. In mammalian females the oocyte begins meiosis during foetal development and arrests part way through meiosis I, therefore homologous chromosome pairs remain associated for months or years dependent on the species (years in humans) in germinal vesicle arrested oocytes (Holt and Jones, 2009). Meiosis I is not completed until ovulation and meiosis II is only completed upon fertilisation of the egg, therefore oogenesis requires several start and stop signals. In contrast, paternal meiosis is a continuous process which begins at puberty, with spermatocytes requiring approximately one week to progress from prophase I to meiosis II completion (Hunt and Hassold, 2002).

1.1.6 Conserved features of meiosis

The process of meiosis remains poorly understood. It is difficult to study the meiotic program in humans for various reasons including the inherent difficulty of obtaining germ cells and the fact that meiosis can take decades to complete in females. Many meiotic factors are highly conserved and model organisms such as *Saccharomyces cerevisiae* and *Schizosaccharomyces pombe* have been used to derive meiotic structures and mechanisms at a molecular level (Page and Hawley, 2004). The same or similar mechanisms are thought to take place in human meiosis.

Meiosis I involves three key features; first, the homologous chromosomes (homologues) pair in order to recombine, forming chiasmata in which a sister chromatid from one homologue covalently binds to a sister chromatid of the other homologue (Longhese *et al.*, 2008). Second, the sister kinetochores attach to the microtubules from the same spindle pole (monopolar attachment). Bipolar attachment is established between homologous chromosomes at metaphase I (Holt and Jones, 2009). Third, arm cohesion is eliminated during anaphase I, whereas centromeric cohesion continues, thus resulting in the separation of the homologues but not the sister chromatids (Nasmyth, 2011). These events are orchestrated by a wide array of meiosis-specific proteins and protein complexes, such as the SC and the cohesin complex.

1.2 Homologous Recombination

In most organisms the homologous chromosomes interact through recombination to produce at least one obligate crossover (CO) event per chromosome, which aids correct segregation at the first meiotic division (Longhese *et al.*, 2009).

1.2.1 DNA double-strand breaks (DSBs)

DNA double-strand breaks (DSBs) are one of the most dangerous forms of DNA damage and can be caused by DNA damaging agents, such as exposure to ionising radiation and chemical modifications of the DNA. DSBs are also deliberately generated after DNA replication during meiosis. If left unrepaired these DNA breaks can cause chromosome aberrations that often result in cell death or mutation. Therefore the correct repair of DSBs is essential for maintaining genome integrity; there are two major repair pathways through which DSBs are repaired, non-homologous DNA end-joining (NHEJ) and homologous recombination (HR). During NHEJ, the DNA ends are recognised and simply rejoined. Although this process is efficient it can cause loss of DNA and is prone to causing mutations. In contrast, the intact sister chromatid/homologue is used as a template for synthesis-dependent repair during HR. In mitotic cells, the sister chromatid is used as the preferred template for HR whereas the homologue is the preferred template for HR in meiotic cells (reviewed in Longhese *et al.*, 2008; 2009).

Evidence suggests that the mechanism through which HR is initiated after DSB formation is broadly conserved (Kan *et al.*, 2011).

1.2.2 Meiotic recombination

Recombination is initiated by meiotically induced DSBs which are created by the topoisomerase type II-like protein, SPO11 (Bergerat *et al.*, 1997; Keeney *et al.*, 1997). SPO11's involvement in meiotic recombination initiation is widely conserved and SPO11 orthologues have been identified in many eukaryotes including yeast and mammals (known as Spo11 in *S. cerevisiae* and Rec12 in *S. pombe*). In some species meiotic DSBs are absent from one sex, for example *Drosophilia melanogaster* males, or occur after the completion of chromosome pairing, for example *Caenorhabditis elegans* (reviewed in Inagaki *et al.*, 2010).

HR processing of meiotic DSBs is essential for the formation of CO events during meiosis I. In humans and mice only a small number of the DSBs created lead to the formation of a CO

event, but at least one CO event is obligate per chromosome pair. Meiotic recombination of the majority of DSBs leads to a non-crossover (NCO) event or gene conversion (Inagaki *et al.*, 2010) (Figure 1.3).

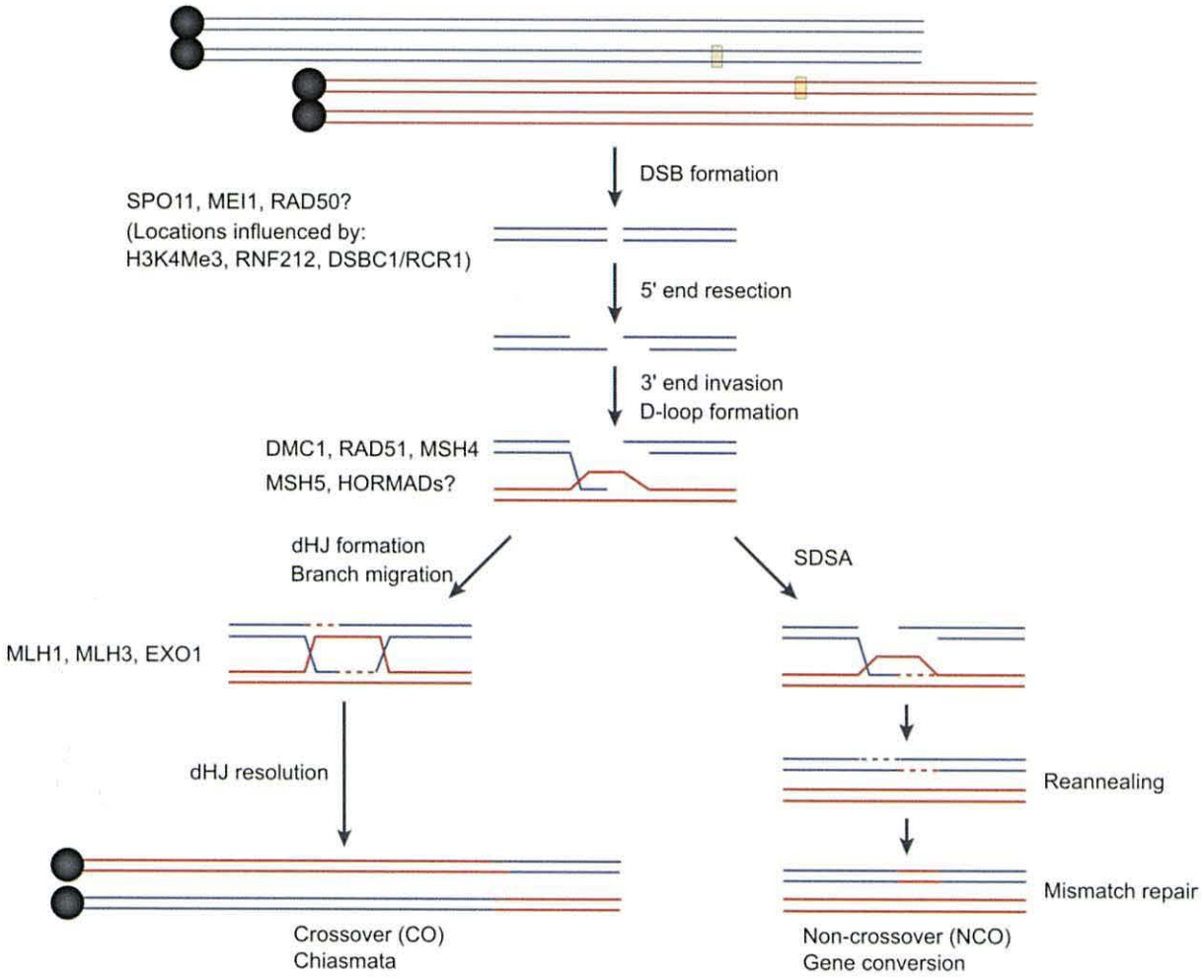

Figure 1.3. Model for meiotic recombination via the double-strand break repair pathway. The two major recombination pathways are shown; the crossover (CO) pathway is shown on the left and the non-crossover (NCO) pathway is shown on the right. The DSB is formed when SPO11 cleaves the DNA and the 5' DNA ends of the DSB are resected to expose 3' single strand DNA (ssDNA) overhangs. One of the overhanging 3' ends invades its homologous chromosome (single end invasion) forming an asymmetric strand exchange intermediate (SEI). DNA synthesis proceeds using the homologue as a template. This intermediate is unstable and the decision to generate a CO or NCO event is made at this step. HR via synthesis dependent strand annealing (SDSA) occurs in both meiotic and mitotic cells and results in NCO events. In the NCO pathway, the transient strand invasion complex is dissociated to allow the newly synthesised DNA to anneal to complementary ssDNA on the other side of the break; DNA synthesis and ligation therefore generate a NCO event. In the CO pathway, the second 3' overhang invades the displaced strand (second end capture) which is followed by DNA synthesis. A double Holliday junction (dHJ) is formed, and a mature CO event with exchanged flanking DNA is produced when the dHJ is resolved.

From Handel and Schimenti (2010).

SPO11 is loaded onto the chromatin during the final stages of S-phase and requires activation through the action of several accessory proteins/factors. The catalytic tyrosine of SPO11 attacks the phosphodiester backbone of the DNA and creates a covalent SPO11-DNA complex. The conserved protein complex; MRN (MRE11-RAD50-NBS1) in fission yeast and mammals, and the MRX (Mre11-Rad50-Xrs2) in budding yeast, is recruited to the DSB (Lisby *et al.*, 2004). SPO11 (Rec12/Spo11) removal is induced by the endonucleolytic activity of the MRN/MRX complex and CtIP in humans (Sartori *et al.*, 2007)/Ctp1 in fission yeast (Hartsuiker *et al.*, 2009)/Sae2 in budding yeast (Neale *et al.*, 2005). The MRN/MRX complex participates in telomere maintenance and DNA damage checkpoint activation in meiotic and mitotic cells (reviewed in Longhese *et al.*, 2010).

The 5' end of the DSB is then resected in a 5'-to-3' direction by the MRN/MRX complex and its associated co-factors, thus exposing 3' single stranded DNA (ssDNA) overhangs on either side of the break (Limbo *et al.*, 2007; Williams *et al.*, 2008). The ssDNA overhangs are incorporated into nucleoprotein filaments which contain the RecA-like strand invasion factors, RAD51 and DMC1 in mammals (Rad51 and Dmc1 in *S. cerevisiae*) (San Filippo *et al.*, 2008). These nucleoprotein filaments are involved in the search for homologous repair templates, with a strong preference towards the homologous chromosome rather than the sister chromatid (Longhese *et al.*, 2008; Neale and Keeney, 2006). Stable strand invasion is initiated by DMC1 and associated accessory proteins once the appropriate homologue has been identified, which leads to the formation of the Dissociation loop (D-loop) using the homologue as the template for extension (Dray *et al.*, 2011). The D-loop is extended by synthesis of the DNA and when DNA synthesis ceases, second end capture occurs. Subsequent extension and ligation (3' ends reattach to the exposed resected 5' ends of the original strand) results in the formation of a double Holliday junction (dHJ). Cleavage of the two HJs in either the same or opposing directions produces a NCO or CO product respectively (Longhese *et al.*, 2008; 2009).

1.2.3 Recombination hotspots

Recombination events are often clustered in narrow regions of the genome in preferred initiation sites, known as hotspots (Cheung *et al.*, 2010; Mihola *et al.*, 2009). PRDM9 (PR domain containing 9) is a zinc finger protein, which is produced specifically in germ cells during meiotic prophase, and acts as a histone methyltransferase that trimethylates lysine4

of histone3 (H3K4me3) (Cheung *et al.*, 2010; Mihola *et al.*, 2009). The zinc-fingers of PRDM9 are thought to mediate DNA-binding specificity and thus target specific sites in the genome (Baudat *et al.*, 2010). The polymorphic forms of PRDM9 have been shown to recognise different DNA sequences and can therefore promote CO events at different chromosomal sites (Cheung *et al.*, 2010). Data suggests that this is a rapidly evolving protein which may explain the lack of hotspot conservation between species (Mihola *et al.*, 2009; Myers *et al.*, 2010). In humans, the recombination hotspots usually occur relatively close to the genes (within 50 kb), but are preferentially outside the transcribed regions (Myers *et al.*, 2005).

Although many recombination interactions are initiated along each chromosome, only a few of them actually mature into COs and the remaining interactions revert into intact gene conversion events (NCO products). The pathway by which gene conversion events are produced is known as the single-strand annealing pathway (Bishop and Zickler, 2004; Kleckner *et al.*, 2003). CO designation is a highly regulated process responsible for the selection of the future COs which occurs at a relatively early stage (Kleckner *et al.*, 2003).

1.2.4 Crossover regulation

CO formation is essential in establishing a physical link between homologous chromosomes, which manifest as cytological structures called chiasmata. The frequency and distribution of CO events are tightly controlled by inter-chromosomal non-random distribution, known as 'the obligate crossover', which ensures that each chromosome has at least one CO event per chromosome pair (often only 1-2 per pair) (Jones and Franklin, 2006). CO events have been observed to exhibit 'interference' which reduces the probability that another CO event will occur simultaneously in an adjacent chromosome region; this is known as CO interference. Subsequently the CO events and the resulting chiasmata appear to be relatively evenly spaced along the chromosomes (reviewed in Hillers, 2004). Kleckner and colleagues have suggested a model whereby CO interference is regulated by local increases or decreases in the mechanical stress along a chromosome (reviewed in Kleckner *et al.*, 2004).

A reduction in the number of DSBs does not result in a subsequent reduction in the frequency of CO events (Martini *et al.*, 2006). This ability to maintain the frequency of CO events is known as CO homeostasis, and suggests that the frequency and distribution of CO events per chromosome pair are pre-designated (Martini *et al.*, 2006). In budding yeast, CO

homeostasis is thought to be regulated by components of the SC and is related to CO interference. Interestingly, *S. pombe* does not exhibit CO interference (Munz, 1994) but has been shown to exhibit CO homeostasis via CO invariance which is regulated by the sister chromatid versus homologue partner choice for DSB repair (Hyppa and Smith, 2010; Kan *et al.*, 2011). CO homeostasis regulates frequency and CO interference regulates the distribution of the resultant CO events, and as such are two distinct processes (Kan *et al.*, 2011).

The *S. pombe* SPO11 orthologue (Rec12) has also been implicated in regulating and deciding the fate of the recombination events, as the CO/NCO decision is thought to be established by a protein-protein interaction at the surface of Rec12 (Kan *et al.*, 2011).

1.2.5 HORMAD1 and HORMAD2

The meiotic HORMA domain-containing proteins (Hop1, Rev7 and MAD2 homology domain), HORMAD1 and HORMAD2, are highly conserved between eukaryotes (the yeast meiotic HORMA domain-containing protein is known as Hop1). Hop1 is a structural component of the SC in *S. cerevisiae* (Kironmai *et al.*, 1998), and promotes inter-homologue recombination during meiosis in *S. cerevisiae* (Niu *et al.*, 2005) and *S. pombe* (Latypov *et al.*, 2010). In mammals, HORMAD1 and HORMAD2 preferentially localise to unsynapsed chromosome axes during prophase I, but are not observed on the synapsed chromosomes in pachytene (Fukuda *et al.*, 2010; Shin *et al.*, 2010). A recent study by Shin *et al.*, (2010) suggested that HORMAD1 is essential for mammalian gametogenesis, as *Hormad1*$^{-/-}$ male and female mice were found to be infertile. HORMAD1 was identified as a fundamental component of the SC with roles in synapsis, meiotic recombination and meiotic sex chromosome inactivation and transcriptional silencing (Shin *et al.*, 2010). HORMAD1 ensures that sufficient unrepaired DSBs are available for a homology search, promoting homologue alignment and SC formation (Daniel *et al.*, 2011).

HORMAD1 and HORMAD2 appear to have non-overlapping functions but both are required for the elimination of *Spo11*$^{-/-}$ mouse oocytes. A HORMAD1- and HORMAD2-dependent meiosis-specific surveillance mechanism has been identified which monitors inappropriate asynapsis and triggers meiocyte elimination (Daniel *et al.*, 2011; Wojtasz *et al.*, 2012). The DNA damage response (DDR) sensor kinase ATR identifies DNA damage (such as DSBs) in

mitotic cells and activates the DNA damage checkpoint which leads to cell cycle arrest. ATR has also been implicated in the control of cell progression through meiotic prophase. HORMAD1 and HORMAD2 recruit ATR and/or its activators to unsynapsed chromosome axes and therefore are required to adapt ATRs function to the meiosis-specific task of identifying asynapsis (Wojtasz *et al.,* 2012).

In budding yeast and mammals, meiotically induced DSBs are a prerequisite for normal SC formation (Zickler and Kleckner, 1999). However, in other species such as *D. melanogaster* and *C. elegans* recombination is not required for SC formation, but is delayed until SC formation is complete. Instead pre-synaptic alignment appears to be mediated by specific chromosomal domains (MacQueen *et al.*, 2002; McKim *et al.*, 2002).

1.3 Chromosome synapsis

In most organisms, chromosome synapsis involves the alignment of homologous chromosomes within the context of a large proteinaceous structure, the SC. The SC is a highly conserved structure which is thought to facilitate crossover formation during prophase I, however its function remains poorly understood. The majority of the current understanding of synapsis and recombination was derived from model organisms, such as *S. cerevisiae*, *C. elegans* and *D. melanogaster* (Page and Hawley, 2004).

Synapsis occurs along the entire length of the homologous chromosomes, except for the sex chromosomes in mammals. The XY chromosomes are sequestered in a specialised nuclear territory known as the XY body during pachytene spermatocytes and form synapsis in pseudoautosomal regions only. This specialised feature accommodates the absence of homology between the sex chromosomes during synapsis (Handel, 2004).

1.3.1 The synaptonemal complex

The SC is a large tri-partite proteinaceous structure, with a ladder-like arrangement, composed of two electron dense structures known as the lateral elements (LEs) and a less electron dense central element (CE). During early prophase, the sister chromatids become organised along well-distributed short linear segments, known as the axial elements (AEs) which lengthen and condense into the filamentous meshwork structures of the LEs. The LEs are fully formed at the beginning of zygotene and become physically linked to the CE via the

transverse filaments (TFs). The CE is thought to be composed of three or four layers of transverse filament components which are longitudinally connected by the pillar-shaped protein structures of the LEs (Figure 1.4). By the end of zygotene the paired homologous chromosomes are fully synapsed in the context of a mature SC structure (reviewed in Page and Hawley, 2004; Vallente *et al.*, 2006).

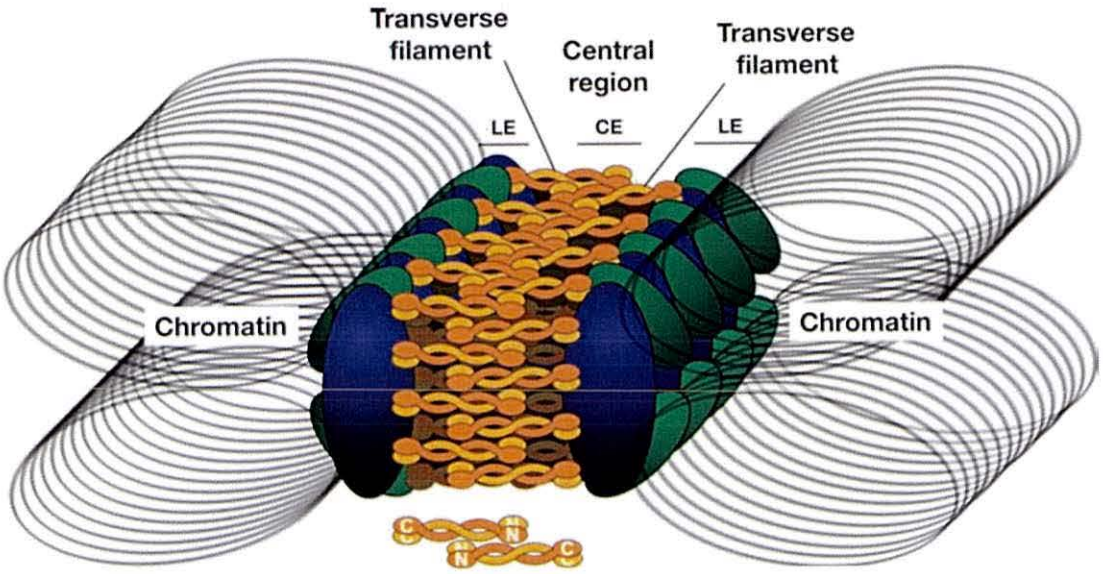

Figure 1.4. The synaptonemal complex structure. This cross section shows the continuous pillar-shaped protein structures of the lateral elements (LE) which are shown in green. Two LEs are linked to the central element by the transverse filaments which are shown in yellow and orange. Loops of chromatin are extended in a perpendicular array from the LEs of the SC. The cohesin and condensin proteins interact with the chromosomes whilst in the SC (shown in blue). C, carboxyl-terminus; N, amino-terminus.

From Page and Hawley (2004).

The transverse filaments maintain a uniform distance between the LEs (approximately 100 nm). The DNA of the homologous chromosomes is organised in a series of chromatin loops which extend out in a perpendicular array to the SC structure. The density of chromatin loops along the SC is relatively well conserved in a variety of organisms, regardless of differing genome size and SC length (Zickler and Kleckner, 1999), which is maintained through differing chromatin loop sizes (Kleckner, 2006). Interestingly, in humans the chromatin loop sizes differ between males and females. The female SC structure is approximately twice the length of the male SC structure (Tease and Hultén, 2004).

Once the SC is fully constructed, the cell is able to progress into the pachynema stage (this is the longest stage during prophase I). During pachynema the chromosomes continue to

condense into their shortest length, whilst remaining fully synapsed. When the CE begins to disassemble during diplonema, the chromosomes repel one another and chiasmata become evident, thus keeping the chromosomes in their appropriate pairs during diakinesis as the chromosomes condense before the onset of metaphase I (Page and Hawley, 2004). The LEs then begin to dissolve as diplonema progresses and the SC is totally dissipated by the end of prophase I (Svetlanov and Cohen, 2004). The chiasmata promote the monopolar orientation of sister kinetochores, which results in the correct segregation of the homologues to opposite poles (Hirose *et al.*, 2011).

1.3.2 The SC proteins

To date, seven essential constituent proteins of the mammalian SC structure have been identified; synaptonemal complex proteins 1, 2 and 3 (SYCP1, SYCP2 and SYCP3), synaptonemal complex central element proteins 1, 2 and 3 (SYCE1, SYCE2 and SYCE3) and testis expressed 12 (TEX12) (Table 1.2).

Table 1.2. Constituent proteins of the synaptonemal complex

Constituent protein	Role within the SC
SYCP1	The TFs are composed of SYCP1 parallel homodimers. The C-terminal domain associates with the LE proteins and the N-terminal domain associates closely with the CE proteins (Page and Hawley, 2004).
SYCP2	Constituent protein of the LEs (Page and Hawley, 2004).
SYCP3	Constituent protein of the LEs (Page and Hawley, 2004).
SYCE1	Central element protein. Co-localises with SYCE3, and is thought to have a role in SC initiation (Schramm *et al.*, 2011).
SYCE2	Central element protein. Co-localises with TEX12, and is thought to have a role in SC extension (Davies *et al.*, 2012).
SYCE3	Central element protein. Co-localises with SYCE1, and is thought to have a role in SC initiation (Schramm *et al.*, 2011).
TEX12	Central element protein. Co-localises with SYCE2, and is thought to have a role in SC extension (Davies *et al.*, 2012).

In mammals, the LEs are composed of SYCP2 and SYCP3, which are linked to the CE by the TFs comprised of SYCP1. SYCE1, SYCE2, SYCE3 and TEX12 are the constituent CE proteins (Figure 1.5).

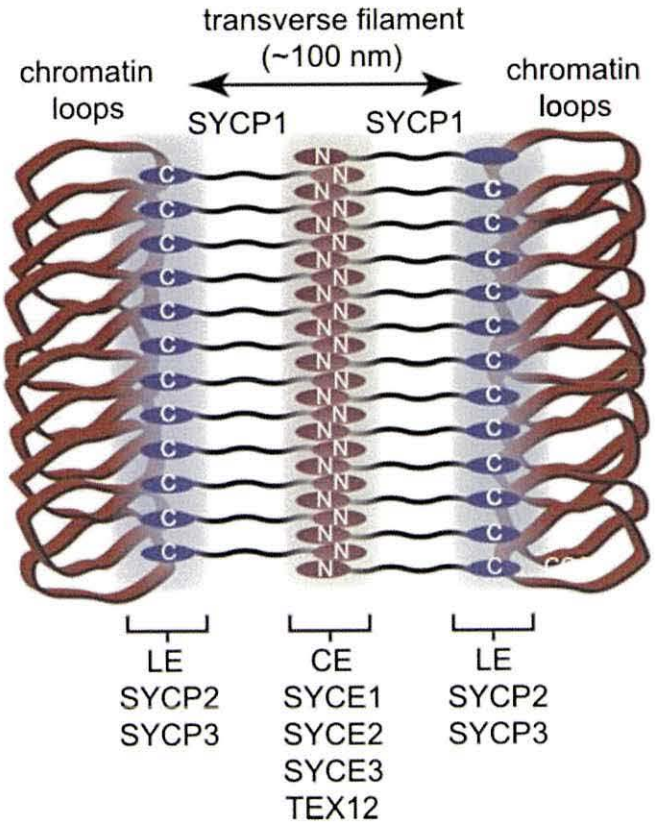

Figure 1.5. Constituent proteins of the mammalian synaptonemal complex. Schematic of the mammalian SC; wherein the two LEs are connected to the CE via the TFs. SYCP1 molecules comprise the TFs, with the N-terminal domain in the CE and the C-terminal domain in the LEs. The LEs are made up of SYCP2 and SYCP3, and the CE contains SYCE1, SYCE2, SYCE3 and TEX12.
From Davies *et al.*, (2012).

Homologous pairing establishes local alignments along the homologous chromosomes. Short sections of LEs form along the length of the chromosomes and are brought into local alignment, through the action of homologous pairing. Synapsis is initiated at these sites and the LEs are brought into 100 nm apposition by TF association. Synapsis is extended via the formation of the CE and TF protein array, thereby converting local alignments into fully synapsed homologous pairs (Page and Hawley, 2004).

Incomplete assembly of the SC has been shown to cause synapsis failure between homologous chromosomes and impaired meiotic recombination. Studies in mice have shown that mutations in the TF and CE proteins result in male/female infertility (Bolcun-Filus *et al.*, 2007; 2009; De Vries *et al.*, 2005; Hamer *et al.*, 2008; Schramm *et al.*, 2011), whereas mutations in the LE proteins produces a sexually dimorphic phenotype; with male infertility and female subfertility (Yang *et al.*, 2006; Yuan *et al.*, 2000). In humans, incorrect

SC assembly causes impaired meiotic recombination and cell death, which can cause male infertility (Judis *et al.*, 2004) and a high aneuploidy rate in oocytes (Hassold and Hunt, 2001).

1.3.2a The lateral element proteins

The cohesin complex (see Section 1.4 for more details) has been implicated in the localisation of the LE-associated proteins to the chromatin (Zickler and Kleckner, 1999). There is evidence to suggest that cohesin complex subunits form an axial chromosome core onto which the LE proteins bind and assemble (Eijpe *et al.*, 2003). The LEs are composed of the meiosis specific proteins, SYCP2 and SYCP3 in mammals and in *S. cerevisiae* Hop1, Red1 and Mek1 are all structural components of the LEs (Zickler and Kleckner, 1999). In *S. cerevisiae*, Red1 localises to the AEs and is required for AE formation. The Red1-Hop1 interaction requires Red1 phosphorylation which is mediated by Mek1, a serine/threonine kinase required for SC assembly (Smith and Roeder, 1997). Red1 remains associated with the bivalents during pachytene, whereas the majority of Hop1 appears to dissociate as the chromosomes synapse. Red1 is capable of associating with the chromosomes in *hop1 S. cerevisiae* mutants, however Hop1 is required for correct chromosomal localisation of Red1 (Smith and Roeder, 1997).

Similarly, in mammals SYCP2 and SYCP3 localise to unsynapsed AEs during lepotene, which mature into the LEs. SYCP3 is required for the normal binding of SYCP2 to the AEs (Pelttari *et al.*, 2001), however SYCP2 can localise to the telomeres by an SYCP3-independent mechanism (Liebe *et al.*, 2004). SYCP3 is able to form fibrous structures when it is expressed in cultured mammalian cells (Yuan *et al.*, 1998), and when SYCP2 and SYCP3 are co-expressed in cultured mammalian cells, they co-localise to short, fibrous structures, distinct from the SYCP3 fibrous structures (Pelttari *et al.*, 2001). SYCP3 accumulation in large protein aggregates was reported in *Sycp2* mutant mice; however SYCP3 was unable to bind to the axial chromosomal cores resulting in absence of AE formation (Yang *et al.*, 2006). The sexually dimorphic phenotype observed in the *Sycp2* mutant mice suggests that SYCP2 is essential for SYCP3 incorporation into the LEs (Yang *et al.*, 2006).

SYCP3 is essential during meiotic progression and synapsis, with studies observing a failure to construct a functional SC in the absence of SYCP3. SYCP3 undergoes major transformations during prophase I and constitutes a major structural template of the SC

(reviewed in Vallente *et al.*, 2006). A study by Yuan and colleagues (2000) found that synapsis was completely eliminated in *Scp3*$^{-/-}$ mouse spermatocytes and observed apoptosis in the germ cells leading to male infertility. Although SYCP3 is required for chiasma formation and maintenance of chromosomal integrity, *Scp3*$^{-/-}$ mature female mouse oocytes can be obtained but they are severely aneuploid because the chromosomes fail to segregate correctly (Yuan *et al.*, 2002).

There is also evidence to suggest that the AE proteins influence the DSB repair partner choice (Li *et al.*, 2011). In *S. cerevisiae*, Mek1/Hop1/Red1 complexes appear to promote inter-homologue DSB repair (Niu *et al.*, 2007). Mek1 suppresses DNA repair between sister chromatids during meiosis by inhibiting Rad51 recombinase activity (Callender and Hollingsworth, 2010). Similarly, the mammalian AE proteins have also been implicated in inter-homologue bias during meiotic recombination. SYCP3 is not required for DSB formation however a decrease in CO formation was observed in *Sycp3*$^{-/-}$ mice (Li *et al.*, 2011). Interestingly, SYCP3 has been shown to form a complex with BRCA2 in cancer cells which therefore inhibits the mitotic recombination DNA repair pathway and induces chromosome instability (Hosoya *et al.*, 2012). This may suggest that SYCP3 promotes inter-homologue recombination during meiosis, by inhibiting inter-sister recombination.

1.3.2b The transverse filament proteins

The SYCP1 molecules are long coiled-coil proteins with two globular heads which form parallel homodimers, with the C-termini embedded in the LEs and the N-termini interacting in the dense region in the middle of the CE (Liu *et al.*, 1996; Schmekel *et al.*, 1996). TF proteins have also been identified in several other species, including Zip1 in *S. cerevisiae*, and SYP1 and SYP2 in *C. elegans* (MacQueen *et al.*, 2002). Although the TF orthologue proteins lack sequence homology, they have similar secondary structures and localisation (Page and Hawley, 2004). Homologous pairing but not chromosome synapsis was observed in *zip1* null mutants in *S. cerevisiae*, therefore suggesting that Zip1 (SYCP1) is the main component of the TFs and essential for SC formation (Sym *et al.*, 1993). Also, *zip1* mutants which affect the length of the protein have been shown to exhibit variations in SC width (Sym and Roeder, 1995). Similar to the lateral element proteins, when Zip1 and SYCP1 are over-expressed in yeast and cultured mammalian cells respectively, they form structures, known as polycomplexes, which closely resemble that of the SC (Ollinger *et al.*, 2005; Sym

and Roeder, 1995). These polycomplexes are also commonly observed in meiotic cells after the dissociation of the SC, but have also been observed before SC formation which may suggest they are just discarded SC structures (Zickler and Kleckner, 1999).

Studies using *S. cerevisiae* have suggested that centromeres undergo homology-independent coupling which depends upon Zip1. Zip1 is also thought to suppress centromere-proximal CO events (Chen *et al.*, 2008; Obeso and Dawson, 2010). The centromeres appear to act as nucleation sites for SC polymerisation, as well as recombination sites along the chromosome arms (Tsubouchi *et al.*, 2008). In budding yeast *spo11* mutants, which fail to initiate recombination, Zip1-mediated centromere coupling is still observed (Tsubouchi and Roeder, 2005), and in the absence of SPO11-mediated recombination the centromeres become the primary sites of SC polymerisation (MacQueen and Roeder, 2009).

1.3.2c The central element proteins

Four CE proteins have been identified in mammals, SYCE1, SYCE2 (Costa *et al.*, 2005), SYCE3 (Schramm *et al.*, 2011) and TEX12 (Hamer *et al.*, 2006). SYCE1 and SYCE3 co-localise to the central region of the SC in a continuous pattern identical to that of SYCP1 (Schramm *et al.*, 2011). Mouse studies in which *Syce1* and *Syce3* were disrupted showed a complete SC failure, although SYCP1 localisation was observed in a discontinuous pattern along the AEs (Bolcun-Filus *et al.*, 2009; Schramm *et al.*, 2011). In contrast, SYCE2 and TEX12 co-localise in a distinct pattern to that observed for SYCP1, SYCE1 and SYCE3. Disruption of *Syce2* and *Tex12* in mice causes synaptic failure, although synapsis is initiated at multiple positions along the chromosomes, with the formation of short stretches containing CE-like structures (Bolcun-Filus *et al.*, 2009; Hamer *et al.*, 2008). Therefore SYCE1 and SYCE3 have been implicated in the initiation of synapsis, whereas SYCE2 and TEX12 have been implicated in synapsis extension (Bolcun-Filus *et al.*, 2009; Davies *et al.*, 2012). SYCE2 and TEX12 spontaneously associate with each other, forming hetero-oligomers (Davies *et al.*, 2012). Extension of the CE is thought to occur via the formation of the SYCE2-TEX12 filament, which takes place simultaneously with the concomitant extension of the TF (SYCP1) array (Davies *et al.*, 2012). Correct formation of the CE is essential for the formation of the SYCP1 head-to-head polymers and thus normal progression of synapsis and meiotic recombination (Bolcun-Filus *et al.*, 2009; Schramm *et al.*, 2011).

In *S. cerevisiae*, the initiation and elongation of the SC is mediated by the synapsis initiation complex, consisting of the ZMM proteins (Zip1, Zip2, Zip3, Zip4, Mer3 and Msh4) (Fung *et al.*, 2004; Lynn *et al.*, 2007). Of these, the Zip2, Zip3 and Zip4 proteins appear to be functionally related to the mammalian CE proteins. Zip3 binds to sites of synapsis initiation and recruits Zip2 and Zip4, which in turn are responsible for Zip1 polymerisation (TF) (Tsubouchi *et al.*, 2006). These proteins are essential for SC formation and efficient meiotic recombination resulting in CO events (Tsubouchi *et al.*, 2006).

1.3.3 The SC function

SC assembly converts local homologous chromosome alignments into fully synapsed chromosome pairs, however its exact function remains poorly understood. Incomplete assembly of the SC has been shown to cause synapsis failure between homologous chromosomes and impaired meiotic recombination, which can cause meiotic arrest and cell death. Therefore correct SC assembly is essential for the accurate completion of meiosis in some organisms, such as humans, mice and *S. cerevisiae* (Page and Hawley, 2004). However, some organisms undergo normal meiosis without the presence of this protein structure, for example *S. pombe* does not have a fully developed SC structure, although it does possess Red1, Hop1 and Mek1 orthologues and structures called linear elements which are thought to be functional orthologues of the axial elements. This may suggest that the full SC is not a prerequisite for meiosis and/or meiotic recombination (Cromie and Smith, 2008).

In most organisms, the homologous chromosomes are aligned through the interaction of meiotically induced DSBs. Homologous pairing aligns the AEs, thus allowing the formation of the SC which in turn is thought to aid homologous recombination (Figure 1.6).

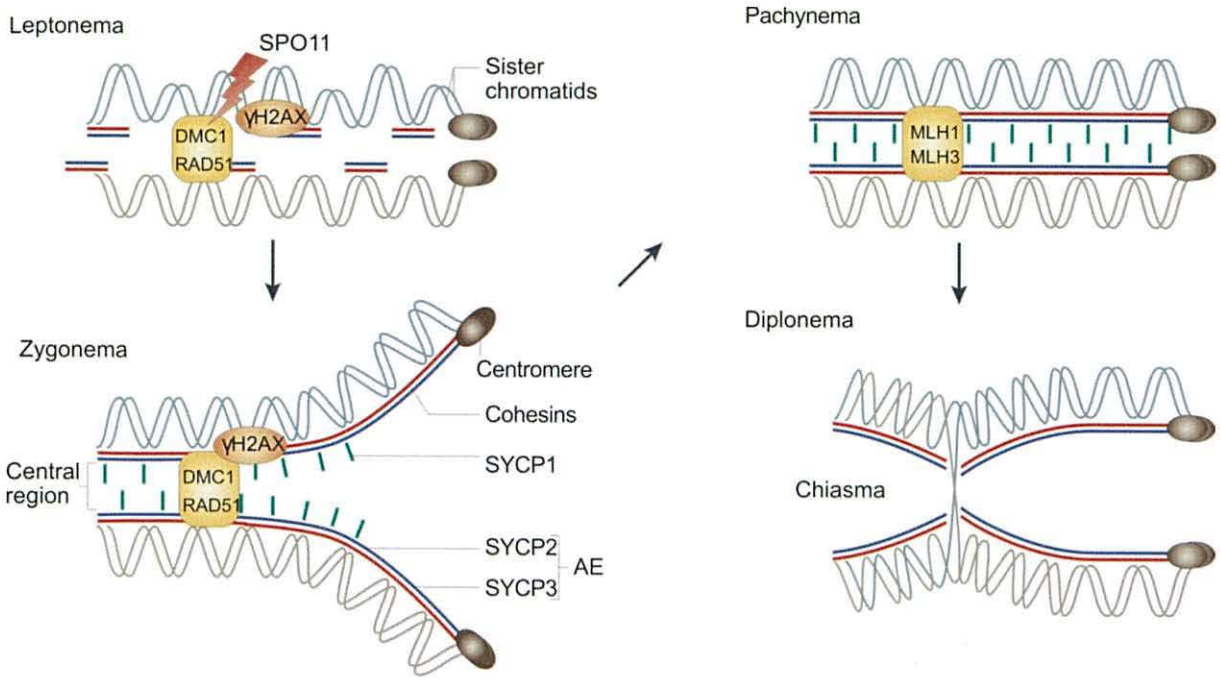

Figure 1.6. Recombination and synaptonemal complex formation in the prophase sub-stages. During leptotene, the homologous chromosomes begin to align. A chromosomal core, containing cohesin proteins (for example REC8 and SMC1β), forms along the chromosomes onto which SYCP2 and SYCP3 localise and begin to form the AEs. Meiotically induced DSBs are created by SPO11, which aids homologous chromosome pairing and alignment. Recombination repair machinery proteins (such as H2AX) are recruited to the DSBs. The 5' DNA is resected on either side of the break, which triggers DMC1 and RAD51 binding. By zygotene, the homologous chromosomes are paired and synapsis is initiated at the sites of future CO sites. The homologous chromosomes are fully synapsed by pachytene, with a clear central element. The central element proteins aid the conversion of DSBs into CO events. The CO events are marked by the mismatch repair proteins MutL protein homologue-1 and -3 (MLH1 and MLH3). After recombination, the SC disassembles at diplonema and the chiasmata are resolved.

From Handel and Schimenti (2010).

'Twisting' of the SC has repeatedly been reported in mammals and other organisms. A model has been proposed for SC-assisted recombination, due to a 'twisting' of the SC structure which is caused by mechanical forces or stress generated by chromatin loop extension. 'Twisting' of the structure would bring the axes of the chromatids into close proximity of one another and thus mediating local changes between DNA, SEI-to-dHJ transition, and axis exchange between the chromatid axes (Borner *et al.*, 2004; Kleckner *et al.*, 2004).

Meiotic recombination and synapsis are two distinct meiotic processes, which appear to be fundamentally interrelated. Recombination has a critical role in promoting homologous pairing and synapsis, and in turn synapsis stabilises homologous pairing and locally

promotes CO formation. Synapsis is often initiated at the sites of future CO events; however it is unclear whether CO-designation triggers synapsis or SC-initiation triggers CO formation (Henderson and Keeney, 2005). Mammalian centromeres do not undergo synapsis and it has been suggested that this is the mechanism by which centromere-proximal CO events are suppressed (Qiao *et al.*, 2012). This may therefore provide evidence that SC initiation may trigger CO formation (Qiao *et al.*, 2012). However, in some species homologous pairing and synapsis occur in the absence of recombination (for example male *D. melanogaster*) (Vazquez *et al.*, 2002). In male *D. melanogaster* homologous pairing is achieved via the pre-synaptic alignment of specific chromosomal domains (McKim *et al.*, 2002).

The TF proteins have been shown to play a role in promoting the maturation of recombination intermediates to form CO products (reviewed in De Boer and Heyting, 2006). Impaired recombination has been reported in mouse mutants lacking a clear CE, therefore it has been suggested that interactions between the recombination machinery proteins and the structural components of the CE are essential for CO formation (Bolcun-Filus *et al.*, 2009). Interactions between RAD51 and both SYCP1 (Tarsounas *et al.*, 1999) and SYCE2 (Bolcun-Filus *et al.*, 2009) have been reported in mice. There is also evidence that the ZMM proteins promote CO formation in *S. cerevisiae* at the sites of synaptic initiation. Zip2, Zip3 and Zip4 are thought to have roles in the polymerisation of TFs (Lynn *et al.*, 2007) and *Zip2* or *Zip3* deletions result in a reduction in the number of COs observed (Agarwal and Roeder, 2000; Chua and Roeder, 1998).

In addition to homologous pairing, stabilisation via synapsis and CO promoting function, a role for the SC structure in CO interference has been suggested in a number of organisms (such as *S. cerevisiae*). Impaired/lack of SC formation has been observed with a simultaneous reduction/elimination in CO interference. *Zip1* mutants exhibiting a slight reduction in SC formation were able to form functional chiasmata however CO interference was completely abolished (Sym and Roeder, 1994). Synapsis initiation complexes (SIC) associate with the chromosomes prior to the formation of the SC. The SICs localise fairly uniformly along the chromosomes and display interference with each other, which is known as physical interference (Fung *et al.*, 2004). Null mutants in the genes encoding the SIC components reduce the number of CO events, but not the number of NCO events. Zip1 has

been shown to inhibit CO formation in the vicinity of the centromeres (Chen *et al.*, 2008). The CE proteins have been shown to play several roles in deciding CO frequency and distribution, including; local CO-promoting activity at sites of future COs, self-polymerisation of the CE proteins enable CO formation at distant sites of synapsis initiation and CO-inhibitory role(s) which limit the number of successful CO events (Hayashi *et al.*, 2010).

Interestingly, *S. pombe* does not have an SC and does not exhibit CO interference (Munz, 1994), therefore providing further evidence supporting a role for the SC in CO interference.

1.4 Chromosome cohesion

Sister chromatid cohesion is established during the DNA replication phases of both mitosis and meiosis by a multiprotein complex called cohesin, which has an essential role in sister chromatid pairing and separation. Cohesion facilitates the generation of tension, which is required for the correct alignment of chromosomes prior to segregation. Subsequent cleavage of cohesin releases the chromosomes, allowing them to migrate towards opposite poles (Lee and Orr-Weaver, 2001; Nasmyth, 2001).

The cohesin complex has been implicated in a wide range of functions additional to that of chromosome cohesion. These functions include; the formation and repair of DNA DSBs in mitotic and meiotic cells (reviewed in Sjogren and Strom, 2010); assembly of replication factories during S-phase (Guillou *et al.*, 2010) and SC AEs during prophase I (Kim *et al.*, 2010); formation and repair of DSBs during mitosis (Sjogren and Nasmyth, 2001) and meiosis (Kim *et al.*, 2010); transcriptional control in yeast (Lin *et al.*, 2011), trypanosomes (Landeira *et al.*, 2009), flies (Pauli *et al.*, 2010), fish (Horsfield *et al.*, 2007) and mammals (Parelho *et al.*, 2008).

1.4.1 The cohesin complex

The cohesin complex is a tripartite ring structure, consisting of two structural maintenance of chromosome (SMC) proteins and an α-kleisin subunit. The two SMC proteins are rod-shaped proteins which consist of 50 nm long intramolecular anti-parallel coiled coils, with a dimerisation domain at one end and an ABC (ATPase bind cassette)-like ATPase head at the other end. Heterotypic interaction between the SMC1 and SMC3 dimerisation domains creates a huge V-shaped structure with ABC ATPase heads at its apices (Gruber *et al.*, 2003).

The SMC3 and SMC1 ATPase heads are bound by the N- and C-terminals of the α-kleisin subunit respectively. The α-kleisin, RAD21 (SCC1) in mammalian cells (also known as Mcd1 in *S. cerevisiae* and Rad21 in *S. pombe*), in turn recruits SCC3/SA (stromal antigen) and the cohesin accessory proteins; PDS5 and WAPL subunits (Nasmyth and Haering, 2005) (Figure 1.7).

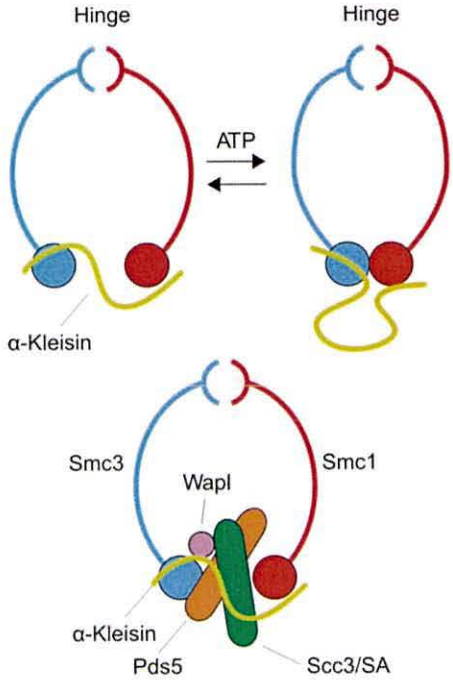

Figure 1.7. Structure of the cohesin ring. The two rod-shaped SMC proteins, SMC1 (red) and SMC3 (blue) with dimerisation domains at one end and ABC-like ATPases at the other, form a V-shape through heterotypic interactions between the dimerisation domains. The tripartite ring is formed through α-kleisin (yellow) association with the SMC1-SMC3 heterodimer. The N- and C-terminal domains of the α-kleisin bind to the nucleotide-binding domains of the SMC3 and SMC1 subunits respectively. The central domain of the α-kleisin binds to the Scc3/SA and PDS5 subunits, and PDS5 in turn binds to WAPL.

Adapted from Nasmyth (2011).

This ring structure is thought to entrap the sister chromatids thus enabling intra- and inter-chromatid cohesion (Gruber *et al.*, 2003; Haering *et al.*, 2008).

1.4.2 Cohesin subunit proteins

In mammals, there are two SMC1 subunits (SMC1α and SMC1β), three α-kleisins (SCC1/RAD21, REC8 and RAD21L), three SCC3/SA subunits (STAG1, STAG2 and STAG3) and two PDS5s (PDS5A and PDS5B); therefore there are 18 possible combinations of the cohesin complex (Nasmyth, 2011).

Four of these cohesin subunit proteins have been identified as being meiosis-specific; SMC1β, REC8, RAD21L and STAG3 (Nasmyth, 2011) (summarised in Table 1.3).

Table 1.3. Cohesin complex subunits

Cohesin subunit	*Saccharomyces cerevisiae*	*Schizosaccharomyces pombe*	*Drosophila melanogaster*	*Homo sapiens*
SMC proteins	Smc1 Smc3	Psm1 Psm3	Smc1 Smc3	SMC1α, SMC1β SMC3
α-kleisins	Mcd1/Scc1, Rec8	Rad21, Rec8	Rad21, C(2)M	RAD21/SCC1, REC8, RAD21L
α-kleisin binding subunits	Scc3 Pds5	Psc3, Rec11 Pds5	SA Pds5	STAG1, STAG2, STAG3 PDS5a, PDS5b/APRIN
Pds5 binding proteins	Rad61/Wapl ?	Wapl ?	Wapl Dalmatian	WAPL Sororin
Kollerin loading complex	Scc2 Scc4	Mis4 Ssl3	Nipped B Scc4	SCC2/Nipbl SCC4/Mau2
Cohesin acetyl transferases	Eco1	Eso1	Deco, San	ESCO1, ESCO2
Shugoshin	Sgo1	Sgo1, Sgo2	MEI-S332	SGO1, SGO2

Orthologous proteins and alternative isoforms are shown on the same line.
The meiosis-specific cohesin subunits are underlined.
? – indicates an unidentified protein.

Adapted from Nasmyth (2011) and Watanabe (2005).

Cohesin is a chromosome-associated multisubunit protein complex that is highly conserved in eukaryotes. The principal mechanisms by which cohesion is mediated by the cohesin complex in eukaryotic cells is highly conserved, however there are differences between yeast and higher eukaryotes in how cohesin is regulated and distributed along the chromosomes (Peters *et al.*, 2008).

1.4.3 Mechanism of cohesion

The mechanism through which this tripartite ring structure entraps the DNA remains poorly understood, however several models have been proposed. The simplest model involves a single monomeric cohesin ring in which sister chromatids are entrapped within a single ring structure. However, it has also been hypothesised that sister chromatids may be entrapped by their own separate cohesin ring (Nasmyth, 2011) (Figure 1.8).

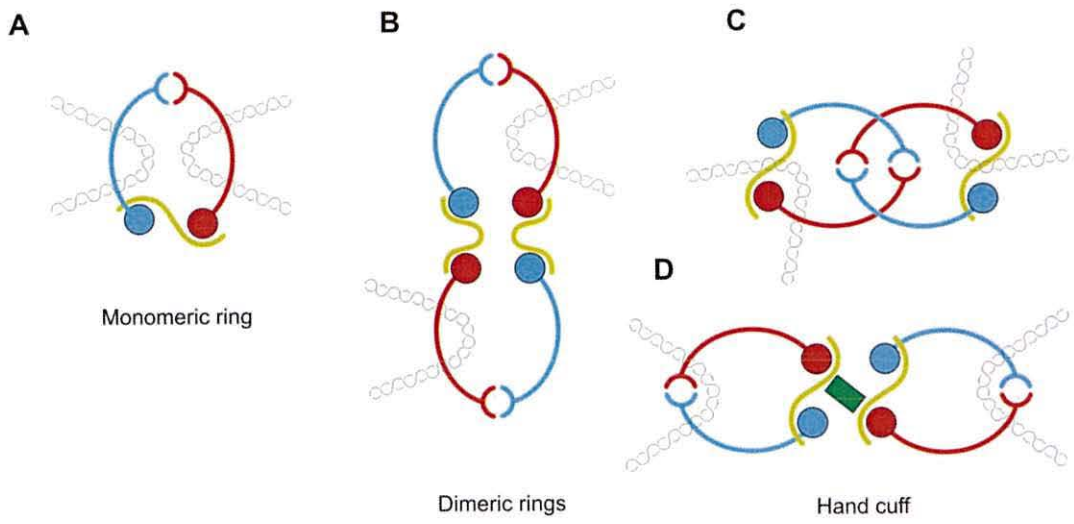

Figure 1.8. Three ring models proposed for cohesin. **A.** A single monomeric cohesin ring entraps the sister chromatids. **B** and **C** present models in which the cohesin complex forms dimeric rings where the sister chromatids are entrapped in separate ring structures. **B.** Proposes that N- and C-terminal α-kleisin binds to the nucleotide-binding domains of different SMC1-SMC3 heterodimers and **C**. proposes that the dimeric rings interact through cohesin ring concatenation. **D.** Another model has been suggested in which two rings bind to the same Scc3/SA subunit, which is known as the handcuff model.

From Nasmyth (2011).

Chemical cross-linking experiments in yeast have suggested that sister minichromosome DNAs are entrapped in a single monomeric cohesin ring (Haering *et al.*, 2008). These findings provide strong evidence to support the single ring model for the cohesin ring structure (Haering *et al.*, 2008).

In mammalian cells, cohesin associates with the DNA following the reformation of the nuclear envelope during telophase (Darwiche *et al.*, 1999) and in lower eukaryotes this occurs at the end of G_1 (Guacci *et al.*, 1997; Michaelis *et al.*, 1997). Loading of the cohesin complex requires the action of the loading complex (Scc2/Scc4) before DNA replication (Ciosk *et al.*, 2000) which is proposed to facilitate opening of the cohesin ring via ATP hydrolysis (Hu *et al.*, 2011). Cohesin persists transiently on the chromosomes, during which it dissociates with a short half life. Cohesin DNA-binding stabilisation is facilitated by the Eco1 acetyl transferase in *S. cerevisiae* (also known as Eso1 in *S. pombe*) during S-phase via Smc3 acetylation (Ben-Shahar *et al.*, 2008).

During mitosis, cohesin is released from the DNA in two waves; the majority of cohesin is released from the sister chromatid arms in the first wave, via an α-kleisin-cleavage

independent mechanism during the prophase pathway. The centromeric cohesin is protected from removal at this stage until its release at the second wave at the onset of anaphase, when the α-kleisin subunit is irreversibly proteolytically cleaved by separase (reviewed in Murayama and Uhlmann, 2013). This dynamic proteinaceous structure contains separate DNA entry and exit gates; DNA enters the cohesin complex through an entry gate at the hinge domain and exits through a distinct gate at the Smc3 head (Chan *et al.*, 2012; Murayama and Uhlmann, 2013) (Figure 1.9).

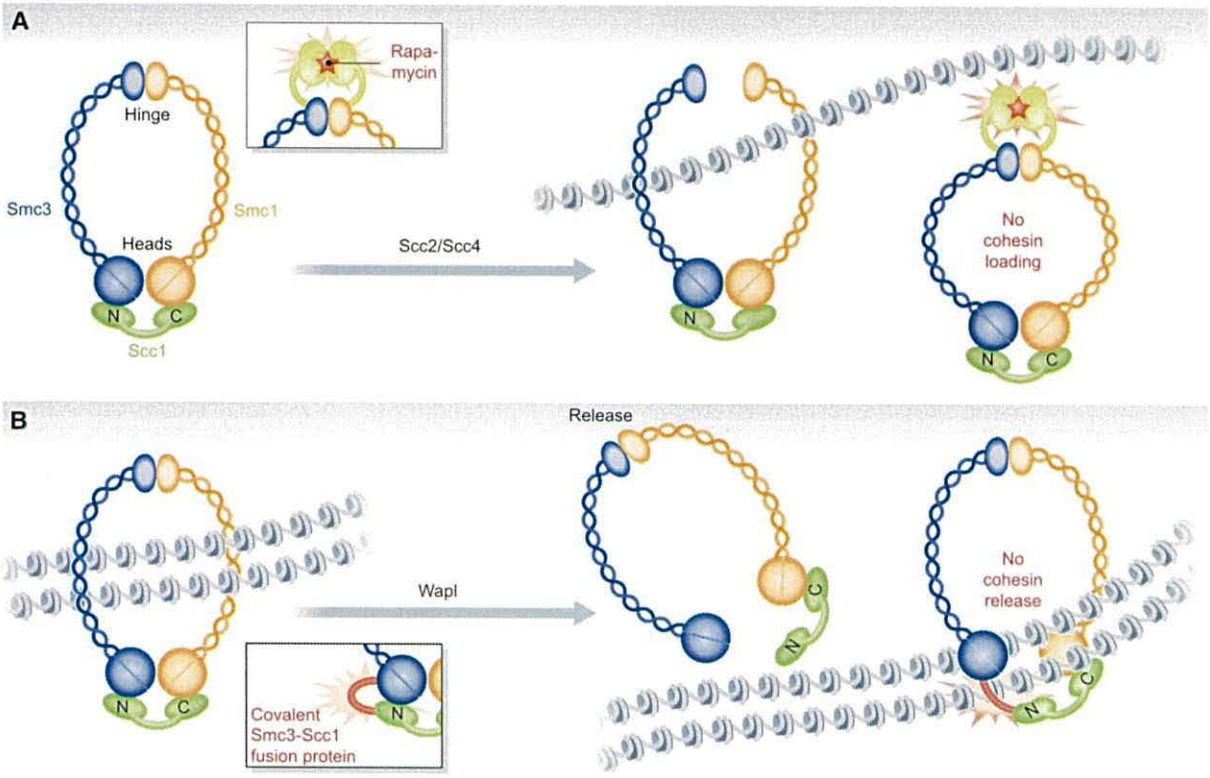

Figure 1.9. The DNA entry and exit gates in the cohesin complex. A model for the distinct DNA entry and exit gates in the cohesin complex was proposed from engineered cohesin gate fusion proteins. **A.** Rapamycin-induced dimerisation of engineered hinge interaction domains SMC1-SMC3 prevents cohesin loading onto DNA. Thus suggesting that cohesin is loaded onto DNA through an entry gate at the SMC1-SMC3 hinge domain. **B.** A covalent SMC3-SCC1 fusion protein prevents the release of cohesin from DNA, by WAPL during interphase and via the prophase pathway. Therefore suggesting that the DNA exit gate is located at the SMC3-SCC1 interface.

From Murayama and Uhlmann (2013).

Studies have shown that the cohesin complex is loaded onto the DNA through an entry gate at the Smc1-Smc3 (SMC1-SMC3) hinge domain in yeast (Gruber *et al.*, 2006) and in humans (Buheitel and Stemmann, 2013). In mammalian cells, WAPL is required for cohesin turnover during interphase via α-kleisin displacement. Cohesin is loaded onto the DNA before replication and persists only transiently. WAPL binds to PDS5 (a large HEAT-repeat

containing protein) and is recruited to the cohesin complex. WAPL does not stably associate with cohesin, and therefore its displacement of the α-kleisin from SMC3 is a temporary event (Nishiyama *et al.*, 2010). Sororin is recruited to the chromatin bound cohesin after SMC3 acetylation, and displaces WAPL from PDS5 but not from cohesin and is therefore thought to induce a change in the topology of these cohesin associated proteins. This displacement is thought to inhibit WAPL's ability to dissociate the cohesin complex from DNA, therefore creating a stable cohesin interaction and thus allowing stable chromosome cohesion (Nishiyama *et al.*, 2010). Eco1 has been detected at the replication forks in *S. cerevisiae*, therefore these events are thought to occur directly at the replication forks (Lengronne *et al.*, 2006). Sororin (known as Dalmatian in *D. melanogaster*) is essential for sister chromatid cohesion in vertebrates (Rankin *et al.*, 2005; Schmitz *et al.*, 2007). Sororin appears to be less conserved than the other cohesin subunits, as no sororin related proteins have been identified in worms or yeast to date (Nishiyama *et al.*, 2010; Peters *et al.*, 2008).

In oocytes, cohesin holds the sister chromatids together for several weeks or years (depending on species) and therefore this stable cohesin state is thought to be very robust (Tachibana-Konwalski *et al.*, 2010).

1.5 Chromosome segregation

Homologous chromosome pairing and cohesion is essential for faithful chromosome segregation in mitosis and meiosis. In mitosis, the cohesin complex is responsible for holding sister chromatids together until the onset of anaphase. The sister chromatid kinetochores are captured by spindle microtubules emanating from opposite poles, known as bipolar attachment. Bipolar attachment of sister chromatids is essential for correct chromosome segregation in mitosis (reviewed in Silkworth and Cimini, 2012).

In meiosis chromosome segregation occurs in two cell divisions, wherein sister chromatids must remain associated until the onset of anaphase II to ensure that they are segregated to the same pole during meiosis I. There are two distinct types of chromosome segregation observed in meiosis; therefore meiosis requires a different mechanism of cohesion and cleavage to that of mitosis (reviewed in Holt and Jones, 2009) (summarised in Figure 1.10).

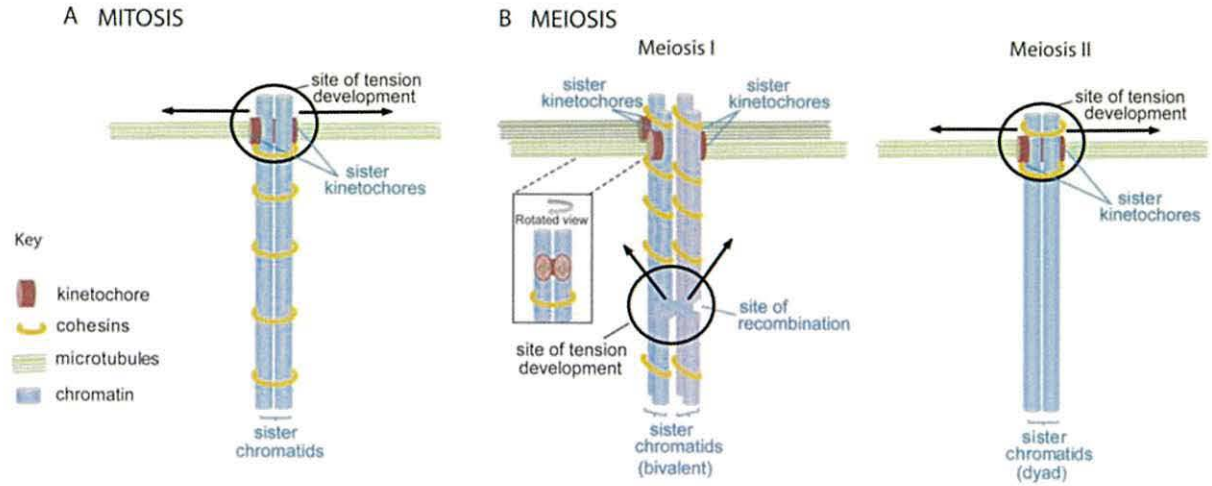

Figure 1.10. Comparison between the kinetochore arrangements during chromosome segregation in mitosis and meiosis. A. In mitosis, sister chromatids are held together by cohesin complexes along their arms. Tension is achieved when the microtubules attach to the centromere and the arm cohesins dissociate, to enable correct segregation at anaphase. The sister kinetochores are arranged in a back-to-back formation and are attached to opposite spindle poles. **B.** In meiosis I, homologous chromosomes are joined via crossovers and cohesin complexes bind sister chromatids together, thus maintaining a bivalent structure. When the microtubules attach to the kinetochores in meiosis I, tension arises from the crossover sites. The sister kinetochores are arranged in a side-by-side formation and are attached to the same spindle pole, thus ensuring that homologues are attached to opposite poles. Centromeric cohesin is protected from degradation during meiosis I, and therefore sister chromatids remain physically linked via centromeric cohesin. Sister kinetochores become arranged in a back-to-back conformation during meiosis II and attach to opposite poles. Tension is achieved at the centromeric cohesin bonds, in a similar way to mitosis.
From Holt and Jones (2009).

In mitosis, arm cohesin is removed via the prophase pathway whilst centromeric cohesion is maintained until the onset of anaphase when RAD21 is cleaved by separase (Uhlmann *et al.*, 1999; 2000). In contrast, during meiosis sister chromatids do not lose their arm cohesin until the onset of anaphase I, which requires REC8 degradation by separase (Kudo *et al.*, 2006; Terret *et al.*, 2003). Centromeric REC8 is not cleaved until the onset of anaphase II, thus maintaining sister chromatid connections at the centromeres. Cleavage of REC8 irreversibly breaks the ring structure, allowing the homologues and the sister chromatids to be pulled apart in meiosis I and meiosis II respectively (Holt and Jones, 2009).

The Shugoshin family of proteins (Japanese for 'guardian spirit') have been identified as key regulators of chromosome segregation in yeast, flies and vertebrates (Watanabe, 2005). In mammals, centromeric RAD21/REC8-containing cohesin complex protection is mediated by the Shugoshins during mitosis and meiosis. Only one Shugoshin has been identified in *S. cerevisiae* and *D. melanogaster* (Sgo1 and MEI-S332 respectively), whereas two Shugoshin

proteins have been identified in *S. pombe* (Sgo1 and Sgo2) and mammals (SGO1/SGOL1 and SGO2/SGOL2) (Watanabe, 2005).

1.5.1 Mitotic chromosome segregation

Cohesin is released from the DNA in two waves during mitosis, therefore suggesting two distinct release mechanisms. The majority of cohesin is released from the chromatid arms during prophase and the remaining cohesin remains chromatin-associated until anaphase.

In mammalian cells, the bulk of cohesin is removed during prophase through a mechanism which requires Polo-like kinase 1 (PLK1) and WAPL. Sororin is inactivated by phosphorylation which initiates cohesin removal via the prophase pathway (Nishiyama *et al.*, 2010). Inactivation of sororin prevents its antagonistic displacement of WAPL from PDS5. WAPL-PDS5 facilitates cohesin ring opening therefore releasing intact cohesin complexes from the chromatid arms (Nasmyth, 2011; Nishiyama *et al.*, 2010). Cohesin release by the prophase pathway also requires phosphorylation of the SCC3 (SA) subunit (Peters *et al.*, 2008). Although yeast cells contain a Wapl orthologue they lack a discernible prophase pathway, and as a result cohesin is removed via a separase-mediated mechanism in *S. cerevisiae* (Ulhmann *et al.*, 1999). Only a small population of Rad21 is cleaved at the onset of anaphase in *S. pombe* cells and the bulk of Rad21 remains associated with the chromosome arms during the metaphase-anaphase transition (Tomonaga *et al.*, 2000).

In fission yeast, Sgo2 is important for chromosome biorientation and controls the localisation of the passenger proteins to the centromeres and telomeres during early mitosis (Vanoosthuyse *et al.*, 2007). Sgo2 is also required to ensure mono-orientation of sister chromatids during meiosis (Rabitsch *et al.*, 2004; Vaur *et al.*, 2005). In contrast, Sgo1 is required to maintain sister chromatid cohesion in meiosis but not mitosis in budding yeast (Katis *et al.*, 2004; Marston *et al.*, 2004). In mammals, the shugoshin protein SGO1 is responsible for protecting centromeric cohesin from removal via the prophase pathway during mitosis (Kitajima *et al.*, 2006; Vanoosthuyse *et al.*, 2007). SGO1 recruits PP2A phosphatase which in turn promotes PDS5-bound sororin dephosphorylation and thus preventing cohesin removal by WAPL. Therefore this site selective dephosphorylation of cohesin and its regulators ensures the protection of centromeric cohesion (Liu *et al.*, 2013) (Figure 1.11).

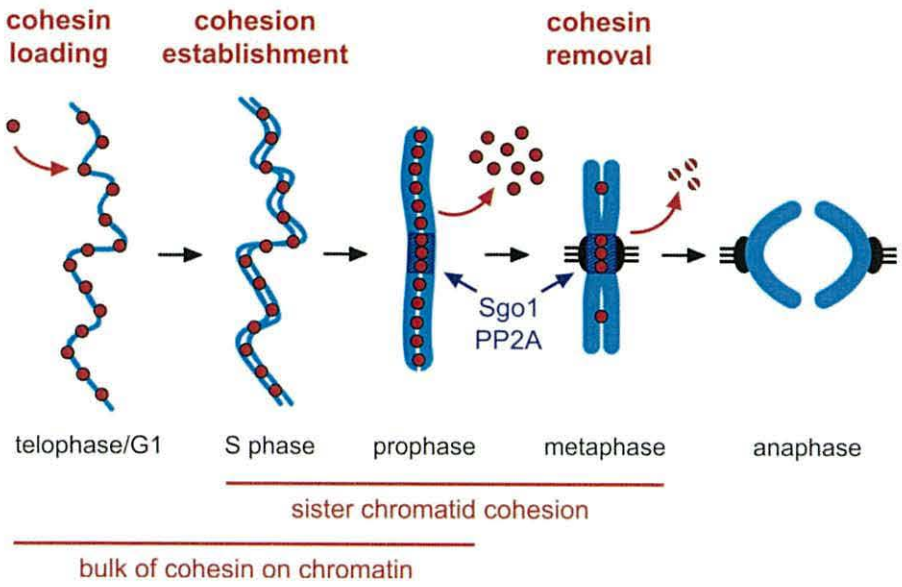

Figure 1.11. Regulation of sister chromatid cohesion during mitosis in mammalian cells. The cohesin complex is loaded onto the chromatin during telophase and G_1 via the action of the loading complex (SCC2/SCC4). Stable chromatid cohesion is established during S-phase. The arm cohesin is removed during prophase via the prophase pathway and the centromeric cohesin is protected by SGO1 until the onset of anaphase. RAD21 cleavage by separase irreversibly opens the cohesin ring complex and allows the sister chromatids to move to opposite poles during anaphase. Adapted from Peters *et al.*, (2008).

Sister chromatid cohesion at the centromere stimulates the pulling force of the spindle microtubules from the poles, and if the sister kinetochores are incorrectly attached to microtubules from the same pole this tension is not created and the attachment is destabilised. Aurora B kinases are required for efficient biorientation of sister chromatids during mitosis, through the destabilisation of erroneous kinetochores attachment (Cimini *et al.*, 2006; Knowlton *et al.*, 2006). Unattached kinetochores and/or lack of tension is sensed by the spindle checkpoint machinery, which prevents premature separation of the sister chromatids (Nezi and Musacchio, 2009; Pinsky and Biggins, 2005).

At the onset of anaphase the SCC1 (RAD21) subunit is proteolytically cleaved by a thiolprotease called separase which irreversibly opens the ring structure and triggers equational chromatid disjunction (Uhlmann *et al.*, 1999; 2000). Separase is maintained in an inactive state through association with the inhibitory chaperone protein, securin (Pds1 in budding yeast and Cut2 in fission yeast) (Mei *et al.*, 2001). When all of the chromosomes are bioriented on the spindle, SAC is inactivated at the metaphase-anaphase transition and securin is targeted for degradation by the ubiquitin E3 ligase protein complex, APC/C (anaphase-promoting complex/cyclosome). APC-dependent degradation of securin frees

separase, which in turn enables SCC1 (RAD21)-cleavage and removal of the cohesin complex from the sister chromatids (reviewed in Holt and Jones, 2009).

Cut2 is essential in fission yeast, whereas studies have shown that Pds1 is not essential in budding yeast, but loss of Pds1 causes genome instability (Yamamoto *et al.*, 1996). There is also evidence to suggest that securin is not essential in mice (Mei *et al.*, 2001) and humans (Pfleghaar *et al.*, 2005). Phosphorylation of separase has also been shown to mediate separase inhibition in vertebrate cells (Stemmann *et al.*, 2001) and this inhibitory phosphorylation functions in the absence of securin (Huang *et al.*, 2005). These studies provide evidence that the securin/separase pathway has diversified during evolution and represents different strategies controlling the metaphase-anaphase transition, used by various organisms (Clift *et al.*, 2009; Mei *et al.*, 2001; Pfleghaar *et al.*, 2005).

1.5.2 Meiotic chromosome segregation

During meiosis the RAD21 (SCC1) subunit is at least in part replaced by REC8. Sister chromatid cohesion is established during pre-meiotic S-phase and mediates two consecutive rounds of chromosome segregation. During meiosis I the sister kinetochores attach to microtubules originating from the same pole (known as syntelic attachment), whereas the sister kinetochores attach to opposite poles (amphitelic attachment) during the second meiotic division (Petronczki *et al.*, 2003).

The maternal and paternal chromosomes align on the spindle at metaphase I and are connected via chiasmata, which ensure that sufficient tension is generated when the maternal and paternal centromeres attach microtubules in a syntelic arrangement (Champion and Hawley, 2002). This tension ensures the correct orientation of the homologous chromosomes at metaphase I, thus aligning the chromosomes for subsequent segregation in anaphase I (Hauf and Watanabe, 2004; Kudo *et al.*, 2006).

The cell systematically suppresses amphitelic attachment, while promoting syntelic attachment of the sister kinetochores during meiosis I. Cleavage of REC8 at anaphase I onset triggers segregation of the maternal and paternal chromosomes to opposite poles. In contrast, amphitelic attachment of the sister kinetochores is promoted during meiosis II, and allows sister chromatids to move to opposite poles during anaphase II (Hauf and Watanabe, 2004; Petronczki *et al.*, 2003) (Figure 1.12).

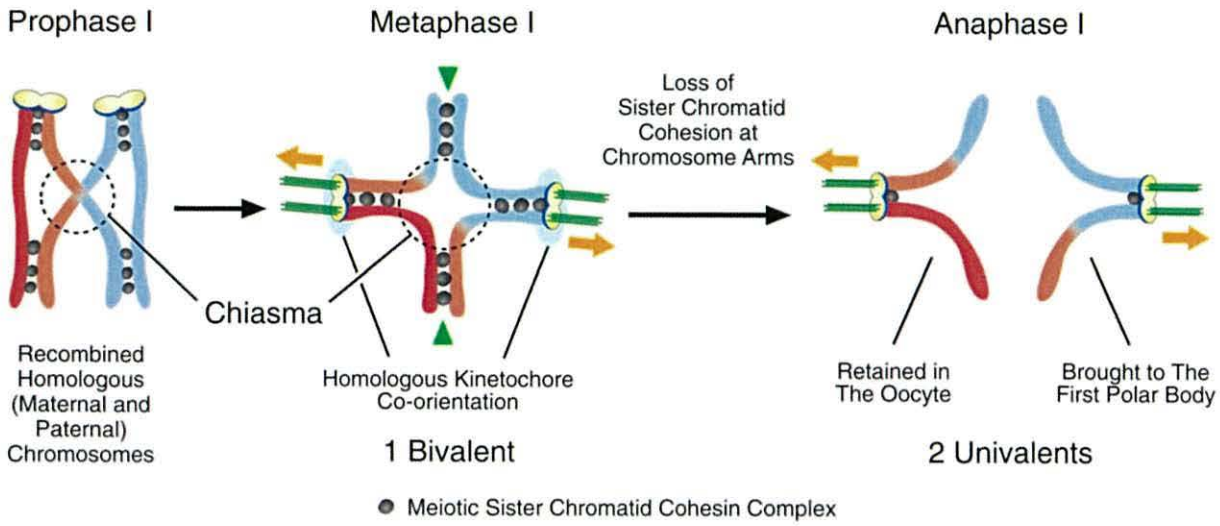

Figure 1.12. Model for the control of REC8 cleavage by REC8 kinases, SGO1-PP2A and separase. Homologous pairing, synapsis and meiotic recombination occur during prophase I, resulting in the formation of chiasmata. The sister chromatids are held together by cohesin, represented by black circles along the length of the chromosomes. Separase cleaves the REC8-containing cohesin along the chromosome arms at the onset of anaphase I, allowing homologous chromosomes to move to opposite poles. Centromeric REC8-containing cohesin is protected from separase cleavage and persists until anaphase II, where it supports the biorientation of sister chromatids during meiosis II. Separase cleavage of REC8 during anaphase II allows the sister chromatids to move to opposite poles.

From Kudo *et al.*, (2006).

REC8-containing cohesin is released via separase cleavage, and unlike mitosis there is no known non-separase mediated removal mechanism to facilitate the stage-dependent release of cohesin during meiosis (Buonomo *et al.*, 2000). Centromeric cohesin is protected from degradation by separase during meiosis I via a unique protection mechanism to ensure faithful segregation of the homologous chromosomes.

Phosphorylation of the SCC1 (RAD21) subunit by Cdc5/PLK during mitosis enhances its cleavability, but is not essential in budding yeast and mammals. In contrast, REC8 phosphorylation is required for efficient separase-mediated cleavage (Kitajma *et al.*, 2006; Llano *et al.*, 2008; Riedel *et al.*, 2006). The Shugoshin proteins recruit protein phosphatase 2A (PP2A) to the centromere, and protect REC8 from phosphorylation and therefore separase cleavage (Katis *et al.*, 2010) (Figure 1.13). Shugoshin-PP2A could mediate the protection of centromeric REC8 by inhibiting the kinase responsible for REC8 phosphorylation or by dephosphorylating REC8 itself (reviewed in Clift and Marston, 2011).

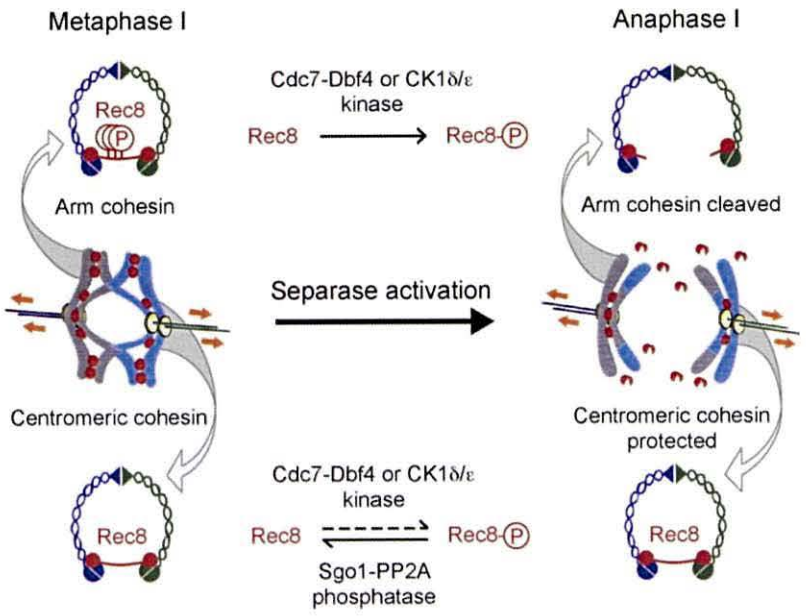

Figure 1.13. REC8 phosphorylation and cleavage during meiosis I. REC8 phosphorylation is required for separase-mediated cleavage. REC8 is phosphorylated along the chromosomes during anaphase I, which allows separase cleavage. Release of cohesin from the chromosome arms leads to chiasmata resolution. Shugoshin proteins recruit PP2A and protect REC8 from phosphorylation and therefore cleavage by separase.

From Katis *et al.*, (2010).

There is evidence to suggest that protection of sister chromatid during meiosis is regulated by tension on the kinetochore (Lee *et al.*, 2008). A study by Lee *et al.*, (2008) suggested that SGO2/PP2A associate with the outer kinetochore and their proximity to the centromeric cohesin is regulated by kinetochore tension, in mammalian oocytes. When the sister kinetochores are not under tension, during anaphase I, SGO2/PP2A are kept in close proximity with the centromeric cohesin. However, in anaphase II and anaphase during mitosis, when the sister kinetochores are under tension SGO2/PP2A is pulled away from the centromeric cohesin and are no longer in close proximity.

Studies in yeast have also shown that the Shugoshin proteins act via sensing tension across the centromere by interacting with members of the chromosomal passenger complex and enabling biorientation (Kawashima *et al.*, 2007; Vanoosthuyse *et al.*, 2007). A study by Kiburz *et al.*, (2008) demonstrated that Sgo1 has a minor role mediating homologous chromosome segregation during meiosis I, but has a key role in sister kinetochore biorientation bias in meiosis II in budding yeast. In both fission yeast and budding yeast cells lacking *SGO1* cohesin is entirely lost from the chromosomes during meiosis I, which resulted

in the random segregation of sister chromatids during meiosis II (Katis *et al.*, 2004; Kitajima *et al.*, 2004; Marston *et al.*, 2004). In budding yeast, *Shugoshin* mutants defective in PP2A binding fail to protect centromeric Rec8 during meiosis I (Xu *et al.*, 2009). In fission yeast, *Sgo1* mutants show random chromosome segregation at meiosis II, whereas *Sgo2* depleted cells show both mitotic and meiotic alterations (Rabitsch *et al.*, 2004; Vanoosthuyse *et al.*, 2007; Vaur *et al.*, 2005). In mice, SGO1 has been implicated in cohesin protection during mitosis and meiosis, but SGO2 has been implicated in protection during meiosis only. *SGO2* mutant mice were able to develop normally and reach adulthood, but were infertile (Llano *et al.*, 2008). Normal homologous chromosome separation was observed at meiosis I, but sister chromatids were unable to biorient on the equational metaphase plate and appeared separated due to loss of centromeric cohesion (Llano *et al.*, 2008).

Centromeric cohesion is established and maintained solely by REC8-containing cohesin until anaphase II (Holt and Jones, 2009; Tachibana-Konwalski *et al.*, 2010). A dramatic switch from REC8- to RAD21-containing cohesin complexes was observed in the oocyte-zygote transition in mice. Prior to fertilisation, sister chromatids are held together exclusively by REC8-containing cohesin and sister chromatid cohesin within the fertilised eggs (upon completion of meiosis) is established exclusively by RAD21-containing cohesin (Tachibana-Konwalski *et al.*, 2010).

There is evidence to suggest that inhibition of APC/C-dependent securin degradation is the only mechanism protecting premature destruction of cohesin in yeast meiosis (Katis *et al.*, 2010). Age-dependent chromosome non-disjunction during extended periods of prophase I arrest has been suggested to be caused by loss of cohesin (Holt and Jones, 2009; Katis *et al.*, 2010; Tachibana-Konwalski *et al.*, 2010).

1.5.3 REC8

REC8 orthologues have been identified in many species (from yeast to humans) and has been reported to be meiosis-specific (Parisi *et al.*, 1999). Centromeric cohesion is established and maintained solely by REC8-containing cohesin during meiosis (Tachibana-Konwalski *et al.*, 2010) and is responsible for ensuring faithful chromosomal segregation and generating tension between sister chromatids during meiosis II with kinetochore attachment (Holt and Jones, 2009). Studies in fission yeast have shown that Rad21 is

recruited to the centromeres in the absence of Rec8, however the Rad21-associated centromeres are unable to form monopolar attachment of sister kinetochores during meiosis I (Yokobayashi *et al.*, 2003). When Rad21 is recruited to the centromere instead of Rec8, no centromeric protection is exhibited, therefore suggesting that Rec8 is essential in the establishment of monopolar attachment of the sister kinetochores (Yokobayashi *et al.*, 2003).

There is also evidence to suggest that REC8 is also required for correct AE formation and SC initiation (Eijpe *et al.*, 2003; Klein *et al.*, 1999). A study using mouse *REC8* mutants has shown that the formation of SC-like structures can occur in the absence of REC8, albeit with a reduced length in the AEs (Xu *et al.*, 2005). This study also reported HR disruption and synapsis between sister chromatids instead of homologous chromosomes (Xu *et al.*, 2005). Therefore providing evidence that REC8 may have a direct/indirect role in partner bias during DNA DSB repair by HR (Kim *et al.*, 2010; Xu *et al.*, 2005).

REC8 and RAD21L are meiosis-specific α-kleisin subunits, which replace most of the RAD21 in the cohesin complexes during meiosis. REC8 and RAD21L localise along the AEs in a mutually exclusive pattern. This localisation pattern suggests that REC8 and RAD21L may have intrinsic loading sites on the chromosomes and form distinct cohesin-enriched domains along the AEs (Ishiguro *et al.*, 2011; Lee and Hirano, 2011). RAD21L localises with known SC proteins and has been suggested to have a role in homologous pairing and synapsis. RAD21L dissociates from the DNA at mid-pachytene and it has been suggested that RAD21L does not have a role in chromatid cohesion, although its role is unclear (Lee and Hirano, 2011). Lee and Hirano (2011) suggested that RAD21L may function by promoting inter-homologue recombination and CO formation. A mutually exclusive localisation pattern is observed for RAD21-, REC8- and RAD21L-containing cohesin complexes, which may indicate different functional roles for the different cohesin complexes (Ishiguro *et al.*, 2011; Lee and Hirano, 2011). The localisation pattern of REC8 and RAD21L along each chromosome is different, and a model has been proposed wherein these unique localisation patterns are thought to aid homologue pairing and synapsis, this proposed model is known as the barcode model (Ishiguro *et al.*, 2011).

Germ cell failure has been observed in *REC8* null mice, therefore demonstrating that REC8 is essential for the completion of meiosis in mammals (Xu *et al.*, 2005). However, this study also reported a high mortality rate and reduced growth for the *REC8* null mice, leading Xu and colleagues (2005) to propose a potential role for REC8 in one or more non-meiotic processes.

1.6 Errors in cell division

The events of cell division must occur in a highly coordinated manner, to achieve faithful chromosome segregation which enables the intact genome to be maintained from one generation to the next. If any of these events go awry, the resultant daughter cells may end up with an incorrect number of chromosomes (reviewed in Nicholson and Cimini, 2011).

1.6.1 Errors in mitosis

Mitotic errors occurring in early development may give rise to abnormal cells in the developing embryo which can cause birth defects or spontaneous abortion. The correct attachment of sister kinetochores to microtubules emanating from opposite poles (amphitelic attachment) is required for accurate chromosome segregation. Defects with the mitotic spindle are associated with kinetochore mis-attachment and subsequent chromosome mis-segregation. Erroneous kinetochore attachments are commonly observed during the early stages of mitosis, but are corrected before anaphase (reviewed in Gregan *et al.*, 2011). Chromosome mis-segregation leads to progeny cells with an incorrect number of chromosomes, in a state known as aneuploidy. Aneuploidy is a common feature of cancer cells, with most cancer cells exhibiting high rates of chromosome mis-segregation. Aneuploidly has been observed in over 70% of cancer cells and is the primary mechanism of chromosome instability (Weaver and Cleveland, 2006). Merotelic kinetochore orientation arises when a single kinetochore is attached to kinetochore microtubules emanating from both poles, and represents the major mechanism of aneuploidy in cancer cells (reviewed in Gregan *et al.*, 2011) (Figure 1.14).

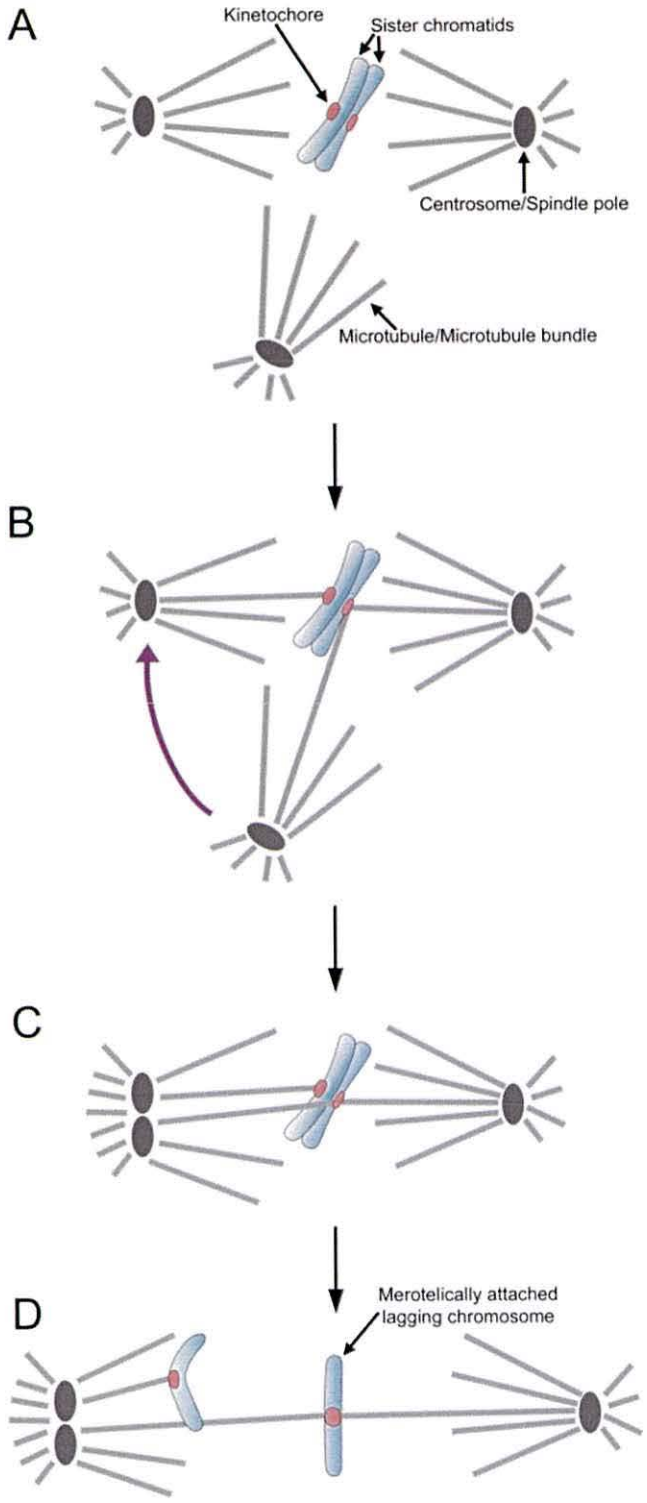

Figure 1.14. Multipolar spindle geometry promotes merotelic kinetochore attachments. **A.** A single kinetochore is more likely to face two spindle poles within a multipolar spindle, than in a bipolar spindle. **B.** As a result of the multipolar geometry, a single kinetochore can easily bind microtubules emanating from two spindle poles. After the establishment of merotelic kinetochore attachment, the spindle bi-polarises by a process known as centrosome clustering. **C.** Merotelic kinetochore attachment can persist through metaphase and into anaphase. **D.** Merotelic kinetochore attachments can cause chromosome lagging during anaphase.

From Silkworth *et al.*, (2009).

The SAC delays anaphase onset until all of the sister kinetochores are attached to the spindle microtubules. Both amphitelic and merotelic kinetochore attachments generate tension across the sister kinetochores, therefore SAC cannot detect merotelic kinetochore attachment (Cimini *et al.*, 2004). Merotelic kinetochore attachments do not trigger SAC-dependent mitotic arrest. Amphitelic-attachments are selectively stabilised and erroneous kinetochore attachments are destabilised through an Aurora B-dependent mechanism (reviewed in Gregan *et al.*, 2011; Silkworth and Cimini, 2012).

Multipolar cell division has been shown to cause cell death in the progeny cells as a result of chromosome mis-segregation. Multipolar spindle assembly is commonly observed in cancer cells and has been linked to chromosome instability (Silkworth *et al.*, 2009). Despite the increased frequency of multipolar spindle assembly, cancer cells are able to avoid multipolar cell division and subsequent cell death. Although the mechanisms by which cancer cells suppress multipolar cell division are not fully understood, there is evidence to suggest that centrosome clustering before the onset of anaphase may play a major role (Kwon *et al.*, 2008; Silkworth *et al.*, 2009).

1.6.2 Errors in meiosis

When meiotic chromosome segregation fails, this is known as non-disjunction and can occur when two homologues fail to pair and/or recombine or fail to move to opposite poles. Non-disjunction can result in aneuploid gametes, which can in turn create aneuploid embryos. Embryos carrying an extra copy of a given chromosome are known as trisomic and a few trisomic zygotes are capable of survival, for example trisomy of chromosome 21 causes Down's Syndrome. Whereas embryos carrying one copy are known as monosomic. There are no viable monosomies for the human autosomes, which therefore result in spontaneous abortion. The frequency of meiotic failure in humans is difficult to determine, but is estimated that 10-30% of fertilised human eggs are aneuploid (reviewed in Hassold *et al.*, 2007).

A significantly greater number of errors arise from maternal meiosis than paternal meiosis, suggesting major differences in the ability to detect errors in male and female germlines. The paternal meiosis process contains two checkpoints which detect; first, errors in early recombination or synapsis and second, unpaired or mis-aligned chromosomes, which the

maternal meiosis process appears to lack (LeMaire-Adkins *et al.*, 1997; Pelttari *et al.*, 2001). Therefore female meiosis is a more error-prone process than male meiosis, due to the lack of these checkpoints and errors in the chiasma placement (Champion and Hawley, 2002; Hunt and Hassold, 2002).

1.7 Cancer

Cancer is a disease in which a group of cells divide uncontrollably, invade and destroy adjacent tissues and potentially spread to other areas of the body. Based on the GLOBOCAN 2008 statistics, there were approximately 12.7 million cancer cases in 2008 and it accounted for 7.6 million deaths. Cancer is the leading cause of death in economically developed countries and the second leading cause of death in economically developing countries (Jemal *et al.*, 2011). Cancer cells have been shown to undergo many complex processes and exhibit phenotypic features which distinguish them from normal cells. Mutations may result in the cancer cells gaining a survival advantage, which allows them to avoid immune surveillance and aid tumorigenesis. Such features included resistance to apoptosis, insensitivity to growth inhibitors, massively increased replicative potential, sustained angiogenesis and the ability to invade neighbouring tissues. Cancer cells are also able to tolerate errors in mitosis, DNA damage and incorrect processing of proteins and transform their microenvironment to favour tumour progression (reviewed in Hanahan and Weinberg, 2011; Mitrus *et al.*, 2012).

1.7.1 Cancer antigens

Many studies have shown cancer cells to have an altered gene expression profile, with genes being up regulated and/or down regulated. Up regulated genes can provide an indicator/marker to the disease state, however their use as a target for therapeutic and/or diagnostic technologies is limited for many of the genes because the resulting antigens are recognised as 'self' by the immune system.

A lot of research has been carried out to find new human tumour-specific antigens as potential immunotherapeutic targets for cancer vaccines and/or antibody–based therapy. To be classified as a potential immunotherapeutic target, an antigen gene must have no, or highly restricted expression in normal cells. The family of tumour antigens known as the

cancer-testis (CT) antigens have been identified as an attractive group of cancer-specific biomarkers (Caballero and Chen, 2009; Costa *et al.*, 2007).

1.8 CT antigens

The CT antigen gene family represents a wide variety of genes which are found to display a highly tissue-restricted expression profile. The genes encoding CT antigens are normally expressed in the testes of adult males, but are aberrantly activated and expressed in various types of human cancer (Almeida *et al.*, 2009). Expression levels of the CT antigen genes have been shown to vary between different tumour types, with the highest frequency of CT antigen gene expression observed in melanoma, lung cancer (particularly the squamous cell type) and ovarian cancer, whereas hematopoietic malignancies such as lymphomas and leukemia have notably low frequencies of CT antigen gene expression (Caballero and Chen, 2009). The frequency of CT antigen expression also appears to be dependent upon the tumour grade, stage and histological type. Expression of CT antigens in malignant cells can induce an immune response which might have an important role in the control of cell transformation (Almeida *et al.*, 2009).

The testes are a site of immune privilege thus avoiding the production of anti-sperm antibodies which would lead to male infertility. An immune barrier known as the blood-testis barrier (BTB) physically divides the blood vessels and the seminiferous tubules of mammalian testes (reviewed in Cheng *et al.*, 2011; Mruk and Cheng, 2010). In addition to this physical barrier, a distinct lack of the major histocompatibility complex (MHC) has been reported in mammalian testes (Fiszer and Kurpisz, 1998). Therefore, from an immunological point of view CT antigens are regarded as tumour specific and considered to be attractive and potentially important therapeutic and diagnostic targets. Several CT antigens have been reported to elicit spontaneous humoral and cell-mediated immune responses. In particular, CT antigen induced spontaneous and co-ordinated humoral and cell mediated immune responses have been observed in a high percentage of *NY-ESO-1* expressing tumours (reviewed in Fratta *et al.*, 2011). NY-ESO-1 is one of the most well characterised CT antigens, and its mRNA presence has been reported in a wide range of cancers, including; melanoma, sarcoma and breast, bladder, lung, ovarian and prostate cancers (Chen *et al.*,

1997). However, not all of the CT antigens identified have been shown to be capable of eliciting an immune response (Almeida *et al.*, 2009; Caballero and Chen, 2009).

The tissue restricted profile together with the strong *in vivo* immunogenicity observed for some CT antigens has identified this family of tumour antigens as strong targets for immunotherapy based treatments. Numerous clinical trials, at various stages, have been conducted for CT antigen-based vaccine therapies, against MAGE-A3 and NY-ESO-1 in particular, in patients with melanoma and lung, prostate and ovarian cancers. Results from various clinical trials have shown that CT antigen-based vaccines are capable of promoting immune and clinical responses in late stage cancer patients (summarised in Cheng *et al.*, 2011; Fratta *et al.*, 2011).

The CT antigens are considered to be ideal targets for cancer immunotherapy due to the restricted expression pattern of their genes (Parmigiani *et al.*, 2006). Despite being apparent in various cancer types, little is known about the role of CT antigens within cancer biology (Cronwright *et al.*, 2005), but there is increasing evidence that expression is linked to the progression of the tumour (Old, 2001). The importance of CT antigen gene expression in cancer remains unclear, but two possible explanations have been proposed. First, expression of these genes may be random and linked to genome instability in tumorigenesis. Second, the activation of the CT antigens may be providing the tumour with a survival advantage. For example, CT antigen gene expression may enhance tumour growth, stimulate DNA repair and/or inhibit apoptosis (Kalejs and Erenpreisa, 2005). There is evidence to suggest a common evolutionary pathway between polyploidy in tumour cells and ploidy cycles in meiosis. Several CT antigens previously identified are related to DNA repair factors by homologous recombination in meiotic prophase of gametogenesis; SPO11, SYCP1, helicase-like CAGE and HAGE (Kalejs and Erenpreisa, 2005). Homologous recombination in tumours has been shown to produce anti-apoptotic effects (Raderschall *et al.*, 2002).

1.8.1 CT antigen classification

More than 100 gene families have been identified as CT antigen genes according to the CTdatabase (http://www.cta.lncc.br/). Many of the genes purported to encode CT antigens have not endured continued scrutiny and many of the genes initially identified as CT

antigens genes have subsequently been found to display some degree of expression in normal somatic tissues (Lim *et al.*, 2012). This has lead to the subsequent redefining of the criteria by which CT antigen genes are characterised. The CT antigens have been classified according to their gene expression patterns; (i) testis-restricted, (ii) testis/brain-restricted, or (iii) testis-selective, genes which have been shown to exhibit additional expression in at least one non-immune privileged somatic tissue (Almeida *et al.*, 2009). The brain is another site of immune privilege, protected by the blood brain barrier (BBB), and therefore it has been proposed that CT antigen gene expression in the brain does not reduce the potential of CT antigens as immunotherapeutic targets. The majority of the CT antigen genes identified to date display a low level of expression in other somatic tissues such as the brain (Ghafouri-Fard and Modarressi, 2009).

A genome-wide survey of expression was carried out for 153 previously reported CT antigen genes in normal and cancer expression libraries, by Hofmann and colleagues (2008). Of these they found that only 39 genes displayed a testis-restricted expression in the normal human tissues used, 14 genes showed a testis/brain-restricted expression profile and the remaining 85 were described as testis-selective. The testis-selective group of genes were shown to display expression in the testis and additional expression in other somatic tissues (Hofmann *et al.*, 2008).

CT antigens have been further sub-classified into X-CT genes (genes encoded on the X chromosome) and non-X-CT genes (autosomally encoded genes). Disproportionately, about 50% of the CT antigens identified are encoded by the X chromosome, and 10% of all the genes encoded by the X chromosome have been attributed to CT genes (Caballero and Chen, 2009; Ghafouri-Fard and Modarressi, 2009). A unique mechanism of transcriptional silencing known as meiotic sex chromosome inactivation (MSCI) occurs during the zygotene-pachytene transition in mammalian spermatogenesis. Meiotic DSBs are formed in unsynapsed chromatin thus inactivating the sex chromosomes (Turner, 2007). The MSCI mechanism suggests that most of the CT antigens are silenced during meiosis and therefore probably have non-meiotic roles within the testis.

1.8.2 Meiosis-specific CT antigens

The process of meiosis is restricted to germ cells; therefore expression of genes encoding meiosis-specific proteins is restricted to the germ cells only. The meiosis-specific proteins; SPO11, SYCP1 (Türeci *et al.*, 1998), HORMAD1 (Chen *et al.*, 2005) and SYCP3 (Mobasheri *et al.*, 2007; Simpson *et al.*, 2005) have previously been identified as CT antigens. Therefore there is potential for other meiosis-specific proteins to be identified as CT antigens. The present work will be concentrating on this sub-group of the CT antigens due to the highly-restricted expression profile of their genes in somatic cells.

Up regulation of meiosis-specific proteins in mitotically dividing cells may cause the cell to undergo a meiotic-like cell division, which could result in oncogenic genetic changes, such as translocations and loss of heterozygocity. Events such as inappropriate non-allelic intra- and/or inter-chromosomal recombination and inter-homologue recombination during tumorigenesis could be orchestrated by the up regulation of meiosis specific proteins (Caballero and Chen, 2009).

1.9 Project aims

The aim of this project was to identify potential novel CT antigen genes from potential meiosis-specific genes. Two screening approaches were used:

- Screening previously reported meiosis-specific genes for RT-PCR expression in normal human tissues and cancer cells.
- A bioinformatics screening program was developed by Julia Feichtinger (Feichtinger *et al.*, 2012a) with the aim of identifying potential novel meiosis-specific CT antigen genes. The potential meiosis-specific genes identified using this bioinformatics screening tool, were screened for expression in normal human tissues and cancer cells using RT-PCR.

Further biochemical and functional analyses of the gene products for genes identified during the RT-PCR screen, were carried out using human cancer cell lines.

Biochemical and functional analysis of the meiotic cohesin subunit REC8 and its mitotic paralogue, RAD21, was performed using human cancer cell lines.

2.0 Materials and Methods

2.1 Source of human cell lines

The NTERA-2 (clone D1) cell line was gifted by Prof. P.W. Andrews (University of Sheffield) and the A2780 cell line was gifted by Prof. P. Workman (Cancer Research UK Centre for Cancer Therapeutics, Surrey, UK). The following cell lines were purchased from the European Collection of Cell Cultures (ECACC); 1321N1, COLO800, COLO857, G-361, HCT116, HT29, LoVo, MCF7, MM127, SW480 and T84. H460 and MDA-MB-453 were purchased from the American Type Culture Collection (ATCC), and two ovarian adenocarcinoma cell lines, PEO14 and TO14, were obtained from Cancer Research Technology Ltd. A fibroblast cell line, normal human dermal fibroblasts (NHDF) from juvenile foreskin, was purchased from PromoCell. The HeLa T-REx cell line containing an miRNA construct (directed at REC8) stably integrated under the control of a tetracycline repressor, was gifted by Prof. A. Goldman (University of Sheffield).

2.2 Cell culture

The cells were grown at 37˚C in a humidified incubator, in a CO_2 enriched environment. The media used for each cell line was supplemented with foetal bovine serum (FBS) from GIBCO, Invitrogen (Catalogue number; 10270, Lot 41Q6208K). The cell lines and their growth conditions are detailed in Table 2.1. All cell lines were routinely checked for mycoplasma contamination using the LookOut® Mycoplasma PCR Detection kit (Sigma Aldrich; MP0035) as per the manufacturer's instructions.

Table 2.1. Description of the cancer cells lines and their growth conditions

Cell Line	Cell Line Description	CO_2	Media
1321N1	Human brain astrocytoma	5%	Dubeco's modified Eagle's medium (DMEM) + GLATAMAX™ (Invitrogen; 61965) + 10% FBS
HeLa T-REx	Human cervical cancer cell line containing a REC8 miRNA construct	5%	
NTERA-2 (clone D1)	Human Caucasian pluripotent embryonal carcinoma	10%	
SW480	Human colon adenocarcinoma	5%	
A2780	Human ovarian carcinoma	5%	DMEM + GLATAMAX™ + 10% FBS and 1xNEAA (non-essential amino acids)
MCF7	Human Caucasian breast adenocarcinoma	5%	
COLO800	Human melanoma	5%	Roswell Park Memorial Institute 1640 medium (RPMI 1640) + GLUTAMAX™ (Invitrogen; 61870) + 10% FBS
COLO857	Human melanoma	5%	
H460	Large cell lung carcinoma	5%	
PEO14*	Ovarian Adenocarcinoma, peritoneal ascites	5%	RPMI 1640 + GLUTAMAX™ + 10% FBS and 2 mM sodium pyruvate
TO14*	Ovarian Adenocarcinoma, solid metastasis	5%	
MM127	Human malignant melanoma	5%	RPMI 1640 + GLUTAMAX™ + 10% FBS and 25 mM HEPES
G-361	Human Caucasian malignant melanoma	5%	McCoy's 5A medium + GLUTAMAX™ (Invitrogen; 36600) + 10% FBS
HCT116	Human colon carcinoma	5%	
HT29	Human Caucasian colon adenocarcinoma	5%	
T84	Human colon carcinoma	5%	Ham's F12 + DMEM (1:1) + GLUTAMAX™ (Invitrogen; 31331) + 10% FBS
NHDF	Human dermal fibroblasts, juvenile foreskin	5%	Fibroblast growth medium (PromoCell; C-23010)
MDA-MB-453	Human breast carcinoma	0%	Leibovitz's (L-15) medium + GLUTAMAX™ (Invitrogen; 31415) + 10% FBS

* These cells lines were from the same patient, collected prior to treatment.

2.3 Preparation of frozen cell stocks

Confluent cells were trypsinised using 1x trypsin-EDTA (Sigma-Aldrich; T3924) and collected. The cells were counted and then centrifuged for 5 minutes at 400x*g*. The cells were then re-suspended in freezing media (10% DMSO, 90% FBS) and transferred into a cryotube and placed at -80˚C for 24 hours before being transferred to liquid nitrogen for long term storage.

2.4 Total RNA extraction

Total RNA extracts were prepared for all of the cell lines grown in the lab (Table 2.1). Confluent cells were collected in 1 ml TRIzol reagent (Invitrogen; 15596-026) and incubated at room temperature for 5 minutes. A volume of 0.2 ml chloroform was added and the samples were vigorously shaken for 15 seconds, followed by a 5 minute incubation at room temperature. The aqueous phase was transferred to a clean tube following centrifugation at 12,000x*g* for 15 minutes at 4°C. The RNA was then precipitated out of solution by adding 0.5 ml isopropanol and incubated at room temperature for 10 minutes. The samples were then centrifuged at 12,000x*g* for 20 minutes at 4°C and the pellet was washed using 70% ethanol and centrifuged again at 7500x*g* for 5 minutes at 4°C. The supernatant was removed and the pellet was allowed to air dry. The total RNA preparations were then re-suspended in 100 µl DEPC treated water and 1 µl DNase I (Sigma-Aldrich; D5319) was added to each sample, and then incubated at 37°C for 10 minutes and 75°C for 10 minutes. The concentration and quality of RNA was measured using a NanoDrop (ND_1000).

2.5 cDNA synthesis

Total RNA preparations from the human tissue panel (Clontech; 636643) and a range of tumour tissues and cell lines were purchased from Clontech and Ambion.

1.0 µg of total RNA was reverse transcribed into cDNA using the SuperScript III First Strand synthesis system (Invitrogen; 18080-051) as per the manufacturer's instructions and the cDNA was then diluted eight times. The quality of the cDNA was tested using a control RT-PCR using primers for *βACT*.

A panel of normalised, first strand cDNA preparations from mouse normal tissues (Clontech; 636745) was also purchased. Primers for mouse *G3PDH* were used as the control for these cDNA samples.

2.6 Reverse transcription (RT-) PCR

The sequences for each of the genes analysed were obtained from the National Center for Biotechnology Information (NCBI; http://www.ncbi.nlm.nih.gov/) and primers specific to each of the genes were designed to span introns where possible. The Primer3 software

(available from: http://www.genome.wi.mit.edu/cgi-bin/primer/primer3www.cgi) was used to aid primer design.

A volume of 2 µl diluted cDNA was used in the PCR with a final volume of 50 µl. BioMix™ Red (Bioline; BIO-25006) was used for the PCR amplification as per the manufacturer's instructions. Samples were amplified with a pre-cycling hold at 96°C for 5 minutes, followed by 40 cycles of denaturing at 96°C for 30 seconds, annealing at a temperature between 58-62°C for 30 seconds and extension at 72°C for 40 seconds, followed by a final extension step at 72°C for 5 minutes.

RT-PCR for *βACT* and *MAGE-A1* (a known X-CT gene) was carried out for all cancer and non-cancer cDNA samples as controls. The products were separated on 1% agarose gels stained with ethidium bromide.

2.6.1 Methylation analysis with RT-PCR

The cells were treated with 0.1, 1 and 10 µM 5-aza-2'-deoxycytidine for 48 hours and/or 300 nM trichostatin A (TSA) for 24 hours. The media was changed and 5-aza-2'-deoxycytidine was added again 24 hours after the initial treatment. Total RNA was then extracted from the treated and untreated cells as per Section 2.4. RT-PCR was then carried out to observe any effect of 5-aza-2'-deoxycytidine and/or TSA treatment on gene expression.

2.6.2 RT-PCR primers

The primers used for RT-PCR screening and their expected PCR products are detailed in Table 2.2.

Table 2.2. Primer sequences and their expected product size in base pairs (bp)

Gene	Primer Name	Primer Sequence	Product region	Product size (bp)
β-ACT	ACTB_F1	5'-AGAAAATCTGGCACCACACC-3'	332-884	553
	ACTB_R1	5'-AGGAAGGAAGGCTGGAAGAG-3'		
	ACTB_F2	5'-TGCTATCCCTGTACGCCTCT-3'	500-1174	675
	ACTB_R2	5'-CGTCATACTCCTGCTTGCTG-3'		
ADAD1	ADAD1_F1	5'-CAGTTGCCTAAAGGATCAGC-3'	1200-1851	652
	ADAD1_R1	5'-AGGAGGCAGACATACACTTAGC-3'		
ARL13A	ARL13A_F1	5'-TGCTGCTCTTGCCTAAGGAC-3'	138-779	642
	ARL13A_R1	5'-GGTGGAGAAGCTGTGTGATG-3'		
CATSPER1	CATSPER1_F1	5'-AGACCTTCGCTGAAGTCGAG-3'	1538-2137	600
	CATSPER1_R1	5'-TCACCAGGTTGAGGAAGATG-3'		
CCDC109A	CCDC109A_F1	5'-GTGCCCTCTGATGATGTTAC-3'	506-1129	624
	CCDC109A_R1	5'-TGCCATGGCACTTCCATAAG-3'		

CYLC1	CYLC1_F1 CYLC1_R1	5'-GACTCTGAACCGAAGGGAGA-3' 5'-GCTTATGAATCCACGGTGCT-3'	1360-1969	610
c1orf59	c1orf59_F1 c1orf59_R1	5'-ATGGAGAGGGGATTCGTTAG-3' 5'-CAGGTGGCTCACTCTTAAGC-3'	493-1099	607
c1orf85	c1orf85_F1 c1orf85_R1	5'-TACCAGGCTGCTTGAGTTTG-3' 5'-ACGTCAGATTGAAGGCACAG-3'	645-1279	635
c5orf47	c5orf47_F1 c5orf47_R1	5'-ATGTGACGCGCTTCGGCTCG-3' 5'-ACCTTTGGCATTTCAGCCTGTGTCT-3'	155-604	450
c7orf72	c7orf72_F1 c7orf72_R1	5'-ATCGAGTTCCCAGACCAGAC-3' 5'-GCAGCACGACTTGTGTTTG-3'	419-1091	673
c9orf117	c9orf117_F1 c9orf117_R1	5'-CCACCAGAAGATCATCCTCA-3' 5'-CACGGGTGATATATGACAGCA-3'	886-1499	614
c17orf98	c17orf98_F1 c17orf98_R1	5'-ATGGCGTACCTGAGCGAGT-3' 5'-GGTAGCCAAACCTTCCATTG-3'	1-394	394
c17orf105	c17orf105_F1 c17orf105_R1	5'-CTGGCCTACCCTGTTATCGT-3' 5'-GCCTTGAATTCTGCCAGTCT-3'	50-476	427
DUSP-21	DUSP21_F1 DUSP21_R1	5'-CATCATCTCAGGGTGTCCAG-3' 5'-GATGTTACCTACCGGCGAGT-3'	156-658	503
EFCAB9	EFCAB9_F1 EFCAB9_R1	5'-TGAGACTGAAGCAAGGATCG-3' 5'-CTCCTCTGTTTTCTGCCTCTTC-3'	3-541	539
FHAD1	FHAD1_F1 FHAD1_R1	5'-GATCCTAGCGCCTCAGAATG-3' 5'-TTCCACTGGGCTTAGAATGC-3'	3768-4369	602
mG3PDH	mG3PDH_F1 mG3PDH_R1	5'–TGAAGGTCGGTGTGAACGGATTTGGC–3' 5'–CATGTAGGCCATGAGGTCCACCAC–3'	55-1037	983
HORMAD1 (CT46)	HORMAD1_F1 HORMAD1_R1	5'-GCCCAGGATCTACACAGTTAG-3' 5'-CCATTCGTTCTCTCTCAGTGG-3'	333-818 (variant 1) 333-797 (variant 2)	486 465
HSBP9	HSBP9_F1 HSBP_R1	5'-TGCAGAGAGTCGGTAACACC-3' 5'-ACCTTCTGTGACATGCGGTA-3'	115-415	301
IQCG	IQCG_F1 IQCG_R1	5'-AGCATCTGCGTGAAAAGCAG-3' 5'-TTCCACCAAGAGTTCCTCTG-3'	417-1025	609
LRRC69	LRRC69_F1 LRRC69_R1	5'-AACCAACTAGCCAGCATTCC-3' 5'-GAACACATTCCAGCCATACG-3'	461-956	496
MAGE-A1	MAGEA1_F1 MAGEA1_R1	5'-GTGAGGGTTCCAGCAGCCGT-3' 5'-GCACCTGCCGGTACTCCAGG-3'	450-983	534
MAS1	MAS1_F1 MAS1_R1	5'-CATCACCCACCTGTCTATCG-3' 5'-GAAGAGCAGGGAAATGTGGT-3'	221-818	598
NUT	NUT_F1 NUT_R1	5'-CACCACCAGTTGCTCAACTG-3' 5'-CTCCTTCACAGCTTCTGGTG-3'	643-1265	623
PPP4R4	PPP4R4_F1 PPP4R4_R1a PPP4R4_R1b	5'-AGCCTCAAGACACCGGAAG-3' 5'-TGCCGACACATACAAGATCG-3' 5'-GTCGTACACTGCTGCCTTCA-3'	 263-858 263-959	 596 697
PSMA8	PSMA8_F1 PSMA8_R1	5'-CAGACGGACACCTTTTTCAA-3' 5'-CCAGACTGGACAACTTCTAGC-3'	155-743 155-611 155-725	589 457 571
PTPN20A	PTPN20A_F1 PTPN20A_R1	5'-TGGACAGCCAGAGGCCCCTT-3' 5'-GGAACACCCCTGTCCGGCCTA-3'	277-1120 275-692	844 418
RAD21	RAD21_F1 RAD21_R1	5'-TACTGAAGCTCTTTACACGCTGTC-3' 5'-TGTGTCAGCTCAATAGCTTGC-3'	1442-2126	685
mRAD21*	mRad21-1745F mRad21-1908R	5'-CTATCAGTTTGCTTGAGCTGTGTCG-3' 5'-TCAGATAATATGGAACCGTGGTCC-3'	1745-1908	164
RAD21L	RAD21L_F1a RAD21L_F1b RAD21L_R1	5'-TTGGAACTTGCACCTCCTAC-3' 5'-TACTTCCTTTGCGGACACAC-3' 5'-AGCCAGCTGTTTCTTTAGGAC-3'	1066-1692 1038-1692	627 655
mRAD21L*	mRad21L-1306F mRad21L-1651R	5'-GGAATGATTTCTCCAGCTGTTGAG-3' 5'-TCACATCTTATAGAACATTGGTCCC-3'	1306-1651	346

REC-8	REC8_F1	5'-GTGAAGCGCGAATACCTGAG-3'	613-1202	590
	REC8_R1	5'-ATCAGCAGGTCCAGTTCTCG-3'		
	REC8_F2	5'-GTTGGTGAAGCGCGAATACC-3'	609-1052	444
	REC8_R2	5'-GGAACTTCAGGAGGGATCTC-3'		
mREC8*	mREC8-1504F	5'-CTGCCCATGCTGCCTGAACTTCCTG-3'	1504-1732	229
	mREC8-1732R	5'-GCTTCTGTTGTTCCACAAGAAGGATC-3'		
SAMD13	SAMD13_F1	5'-CAAGGAAAATGGCTCTGTCG-3'	96-315	220
	SAMD13_R1	5'-AGCAGGCCCCAATTTTAACTG-3'		
SLC25A2	SLC25A2_F1	5'-TGCTTCCTGAAGACATACGC-3'	328-925	598
	SLC25A2_R1	5'-ATCCTGCCTGTTTCCCATAC-3'		
SMC1α	SMC1A_F1	5'-AGTGTGCTTCAGCGTATTGC-3'	3112-3736	625
	SMC1A_R1	5'-ACTTGGTGAGGTCGAAGGTC-3'		
SMC1β	SMC1B_F1a	5'-GCAGCCCCAAACCTACGAGCA-3'	3101-3395	295
	SMC1B_R1	5'-CTGGGGCCACACAGTTATAG-3'		
	SMC1B_F1b	5'-TCAAGAAATCGAGGCCCACC-3'	3028-3395	368
mSMC1β	mSMC1B-3329F	5'-GTGTGGCTCCAGGCAAACGG-3'	3329-3704	376
	mSMC1B-3704R	5'-ACTCTGGGCTTCCGGTGGCT-3'		
SMC3	SMC3_F1	5'-ACCTTCATGCCTAAGCAACG-3'	2380-3044	665
	SMC3_R1	5'-TTGCACTGCTCAAGTTTTCG-3'		
SNTG1	SNTG1_F1	5'-TGCAAGATCCTCAAGGACAG-3'	1321-1839	519
	SNTG1_R1a	5'-CTTTGCTTTGCTCGTGGTAG-3'		
	SNTG1_R1b	5'-GAGGGTCCAAACAAGCTACC-3'	1321-1774	454
SOX30	SOX30_F1	5'-GCCAACAATGCAGAAATCAG-3'	1426-2216	691
	SOX30_R1	5'-AGACATGTGGGTGTGGAATG-3'		
STAG1	STAG1_F1	5'-CACTTCACAAGGATGGCATAG-3'	3219-3843	625
	STAG1_R1	5'-TGCCTCACTCCAGTTCTCAC-3'		
STAG2	STAG2_F1	5'-GAACTTGCTCGACGTTTTGC-3'		
	STAG2A_R1a	5'-CATCCATGTTACCTGCGTGT-3'	3161-3799	639
	STAG2B_R1b	5'-TGTGCCACGCCGATTATAATC-3'	3096-3728	633
STAG3	STAG3_F1	5'-CAGTGGAGGCTGTCAGATTAC-3'	1363-1953	591
	STAG3_R1	5'-GAGTGACCTTCTCTGCATCAG-3'		
	STAG3_F2	5'-CTCTTCCATCAGGACAAGCAG-3'	3210-3704	495
	STAG3_R2	5'-CTCTTCTTCCTCGTCCTCTTC-3'		
mSTAG3*	mSA3-3537F	5'-TTCAGGCTCTGGCTTGGGCAAGCAGC-3'	3537-3722	186
	mSA3-3722R	5'-CAGAAATCCTCCATGTTCAGCTCTG-3'		
SYCE2	SYCE2_F1	5'-CTTCTCCTCTCTGGACTCAAG-3'	192-530	339
	SYCE2_R1	5'-CATCTGAGTCTTAGGCTCTGC-3'		
SYCP2	SCP2_F1	5'-CTTGGGAGACCTGGCAAAATG-3'	4173-4526	354
	SCP2_R1	5'-GATGAAGCCTCTGTTGTTCGC-3'		
mSYCP2*	mSCP2-86F	5'-TGCGCCCACAGCCTAAAGTGTCTGC-3'	86-309	224
	mSCP2-309R	5'-TATTAAGTCATCCAACTTGCGGAGG-3'		
SYCP3	SCP3_F1	5'-TGCTGGAAGGAGTTGGAGTTGACA-3'	357-823	467
	SCP3_R1	5'-CCGAACACTTGCTATCTCTTGCTGC-3'		
	SCP3_F2	5'-GGGGTGAAGTGCAGAATATGCTGG-3'	339-822	484
	SCP3_R2	5'-CGAACACTTGCTATCTCTTGCTGCT-3'		
	SCP3_F3	5'-TGGAAGATCAGTTTACGAGAGC-3'	189-806	618
	SCP3_R3	5'-CTTGCTGCTGAGTTTCCATC-3'		
	SCP3_F4	5'-TGAAGGGAAGACTGCAGTCA-3'	268-816	549
	SCP3_R4	5'-CTTGCTATCTCTTGCTGCTGAG-3'		
TEX12	TEX12_F1	5'-TGCAAGAGGCCAAGAGAATTGGAG-3'	172-481	310
	TEX12_R1	5'-TCACTGTAAACCTCTGTCGCAGGA-3'		
TDRD5	TDRD5_F1	5'-GCCAGAGGACATTGTCTTGA-3'	2570-3224	655
	TDRD5_R1	5'-GCTTTCCACAGAACCAGAGG-3'	2283-3099	817
ZCCHC13	ZCCHC13_F1	5'-TGGCAGAGGTTCTCAATGTG-3'	173-576	404
	ZCCHC13_R1	5'-ACTGGGACATTCCTTGGCTA-3'		

* Primer sequences from Ishiguro *et al.*, (2011).

Primers were also designed to assess the presence of the REC8 miRNA construct in the HeLa T-REx cell line, shown in Table 2.3.

Table 2.3. REC8 miRNA construct primers and the expected product size in base pairs (bp)

Target	Primer Name	Primer Sequence	Product size (bp)
Tet operator site	TetO_F	5'-TCCCTATCAGTGATAGAGATC-3'	-
REC8 miRNA sequence	miRNA_R	5'-ACCACATTCACTCAGGTATG-3'	1063bp
BGH (bovine growth hormone)	BGH_R	5'-TAGAAGGCACAGTCGAGG-3'	1223bp

2.6.3 Purification of RT-PCR products using phenol chloroform

Sodium chloride was added to the PCR product to a final concentration of 0.1 M. 100 µl Phenol-chloroform-isoamyl alcohol (Sigma-Aldrich; 77617) was added and the samples were vortexed vigorously before centrifugation at 17,000x*g* for 15 minutes. The aqueous layer was transferred to a clean Eppendorf tube and the PCR product was precipitated in 1 ml 100% ethanol at -80°C for 1 hour. The samples were centrifuged at maximum speed for 30 minutes at 4°C and then washed with 1 ml 70% ethanol. The samples were centrifuged again at maximum speed for 3-4 minutes and the liquid was removed. The pellet was air dried and re-suspended in ddH_2O.

2.6.4 Purification of RT-PCR products using the Roche purification kit

PCR products were separated on a 1% agarose gel containing ethidium bromide and the band(s) were cut out of the gel using a sterile blade. The products were then purified using the High Pure PCR Product Purification Kit (Roche Applied Science; 11732676001), as per the manufacturer's instructions. The purified PCR product was eluted from the column in ddH_2O.

2.6.5 Sequencing RT-PCR products

A minimum amount of 5 ng/µl DNA was sent at room temperature in a clean Eppendorf tube to Eurofins MWG, with 15 pmol of the corresponding forward and/or reverse primers.

The sequencing results were blasted and aligned against the expected PCR product sequence, using the Geneious software.

2.7 Quantitative real time RT-PCR (qRT-PCR)

Total RNA was extracted from confluent cell cultures using the RNeasy Plus Mini Kit (Qiagen; 74134) as per the manufacturer's instructions. The concentration and quality of RNA was measured using a NanoDrop (ND_1000). 1.0 µg of total RNA was reverse transcribed into cDNA using the QuantiTect® Reverse Transcription Kit (Qiagen; 205310) as per the manufacturer's instructions and the cDNA was then diluted ten times.

Commercial qRT-PCR primer assays (Qiagen) were used to carry out SYBR® Green-based real time RT-PCR (Table 2.4). The real time RT-PCR results for the genes of interest were normalised against the real time RT-PCR results for *LAMIN A* and *GAPDH*.

The QuantiTect SYBR Green PCR Kit (Qiagen; 204141) was used to set up the real time PCR reactions, as per the manufacturer's instructions. 1.5 µl cDNA was used per 25 µl reaction, in a 96 well plate, and three repeats were used for each reaction. Samples were amplified with a pre-cycling hold at 95°C for 5 minutes, followed by 40 cycles of 95°C for 10 seconds and 60°C for 30 seconds, then 95°C for 10 seconds. Melt curve analysis was carried out following completion of the 40 cycles. The BioRad CFX machine was used to carry out qRT-PCR and the results were analysed using the BioRad CFX Manager Software (version 2).

Table 2.4. Primer assay details used for SYBR® Green-based real time RT-PCR

Gene	Assay Name	Source
GAPDH	Hs_GAPDH_1_SG	Qiagen; QT00079247
LAMIN A	Hs_LMNA_2_SG	Qiagen; QT01678495
RAD21	Hs_RAD21_1_SG	Qiagen; QT00014301
REC8	Hs_REC8_1_SG	Qiagen; QT00060340

2.8 Western blot analysis

Whole cell extracts (WCEs) were prepared from confluent cell cultures; the cells were scraped from the surface of the flask or plate in cold 1xPBS. The cells were counted and centrifuged at 400x*g* for 5 minutes before lysis.

Lysates were also prepared from normal colon tissue; the tissue was kept on dry ice. Approximately 5 mg tissue sample was added to 300 µl lysis buffer and 3 µl antifoam Y-30 (Sigma; A6457) in an M-tube. The tissue sample was then homogenised using the Gentle MACS dissociator using the Protein 01.01 M-tube program. The M-tubes were centrifuged

at 4,000x*g* for 5 minutes to collect the samples which were then centrifuged into 15 ml tubes through Pierce® tissue strainers (Thermo Scientific; 1825505). The lysates were prepared and the amount of protein in each sample was measured using the BCA assay, before the loading dye was added. Approximately 20 µg protein was loaded per well.

2.8.1 Whole cell extract preparation (technique A)

Whole cell protein lysates were prepared from the cell lines using lysis buffer A (50 mM Tris-HCl pH 7.4, 200 mM NaCl, 0.5% Triton X-100, 1 mM AEBSF [4-(2-aminoethyl)-benzenesulfonyl fluoride] (Sigma-Aldrich; A8456) with complete, mini, EDTA-free protease inhibitor cocktail (Roche Applied Science; 11836170001)) and an equal volume of 2x Laemmli buffer (Sigma-Aldrich; S3401).

2.8.2 Whole cell extract preparation (technique B)

Cells were trypsinised and harvested, washed with 1xPBS and pelleted. The pelleted cells were re-suspended in an equal volume of RIPA buffer (50 mM Tris-HCl pH 7.5, 150 mM NaCl, 0.1% SDS, 1% IGEPAL, 100 mM PMSF, EDTA-free protease inhibitor cocktail (Roche Applied Science)) and mixed by pipetting. The samples were vortexed, and then incubated on ice for 30 minutes (vortexing every 10 minutes). The samples were then passed through a 25G needle 5 times, and centrifuged at maximum speed, 10 minutes at 4˚C. The protein concentration was assessed using the Bradford assay and approximately 25 µg protein was loaded per well.

2.8.3 Crude fractionation

The cytoplasmic fraction was prepared by re-suspending the cells in hypotonic buffer (50 mM Tris-HCl pH 7.4, 0.1 M sucrose, 1 mM AEBSF, Roche complete protease inhibitor cocktail) and an equal volume of lysis buffer C (1% Triton-X-100, 10 mM MgCl, 1 mM AEBSF, Roche complete protease inhibitor cocktail). Cells were then incubated on ice for 30 minutes and centrifuged at 6,000x*g* for 2 minutes. The supernatant was transferred to a clean Eppendorf tube and an equal volume of Laemmli buffer was added.

For the nuclear fraction, the pellet was then re-suspended in lysis buffer N (50 mM Tris-HCl pH 7.4, 100 mM KAc, 1 mM AEBSF, Roche complete protease inhibitor cocktail) and an equal volume of Laemmli buffer was added.

2.8.4 Western blot analysis (technique A)

Western blot analysis technique A was used to analyse lysates prepared as per Sections 2.8.1 and 2.8.3, at Bangor University.

The samples were boiled and an aliquot containing 70,000 cells was loaded and subjected to denaturing gel electrophoresis using a NuPAGE® 4-12% Bis-Tris gel (Invitrogen; NP0322) in 1xMOPS buffer (Invitrogen; NP0001) at 100 V for 1-2 hours, and then transferred to a PVDF membrane (Millipore; IPVH00010) at 400 mA for 1 hour using 1xTowbin transfer buffer. Membranes were blocked for one hour using 1xPBST (0.2% Tween-20) containing 5% non-fat dry milk, followed by an overnight incubation at 4˚C with the primary antibody. Membranes were washed three times for 15 minutes using 5% milk/1xPBST and then 15 minutes using 1xPBST. The HRP-conjugated IgG secondary antibody was diluted in 1xPBST and incubated with the membranes for 1 hour at room temperature. The membranes were washed three times for 15 minutes using 1xPBST before ECL detection using SuperSignal West Pico Chemiluminescent Substrate (Thermo Scientific; 34087) and visualised using X-Ray films (Thermo Scientific; 34091).

2.8.5 Western blot analysis (technique B)

Western blot analysis technique B was used to analyse lysates prepared as per Section 2.8.2, at the University of Sheffield.

The samples were prepared by adding 5x SDS-PAGE sample buffer (250 mM Tris pH 6.8, 10% SDS, 50% glycerol, 250 mM DTT, 0.02% bromophenol blue) and water, and were then boiled. Aliquots of approximately 25 µg protein were loaded and subjected to denaturing gel electrophoresis using either an 8% or 10% SDS-PAGE gel (SDS-PAGE gel composition shown in Table 2.5) at 200 V for 1 hour in SDS-PAGE running buffer (25 mM Tris base, 200 mM glycine, 0.1% SDS). The western blot was transferred to a Hybond-C nitrocellulose membrane (Amersham; RPN303D) at 400 mA for 1 hour using 1xTowbin transfer buffer (25 mM Tris base, 200 mM glycine, 20% MeOH).

Table 2.5. Resolving and stacking gel compositions

Resolving	8%	10%	Stacking	5%
30% Acrylamide/Bis-acrylimide	2.6 ml	3.3 ml	30% Acrylamide/Bis-acrylimide	0.67 ml
1.5 M Tris-HCl (pH 8.8)	1.95 ml	2.5 ml	1.5 M Tris-HCl (pH 8.8)	0.5 ml
10% SDS	0.05 ml	100 µl	10% SDS	40 µl
Ammonium persulphate	0.1 ml	100 µl	Ammonium persulphate	40 µl
TEMED	0.01 ml	4 µl	TEMED	4 µl
Water	5.4 ml	4 ml	Water	2.7 ml

Membranes were blocked for one hour using 1xPBST (0.2% Tween-20) containing 5% non-fat dry milk, followed by an overnight incubation at 4˚C with the primary antibody. Membranes were washed three times for 15 minutes using 5% milk/1xPBST and then 15 minutes using 1xPBST. The HRP-conjugated IgG secondary antibody was diluted in 1xPBST and incubated with the membranes for 1 hour at room temperature. The membranes were washed three times for 15 minutes using 1xPBST before ECL detection using the Amersham ECL western blotting detection reagents (GE Healthcare; RPN2209) and visualised using Kodak X-Ray films.

2.8.6 Primary antibodies

A range of primary antibodies were used to carry out western blot analysis (WB) and immunofluorescent staining of fixed cells (IF) as described in Section 2.13. The primary antibody details and the dilutions at which they were used are summarised in Table 2.6.

Table 2.6. Primary antibodies and the dilution at which they were used

Primary antibodies	Source	Application	Dilution
Polyclonal rabbit anti-RAD21	Abcam; ab992	WB	1/1000
Polyclonal rabbit anti-RAD21 (D213)	Cell Signaling Technology; 4321	IF	1/50
Polyclonal rabbit anti-hREC8	ProteinTech Group; 10793-1-AP	IF WB (BU) WB (SU)	1/50 1/200 1/2000
Monoclonal rabbit anti-NUT (C52B1)	Cell Signaling Technology; 3625	IF WB	1/50 1/500
Monoclonal mouse anti-CENP-A [3-19]	Abcam; ab13939	IF	1/100
Monoclonal mouse anti-Cyclin A (BF683)	Cell Signaling Technology; 4656	WB	1/500
Monoclonal mouse anti-Cyclin B1 (V152)	Cell Signaling Technology; 4135	WB	1/2000
Monoclonal mouse anti-Cyclin E (HE12)	Cell Signaling Technology; 4129	WB	1/1000
Monoclonal mouse anti-SMC1 (8E6)	Cell Signaling Technology; 6892	WB	1/1000
Monoclonal rabbit anti-SMC3 (D47B5)	Cell Signaling Technology; 5696	WB	1/2000
Monoclonal mouse anti-STAG1 (2E9)	Sigma-Aldrich; WH0010274M1	WB	1/500
Polyclonal rabbit anti-STAG2	Cell Signaling Technology; 4239	WB	1/500
Polyclonal rabbit anti-Actin-α-1	Sigma Aldrich; SAB-4502543	WB	1/2000
Monoclonal mouse anti-Histone H3 (96C10)	Cell Signaling Technology; 3638	WB	1/1000
Monoclonal mouse anti-Lamin A/C (636)	Santa Cruz Biotechnology; sc-7292	IF WB	1/50 1/100
Monoclonal mouse anti-α-Tubulin	Sigma; T6074	IF WB	1/2000 1/8000

Bangor University (BU), University of Sheffield (SU)

2.8.7 Secondary antibodies

The corresponding IgG secondary antibodies for the primary antibodies listed in Table 2.6 are summarised in Table 2.7.

Table 2.7. Secondary antibodies and the dilutions at which they were used

Secondary antibodies	Source	Application	Dilution
Peroxidase-conjugated AffiniPure donkey anti-mouse IgG (H+L)	Jackson ImmunoResearch Laboratories Inc.; 715-035-150	WB	1/50,000
Peroxidase-conjugated AffiniPure donkey anti-rabbit IgG (H+L)	Jackson ImmunoResearch Laboratories Inc.; 711-035-152	WB	1/50,000
Anti-rabbit IgG, HRP-linked (H+L)*	Cell Signaling; 7074	WB	1/2000
Alexa Fluor® 488 goat anti-mouse IgG (H+L)	Invitrogen; A11029	IF	1/200
Alexa Fluor® 568 goat anti-rabbit IgG (H+L)	Invitrogen; A11036	IF	1/200

* Anti-rabbit secondary antibody used for western blot analysis at the University of Sheffield.

2.9 siRNA (small interfering RNA) knockdown

A two "hit" approach was used for the siRNA knockdown, with the first siRNA treatment added at 0 hours and the second added at 24 hours after seeding the cells.

The transfection complex was formed by mixing 6 µl HiPerfect transfection reagent (Qiagen; 301705), 5-10 nM siRNA (Qiagen) and 100 µl serum free media, which was incubated at room temperature for 25 minutes. The cells were seeded at $2x10^5$ cells per well in a 6 well plate and the transfection mixture was added dropwise to the cells whilst gently shaking the plate. The media was changed when the second siRNA "hit" was added to the cells.

The cells were collected by trypsinisation and the cells were counted before preparing WCEs, as per Sections 2.8.1 and 2.8.2.

2.9.1 siRNAs

Several siRNAs were used to carry out siRNA knockdown in cultured cells; the details are summarised in Table 2.8.

Table 2.8. siRNA sequences used for siRNA knockdown

Gene	siRNA Name	Target Sequence	Source
NUT	Hs_NUT_7	5'-ATGACTGTGGCCTCCAACTAA-3'	Qiagen; SI04345810
	Hs_NUT_8	5'-CAGCATCTAATGTGAAGACCA-3'	Qiagen; SI04362554
RAD21	Hs_RAD21_8	5'-ATCGATGAGCCCATTATTGAA-3'	Qiagen; SI02653623
REC8	Hs_REC8_1	5'-CAGCCGGTTGGTGAAGCGCGA-3'	Qiagen; SI04257834
	Hs_REC8_2	5'-ATCCGCGTCTATTCTCAACAA-3'	Qiagen; SI04269034
	ON-TARGET plus SMART pool*	-	Thermo Scientific; L-021277-00
NI siRNA	AllStars Negative Control siRNA	-	Qiagen; 1027280

(NI) non-interfering siRNA
*The Dharmacon ON-TARGET plus SMART pool siRNA, is a combination of four unique siRNAs directed at REC8

2.9.2 Cell viability counting

Cell viability counts were carried out at time points after siRNA knockdown. Cell viability was determined by mixing 10 µl cell suspension with an equal volume of 0.4% (w/v) Trypan blue (Invitrogen; 15250-061) and counted using a hemocytometer. Cell viability was calculated as a percentage of unstained cells out of the total number of cells.

2.9.3 Phleomycin assay

Phleomycin treatment was carried out in conjunction with siRNA knockdown to detect any affect that the knockdown may have on the cells susceptibility to cell death by this DNA damaging reagent.

The cells were seeded and the siRNA was added at 0 hours and 100 µg/ml phleomycin was added after about 24 hours. Several incubation times were used for the phleomycin; 15 seconds, 1 hour, 3 hours and 8 hours. After incubation the cells were washed twice with warm media, before adding the second "hit" of siRNA.

Cells were collected 24 hours and 48 hours after phleomycin treatment, receiving two and three "hits" of siRNA respectively. Three repeats were carried out for each condition, and the cells were collected using trypsin. Cell viability counts were then carried out for each repeat.

2.9.4 REC8 Knockdown using a stable cell line

A stable T-REx^{TM}-HeLa cell line with a tetracycline-induced miRNA expression system for REC8 knockdown was created by Adam Croucher (University of Sheffield). The T-REx^{TM}

system (Invitrogen) contains an miRNA construct, directed at REC8, stably integrated under the control of a tetracycline repressor. The cells were grown in complete media, supplemented with 15 µg/ml Blasticidin S HCl to maintain the tetracycline repressor protein expression and 100 µg/ml Hygromycin B to maintain the miRNA construct expression within the cell line.

Cells were seeded at $1x10^6$ cells in a 10 cm plate and knockdown was induced using 1 µg/ml tetracycline. Cells were incubated in a humidified chamber for 24 hours and 48 hours and then collected by scraping in 1xPBS. WCEs were prepared and subjected to western blot analysis, as per Section 2.8.

2.10 Clonogenic survival assays

Knockdown was set up using the two "hit" siRNA protocol as described in Section 2.9. 48 hours after the first siRNA treatment the clonogenic survival assay was set up, comparing the knockdown cells to cells treated with non-interfering siRNA.

Cells were trypsinised and seeded at a range of seeding densities in 10 cm plates, then allowed to grow undisturbed for 10-14 days until colonies could be seen. Once the colonies were visible, the plates were fixed and stained for approximately 30 minutes using 0.4% (w/v) Methylene blue (Fisher Scientific; M291) in methanol. The colonies consisting of 50 cells or more were then counted. The survival fraction was calculated for the cells which received the siRNA knockdown treatment against the ones that received the non-interfering siRNA treatment.

2.10.1 γ-Irradiation toxicity assays

Set up as previously described in Section 2.10, but the cells were irradiated by exposure to Caesium 137 (Cis Bio International) before seeding in 10 cm plates. The cells were exposed to a range of doses; 0 Gy, 2.5 Gy, 5 Gy and 10 Gy, and the cells exposed to each dose were seeded at a range of seeding densities; 500, 2500 and 5000 cells per plate. The cells were incubated undisturbed for 10-14 days until colonies had formed. The colonies were stained and counted as previously described.

2.11 Association of proteins with chromatin

2.11.1 Cell cycle synchronisation

Adapted from Bermudez *et al.*, (2012).

Cells were synchronised in the G_1/S phase using 2 mM thymidine, which was added to the cells when they were approximately 25-30% confluent and incubated for 16 hours. After incubation the cells were washed with 1XPBS and grown in fresh media for 8 hours. Then a second treatment with 2 mM thymidine was added to the cells and incubated for 16 hours. The cells were again washed with 1xPBS and grown for 4 and 8 hours in fresh media, before collecting by trypsinisation, for S phase and G_2 phase cells respectively.

In order to collect cells within the G_1 and M phases of the cell cycle, the cells were synchronised in the G_1/S phase using 2 mM thymidine as above. The cells were washed with 1xPBS after the 16 hour incubation and fresh media containing 40 ng/ml nocodazole was added and the cells were grown for a further 17 hours. The cells were collected using mitotic shake-off for the M phase cells; these cells were grown for a further 3 hours in fresh media and collected by trypsin for G_1 phase cells.

2.11.2 Chromatin association lysate preparation

Adapted from Bermudez *et al.*, (2012).

Cells were synchronised and collected in the G_1, S, G_2 and M phases of the cell cycle, as previously described, or synchronised at metaphase using an overnight incubation with 0.1 µg/ml colcemid (Invitrogen; 15212-012).

Cells collected at each stage were washed using 1xPBS and counted. The cells were lysed in lysis buffer Ch [100 mM NaCl, 50 mM Hepes-NaOH (pH 7.5), 5 mM $MgCl_2$, 1 mM EDTA, 0.5% Triton X-100, 1 mM ATP, phosphatase, and protease inhibitors] and incubated on ice for 10 minutes. The samples were then centrifuged at 15,000x*g* for 10 minutes. The supernatant was transferred to a clean Eppendorf and an equal volume of Laemmli buffer was added.

The pellet was re-suspended in lysis buffer Ch containing 0.4 M NaCl and incubated on ice for one hour, then centrifuged at 8000x*g* for 10 minutes. The supernatant was transferred to a clean Eppendorf and an equal volume of Laemmli buffer was added.

The pellet was re-suspended in lysis buffer Ch containing 1 M NaCl, and then sonicated at 3 microns for 10 seconds (1 second on and 1 second off) using a SoniPrep 150. The samples were incubated on ice for one hour, and centrifuged at 8000x*g* for 10 minutes. The supernatant was transferred to a clean Eppendorf and an equal volume of Laemmli buffer was added.

The lysates were boiled at 100˚C for 5 minutes and subjected to western blot analysis as per Section 2.8.4.

2.12 Size exclusion chromatography (SEC)

WCEs were prepared using approximately $3x10^8$ cells. The cells were harvested using tryspin, and then washed twice with cold 1xPBS. The cells were lysed in a volume of 900 µl physiological salt lysis buffer [150 mM NaCl, 40 mM Tris-HCl (pH 7.4), 1 mM EDTA, 0.5 mM DTT, 5% glycerol, 1% Triton, Roche complete protease inhibitors] or high salt lysis buffer [1 M NaCl, 40 mM Tris-HCl (pH 7.4), 1 mM EDTA, 0.5 mM DTT, 5% glycerol, 1% Triton, Roche complete protease inhibitors]. 5 µl benzonase (Novagen; 70746) with 2 mM Mg^{2+} was added and the cells were lysed on ice for 30 minutes, shaking every 10 minutes. The cell lysate was then centrifuged at maximum speed for 30 minutes, at 4˚C. The supernatant transferred to a clean tube and kept on ice, this was used as the input sample for the SEC. The protein concentration of the input sample was estimated using the Bradford Assay before running the SEC.

The Superdex 200 10/300 GL column (GE Healthcare; 17-5175-01) was used to carry out SEC. The column was calibrated using a gel filtration high molecular weight (HMW) calibration kit (GE Healthcare; 28-4038-42).

The column was equilibrated with two column volumes of either physiological salt column buffer [150 mM NaCl, 40 mM Tris-HCl (pH 7.4), 1 mM EDTA, 0.5 mM DTT, 5% glycerol, 0.001% Triton, 10 mM NaF) or high salt column buffer [1 M NaCl, 40 mM Tris-HCl (pH 7.4), 1 mM EDTA, 0.5 mM DTT, 5% glycerol, 0.001% Triton, 10 mM NaF]. Once the sample was injected into the machine, the column was run at a flow-rate of 0.5 ml/minute and 1 ml fractions were collected.

The fractions were analysed using western blot analysis as described in Section 2.8.4.

2.13 Immunofluorescent staining of fixed cells

Adapted from Erenpreisa *et al.*, (2009).

Cells were seeded in a 24 well plate on glass coverslips, at $1x10^4$ cells per well and grown until 70-80% confluent. The cells were washed twice using cold 1xPBS, then fixed in methanol for 10 minutes at -20°C and washed 10 times with ice cold acetone. The cells were allowed to semi-air dry before washing once with 1xTBS and three times with 1xTBS/0.01%Tween-20 (TBS-T). Blocking was carried out using 1xTBS/1%BSA/0.05%Tween-20 (TBT) for 15 minutes at room temperature [N.B: 1xTBS/1%BSA/0.05%Tween-20/5% FBS (TBTS) was added to the blocking buffer when immunostaining for REC8].

The primary antibody was diluted in the blocking buffer and incubated with the cells at 37°C for 1 hour or overnight at 4°C in a humidified chamber. The cells were then washed three times using TBS-T. The secondary antibody was diluted in the blocking buffer and incubated at room temperature for 40 minutes, followed by two five minute washes in TBS-T and one five minute wash in 1xTBS. The cells were counterstained with DAPI, before sealing the coverslips onto glass slides.

Staining was viewed with a Zeiss Axioskop 2 fluorescent microscope, and the pictures were taken using an Axiocam digital camera.

2.14 Staining of unfixed metaphase spreads

Cells were grown until the exponential phase (70-80% confluence), then a final concentration of 0.1 µg/ml colcemid was added. The cells were treated for 2-4 hours at 37°C and collected by mitotic shake off. The cells were washed twice with ice cold 1xPBS, then re-suspended in 75 mM KCl to a concentration of $2x10^5$ cells/ml and incubated at room temperature for 10 minutes.

200 µl of the cell suspension was spread onto ethanol washed glass slides by centrifuging at 1,800 rpm for 10 minutes using a CytoSpin4 Rotofix 32A. The area of chromosome spreading was marked on the reverse side of the slide, and then the slides were immediately immersed in KCM buffer (120 mM KCl, 20 mM NaCl, 10 mM Tris-HCl pH 8.0, 0.5 mM EDTA, 0.1% v/v Triton-X-100) for 10 minutes at room temperature. Excess buffer was

removed and the primary antibody, diluted in 50 µl 1% BSA/KCM, was added directly to the area of chromosome spreading. The spreads were incubated with the primary antibody overnight at 4°C in a humidity chamber. The spreads were washed twice for 5 minutes in KCM buffer, and then the excess was drained before the secondary antibody was added. The secondary antibody was added directly to the area of chromosome spreading, diluted in 50 µl 1% BSA/KCM, and incubated for 1 hour at 4°C in a humidity chamber. The spreads were then washed twice for 5 minutes in KCM buffer at room temperature, and fixed for 10 minutes using 4% PFA. The spreads were washed with de-ionised water before counter staining with DAPI.

Staining was viewed with a Zeiss Axioskop 2 fluorescent microscope, and the pictures were taken using an Axiocam digital camera.

2.15 Flow cytometry

Flow cytometry analysis was carried out after siRNA knockdown (as per Section 2.9). Between $1x10^5$ and $1x10^6$ cells were used; cells were collected by trypsinisation and gently centrifuged. The media was aspirated off the pellet and the cell pellet was disturbed by gently flicking the 15 ml tube. The cell pellet was re-suspended in 0.5 ml ice cold 1xPBS and pipetted up and down to avoid clumping. The cells in 1xPBS were then added dropwise to 4.5 ml ice cold 80% ethanol. The fixed cells were stored at -20˚C for no more than a week before staining.

A propidium iodide/RNase A solution was prepared (0.5 mg/ml RNase A, 50 µg/ml propidium iodide in 1xPBS). The ethanol-fixed cells were then centrifuged at approximately 500x*g* for 5 minutes, the supernatant was discarded and the cells were washed using ice cold 1xPBS. Then centrifuged at 1500 rpm for 5 minutes, the cells were re-suspended in 1 ml propidium iodide/RNase A solution and incubated at 37˚C for 30 minutes (unstained samples were also incubated in 1 ml 1xPBS with 0.5 mg/ml RNase A). The samples were vortexed and analysed using the Partec PAS III flow cytometer.

3.0 RT-PCR screening of meiosis-specific genes for potential novel CT antigen gene candidates

3.1 Introduction

Meiotic cell division results in the production of four genetically unique haploid daughter cells, in contrast to mitotic cell division which produces two genetically identical diploid daughter cells. Somatic cells undergo mitosis which enables tissue homeostasis and regeneration of damaged tissues, in adults. In contrast, the process of meiosis is restricted to the germ cells and is required for the production of gametes (sperm and egg in humans). Meiosis is strictly regulated and orchestrated by a wide range of meiosis-specific proteins and ensures that ploidy is maintained from generation to generation, as diploidy is re-established upon fertilisation (Kleckner, 1996).

Cell cycle checkpoints regulate the cell cycle and ensure faithful chromosome segregation, however in some diseases one or more of these checkpoints are switched off or do not function properly. For example, errors in the chromosomal segregation are common during cancer cell division. Errors in cell division may lead to the incorrect separation of chromosomes which results in the production of aneuploid and polyploid cells (Nicholson and Cimini, 2011). Genetic instability is a hallmark of cancer, which allows successive mutations in the cancer cells and leads to selection of cancer cells which exhibit specific phenotypic traits (Merlo *et al.*, 2006; Negrini *et al.*, 2010). Cancer cells have been shown to undergo many complex processes and exhibit phenotypic features which distinguish them from normal cells. These mutations may result in the cancer cells gaining a survival advantage which allows them to avoid immune surveillance. Such features include resistance to apoptosis, insensitivity to growth inhibitors, massively increased replicative potential, sustained angiogenesis and the ability to invade neighbouring tissues. Cancer cells are also able to tolerate DNA damage and incorrect processing of proteins (Mitrus *et al.*, 2012).

A number of reported meiosis-specific genes have been shown to display expression in cancers, such as *SPO11*, *SYCP1* (Türeci *et al.*, 1998), *HORMAD1* (Chen *et al.*, 2005) and *SYCP3* (Mobasheri *et al.*, 2007; Simpson *et al.*, 2005). These genes have a role in chromosome alignment and homologous recombination, within meiosis. Up-regulation of meiosis-specific proteins in cancer cells could induce meiosis-like chromosome dynamics during tumorigenesis, which may then confer a survival advantage. For example, homologous recombination has been shown to produce anti-apoptotic effects in tumours (Raderschall *et al.*, 2002).

Tumours have been shown to display aberrant expression of a large number of genes. Identifying and characterising this altered expression profile may highlight good candidates for diagnostic markers and/or immunotherapeutic targets. However, many genes found to be up-regulated in cancers are limited in the immunotherapeutic target potential of their products, due to their expression in somatic cells. A subclass of cancer genes with a restricted expression profile in somatic cells has been identified, which is known as the cancer testis (CT) antigen genes. Expression of CT antigen genes is restricted to the human testicular cells in normal tissue, with expression shown in a wide range of cancers (Caballero and Chen 2009; Costa *et al.*, 2007; Lim *et al.*, 2012; Simpson *et al.*, 2005). The testes are an immune privileged site, therefore the products of these genes should not be recognised as 'self' by the immune system (Fijak and Meinhardt, 2006; Mruk and Cheng, 2010). Although the expression levels of CT antigen genes have been shown to differ between different types of tumour, they present attractive potential targets for new immunotherapeutic strategies, diagnostic targets and/or drug targets.

Due to the differences in meiosis in males and females, expression of many of the genes encoding meiosis-specific proteins is restricted to the testes in adult humans (Holt and Jones, 2009). We hypothesised that meiosis-specific genes may provide a potential source for identifying new CT antigen candidate genes, due to their highly restricted expression profile in somatic cells. This idea is supported by the fact that a number of meiosis-specific proteins have previously been identified as CT antigens.

The literature was searched to identify genes with predicted meiosis-specific expression and a number of genes were chosen to carry out an initial screen to validate this hypothesis.

The genes selected for this initial screen included the meiosis-specific cohesin subunit genes and genes encoding the subunits for a meiosis-specific chromosomal structure, the synaptonemal complex (SC). The SC is a highly conserved structure, which mediates synapsis between homologous chromosomes during prophase I, however its function remains poorly understood (Bhalla and Dernburg, 2008; Qiao *et al.*, 2012). Cohesin complexes are multi-protein complexes which play roles in maintaining sister chromatid cohesion in both mitotic and meiotic cell division. Several cohesin complex subunits are meiosis-specific, and are not present in the mitotic cohesin complex (reviewed in Nasmyth, 2011).

The aim of this initial screen was to determine the meiosis-specificity of the predicted meiosis-specific genes, in a range of normal tissues and to establish if any of the genes demonstrate expression in a variety of cancer cells, using RT-PCR analysis.

3.2 Meiosis-specific genes to be screened

Nine genes predicted to be meiosis-specific, with reported meiosis-specific functions were selected from the literature for the initial screen. A number of non-meiosis-specific genes were also selected; the mitotic cohesin subunit genes were screened alongside their meiotic counterparts as a control for expression in normal tissues. Details of the genes and their functions are given in Table 3.1

Table 3.1. Meiosis-specific genes selected for the initial screen and their known functional roles

Gene	Known Function	Reference
***HORMAD1* (*CT46*)**	Synaptonemal complex component and DSB repair	Shin *et al.*, 2010 Wojtasz *et al.*, 2009
***RAD21** (*SCC1*)**	Mitotic cohesin subunit	Xu *et al.*, 2004
RAD21L	Meiotic cohesin subunit	Ishiguro *et al.*, 2011 Lee and Hirano, 2011
REC8	Meiotic cohesin subunit	Bardhan, 2010 Eijpe *et al.*, 2003
SMC1α*	Mitotic cohesin subunit	Eijpe *et al.*, 2000 Kouznetsova *et al.*, 2005
SMC1β	Meiotic cohesin subunit	Bardhan, 2010 Kouznetsova *et al.*, 2005 Revenkova *et al.*, 2001
SMC3*	Mitotic and meiotic cohesin subunit	Eijpe *et al.*, 2000 Kouznetsova *et al.*, 2005
***STAG1** (*SA1*)**	Mitotic cohesin subunit	Canudas and Smith, 2009
***STAG2** (*SA2*) isoforms a and b**	Mitotic cohesin subunit	Canudas and Smith, 2009
***STAG3* (*SA3*)**	Meiotic cohesin subunit	Bardhan, 2010 Kouznetsova *et al.*, 2005 Prieto *et al.*, 2001
SYCE2	Synaptonemal complex central element component	Bolcun-Filas *et al.*, 2007
SYCP2	Synaptonemal complex component	Offenberg *et al.*, 1998 Schalk *et al.*, 1998
SYCP3	Synaptonemal complex component	Schalk *et al.*, 1998
TEX12	Synaptonemal complex central element component	Davies *et al.*, 2012 Schramm *et al.*, 2011

*Non-meiosis-specific genes, which were used as a control for the meiosis-specific cohesin subunit genes.

3.3 RT-PCR with normal tissues

The genes listed in Table 3.1 were screened for expression in a range of normal tissues to assess their predicted meiosis-specificity. The expected expression profiles for these genes are testis-specific with no expression in the other normal tissues.

Total RNA preparations from 21 normal human adult tissues, including testis, ovary and CNS (obtained *post mortem*) were purchased from Clontech and Ambion. cDNA was synthesised from the total RNA and intron-spanning primers were designed for each gene. The expression profiles of the genes were assessed using RT-PCR.

The genes screened here were categorised depending on the RT-PCR profiles observed in the normal tissues, as follows; dismissed, testis-restricted, testis/CNS-restricted, testis-selective and testis/CNS-selective. The testis-restricted genes display expression in the testis tissue only, and the testis/CNS-restricted genes display expression in the testis and CNS tissues only. The testis-selective genes display expression in the testis and no more than two additional non-CNS tissues, and the testis/CNS-selective genes display expression in the testis and CNS tissues with expression in no more than two additional tissues. The genes which were observed to display expression in more than two additional tissues to the testis and/or CNS were dismissed as CT antigen gene candidates.

3.3.1 Literature selected genes

The genes encoding several of the SC component proteins were selected to be screened; *HORMAD1*, *SYCE2*, *SYCP2*, *SYCP3* and *TEX12*. The RT-PCR expression profiles for these genes in the normal tissues are shown in Figures 3.1 and 3.2.

Although *SYCE2*, *SYCP2* and *TEX12* are believed to be meiosis-specific, their RT-PCR profiles appear to display expression in a number of normal tissues. This may suggest that these predicted meiosis-specific genes are not as tightly tissue restricted as previously believed. The expression of *SYCE2*, *SYCP2* and *TEX12* in the normal tissues is not selective for the testis and CNS tissues and do not fit the expected profile of a CT antigen gene, consequently they were dismissed as potential CT antigen genes.

HORMAD1 was previously identified as a CT antigen gene in a study Chen *et al.*, (2005) however here *HORMAD1* is shown to display expression in a range of normal tissues and was dismissed as a candidate. The PCR products were purified and sequenced to ensure the correct target was being amplified, the sequencing results are summarised in Table 3.2.

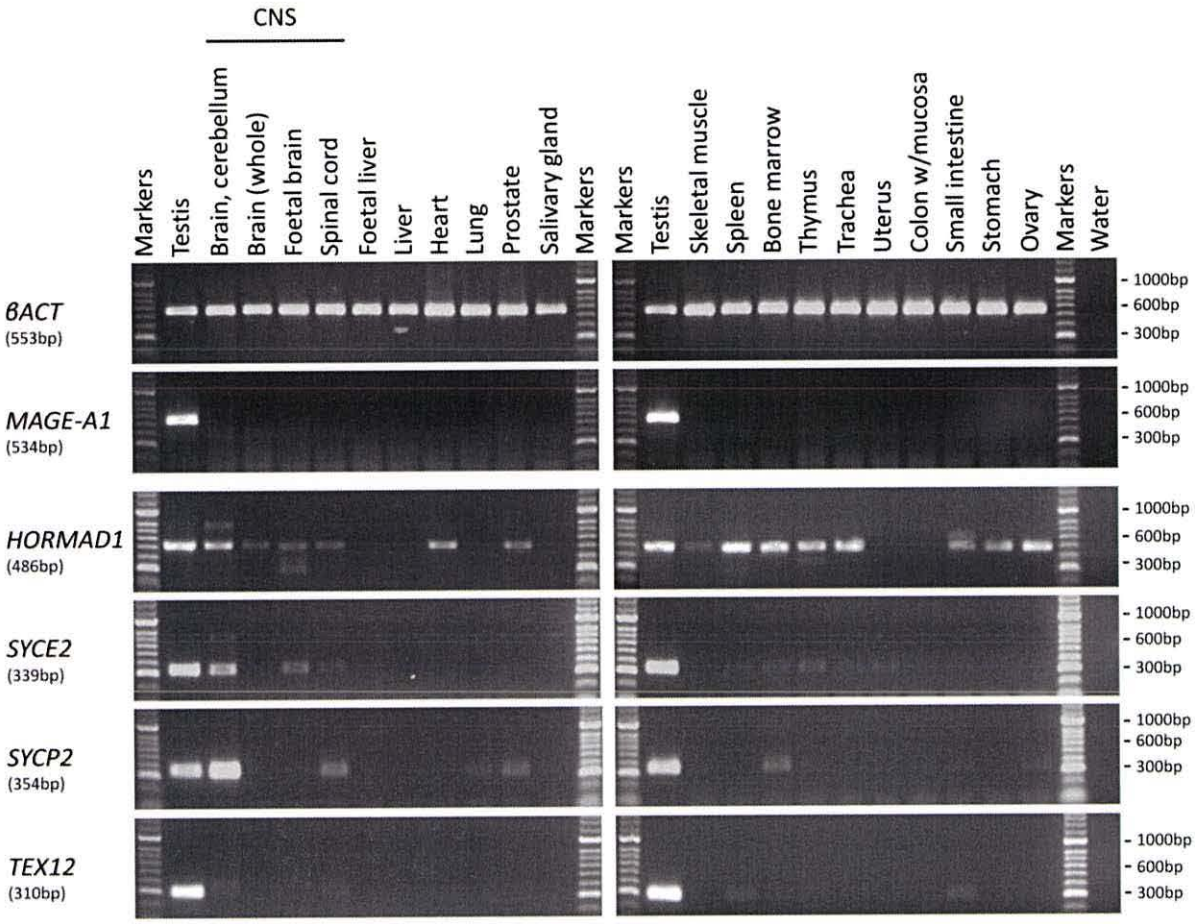

Figure 3.1. RT-PCR profiles for four predicted meiosis-specific genes in normal human tissues. Agarose gels showing the expression profiles of *HORMAD1*, *SYCE2*, *SYCP2*, and *TEX12* in normal human tissues (the expected PCR product size is shown in brackets). cDNA was generated from the total RNA from a range of normal tissues (obtained *post mortem*). The expression profiles of these genes do not appear to be meiosis-specific and do not fit the expected profile of a CT antigen gene in normal tissues. The expression profile for *βACT* is shown as a positive control for the cDNA samples (top) and the expression profile of *MAGE-A1*, a known CT antigen gene, is shown to demonstrate the expected testis-restricted expression profile of a CT antigen gene in normal tissues (top). These results appear to be reproducible as these PCRs were repeated at least two times.

Previous studies have also identified *SYCP3* as a CT antigen gene (Mobasheri *et al.*, 2007; Niemeyer *et al.*, 2003). A number of primer pairs were designed for *SYCP3*, the RT-PCR profile of *SYCP3* in normal human tissues is shown in Figure 3.2. The mRNA expression profile of *SYCP3* appears to be restricted to the testis in normal tissues and was therefore not dismissed as a candidate gene.

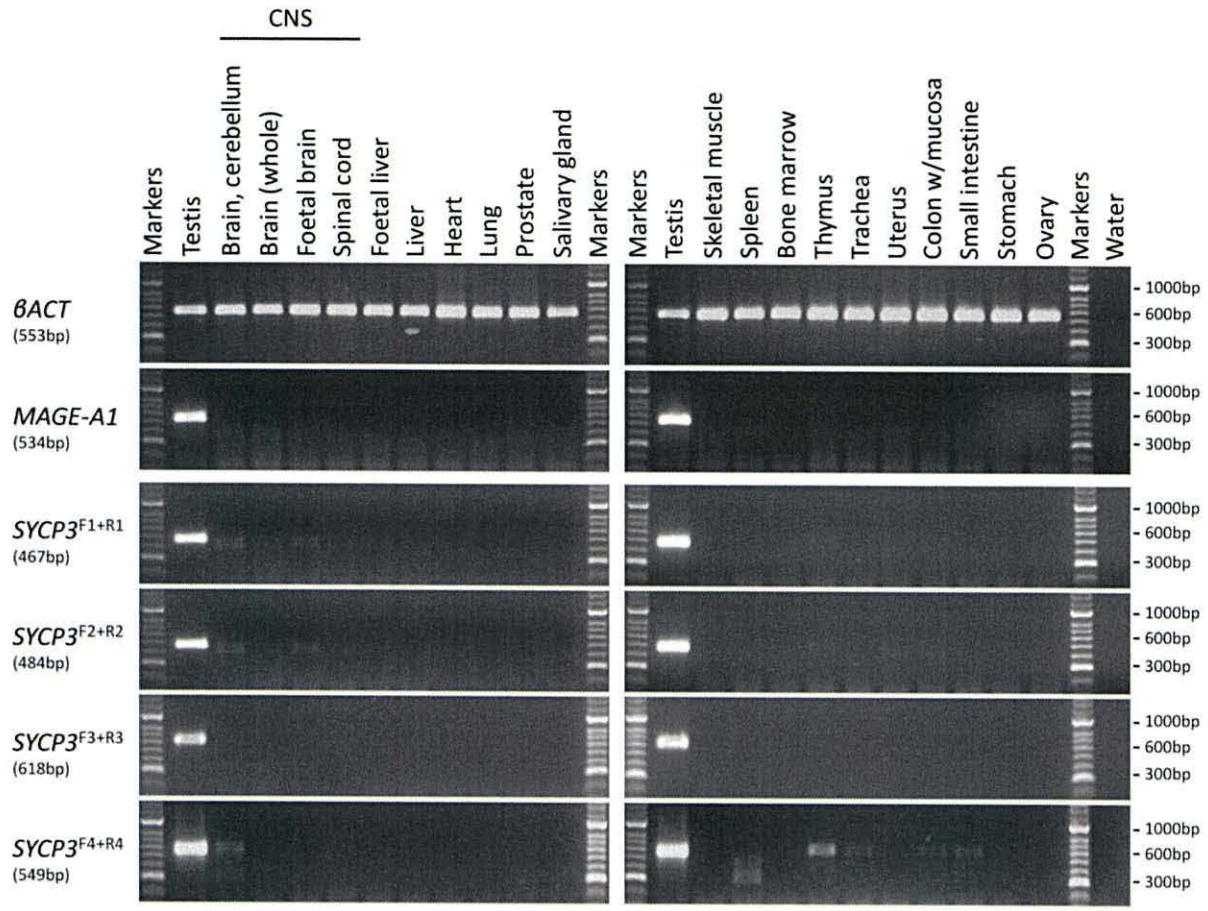

Figure 3.2 RT-PCR profile of *SYCP3* in normal human tissues. Agarose gels showing the expression profile of *SYCP3* in normal human tissues (the expected PCR product size is shown in brackets). cDNA was generated from the total RNA from a range of normal tissues (obtained *post mortem*). Four pairs of primers were used to screen for *SYCP3* expression, F3+R3 appears to show a testis-restricted profile, whereas the other three primer pairs show faint bands in various non-testis/CNS normal tissues. Sequencing of these faint bands in the normal tissues, showed no significant similarity to *SYCP3*. Therefore *SYCP3* appears to fit the testis-restricted expression profile of a CT antigen gene in normal tissues. The expression profile for *βACT* is shown as a positive control for the cDNA samples (top) and the expression profile of *MAGE-A1*, a known CT antigen gene, is shown to demonstrate the expression profile of a CT antigen gene in normal tissues (top). These results appear to be reproducible as these PCRs were repeated at least three times.

3.3.2 Cohesin complex subunit genes

Sister chromatid cohesion is established during the DNA replication phases of both mitosis and meiosis by a multiprotein complex called cohesin, which has an essential role in sister chromatid pairing and separation (Lee and Hirano, 2011; Nasmyth, 2011). The mammalian mitotic cohesin complex is made up of the structural maintenance of chromosomes (SMC) subunits; SMC1 and SMC3, stromal antigens; STAG1/SA1 or STAG2/SA2 and the α-kleisin; RAD21 (SCC1) (Nasmyth, 2011). During meiosis, RAD21 is largely replaced by the purported meiosis-specific proteins; RAD21L (Ishiguro *et al.*, 2011) and REC8 (Watanabe, 2005). The

mitotic α-kleisin binding proteins, STAG1 and STAG2, are replaced by the predicted meiosis-specific subunit, STAG3. The mitotic cohesin complex contains two members of the SMC family, SMC1α and SMC3, whereas the meiosis-specific cohesin complex contains two of three members of the SMC family, SMC1α, SMC1β and SMC3, as SMC1α is partially replaced by SMC1β in the meiotic complex (Gutiérrez-Caballero *et al.*, 2011). The genes encoding the purported meiosis-specific cohesin complex subunits were selected for screening.

The meiosis-specificity of the cohesin subunit genes was assessed by RT-PCR. The expression profiles of the genes encoding the mitotic cohesin subunits were expected to show expression in a wide range of normal tissues, whilst the expression of the reported meiosis-specific cohesin genes was expected to be restricted to the testis in normal tissues. The expression profiles of genes from the STAG, SMC and α-kleisin gene families were assessed here. The RT-PCR profiles for the STAG family genes, *STAG1*, *STAG2A*, *STAG2B* and *STAG3*, in normal human tissues are shown in Figure 3.3.

The *STAG1*, *STAG2A* and *STAG2B* genes encode cohesin subunit proteins which are involved in the mitotic cohesin complex, therefore these genes were expected to be widely expressed. On the other hand, the *STAG3* gene encodes a purported meiosis-specific cohesin subunit and was therefore expected to display a testis-restricted expression profile. Expression was observed in a wide range of tissues for the *STAG1*, *STAG2A* and *STAG2B* genes, thus in line with the literature. A number of different cohesin complexes exist, which may explain why expression was not observed in all of the tissues for these three genes. Interestingly *STAG3* also appears to display expression in a wide range of normal tissues, which may suggest that *STAG3* is not expressed in a meiosis-specific fashion, as was previously believed. Therefore *STAG3* was dismissed as a potential CT gene candidate (Figure 3.3). Sequencing was carried out on purified PCR product to ensure that the correct target was being amplified, summarised in Table 3.2.

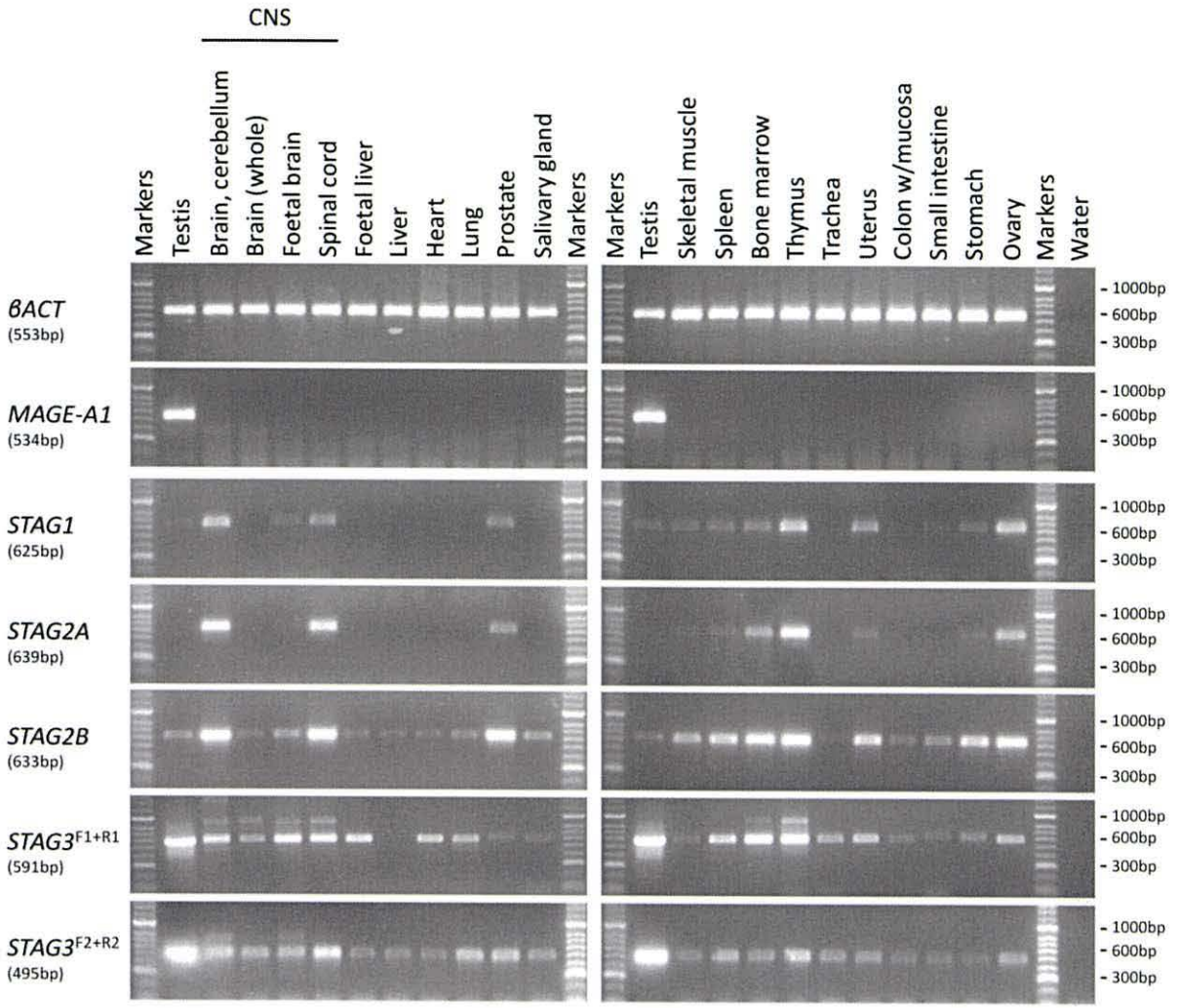

Figure 3.3. RT-PCR profiles for the STAG family genes in normal human tissues. Agarose gels showing the expression profiles for the STAG cohesin genes in normal human tissue (the expected PCR product size is shown in brackets). cDNA was generated from the total RNA from a range of normal tissues (obtained *post mortem*). The *STAG1*, *STAG2A* and *STAG2B* genes encode proteins which are involved in mitotic chromosome cohesion, whereas *STAG3* encodes a reportedly meiosis-specific cohesin subunit. *STAG1, STAG2A* and *STAG2B* display expression in a wide range of normal tissues as expected. *STAG3* also shows expression in a wide range of normal tissues and does not fit its predicted meiosis-specific profile, which was verified using two pairs of primers. The expression profile for *βACT* is shown as a positive control for the cDNA samples (top) and the expression profile of *MAGE-A1*, a known CT antigen gene, is shown to demonstrate the expression profile of a CT antigen gene in normal tissues (top). These results appear to be reproducible as these PCRs were repeated at least three times.

The RT-PCR profiles for the SMC family genes, *SMC1α*, *SMC1β* and *SMC3* in normal human tissues are shown in Figure 3.4.

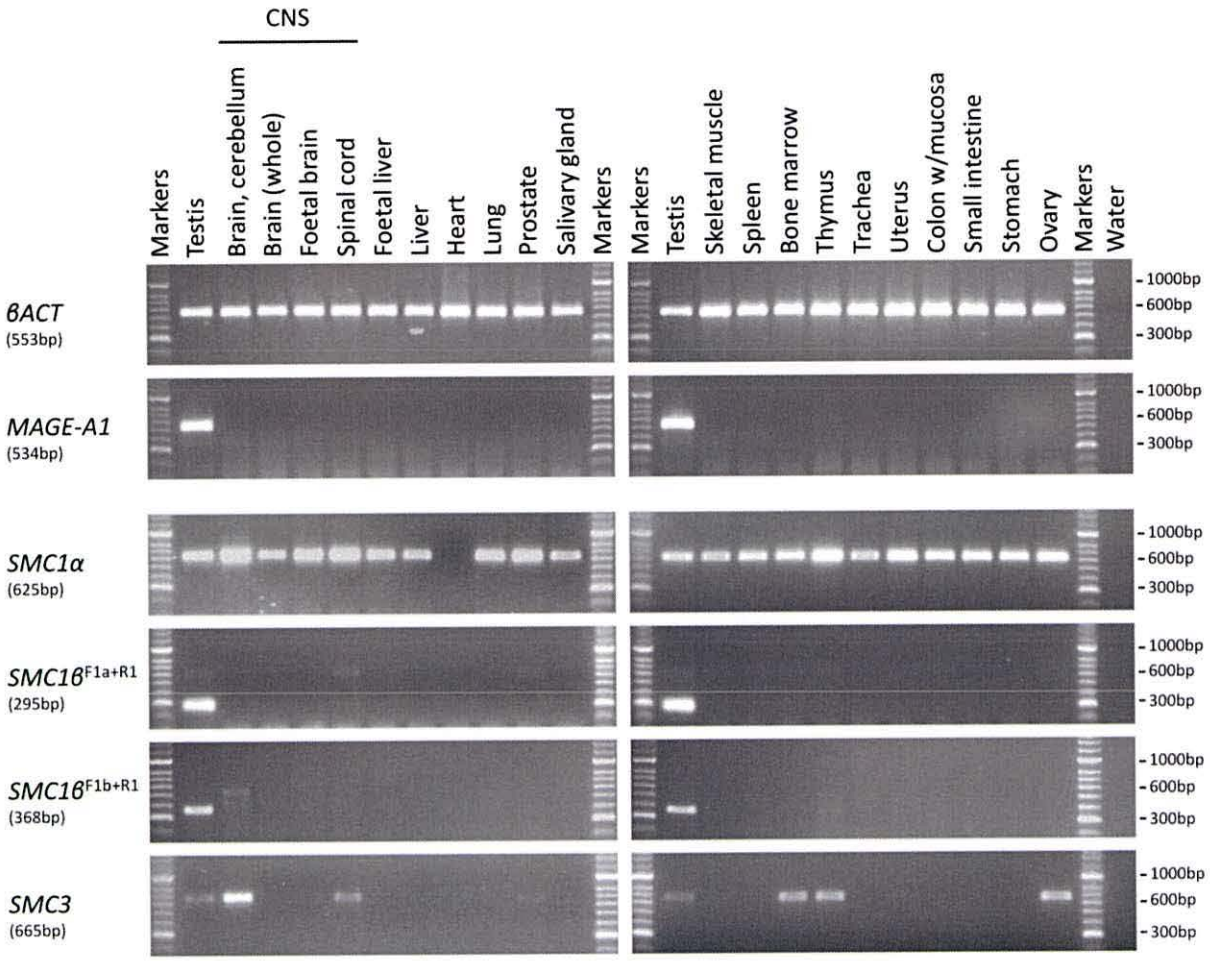

Figure 3.4. RT-PCR profiles for the SMC family genes in normal human tissues. Agarose gels showing the expression profiles for the SMC cohesin genes in normal human tissue (the expected PCR product size is shown in brackets). cDNA was generated from the total RNA from a range of normal tissues (obtained *post mortem*). The *SMC1α* and *SMC3* genes encode proteins which are involved in mitotic chromosome cohesion, whereas *SMC1β* encodes a meiosis-specific cohesin subunit. *SMC1α* and *SMC3* both show expression in a range of normal tissues as expected. Two pairs of primers were used to screen for *SMC1β*, and both pairs of primers amplified fainter bands at an unexpected size in a range of normal tissues. Sequencing results indicated no significant similarity to *SMC1β* for these PCR amplifications. *SMC1β* expression appears to be restricted to the testis in normal tissue, thus fitting the expected profile of a CT antigen gene in normal tissues. The expression profile for *βACT* is shown as a positive control for the cDNA samples (top) and the expression profile of *MAGE-A1*, a known CT antigen gene, to show the expression profile of a CT antigen gene in normal tissues (top). These results appear to be reproducible as these PCRs were repeated at least three times.

The *SMC1α* and *SMC3* genes encode cohesin complex subunits involved in both mitotic and meiotic chromosome cohesion, therefore *SMC1α* and *SMC3* were expected to display expression in a wide range of normal tissues. In contrast, the *SMC1β* gene encodes a predicted meiosis-specific cohesin subunit and was therefore expected to display a testis-restricted expression profile in the normal tissues. Expression was observed for *SMC1α* in

all of the normal tissues tested except for the heart, this is potentially interesting because the ability of the heart to self renew is not preserved in aging mammals (Anversa *et al.*, 2006). The *SMC3* gene also appears to be expressed in a wide range of normal tissues, but was not as widely expressed as expected. Faint PCR bands were observed for *SMC3* in a number of normal tissues, which may suggest a low level of expression which may have been under the threshold of sensitivity in the other tissues.

SMC1β shows a testis-restricted expression profile, which fits the expression profile of a meiosis-specific gene and a CT-antigen gene in normal tissues, therefore *SMC1β* was not dismissed at this stage. Sequencing was carried out on purified PCR products to ensure the correct target was being amplified (summarised in Table 3.2).

The RT-PCR profiles for the α-kleisin family genes, *RAD21*, *REC8* and *RAD21L*, in normal tissues are shown in Figure 3.5. *RAD21* encodes a cohesin complex subunit which is involved in mitotic chromosome cohesion and was expected to be widely expressed, whereas *RAD21L* and *REC8* encode cohesin subunits which are both reported to be meiosis-specific (Ishiguro *et al.*, 2011; Lee and Hirano, 2011; Nasmyth, 2011). The RT-PCR profile of *RAD21* shows expression in all of the tissues tested here, thus fitting the expected expression profile. Surprisingly *REC8* was also observed to display expression in all of the normal tissues tested, which does not fit with the expected expression profile of a meiosis-specific gene. *REC8* was therefore dismissed as a potential CT antigen gene and the possibility that REC8 might have a role in mitotic cells is explored in Chapter 6.0. A testis-restricted expression profile was observed for *RAD21L*; therefore *RAD21L* was not dismissed as a potential CT gene candidate (Figure 3.5).

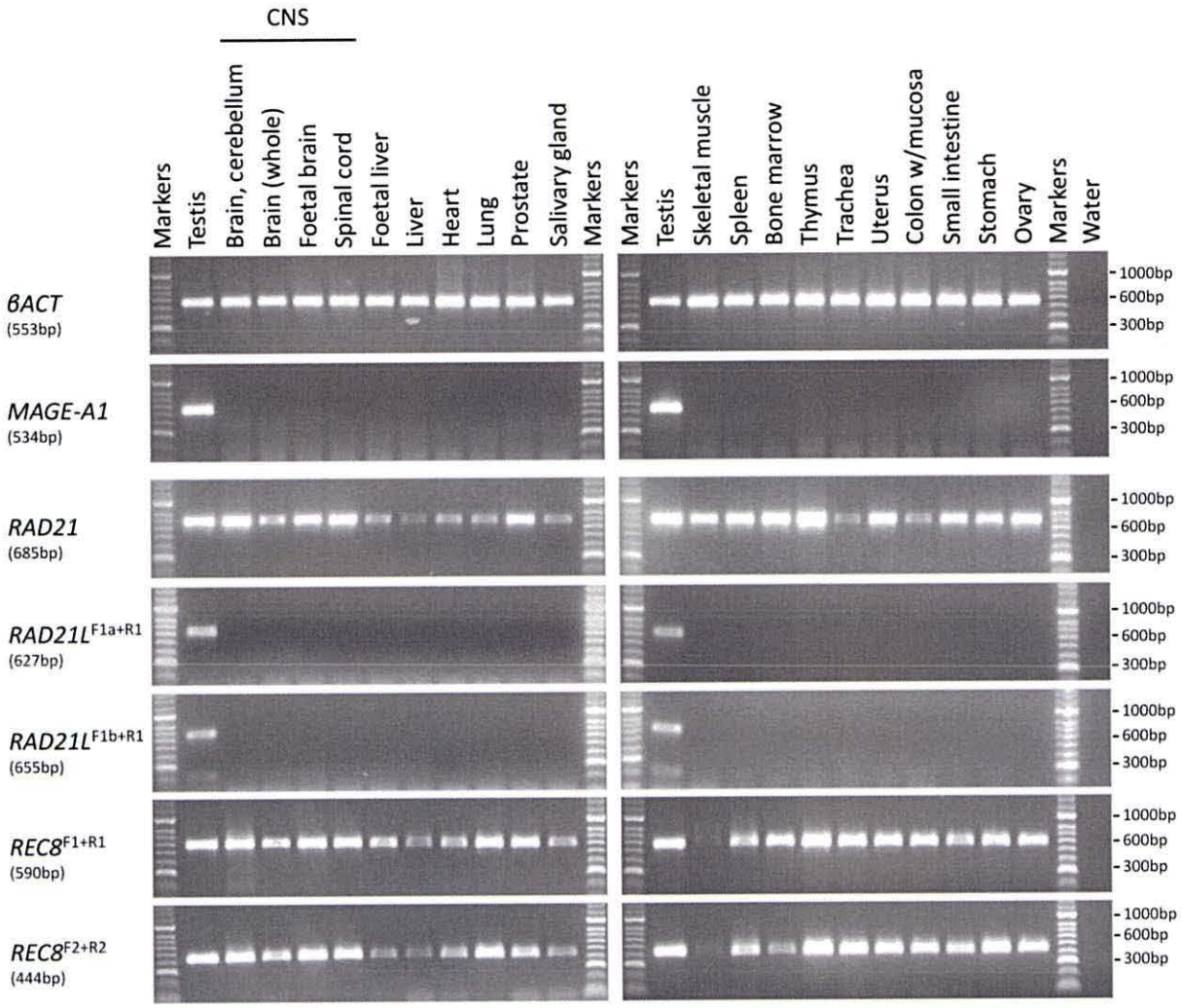

Figure 3.5. RT-PCR profiles for the α-kleisin family genes in normal human tissues. Agarose gels showing the expression profiles, for the α-kleisin cohesin genes, in normal human tissue (the expected PCR product size is shown in brackets). cDNA was generated from the total RNA from a range of normal tissues (obtained *post mortem*). *RAD21* encodes a protein which is involved in mitotic chromosome cohesion, whereas *REC8* and *RAD21L* are reported to be meiosis-specific cohesin subunits. Two pairs of primers were used to amplify both *REC8* and *RAD21L*. *RAD21* appears to be expressed in all of the normal tissues tested here, as expected. *REC8* and *RAD21L* were expected to show meiosis-specific profiles, however *REC8* displays expression in all of the normal tissues tested here. *RAD21L* appears to show a testis-restricted expression profile in the normal tissues, therefore fitting the expected profile of a CT antigen in normal tissues. The expression profile for *βACT* is shown as a positive control for the cDNA samples (top) and the expression profile of *MAGE-A1*, a known CT antigen gene, is shown to demonstrate the expression profile of a CT antigen in normal tissues (top). These results appear to be reproducible as these PCRs were repeated at least three times.

PCR products were purified and sequenced to ensure the correct target was being amplified, the sequencing results are summarised in Table 3.2.

3.3.3 Mouse cohesin complex subunit expression

Surprisingly, the RT-PCR results presented above showed expression in a wide range of normal human tissues for a number of cohesin subunit genes, which were previously reported to be meiosis-specific (Nasmyth, 2011). A study by Ishiguro and colleagues (2011) demonstrated a strict meiosis-specific mRNA expression of *RAD21L*, *REC8*, *STAG3* and *SMC1β* in mice, with expression restricted to the testis and the ovary only. As these genes are known to be meiosis-specific in mouse, RT-PCR for these genes was carried out using cDNA from mouse normal tissue, using the same primer sequences used in the study by Ishiguro *et al.*, (2011). This PCR was carried out to confirm the murine meiosis-specficity these genes (Figure 3.6), as opposed to the wider expression observed here for *REC8* and *STAG3* in the human tissues.

A panel of cDNA from a range of mouse normal tissue was purchased from Clontech and RT-PCR was carried out using primers specific for the non-meiosis-specific cohesin, *mRAD21,* and the meiosis-specific cohesins, *mRAD21L*, *mREC8*, *mSTAG3* and *mSMC1β* and *mSYCP2*. Although Ishiguro and colleagues (2011) showed these genes to be strictly meiosis-specific, here we demonstrate expression in a wider range of normal mouse tissues. Expression of *mRAD21L* was restricted to the testis (no normal ovary tissue was used for this RT-PCR), whereas the expression profile for *mSMC1β* appears to be mostly meiosis-specific, with expression clearly shown in the testis and a weaker band shown in the spleen. *mSYCP2* expression was observed in the testis and the heart, but *SYCP2* does not appear to be as widely expressed in the mouse tissues as in the human tissues.

mSTAG3 appears to be widely expressed in the mouse normal tissues, as *mSTAG3* expression was detected in almost all of the mouse tissues tested. Although *mREC8* expression appears to be more widely expressed than previously reported by Ishiguro *et al.*, (2011), it does not appear to correspond with *REC8* expression observed in the human normal tissues. Interestingly, the PCR band intensity observed for the meiotic genes in the normal human tissues was comparable to that observed for the mitotic genes, whereas in the normal mouse tissues the PCR band intensity was significantly weaker than that observed for *mRAD21*.

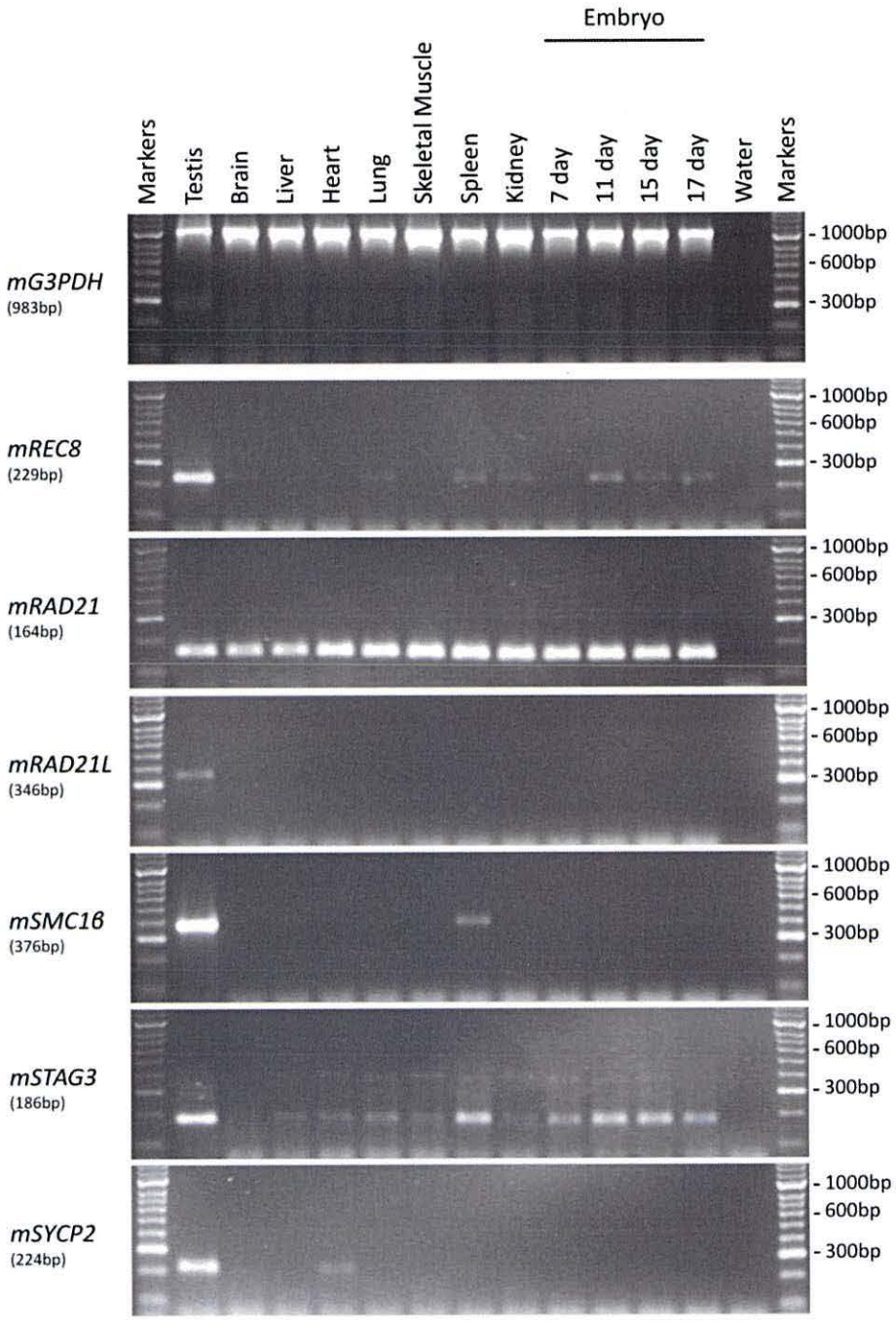

Figure 3.6. RT-PCR profiles for the mouse cohesin genes in normal mouse tissues. Agarose gels showing the expression profiles for the mouse cohesin genes (the expected PCR product size is shown in brackets). A panel of cDNA from a range of normal mouse tissues was used to carry out RT-PCR (Clontech). As in humans, *mRAD21* encodes a mitotic cohesin subunit, whereas *mREC8*, *mRAD21L*, *mSMC1β*, *mSTAG3* and *mSYCP2* are reported to encode meiosis-specific proteins. *mRAD21* shows expression in all of the normal tissues tested. *mRAD21L* shows a testis-restricted expression profile, whereas *mSMC1β* and *mSYCP2* show testis-selective expression profiles. The RT-PCR profiles of *mREC8* and *mSTAG3* show expression in multiple normal tissues. The expression profile for *mG3PDH* is shown as a positive control for the cDNA samples (top). The PCR products were separated on a 2% agarose gel. See Table 3.2 for a summary of the sequencing results. These results appear to be reproducible as these PCRs were repeated at least two times.

3.4 RT-PCR with cancer samples

Three of the meiosis-specific genes screened displayed a testis-restricted expression profile in the normal human tissues tested; *RAD21L, SMC1β* and *SYCP3*. These genes were then screened for expression in a range of human cancer cells, comprised of 33 RNA samples extracted from cancer cell lines and primary cancer tissue (purchased from Clontech and Ambion). The RT-PCR profiles of *RAD21L* and *SMC1β* in the cancer cell lines and tissues are shown in Figure 3.7.

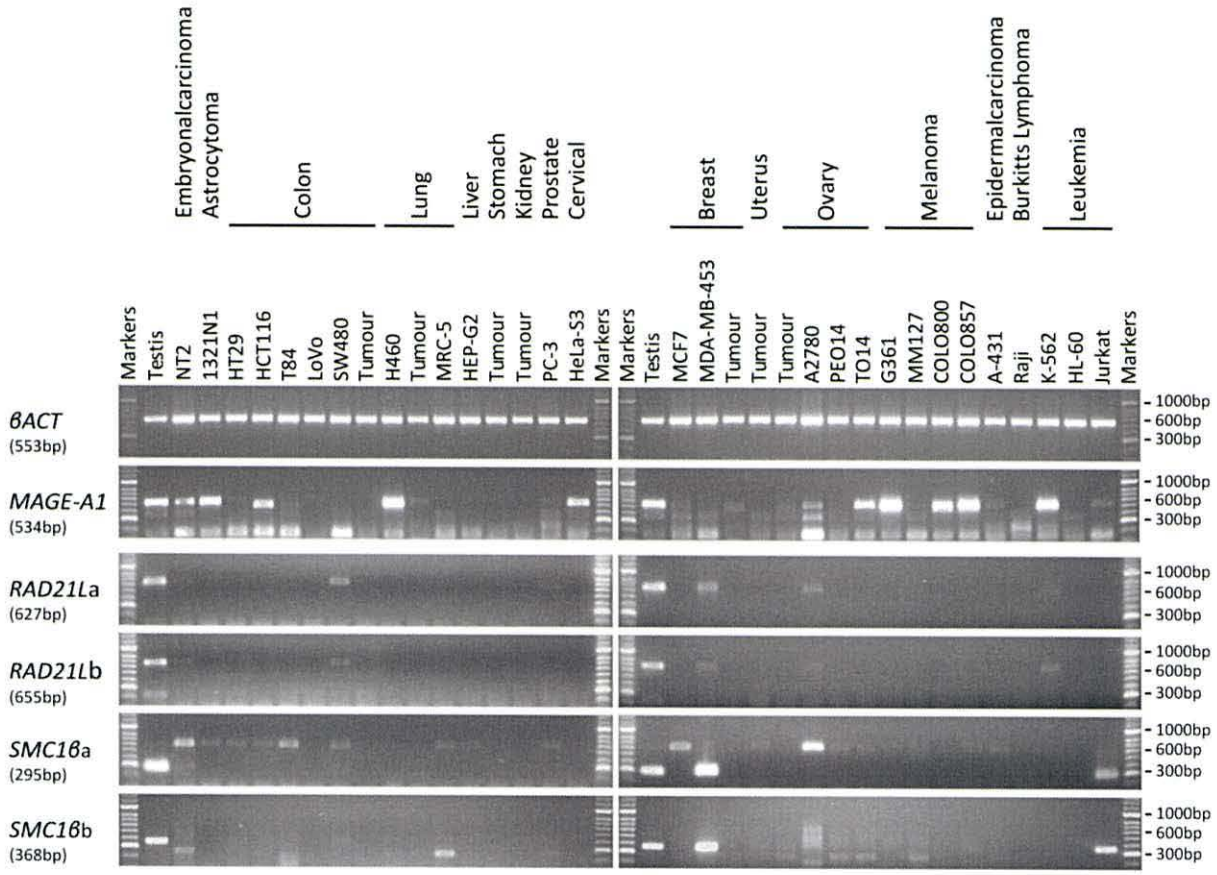

Figure 3.7. RT-PCR profiles for *RAD21L* and *SMC1β* in cancer cell lines and tissues. Agarose gels showing the expression profiles, for *RAD21L* and *SMC1β* meiotic cohesin subunit genes in cancer cells (the expected PCR product size is shown in brackets). cDNA was generated from the total RNA extracted from cancer cell lines and a range of tumour tissues. *RAD21L* and *SMC1β* both show expression in one or more cancer sample. The expression profile for *βACT* is shown as a positive control for the cDNA samples (top) and *MAGE-A1* is shown as a positive control for the expression profile of a known CT antigen gene (top). These results appear to be reproducible as these PCRs were repeated at least three times.

RAD21L and *SMC1β* both displayed a testis-restricted expression profile in normal tissues, and also display expression in one or more cancer samples tested here. The RT-PCR expression profiles for *RAD21L* and *SMC1β* appear to fit the expected profile of a testis-

restricted CT antigen gene. PCR products were purified and sequenced to ensure the correct target was being amplified, sequencing results are summarised in Table 3.2.

RT-PCR was carried out for *SYCP3* expression in the cancer cell lines and tissues, using three pairs of primers, the results are shown in Figure 3.8.

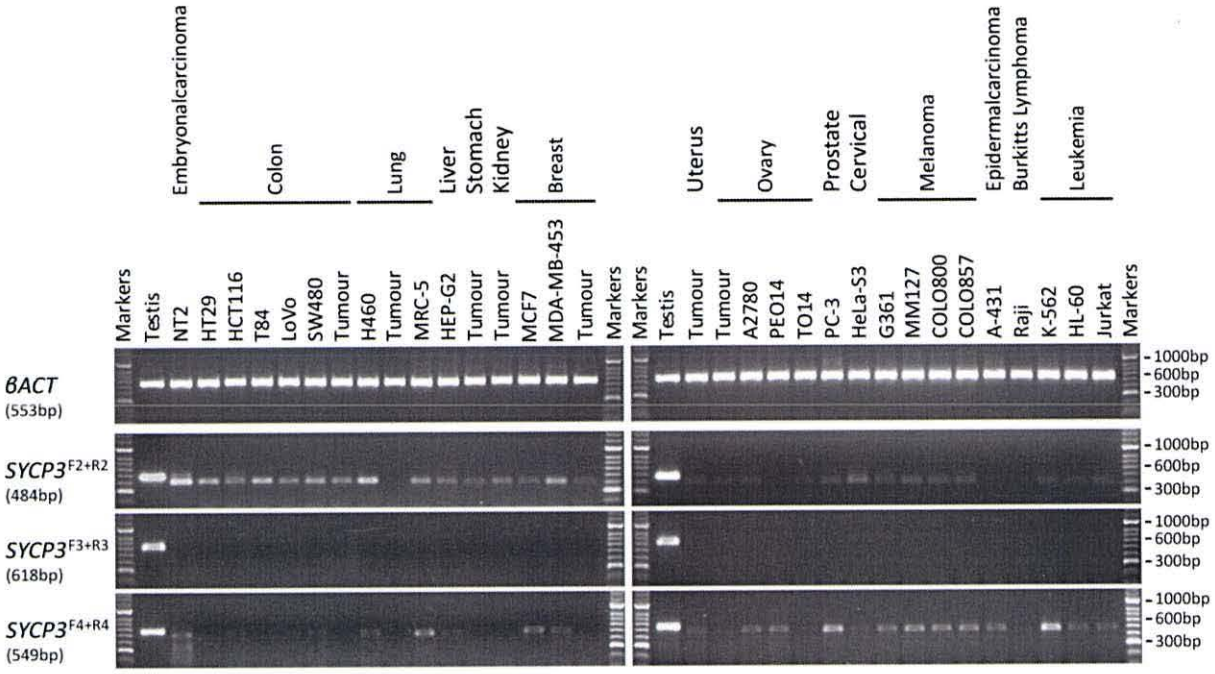

Figure 3.8. RT-PCR profile for the meiosis-specific gene, *SYCP3*, in cancer cell lines and tissues. Agarose gels showing the expression profile for *SYCP3*, in cancer cell lines and tissues (the expected PCR product size is shown in brackets). cDNA was generated from the total RNA extracted from cancer cell lines and a range of cancer tissues. PCR using the primer pairs, F2+R2 and F4+R4, show a band of unexpected size in multiple cancer cells and normal tissues (Figure 3.2). Sequencing found that these PCR products show no significant similarity to *SYCP3*. Therefore RT-PCR using three pairs of primers show a testis-restricted expression profile for *SYCP3*. The expression profile for *βACT* is shown as a positive control for the cDNA samples (top) and the expression profile of *MAGE-A1*, a known CT antigen gene, to show the expression profile of a CT antigen gene in normal tissue (top). These results appear to be reproducible as these PCRs were repeated at least two times.

Sequencing results found that the lower band amplified by the primer pairs F2 + R2 and F4 + R4 did not show any significant sequence similarity to *SYCP3*, therefore this band represents an undesired PCR amplification (summarised in Table 3.2). These RT-PCR results suggest that *SYCP3* displays a meiosis-specific expression profile, in line with the expected expression profile for a meiosis-specific gene. Although *SYCP3* expression was not shown in any of the cancer cells, it was not dismissed as a potential CT gene.

3.5 Summary of sequencing results

The PCR products were purified and sequenced to ensure that the correct sequence was being amplified, the results are summarised in Table 3.2. The sequencing results for the two control genes, *βACT* and *MAGE-A1* (a known CT antigen gene), are shown also at the top of the table. *Italics* (and brackets) have been used to indicate the sequencing results which did not have a strong sequence identity with the expected sequence and thus suggesting that an unexpected product was being amplified by the PCR.

Table 3.2. Summary of the sequencing results for the RT-PCR screen of the meiosis-specific genes

Gene	Primers	Sequenced in Normal tissue	Sequenced in cancer sample	Sequence Identity (%)*	Classification following validation
ACTB	F1 + R1	Testis	-	99.4	-
	F2 + R2	Testis	-	99.5	
MAGE-A1	F1 + R1	Testis	-	97.7	-
		LITERATURE SELECTED MEIOTIC GENES			
HORMAD1	F1 + R1	Testis	-	99.2	Dismissed
		Brain (whole)		99.5	
RAD21	F1 + R1	Testis	-	98.9	-
		Brain (cerebellum)		99.5	
mRAD21	F + R	Testis	-	98.3	-
RAD21L	F1a + R1	Testis		97.7	Restricted CT gene
			NT2	99.0	
			A2780	98.2	
	F1b + R1	Testis		97.5	
			NT2	98.2	
			MDA-MB-453	98.0	
		(Testis (bottom))		*(50.0)*	
mRAD21L	F + R	Testis	-	99.2	-
REC8	F1 + R1	Testis	-	97.9	Dismissed
		Spinal cord		99.4	
		Heart		99.1	
		Thymus		99.1	
		Trachea		98.8	
	F2 + R2	Brain (cerebellum)	-	98.2	
		Thymus		98.9	
mREC8	F + R	Testis	-	98.3	-
		Kidney		98.6	
SMC1α	F1 + R1	Testis	-	100	-
		Brain (cerebellum)		98.9	
SMC1β	F1a + R1	Testis		99.0	Restricted CT gene
			MDA-MB-453	100	
			(NT2)	*(53.5)*	
			(MCF7)	*(52.0)*	
	F1b + R1	Testis		100	
			MDA-MB-453	99.7	
			(Stomach tumour)	*(52.3)*	
mSMC1β	F + R	Testis	-	99.6	-

SMC3	F1 + R1	Brain (cerebellum)	-	99.3	-
		Ovary		99.1	
STAG1	F1 + R1	Brain (cerebellum)	-	99.5	-
		Ovary		99.3	
STAG2 A	F1 + R1a	Brain (cerebellum)	-	99.0	-
		Ovary		99.5	
STAG2 B	F1 + R1b	Brain (cerebellum)	-	98.8	-
		Ovary		98.6	
STAG3	F1 + R1	Testis	-	98.7	Dismissed
	F2 + R2	Testis	-	99.0	
mSTAG3	F + R	Testis	-	98.5	-
		Heart		100	
		Spleen		100	
		Embryo, day 11		98.5	
		Embryo, day 17		99.2	
SYCE2	F1 + R1	Testis	-	99.1	Dismissed
		Brain (cerebellum)		99.3	
		Foetal brain		98.5	
		Spinal cord		99.1	
SYCP2	F1 + R1	Brain (cerebellum)	-	97.7	Dismissed
		Spinal cord		97.8	
		Bone marrow		97.8	
SYCP3	F1 + R1	Testis	-	99.1	Testis-restricted
	F2 + R2	Testis		99.3	
		(Brain, cerebellum)		*(55.3)*	
		(Spinal cord)		*(50.7)*	
		(Thymus)		*(51.0)*	
			(NT2 (top))	*(53.9)*	
			(NT2 (bottom))	*(53.3)*	
			(Brain Tumour)	*(53.9)*	
	F3 + R3	Testis	-	99.7	
	F4 + R4	Testis		99.2	
		(Brain, cerebellum)		*(52.9)*	
		(Brain, whole)		*(51.1)*	
			(NT2)	*(52.2)*	
			(A2780)	*(49.4)*	
			(Leukemia)	*(50.6)*	
TEX12	F1 + R1	Testis	-	99.6	Dismissed
		Spinal cord		99.5	
		Spleen		98.7	
		Small Intestine		99.5	

*The percentage of pair wise residues which are identical in the alignment, including gap versus non-gap residues, but excluding gap versus gap residues; calculated using Geneious software.

The sequences recovered from sequencing were aligned with the expected PCR product sequence using the Geneious software; see Appendix for the corresponding sequence alignments.

3.6 Methylation

Gene expression can be regulated and silenced via epigenetic modifications to the genome, such as DNA methylation. CpG (-cytosine-phosphate-guanine-) sites, also known as CpG

islands, are often over represented within the promoter regions of mammalian genes. When promoter CpG islands are unmethylated this usually permits transcription initiation (De Smet *et al.*, 1999; Mikeska *et al.*, 2012). DNA methylation is very stable and is passed on to subsequent cell generations; however DNA methylation reprogramming occurs during gametogenesis and after fertilisation (De Carvalho *et al.*, 2010; Hassler and Egger, 2012). Methylation of the cytosine within promoter CpG islands represses promoter activity because it prevents the binding of transcription factors and can result in gene silencing, for example, a tumour suppressor gene may be silenced via hypermethylation (Egger *et al.*, 2004). An altered methylation status of genes has been associated with many different types of cancers; both global hypomethylation (a decrease of the overall DNA methylation levels) and localised hypermethylation have been observed in cancer (Mikeska *et al.*, 2012). Hypomethylation of the CpG islands can cause aberrant and/or over-expression of genes (Irizarry *et al.*, 2009).

Histones are highly conserved basic proteins and are an essential component of chromatin which can be post-translationally modified to alter their interaction with DNA and nuclear proteins. Histone deacetylation causes chromatin remodelling, where the chromatin condenses into an inactive state and results in gene repression (Berger, 2007; Chervona and Costa, 2012). Unmethylated DNA associated with acetylated histone is transcriptionally competent; therefore DNA methylation and histone deacetylation prohibit transcription which in turn leads to gene silencing.

A study carried out by Cho and colleagues (2003) found that expression of *CAGE*, a well known CT antigen gene, was affected by changes in DNA methylation status. This study used a DNA methyltransferase inhibitor (5-aza-2'-deoxycytidine) and a histone deacetylase inhibitor (TSA) to assess the effect of DNA methylation and/or histone acetylation status on *CAGE* gene expression. Methyltransferase inhibitors cause hypomethylation of the DNA, and histone deacetylase inhibitors prevent the removal of acetyl groups from histones. The study found that 5-aza-2'-deoxycytidine had a bigger effect than TSA on *CAGE* expression, suggesting that DNA methylation has a dominant role over histone deacetylation in the silencing of *CAGE* gene expression (Cho *et al.*, 2003).

Both *RAD21L* and *SMC1β* were found to display CT-restricted expression profiles within the tissues and cell lines tested here. As epigenetic signals have been shown to effect gene expression of several known CT antigen genes such as *CAGE*, they may also have a role in regulating the gene expression of other CT genes. The effect of DNA methylation and histone acetylation status on the expression of *RAD21L* and *SMC1β* was assessed using 5-aza-2'-deoxycytidine and TSA treated HCT116 cells, a colorectal cancer cell line in which *RAD21L* and *SMC1β* gene expression cannot be detected without drug treatment. Gene expression of *RAD21L* and *SMC1β* was assessed using RT-PCR; the results are shown in Figure 3.9.

Treatment of the HCT116 cells with 5-aza-2'-deoxycytidine and/or TSA appears to cause a change in the expression of both *RAD21L* and *SMC1β*. The significance of these results was assessed by comparing these expression changes with the number of CpG dinucleotides upstream of *RAD21L* and *SMC1β* as predicted by the gene sequences. The predicted number of CpG dinucleotides near the transcription start site (TSS) (usually ±1.5 Kb from the TSS) was obtained for both *RAD21L* and *SMC1β,* from the UCSC genome browser (http://www.genome.ucsc.edu; Gardiner-Garden and Frommer, 1987) (Table 3.3). The number of CpG dinucleotides near the TSS for *CAGE1* is also shown in Table 3.3.

Table 3.3. Predicted CpG islands upstream of the *RAD21L* and *SMC1β* genes

Gene	Chromosome Location	CpG Island size*	CpG count**	% CpG	% C or G	Ratio observed to expected
CAGE1	6p24.3	845	84	19.9	70.3	0.80
RAD21L	20p13	440	46	20.9	70.7	0.84
SMC1β	22q13.31	1105	106	19.2	68.4	0.82

*The CpG islands were defined by the following criteria, as per Gardiner-Garden and Frommer, (1987):

- GC content of 50% or greater.
- Greater than 200 bp in length.
- Ratio of greater than 0.6 for the observed number of CG dinucleotides to expected number of CG dinucleotides. The ratio is calculated according to the formula cited in Gardiner-Garden and Frommer, (1987).

**The CpG count represents the number of CpG dinucleotides in the CpG island.

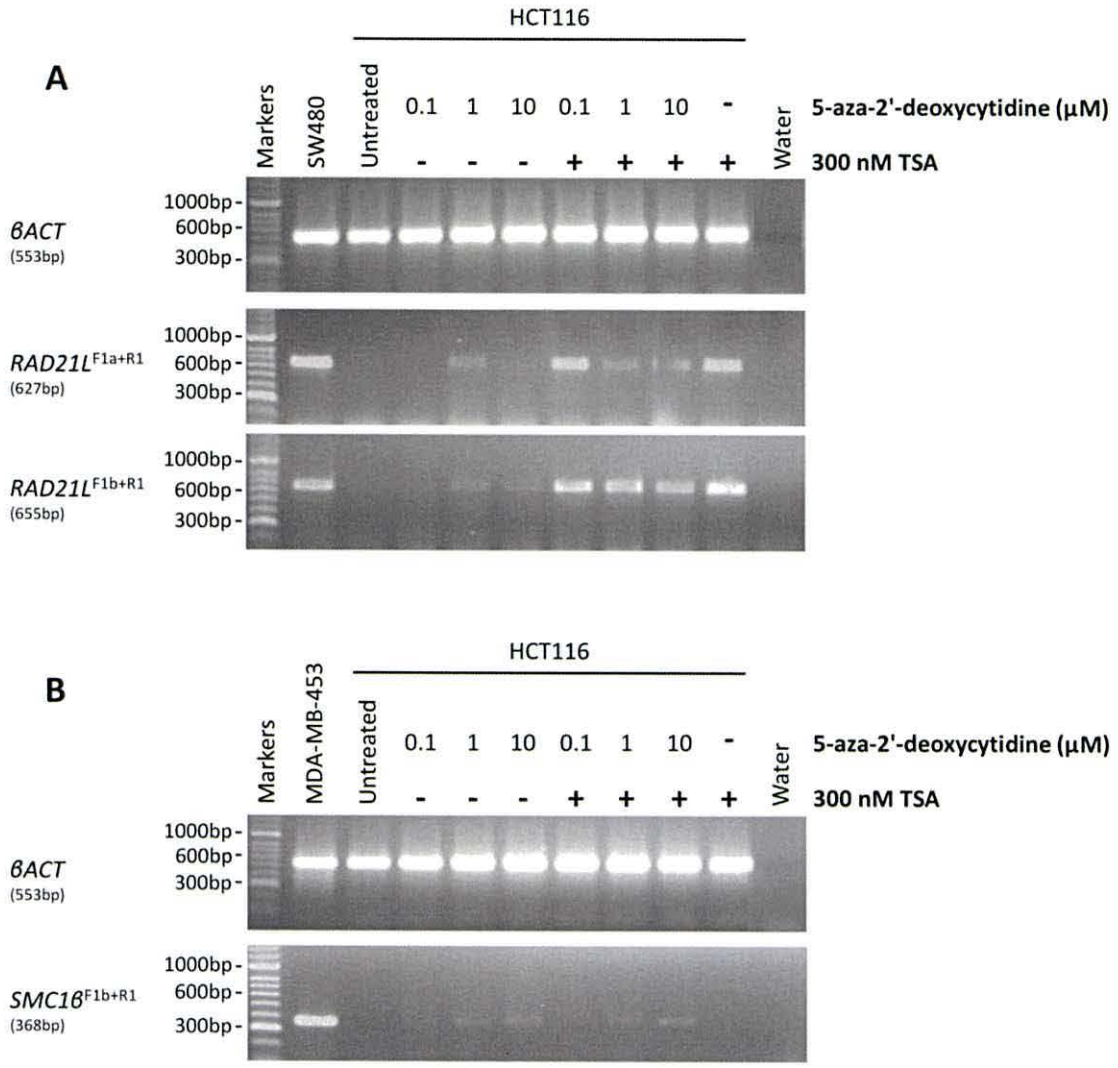

Figure 3.9. The effect of 5-aza-2'-deoxycytidine and TSA on *RAD21L* and *SMC1β* expression in HCT116 cells. Agarose gels showing the expression of *RAD21L* and *SMC1β* in HCT116 cells after treatment with 5-aza-2'-deoxycytidine (0.1, 1 and 10 μM) for 48 hours, and/or 300 nM TSA for 24 hours. cDNA was generated from the total RNA extracted from the HCT116 cells after treatment. **A.** *RAD21L* primer pairs F1a+R1 and F1b+R1 were used to assess the effect of 5-aza-2'-deoxycytidine and TSA on *RAD21L* expression. SW480 cells were used as the positive control for *RAD21L* expression. *RAD21L* expression in 5-aza-2'-deoxycytidine and TSA treated HCT116 cells, was compared against untreated HCT116 cells. 5-aza-2'-deoxycytidine appears to have a slight effect on *RAD21L* expression, but TSA appears to have a greater effect on *RAD21L* expression. **B.** *SMC1β* primer pair F2+R2 was used to assess the effect of 5-aza-2'-deoxycytidine and TSA on *SMC1β* expression. MDA-MB-453 cells were used as the positive control for *SMC1β* expression. *SMC1β* expression in 5-aza-2'-deoxycytidine and TSA treated HCT116 cells, was compared against untreated HCT116 cells. The strength of the band observed for *SMC1β* appears to be stronger with increased concentration of 5-aza-2'-deoxycytidine; however TSA appears to have no detectable effect on *SMC1β* expression. *βACT* is shown as a positive control for the cDNA (top) in both cases. These results appear to be reproducible as these PCRs were repeated two times.

The faint bands indicating *RAD21L* expression after 5-aza-2'-deoxycytidine treatment in Figure 3.9, could suggest a possible role for DNA methylation in the regulation of *RAD21L*

gene expression. The data from the UCSC genome browser predicts a CpG island in the upstream promoter region, of *RAD21L*, containing 46 CpG dinucleotides (Table 3.3), which supports a potential role for DNA methylation in *RAD21L* gene silencing. A stronger band was observed for *RAD21L* after treatment with TSA, and *RAD21L* expression in TSA-treated cells is comparable to *RAD21L* expression in the cells treated with TSA in conjunction with 5-aza-2'-deoxycytidine. This suggests that histone deacetylation may have a greater effect on *RAD21L* gene silencing than DNA methylation.

The RT-PCR results in Figure 3.9 suggest that *SMC1β* expression may be slightly effected by 5-aza-2'-deoxycytidine treatment, whereas TSA treatment appears to elicit no effect. Although faint, the bands appear to suggest a correlation between expression and the concentration of 5-aza-2'-deoxycytidine. The data shown in Table 3.3 suggests that there is a CpG island in the upstream promoter region of *SMC1β*, containing 106 CpG dinucleotides. These results may suggest a possible role for DNA methylation in *SMC1β* gene silencing, however the bands observed for *SMC1β* in the 5-aza-2'-deoxycytidine treated HCT116 cells are significantly weaker than the band observed in the positive control (MDA-MB-453 cell line), which could indicate that another mechanism is controlling the expression of *SMC1β*.

3.7 Discussion

3.7.1 Summary of RT-PCR expression profiles

Meiosis is a highly regulated process, which is restricted to the testes in adult humans; therefore it was reasonable to predict that the expression profiles for the meiosis-specific genes tested here would be restricted to the testis in normal tissue. Surprisingly, a number of the predicted meiosis-specific genes selected from the literature displayed expression in one or more non-germ cell normal tissue. The expression profiles observed for the predicted meiosis-specific genes in human and mouse normal tissues and/or cancer cells are summarised in Figure 3.10.

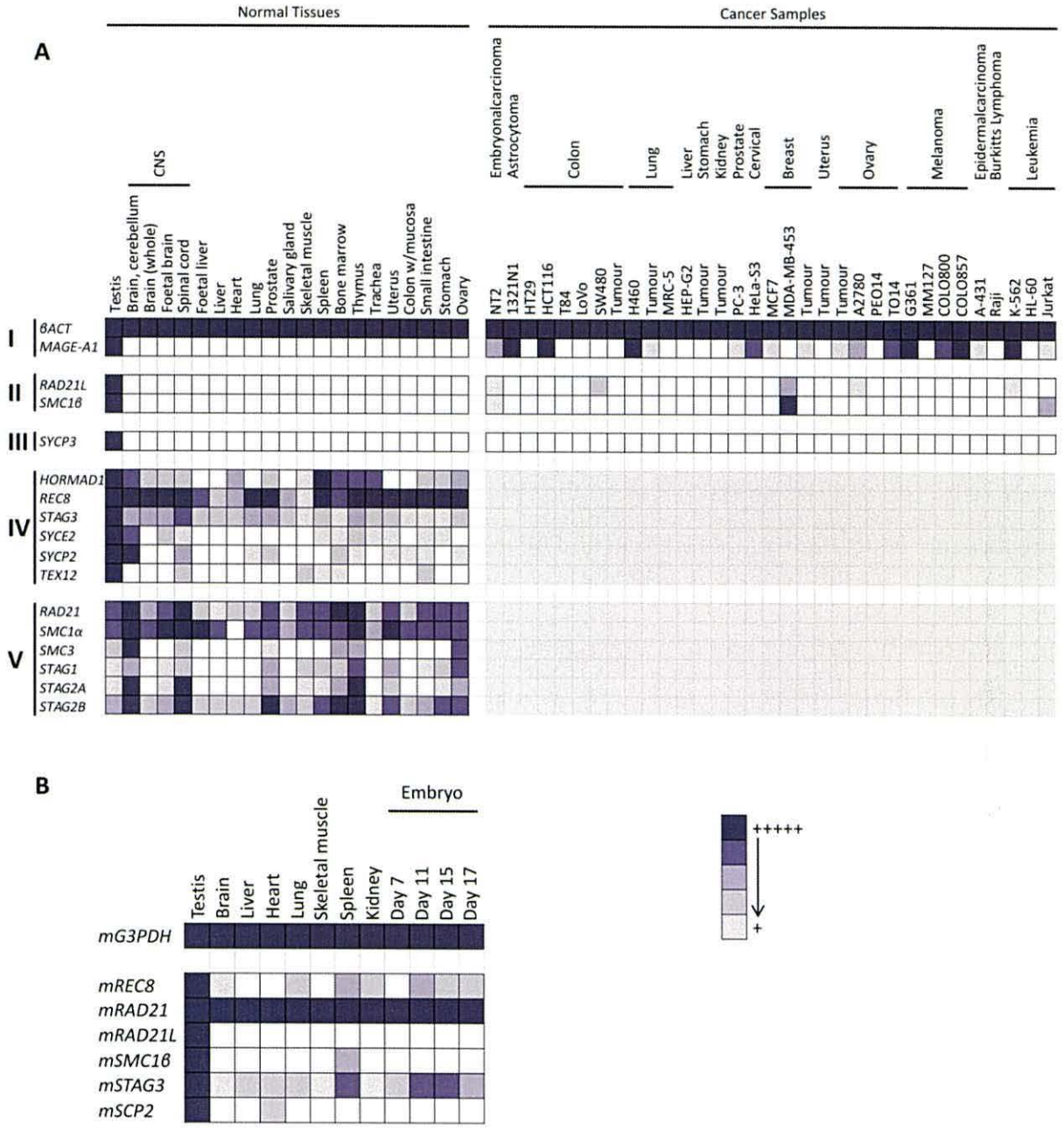

Figure 3.10. Chart summarising the gene expression profiles for the predicted meiosis-specific genes selected from the literature. The expression profile of each gene is represented by a row in the grid, with the columns corresponding to the tissues and cell lines used. The intensity of each PCR product viewed in an ethidium bromide stained agarose gel was ranked 1-5, which is represented in the grid with various shades of purple; thus giving a qualitative representation of the RT-PCR profiles. The darkest shade of purple signifies PCR products ranked 5 (strong band), with lighter shades indicating fainter bands (key shown at the bottom right). **A.** Human predicted meiosis-specific genes from the literature; **I.** Control genes, *βACT* and *MAGE-A1*, **II.** Reported meiosis genes found to display a CT-restricted expression profile, *RAD21L* and *SMC1β*, **III.** The testis-restricted expression profile observed for *SYCP3*. **IV.** The reported meiosis-specific genes shown to display expression in multiple non-testis and non-CNS normal tissues, **V.** The expression profiles of the cohesin subunit genes, with a known role in mitosis, which were screened alongside the purported meiosis-specific cohesin genes. **B.** The expression profiles for the mouse meiosis-specific genes screened in normal mouse tissue.

Although many of the predicted meiosis-specific genes displayed expression profiles more closely resembling that of their non-meiosis counterparts, three genes displayed strictly meiosis-specific expression profiles in the normal tissues tested here, *RAD21L*, *SMC1β* and *SYCP3*. *RAD21L* and *SMC1β* were shown to display a testis-restricted expression profile in the normal tissues, with additional expression observed in one or more of the cancer cell lines or tissues tested here. Neither *RAD21L* nor *SMC1β* have previously been reported to be CT antigen genes, therefore these results suggest that this screen has identified two potential novel CT-restricted CT antigen genes.

3.7.2 *RAD21L* and *SMC1β* identified as novel CT genes

A study by Lee and Hirano (2011) found that RAD21L is responsible for recruiting SYCP1 to the axial elements during SC formation and helps initiate synapsis. This interaction was not observed for the other two α-kleisins, RAD21 and REC8 (Lee and Hirano, 2011). The results presented here represent part of a larger gene screen, which is summarised in Feichtinger *et al.*, (2012a); during the gene screen *SYCP1* was also identified as a CT gene. The expression profile of *RAD21L* observed in the cancer cells was compared with the expression profile observed for *SYCP1*. Expression of *SYCP1* was found in NT2 (an embryonalcarcinoma cell line), ovary tumour tissue, G361 and COLO857 (two melanoma cell lines) (Feichtinger *et al.*, 2012a). The only overlap observed for *RAD21L* and *SYCP1* expression was observed in NT2 cells, which therefore suggests that *RAD21L* and *SYCP1* are not uniformly co-expressed in cancer.

Meta-analysis of gene expression profiles was carried out on *RAD21L* and *SMC1β* after RT-PCR validation, using the CancerMA online tool (http://www.cancerma.org.uk; Feichtinger *et al.*, 2012b), to assess their gene expression in cancer microarray data. The analysis found no significant mean up-regulation or down-regulation for *RAD21L* in the cancer array data, whereas, a significant mean up-regulation of *SMC1β* was observed for brain cancer. This analysis therefore provides evidence that *SMC1β* is expressed in clinically relevant material. Interestingly, *SMC1β* expression was not found in the brain cancer cell line (1321N1) used in this study. Further screening is required to identify any potential cancer-specific expression profiles which *RAD21L* and *SMC1β* may display.

These RT-PCR results suggest that *RAD21L* and *SMC1β* are expressed in cancer cells, however this gene expression may not equate to RAD21L and SMC1β protein levels. The correlation between changes in gene expression and protein abundance is effected by numerous post-transcriptional mechanisms (Tan *et al.*, 2009; Waters *et al.*, 2006). If the *RAD21L* and *SMC1β* gene products are not produced in the cancer cells, then this severely limits their potential use in cancer diagnosis and/or therapy. Further characterisation is required to establish the protein expression (if any) of RAD21L and SMC1β in cancer cells. Therefore, here we have identified *RAD21L* and *SMC1β* as novel CT genes, because their potential CT antigenicity (if any) is yet to be shown.

3.7.2.1 Epigenetic control of *RAD21L* and *SMC1β*

Previous studies have shown that the expression of several CT antigen genes is regulated by epigenetic signals such as DNA methylation (Cho *et* al., 2003; Link *et al.*, 2009). HCT116 cells, a colorectal cancer cell line in which *RAD21L* and *SMC1β* gene expression cannot be detected without drug treatment, were used to assess the effect of 5-aza-2'-deoxycytidine (DNA methyltransferase inhibitor) and TSA (histone deacetylase inhibitor) treatment on *RAD21L* and *SMC1β* expression. RT-PCR after 5-aza-2'-deoxycytidine treatment produced a faint band for *RAD21L*, which may suggest a potential role for DNA methylation in the regulation of *RAD21L* gene expression. The data from the UCSC genome browser predicted 46 CpG dinucleotides near the *RAD21L* TSS, which supports a potential role for DNA methylation in *RAD21L* gene silencing. Whilst there is a minimal effect for 5-aza-2'-deoxycytidine treatment, the effect of TSA treatment is clearly stronger which may indicate a more prominent role for histone acetylation in the regulation of *RAD21L* gene expression. Quantitative real time PCR (qRT-PCR) could be carried out to determine the extent of gene regulation by DNA methylation and/or histone acetylation.

The RT-PCR results for *SMC1β* gene expression after 5-aza-2'-deoxycytidine and/or TSA treatment suggested a role for DNA methylation but not histone acetylation in gene expression regulation. The CpG island map from the UCSC genome browser predicted 106 CpG dinucleotides near the *SMC1β* TSS, which supports the proposal for a potential role for DNA methylation in *SMC1β* silencing. However, the PCR band for *SMC1β* in the 5-aza-2'-deoxycytidine treated HCT116 cells shows a significantly lower intensity than that of the positive control (untreated MDA-MB-453 cells) which may suggest that other mechanisms

and/or factors also control *SMC1β* gene expression. A greater number of CpG dinucleotides are predicted near the *SMC1β* TSS, than near the TSS of *CAGE1* (106 for *SMC1β* and 84 for *CAGE1*, as shown in Table 3.3). However a greater effect for 5-aza-2'-deoxycytidine treatment has been reported for *CAGE1* expression (Cho *et al.*, 2003) than that observed here for *SMC1β*, thus supporting the possibility that other factors may contribute to the regulation of *SMC1β* expression.

More than 50% of all human genes have elevated GC content within their promoter regions. CpG islands (defined by a clustering of CpG dinucleotides) have been shown to co-localise with the promoter regions of all constitutively expressed genes and approximately 40% of those genes with a tissue restricted expression profile (Fatemi *et al.*, 2005; Saxonov *et al.*, 2005). CpG island density varies between the chromosomes and large sections of the genome have been reported to be GC poor, for example a low GC content has been observed for the Y chromosome (reviewed in Illingworth and Bird, 2009). X chromosome inactivation in females is mediated via epigenetic regulation (Chow *et al.*, 2005), which is potentially interesting because a disproportionate number of CT antigen genes are encoded on the X chromosome. Therefore it is unsurprising that previous studies have reported an important role for DNA methylation in the regulation of expression for several X-CT genes (De Smet *et al.*, 1996; 1999; Weber *et al.*, 1994). The regulation of CT antigens by epigenetic signals offers a potential therapeutic opportunity due to the reversible nature of DNA methylation, for example demethylating agents could be used to restore the normal epigenome (Mikeska *et al.*, 2012).

3.7.3 Gene expression profiles of the previously identified CT antigen genes *HORMAD1* and *SYCP3*

HORMAD1 was previously identified as a CT antigen gene using an EST (expressed sequence tag)-based analysis and expression was shown in the normal testis tissue as well as in lung, breast, esophageal, endometrial bladder and colon cancers (Chen *et al.*, 2005). Two transcript variants have been identified for *HORMAD1* (*CT46*), the predominant, full-length variant (variant 1) encodes a longer isoform than the alternative transcript variant (variant 2) which lacks an exon in the coding region. The study by Chen *et al.*, (2005) screened 16 normal tissues for *HORMAD1* expression using qRT-PCR and the highest level of expression they reported was <1% of the expression observed in testis, for the following somatic

tissues; brain, breast, colon, placenta and spleen. However, here the RT-PCR results show *HORMAD1* expression in a wider range of normal tissues and the qualitative RT-PCR analysis (Figure 3.10) suggests that *HORMAD1* expression in the somatic tissues is comparable to that observed in the normal testis tissue. *HORMAD1* expression does not appear to fit the expression profile of a CT antigen gene in normal tissues, which may suggest that *HORMAD1* expression is not as meiosis-specific in humans as previously believed. The sequencing results indicated that the correct PCR product was being amplified by the primers; therefore *HORMAD1* was dismissed as a CT gene. These results also suggest that *HORMAD1* may have been incorrectly identified as CT antigen gene previously, and is in fact a selective CT antigen gene. A high number of PCR cycles were used here to screen for gene expression in the normal tissues and the cancer cell lines and tissues, therefore potentially identifying low levels of expression. Consequently, differences in the expression profiles may be due to differences in RT-PCR sensitivity. qRT-PCR could be carried out to quantitatively establish the level of *HORMAD1* expression in these normal tissues.

A recent study demonstrated that true meiosis-specific genes are tightly transcriptionally silent in *S. pombe* mitotic cells (Ioannoni *et al.*, 2012). Therefore if we are detecting low levels of gene expression here, it is not likely to be a general low transcript level shown for all meiotic genes. As previously mentioned, the post transcriptional mechanisms affect the relationship between gene expression levels and protein abundance. Therefore the *HORMAD1* expression observed here may not correlate to HORMAD1 production in these non-meiotic cells. Further analysis, may cause HORMAD1 to be re-assessed/re-classified as a CT antigen.

SYCP3 was also previously identified as a CT antigen gene (Mobasheri *et al.*, 2007; Niemeyer *et al.*, 2003). The RT-PCR results presented here show a testis-restricted expression profile for *SYCP3*, with no *SYCP3* expression observed in the cancer cells. *SYCP3* was not dismissed because only a relatively small number of cancer cell lines and tissues were screened here and further analysis may reveal *SYCP3* expression in other cancer cells. These results do however confirm the meiosis-specificity of *SYCP3* in human somatic tissues and provides further evidence to support its CT-tissue restricted profile. A study by Mobasheri *et al.*, (2007) showed *SYCP3* expression in 4/156 of the solid tumour samples using nested PCR. The use of nested PCR in the Mobasheri *et al.*, study may indicate that *SYCP3* was expressed

at very low levels in the tumour cells. Therefore qRT-PCR may identify low levels of expression which were not detected by RT-PCR.

3.7.4 Gene expression of the cohesin subunits genes

Two cohesin subunit genes which were previously reported to be meiosis-specific, *REC8* and *STAG3*, were found to display expression in all of the normal human tissues tested here. The expression profiles observed for *REC8* and *STAG3* look very similar to the expression profiles observed for their mitotic paralogues *RAD21* and *STAG1/STAG2* respectively. The idea that these genes are meiosis-specific is well established in the literature (reviewed in Nasmyth, 2011); therefore these results are potentially interesting because they suggest that *REC8* and *STAG3* may not be as tightly meiosis-specific as previously thought in humans. Excepting the testis and the ovary, the normal tissues tested here are comprised of mitotically dividing cells; hence these results could potentially indicate a role for these gene products in mitotic human cells, this possibility is explored in Chapter 6.0. The results from this gene screen also suggest that several other predicted meiosis-specific genes may not be as tightly regulated as previously believed; *SYCE2*, *SYCP2* and *TEX12*.

The literature also shows the mouse ortholgues of these predicted meiosis-specific genes to display sex organ-restricted expression. A strict meiosis-specific mRNA expression profile for *RAD21L*, *REC8*, *STAG3* and *SMC1β* with expression restricted to the testis and the ovary only, was demonstrated in mice by Ishiguro *et al.*, (2011). Therefore, the expression profiles of these predicted meiosis-specific genes were assessed in normal mouse tissues also. *mRAD21L* displayed a meiosis-specific RT-PCR profile, with expression in the mouse testis only, which corresponds to the expression profile observed for *RAD21L* in the human tissues. Whereas *mSMC1β* appears to show a mostly meiosis-specific expression profile, with additional expression shown in the spleen, which does not strictly match the profile observed for *SMC1β* in the normal tissues, however is comparable. *mSTAG3* appears to be widely expressed in the normal mouse tissues, similar to the RT-PCR profile observed for *STAG3* in the normal human tissues. Faint bands were observed for *mREC8* in the mouse normal brain, lung, spleen and kidney tissues, whereas in a strong band was observed for *REC8* in all of the normal human tissues. Although, these RT-PCR profiles do not match the results reported by Ishiguro and colleagues (2011), they suggest that these meiotic genes may not be as widely expressed in normal mouse tissues as in normal human tissues. Also

the band-intensities observed for the PCR products for these genes were significantly stronger in human normal tissues than in mouse normal tissues. This may imply differences in the way the expression of these meiotic genes are controlled in mice and humans, and thus suggesting a greater dissimilarity in the meiotic programs of mouse and human that previously presumed.

Several studies using the fission yeast, *S. pombe*, have shown that a number of meiosis-specific mRNAs, including *REC8*, are expressed during mitosis and meiosis, but are selectively eliminated during mitosis (Harigaya *et al.*, 2006). Meiotic mRNAs transcribed during mitosis are targeted by an RNAi-related system known as the determinant of selective removal (DSR)-Mmi1 system. Post-transcriptional processing of the RNA ensures that the primary transcripts are not processed into mature mRNAs. Inactivation of the DSR-mediated mRNA elimination pathway allows these meiotic genes to become functionally expressed when the cell enters meiosis (Chen *et al.*, 2011; Cremona *et al.*, 2011; Yamanaka *et al.*, 2010). If a similar post-transcriptional degradation pathway were also present in mammals, the meiotic gene transcripts detected in the mouse and human somatic cells may not give rise to proteins. Therefore, further analysis is required to establish the meiotic-specificity of the meiotic gene products (this is explored further in Chapter 6.0).

Cohesin subunit genes with a known role in mitosis were also screened alongside their meiotic counterparts, as a control. Surprisingly the expression profiles showed that some of these mitotic cohesin subunit genes were not as widely expressed as expected. The RT-PCR profiles for *RAD21* and *STAG2B* showed expression in all of the normal tissues, and *SMC1α* displayed expression in all of the normal tissues except for the heart. Interestingly, there appears to be a lack of mitotic gene expression in the normal heart tissue, with only *RAD21* and *STAG2B* expression detected in the heart. Cardiomyocytes are fully differentiated and no longer retain the capability to undergo mitosis, and so the cell number within the heart is controlled by a stem cell compartment. The ability to self-renew is not preserved in the aging heart of mammals (Anversa *et al.*, 2006). *STAG1* and *STAG2A* both display expression in a large number of normal tissues, which appear to correspond with each other. SMC3 is an essential subunit within the cohesin complex and was expected to be expressed in all of the normal tissues; however expression was observed for less than half of the normal

tissues tested. This may be due to a low level of gene expression which was not detected by the PCR, which can be due to gene transcription by an unstable mRNA.

3.7.5 Concluding remarks

The total RNA for the 21 normal tissues used here was purchased from Clontech and Ambion. The tissues were obtained *post mortem*, and although the companies classified these tissues as normal, there is no definite way of verifying the 'normality' of these tissue samples. Clinical evidence, from detailed autopsy studies, suggests that a large proportion of the population carry microscopic cancers which remain dormant and never progress into a clinically detectable disease (Naumov *et al.*, 2009). Therefore it is possible that the normal tissues from which the RNA was extracted contained microscopic cancers which remained undetected. Although the microscopic cancers are dormant and do not behave like a tumour, the potential affect on the gene expression profiles is unknown. However, the expression profiles observed for the well characterised CT antigen gene, *MAGE-A1*, and the two novel CT genes identified here did not show any unexpected expression in the normal tissues. Therefore we can assume that these tissue samples represent relatively 'normal' tissue expression profiles.

CT antigen genes are known to display a highly restricted expression profile in normal tissues; therefore we hypothesised that meiosis-specific genes could possibly provide good candidate genes from which to identify potential new CT antigen genes due to their restricted expression profiles in normal tissues. Two of the nine predicted meiosis-specific genes selected from the literature were identified as potential new CT antigen genes, thus supporting the original hypothesis. If meiosis-specific genes are up-regulated in cancer cells, this may indicate the potential for meiotic-like cell division during tumorigenesis.

4.0 RT-PCR screening of genes identified through a bioinformatics pipeline for potential novel CT antigen gene candidates

4.1 Introduction

In Chapter 3.0, predicted meiosis-specific genes were identified from the literature and a selection of genes was chosen to screen for expression in a wide range of normal tissues and cancer cells. This approach identified two novel CT genes with CT-restricted expression profiles. These results suggested that meiosis-specific genes are a good source from which further potential CT antigen genes can be identified. Although the approach used for the initial screen identified two new potential CT antigen gene candidates, a more systematic approach was developed for a larger screening program. A bioinformatic approach was developed to identify potential candidates from published microarray data and EST analysis data (Feichtinger *et al.*, 2012a; 2012b), which were then validated using RT-PCR.

A large scale microarray study was carried out by Chalmel and colleagues (2007) which studied the meiotic transcriptome of mice. This study analysed total testis, isolated seminiferous tubules in addition to enriched populations of Sertoli cells, spermatogonia, pachytene spermatocytes, and round spermatids against 17 somatic non-testicular control tissues. The study identified a large number of genes with expression associated specifically with meiosis and spermatocyte development in mammals. The expression was assigned to the meiotic or post-meiotic clusters as defined by the study; of the genes studied, 744 mouse genes were classified as meiosis-specific.

In our group, human orthologues were assigned to the 744 mouse meiosis-specific genes, giving 408 human genes (Feichtinger *et al.*, 2012a). These 408 genes were then filtered using MitoCheck (http://www.mitocheck.org; Neumann *et al.*, 2010) to remove the mitosis-associated genes, which left 375 human genes. These genes were then analysed using a bioinformatics pipeline, using previously published microarray data and EST analysis data (Feichtinger *et al.*, 2012a).

Microarray analysis allows the expression of thousands of genes from different populations of cells to be surveyed in a single experiment; visualising which genes are expressed in a particular tissue, at a particular time, under a certain set of conditions, as set by the microarray study (Gibson, 2003). Microarrays provide a powerful tool, as they are able to discriminate between different cell types and also between the effects of various drugs (Miklos and Maleszka, 2004). Thousands of probes can be tested at once on one microarray platform; each probe represents the complement of at least part of a transcript which may be expressed in a tissue. The target mRNA population is labelled with fluorescent dye and the amount of hybridisation of the labelled mRNA to a complementary probe is measured using fluorophore detection. The intensity of the signal is directly related to the number of hybridised molecules, therefore microarray analysis uses relative signal intensity to determine transcript abundance (Gibson, 2003; Miklos and Maleszka, 2004). Although microarray analysis allows expression of thousands of genes to be surveyed in different populations of cells, it is limited by poor sensitivity and background noise which may result in false positives. This technique is also restricted by the lack of gene coverage on the array platforms and the number of cancer microarrays available (Russo *et al.*, 2003).

The 375 human orthologues for the meiosis-specific genes derived from the study by Chalmel and colleagues (2007) were analysed against 80 cancer microarray datasets for up-regulation. This analysis identified 40 candidate genes based on 58 cancer datasets (Feichtinger *et al.*, 2012a).

Given the limitations of the array-based approach, a second bioinformatics pipeline was developed to identify potential CT antigen gene candidates, from the human orthologues of the mouse meiosis-specific genes identified in Chalmel *et al.*, (2007). An expressed sequence tag (EST) analysis pipeline was used to analyse the 375 putative meiosis-specific human genes (Feichtinger *et al.*, 2012a; http://www.cancerest.org.uk). ESTs are short (200-800 nucleotide bases), unedited, single pass DNA sequence reads derived from cDNA (complementary DNA) libraries. An EST dataset represents the mRNAs present in the original tissue used for the construction of the cDNA bank, and can therefore can be analysed to provide an informative overview of the major transcripts in specific tissues. EST analysis has been successfully used in gene discovery, for drug target or vaccine candidate identification (Bernstein *et al.*, 2009; Nagaraj *et al.*, 2006). A very stringent approach was

adopted here because every gene which gave even a single EST hit was screened. The EST analysis pipeline identified 177 candidate genes, which were then classified according to their expression profiles shown in the EST data. Class 1 consists of 9 genes which are cancer/testis-restricted; class 2 contains 75 testis-restricted genes; class 3 contains 21 genes were cancer/testis/CNS-restricted and class 4 contains 72 testis/CNS-restricted genes.

The majority of the CT antigen genes identified to date display a low level of expression in other somatic tissues, such as the brain (Ghafouri-Fard and Modarressi, 2009). As the brain is an immune-privileged site, Almeida *et al.*, (2009) proposed a testis/brain-restricted CT antigen sub-class of genes. Here we have extended this to include all of the CNS tissues, because the CNS is protected by the blood-brain barrier (BBB) which restricts the passage of substances from the blood into the CNS in a highly selective manner (Carson *et al.*, 2009). Therefore candidate genes were dismissed if they were represented in a non-testis and/or non-CNS normal tissue EST library.

The EST analysis identified a considerably larger number of potential candidate genes compared to the microarray analysis. Here, 10 genes were randomly selected from the 40 candidate genes identified through the microarray analysis pipeline and 23 genes were randomly selected from classes 1-4 of the 177 candidate genes identified through the EST pipeline. The genes were screened using RT-PCR for expression in a range of normal tissues and cancer cell lines and tissues. RT-PCR of the candidate genes was used to validate the genes as CT genes and thereby validating the bioinformatic pipelines through which they were identified.

4.2 Screening genes identified from the microarray analysis

4.2.1 Microarray analysis genes to be screened

Ten predicted meiosis-specific genes identified from the microarray data analysis pipeline were selected for screening by RT-PCR. Details of the selected predicted meiosis-specific genes and their functions are given in Table 4.1.

Table 4.1. Predicted meiosis-specific genes identified from the microarray analysis and their known functional roles

Gene	Known Function	Reference
C1orf59	Uncharacterised gene, function unknown	-
C9orf117	Uncharacterised gene, function unknown	-
CCDC109A	Also known as mitochondrial calcium uniporter (MCU) and is involved in the transport of Ca2+ across the inner membrane of the mitochondria	Csordás *et al.*, 2012
FHAD1	Forkhead-associated (FHA) phosphopeptide binding domain 1, precise function not known	-
IQCG	IQ motif containing G, precise function not known	-
LRRC69	Leucine rich repeat containing 69, precise function not known	-
PLD6	Phospholipase D6, precise function not known, but is reported to be widely expressed.	Kerkel *et al.*, 2010
PPP4R4	Protein phosphatase 4 regulatory subunit 4, precise function not known	-
SAMD13	Sterile alpha motif domain-containing 13, precise function not known	-
TDRD5	Tudor domain-containing 5, found to have a role in germ cell development in mice	Yabuta *et al.*, 2011

A previous study reported that *PLD6* is widely expressed (Kerkel *et al.*, 2010), therefore this gene was dismissed at this stage and not screened by RT-PCR, because this expression profile does not fit the expression profile of a CT antigen gene.

4.2.2 RT-PCR with normal tissues for the microarray analysis genes

The genes listed in Table 4.1 were screened for expression in a range of 21 normal tissues, in order to assess their meiosis-specificity. RNA preparations from a range of normal tissues (obtained *post mortem*) were purchased from Clontech and Ambion. Intron-spanning primers were designed for each gene and were used to carry out RT-PCR using cDNA synthesised from the RNA preparations. The RT-PCR profiles for the predicted meiosis-specific genes identified by the microarray analysis pipeline are shown in Figure 4.1.

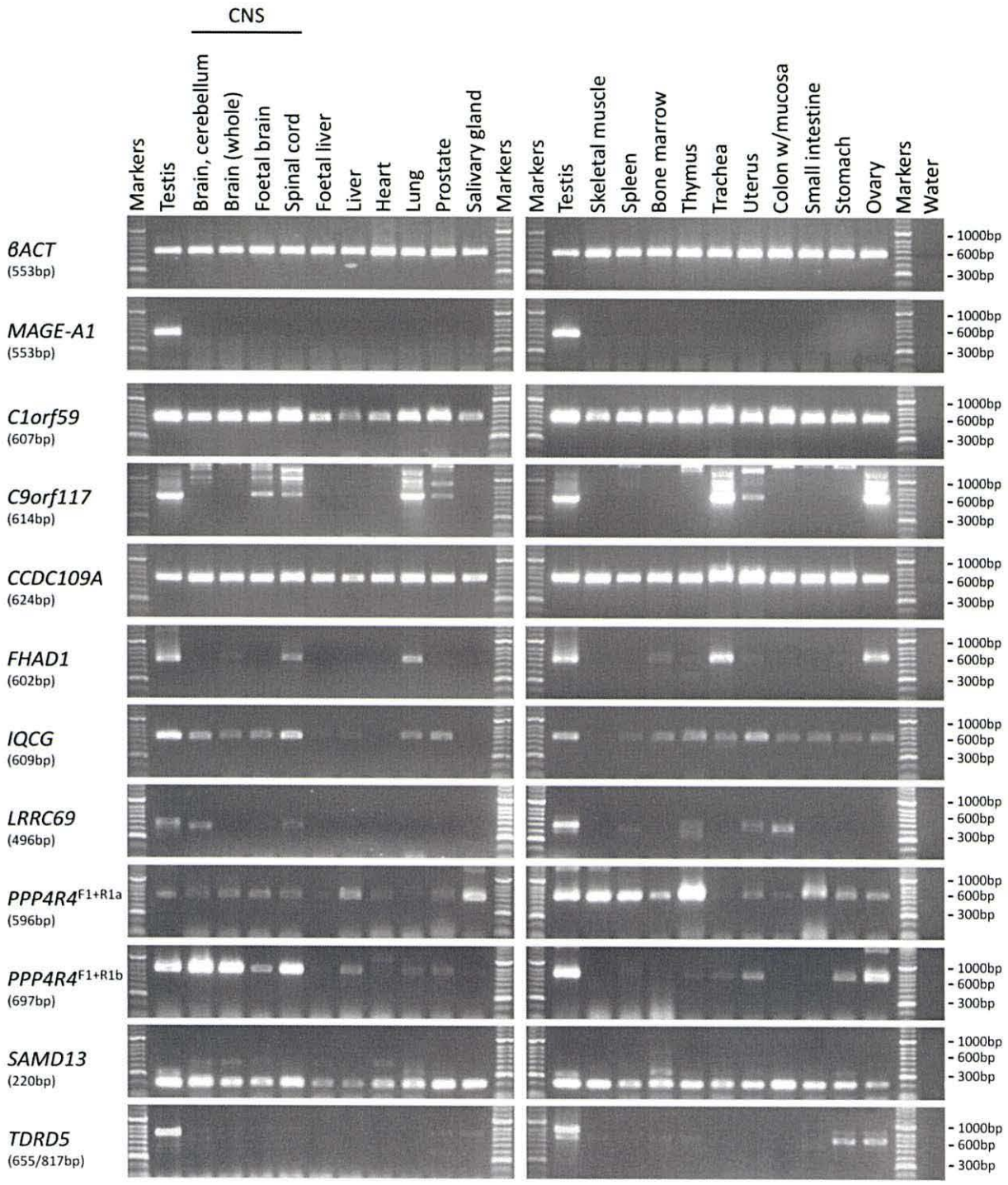

Figure 4.1. RT-PCR profiles for the microarray analysis derived genes in normal human tissues. Agarose gels showing the expression profiles for the microarray analysis genes in normal human tissues (the expected PCR product size is shown in brackets). cDNA was generated from the total RNA from a range of normal tissues (obtained *post mortem*). All of the genes displayed expression in multiple normal tissues. The expression profile for *βACT* is shown as a positive control for the cDNA samples (top) and the expression profile of *MAGE-A1*, a known CT antigen gene, to show the expression profile of a CT antigen gene in normal tissue (top). These results appear to be reproducible as these PCRs were repeated at least three times.

The RT-PCR profiles for the nine putative meiosis-specific genes predicted by the microarray analysis pipeline suggested that all of these genes displayed expression in multiple normal tissues, thus not fitting the expected expression profile of a meiosis-specific gene or that of a CT antigen gene in normal tissues. These genes were all dismissed and were not screened for expression in the cancer cell lines or tissues.

4.2.3 Summary of microarray analysis gene sequencing

The PCR products were purified and sequenced to ensure that the correct sequence was being amplified, the sequencing results and the gene classifications are summarised in Table 4.2. The sequencing results for the two control genes, *βACT* and *MAGE-A1* (a known CT antigen gene), are also shown at the top of the table. *Italics* (and brackets) indicate the sequencing results which did not have a strong sequence identity with the expected sequence and therefore suggesting that an undesired product was being amplified by the PCR. The genes were classified following their validation by RT-PCR, these genes were all dismissed, because they all displayed expression in a wide range of normal tissues.

Table 4.2. Summary of the sequencing results for the RT-PCR screen of the genes identified by the bioinformatics pipeline using the microarray analysis data

Gene	Primers	Normal tissue	Cancer sample	Sequence identity % *	Classification following validation
ACTB	F1 + R1	Testis	-	99.4	-
	F2 + R2	Testis	-	99.5	
MAGE-A1	F1 + R1	Testis	-	97.7	-
C1orf59	F1 + R1	Lung	-	98.0	Dismissed
		Ovary		99.5	
C9orf117	F1 + R1	Testis	-	99.1	Dismissed
		Lung		98.3	
		Trachea		95.7	
		Ova8ry		96.8	
CCDC109A	F1 + R1	Lung	-	99.3	Dismissed
		Ovary		98.4	
FHAD1	F1 + R1	Testis	-	100	Dismissed
		Lung		99.0	
		Ovary		99.5	
IQCG	F1 + R1	Lung	-	99.3	Dismissed
		Ovary		99.1	
LRRC69	F1 + R1	Testis (upper band)	-	99.8	Dismissed
		Testis (lower band)		97.7	
		Spinal cord		99.5	
		Spleen (upper band)		93.4	
		Thymus (upper band)		99.5	
		(Brain, cerebellum)		*(52.2)*	
PPP4R4	F1 + R1a	Lung	-	100	Dismissed
		Ovary		99.2	
	F1 + R1b	Lung		91.5	
		Ovary		77.5	
SAMD13	F1 + R1	Ovary	-	98.6	Dismissed
TDRD5	F1 + R1	Testis (upper band)	-	97.5	Dismissed
		Stomach (upper band)		97.3	
		Ovary (upper band)		99.2	

*The percentage of pair wise residues which are identical in the alignment, including gap versus non-gap residues, but excluding gap versus gap residues; calculated using Geneious software.

The sequences recovered from sequencing were aligned with the expected PCR product sequence using the Geneious software; see Appendix for the corresponding sequence alignments.

4.3 Screening genes identified from the EST-based pipeline

4.3.1 Genes identified in the EST pipeline to be screened

The EST pipeline identified a large number of genes with predicted meiosis-specific expression in normal tissues, 23 of these genes were randomly selected for screening here. Details of the predicted meiosis-specific genes and their functions are given in Table 4.3.

Table 4.3. Predicted meiosis-specific genes identified from the EST pipeline and their functional roles

Gene	Known Function	Reference
	CLASS 1: Cancer/Testis-restricted	
C17orf98	Uncharacterised protein, function unknown	-
HSPB9 (CT51)	Testis specific human small heat shock protein, with a possible role in spermatogenesis. Expression has been reported in testis, lung and pancreas normal tissues	De Wit *et al.*, 2004 Vos *et al.*, 2009
LRRC69*	Leucine rich repeat containing 69, precise function not known	-
	CLASS 2: Testis-restricted	
ARL13A	ADP-ribosylation factor-like 13A, precise function not known	-
C1orf85	Uncharacterised protein, function unknown	-
C5orf47	Uncharacterised protein, function unknown	-
C7orf72	Uncharacterised protein, function unknown	-
C17orf105	Uncharacterised protein, function unknown	-
CYLC1	Proposed to encode a basic protein of the sperm head cytoskeleton, but it appears to be expressed in other cell types such as brain and kidney cells and may be expressed at low levels in cells of lymphoid origin	Siddiqui *et al.*, 2009
DUSP21	Dual specificity phosphatatse 21; functions to remove phosphate groups from phosphotyrosine and phosphothreonine residues	Hood *et al.*, 2002
EFCAB9	EF-hand calcium binding domain 9, precise function not known	-
MAS1	Transmembrane G-protein-coupled receptor. Acts as a receptor for angiotensin-(1-7) and activates the phospholipase C signalling pathway. Possible role in hypotension, smooth muscle relaxation and cardioprotection by mediating the effects of angiotensin-(1-7)	Canals *et al.*, 2006 Kostenis *et al.*, 2005
MS4A13	Membrane-spanning 4-domains, subfamily A member 13, precise function unknown	-
PSMA8	Proteasome (prosome, macropain) subunit, alpha type-8, precise function not known	-
SLC25A2	Likely to play a role in metabolism as a mitochondrial transport protein. Reported to display tissue specificity for liver, kidney, pancreas and cultured fibroblasts	Camacho *et al.*, 2003
SYCP3*	Synaptonemal complex component	
USP50	Role at the G_2/M checkpoint in mitosis	Aressy *et al.*, 2010
ZCCHC13	Zinc finger CCHC domain 13, precise function not known	
	CLASS 3: Cancer/Testis/CNS-restricted	
ADAD1	Adenosine deaminase domain containing 1 (testis-specific), precise function not know	-
CATSPER1	Cation channel sperm associated-1; meiotically and post-meiotically expressed in human testis tissue. Calcium ion channel required for sperm mobility and hyperactivation	Li *et al.*, 2006
SNTG1	Syntrophin, gamma 1; precise function unknown, but expression has been reported in the CNS	Piluso *et al.*, 2000
SOX30	SRY (sex determining region Y)-box 30; transcriptional activator with a possible role in spermatogonial differentiation and spermatogenesis	Han *et al.*, 2010 Osaki *et al.*, 1999
	CLASS 4: Testis/CNS-restricted	
PTPN20A	Protein tyrosine phosphatase, non-receptor type 20A; widely expressed in cell lines with a possible role in the modulation of actin dynamics or cellular processes dependent on cytoskeletal re-organisation	Fodero-Tavoletti *et al.*, 2005

*Screened during the initial screen (Chapter 3.0)/the microarray analysis screen (Section 4.2), but was also identified by the bioinformatics tool using the EST analysis data.

The genes were classified after the EST analysis pipeline and this classification is indicated for each of the selected genes in Table 4.3. Two of the genes identified by the EST pipeline were also identified as predicted meiosis-specific genes in one of the two strategies previously described; *SYCP3* was identified from the literature and was screened during the initial screen, as described in Chapter 3.0, and *LRRC69* was identified from the microarray data analysis and was screened as described in Section 4.2.

Several pairs of primers were designed for both *MS4A13* and *USP50*, but RT-PCR was unsuccessful for these two genes and therefore they could not be screened for expression in the normal tissues or the cancer cell lines and tissues. A study by Aressy *et al.*, (2010) suggests a possible functional role for *USP50* in mitosis; this gene would therefore not have fitted the expected expression profile of a CT antigen gene.

4.3.2 RT-PCR with normal tissues

The genes listed in Table 4.3 were screened for expression in a range of 21 normal tissues, in order to assess their meiosis-specificity and their potential as a CT antigen gene. RNA preparations from a range of normal human tissues (obtained *post mortem*) were purchased from Clontech and Ambion. Intron-spanning primers were designed where possible and RT-PCR was carried out using cDNA synthesised from the RNA preparations. The coding sequences for four of these genes did not contain any introns and therefore intron-spanning primers could not be designed for the following genes; *HSPB9*, *MAS1*, *ZCCHC13* and *DUSP21*. The RT-PCR expression profiles for the EST pipeline genes which displayed expression in multiple normal non-testis/CNS tissues are shown in Figure 4.2.

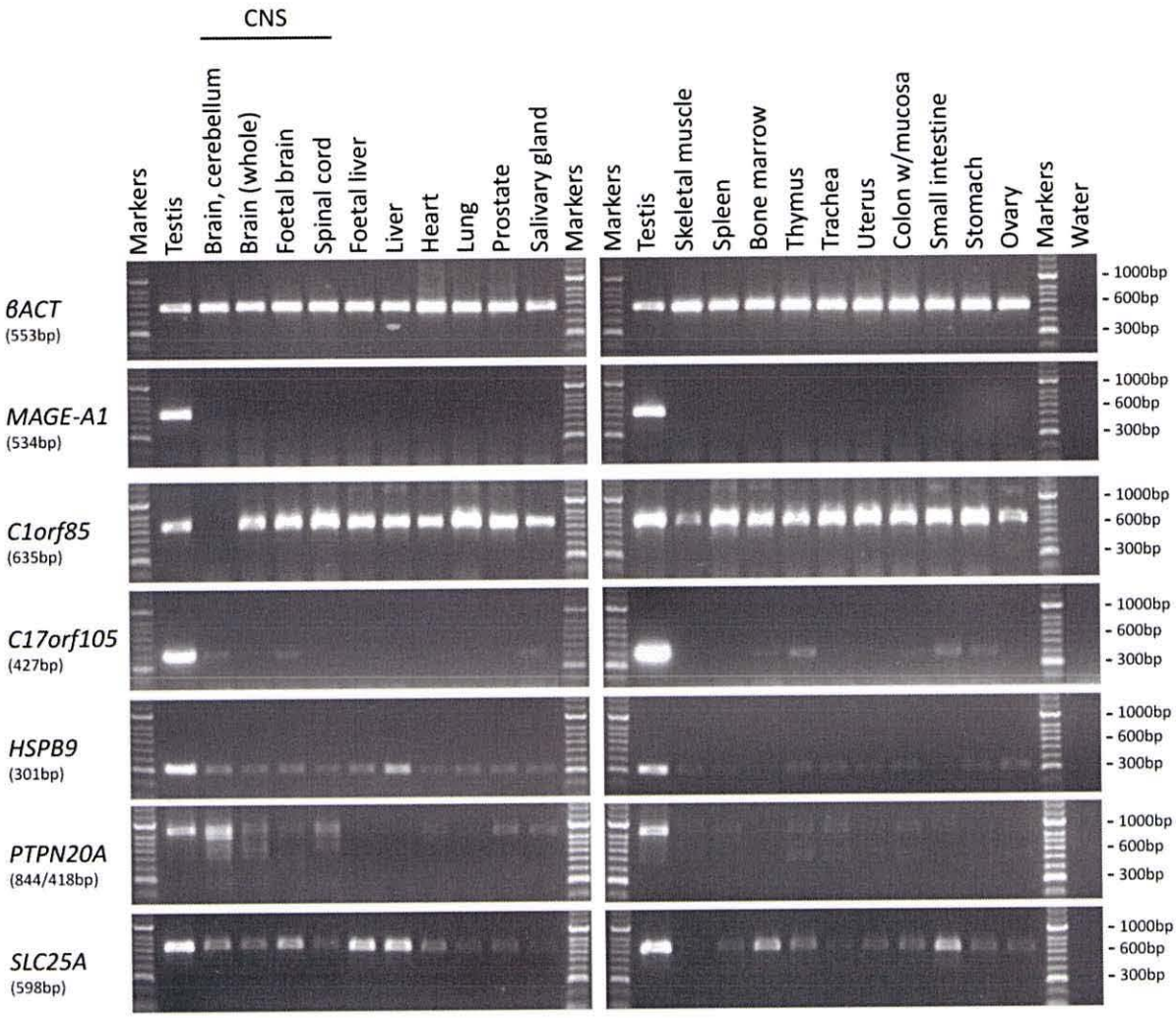

Figure 4.2. RT-PCR profiles for the genes dismissed from the EST pipeline analysis. Agarose gels showing the RT-PCR profiles of the genes from the EST pipeline which were dismissed; *c1orf85*, *c17orf105*, *HSPB9*, *PTPN20A* and *SLC25A* (the expected PCR product size is shown in brackets). cDNA was generated from the total RNA prepared from 21 normal human tissues (obtained *post mortem*). All of these genes were found to display expression in multiple non-testis and/or CNS tissues. The expression profile for *βACT* is shown as a positive control for the cDNA samples (top) and the expression profile of *MAGE-A1*, a known CT antigen gene, to show the expression profile of a CT antigen gene in normal tissue (top). These results appear to be reproducible as these PCRs were repeated at least three times.

HSPB9 was identified as a CT gene, with testis-specific expression in normal tissues, in a study by De Wit and colleagues (2004). Here, however *HSPB9* appears to be widely expressed because the RT-PCR profile shows a strong band in the testis and a faint band in all of the other normal tissues tested. Intron-spanning primers could not be designed for *HSPB9*, therefore we cannot rule out the possibility of genomic DNA contamination giving rise to this expression profile. However, genomic DNA contamination is not apparent in the

gene expression profiles of the other genes, for which intron-spanning primers were used, therefore *HSPB9* was dismissed as a CT gene candidate.

The two uncharacterised genes, *c1orf85* and *c17orf105*, were found to display expression in multiple normal tissues. Expression was observed for *c1orf85* in all of the normal tissues tested except for the cerebellum; it may be potentially interesting that this gene appears to be expressed in the brain but not in the cerebellum. Whereas a faint band was observed for *c17orf105* in a wide range of normal tissues, but it does not appear to be as widely expressed as *c1orf85*. *PTPN20A* was previously found to be widely expressed in cell lines (Fodero-Tavoletti *et al.*, 2005) and *SLC25A* was reported to display expression in normal tissues (Camacho *et al.*, 2003). Here, both *PTPN20A* and *SLC25A* were both found to display expression in multiple normal tissues, in line with what has been previously reported for these genes. The PCR products were purified and sequenced to ensure the primers were amplifying the correct sequence (summarised in Table 4.4). These five genes were all dismissed, as their expression profiles did not fit that of a CT antigen gene in normal tissues.

Another gene identified from the EST pipeline was dismissed due to its expression profile; *SNTG1*. Although *SNTG1* was class 3 gene (cancer/testis/CNS-restricted) after EST pipeline analysis, this gene did not appear to display any expression in the normal testis tissue. With no apparent expression in the normal testis, *SNTG1* does not appear to fit the expression profile of a CT antigen gene in normal tissues. *SNTG1* expression appears to be restricted to the CNS and spleen tissues, as shown in Figure 4.3.

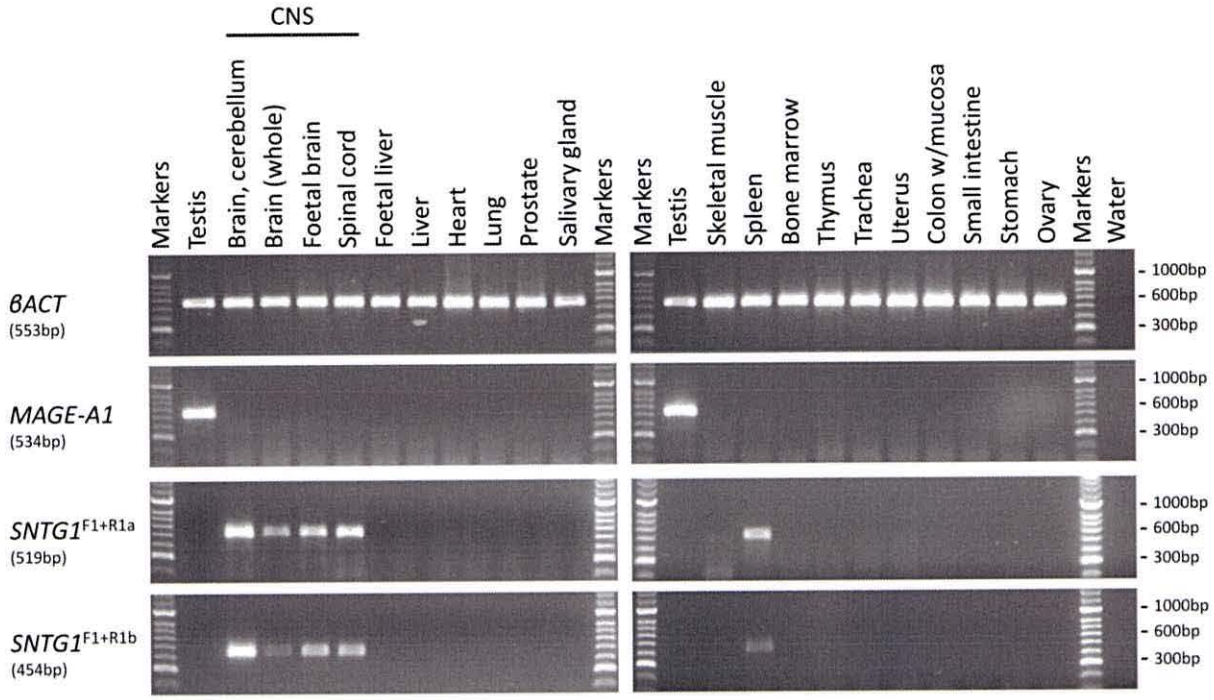

Figure 4.3. RT-PCR profile for *SNTG1* in normal human tissues. Agarose gels showing the RT-PCR profile of the *SNTG1* (the expected PCR product size is shown in brackets) using cDNA which was generated from the total RNA from 21 normal human tissues (obtained *post mortem*). *SNTG1* displays expression in all of the CNS samples tested, as well as in the spleen, with no expression in the testis, which was confirmed with the use of two pairs of primers. *SNTG1* was dismissed due to this apparent CNS-selective expression profile in the normal tissues. The expression profile for *βACT* is shown as a positive control for the cDNA samples (top) and the expression profile of *MAGE-A1*, a known CT antigen gene, to show the expression profile of a CT antigen gene in normal tissue (top). These results appear to be reproducible as these PCRs were repeated at least three times.

The remaining 13 genes displayed more meiosis-specific expression profiles, which have been categorised into three groups depending on the expression profile observed in the normal tissues; testis-restricted, testis-selective and testis/CNS-selective. Nine of the genes identified from the EST pipeline displayed a testis-restricted expression profile in the normal human tissues. The RT-PCR profiles for these genes are shown in Figure 4.4.

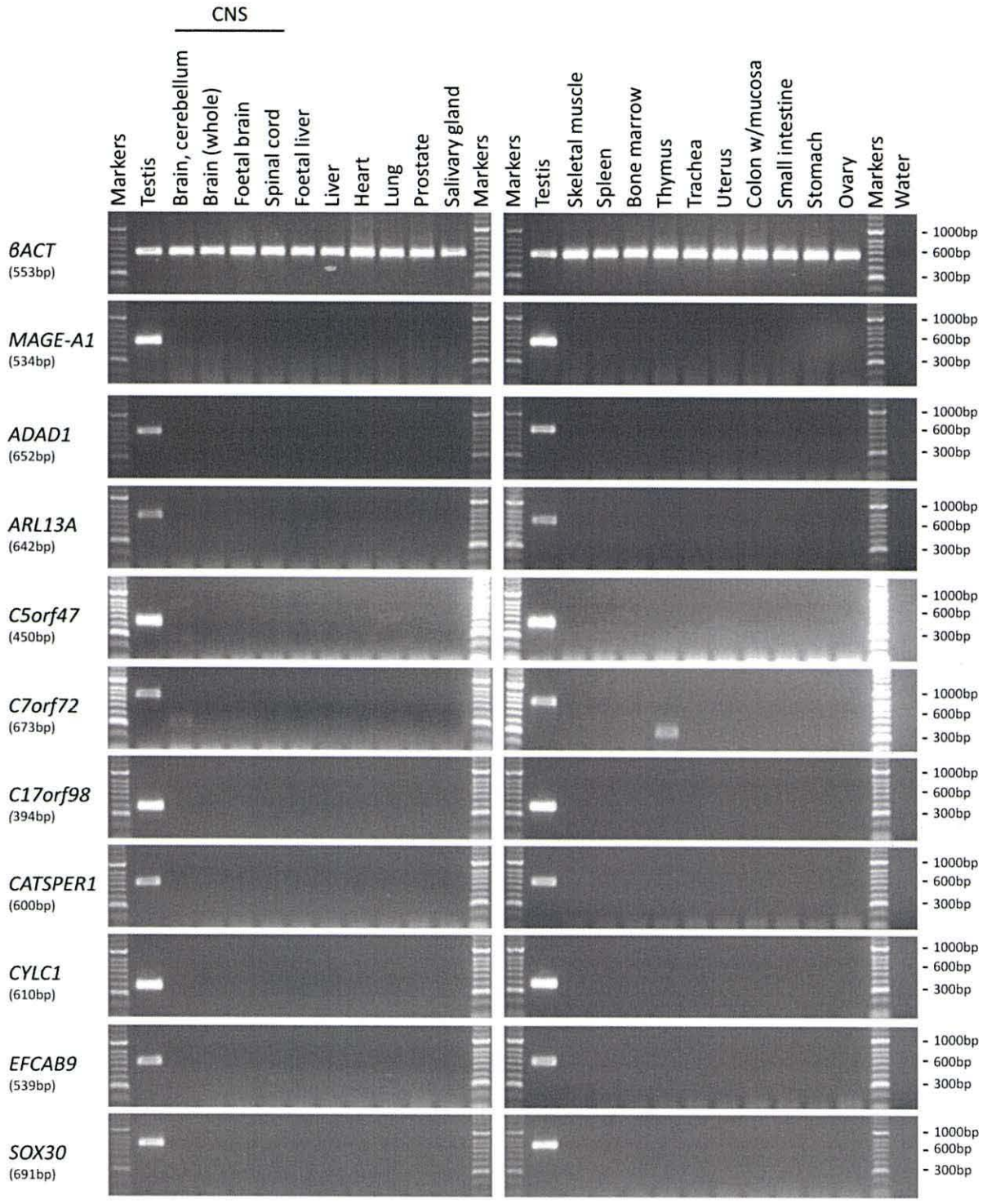

Figure 4.4. RT-PCR profiles for the testis-restricted genes, from the EST pipeline, with normal human tissues. Agarose gels showing the RT-PCR profiles for the testis-restricted genes from the EST analysis (the expected PCR product size is shown in brackets). cDNA was generated from the total RNA from 21 normal human tissues (obtained *post mortem*). The expression profile for *βACT* is shown as a positive control for the cDNA samples (top) and the expression profile of *MAGE-A1*, a known CT antigen gene, to show the expression profile of a CT antigen in normal tissue (top). These results appear to be reproducible as these PCRs were repeated at least three times.

The expression profiles for these nine genes are clearly testis-restricted, as no expression is observed in any of the non-testis normal tissues, except for *c7orf72*. The RT-PCR expression profile of *c7orf72* shows a band of unexpected size (approximately 300 bp) in the cerebellum and thymus normal tissues. Sequencing of this PCR product did not show any significant sequence similarity to *c7orf72* (sequencing results summarised in Table 4.4); therefore *c7orf72* was found to display a testis-restricted expression profile in the normal tissues tested. This expression profile fits that of a meiosis-specific gene and that of a CT antigen gene in normal tissues, these genes were therefore not dismissed.

Of the nine genes displaying a testis-restricted expression profile here, only six genes were predicted to be testis-restricted according to the classification of the genes from the original EST data. One of these genes was classified as cancer/testis-restricted, *c17orf98*, and five genes were classified as testis-restricted according to the expression profile observed in the EST data, *ARL13A*, *c5orf48*, *c7orf72*, *CYLC1* and *EFCAB9*. Whereas, *ADAD1*, *CATSPER1* and *SOX30* were classified as cancer/testis/CNS-restricted according to the expression profiles observed in the original EST data.

Four of the genes identified by the EST pipeline displayed less meiosis-restricted expression profiles, as they displayed additional expression in non-testis/CNS normal tissues. One of these genes displayed a testis-selective expression profile in the normal tissues; *DUSP21*. The RT-PCR profile for *DUSP21* is shown in Figure 4.5.

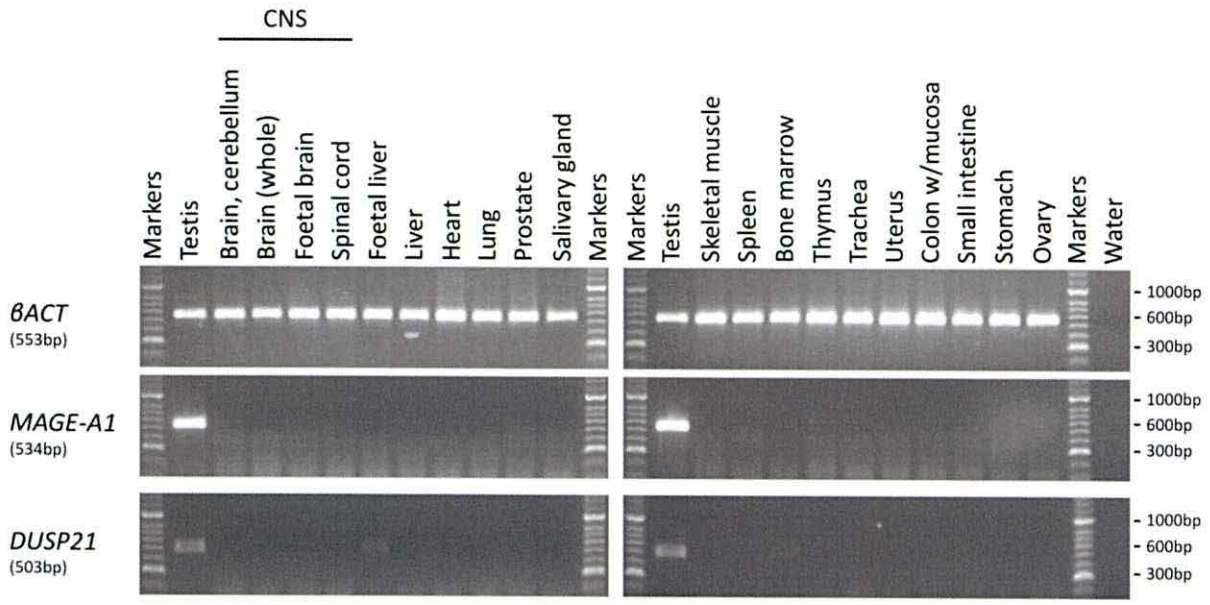

Figure 4.5. RT-PCR profiles for the testis-selective gene, from the EST pipeline, with normal human tissues. Agarose gels showing the RT-PCR profile for the testis-selective gene, *DUSP21*, identified from the EST pipeline (the expected PCR product size is shown in brackets). cDNA was generated from the total RNA from 21 normal human tissues (obtained *post mortem*). *DUSP21* appears to be expressed in the foetal liver and bone marrow normal tissues as well as in normal testis, therefore following a testis-selective expression profile. The expression profile for *βACT* is shown as a positive control for the cDNA samples (top) and the expression profile of *MAGE-A1*, a known CT antigen gene, to show the expression profile of a CT antigen gene in normal tissue (top). These results appear to be reproducible as these PCRs were repeated at least three times.

DUSP21 was originally classified as a testis-restricted gene according to the expression profile observed in the original EST data. However, expression was observed in the foetal liver and bone marrow tissues in addition to the normal testis tissue (see Table 4.4 for sequencing results). Therefore *DUSP21* was classified as testis-selective according to its expression profile in the normal human tissues tested here, and was not dismissed.

The remaining three genes were found to display testis/CNS-selective expression profiles in the normal tissues; *MAS1*, *PSMA8* and *ZCCHC13*. The RT-PCR profiles for *MAS1*, *PSMA8* and *ZCCHC13* are shown in Figure 4.6.

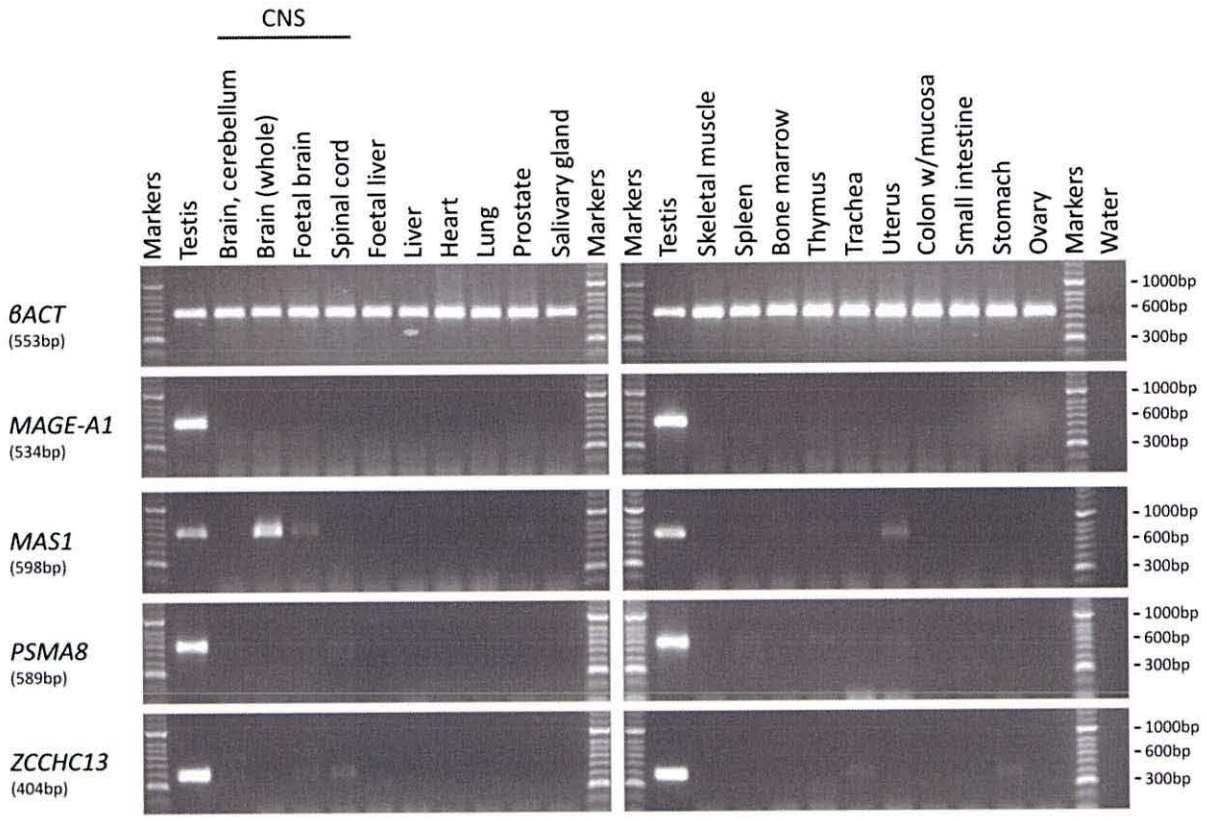

Figure 4.6. RT-PCR profiles for the testis/CNS-selective genes, from the EST pipeline, with normal human tissues. Agarose gels showing the RT-PCR profiles for the testis/CNS-selective genes from the EST pipeline (the expected PCR product size is shown in brackets). cDNA was generated from the total RNA from 21 normal human tissues (obtained *post mortem*). Expression of *MAS1*, *PSMA8* and *ZCCHC13* was shown in a number of normal tissues as well as in the testis and CNS normal tissues, thus following the testis/CNS-selective profile. The expression profile for *βACT* is shown as a positive control for the cDNA samples (top) and the expression profile of *MAGE-A1*, a known CT antigen gene, to show the expression profile of a CT antigen gene in normal tissue (top). These results appear to be reproducible as these PCRs were repeated at least three times.

MAS1, *PSMA8* and *ZCCHC13* were all class 2 genes (testis-restricted genes); according to their expression profiles observed in the EST data. However, these RT-PCR results show testis/CNS-selective expression profiles for these genes. *MAS1* shows additional expression in the following CNS tissues; brain (whole) and foetal brain, with fainter bands for the following non-CNS tissues; prostate, bone marrow, thymus and uterus. Expression of *PSMA8* was shown in the following CNS-tissues; foetal brain and spinal cord, with fainter bands indicating expression in the following non-CNS tissues; prostate, thymus, trachea and uterus. *ZCCHC13* expression was shown in three CNS tissues; brain (cerebellum), foetal brain and spinal cord, and two non-CNS tissues; trachea and stomach. PCR products were purified and sequenced to ensure the correct target was being amplified, sequencing results are summarised in Table 4.4.

4.3.3 RT-PCR with cancer samples

RT-PCR for the candidate genes identified from the EST pipeline found that 13/21 genes displayed an expression profile similar to that expected of a CT antigen gene in normal tissues. The expression of these genes was then assessed by RT-PCR in a range of cancer cell lines and tissues. Eight of the genes which, were found to display a testis-restricted expression profile in the normal tissues, displayed no measurable expression in the cancer cells also, as shown in Figure 4.7.

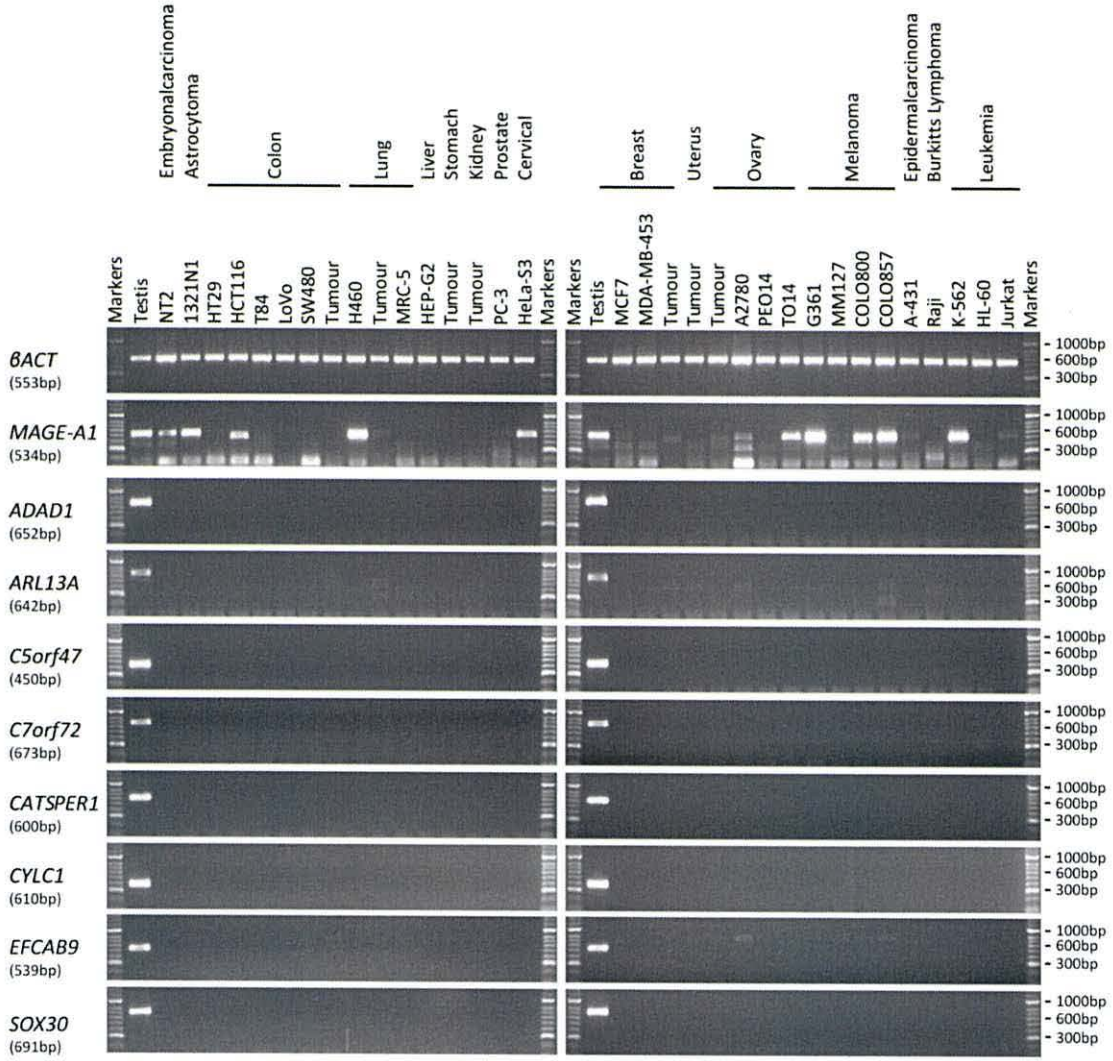

Figure 4.7. RT-PCR profiles for the testis-restricted genes, from the EST pipeline, with cancer cell lines and tissues. Agarose gels showing the RT-PCR profiles for the testis-restricted genes from the EST analysis (the expected PCR product size is shown in brackets). cDNA was generated from the total RNA extracted from cancer cell lines and tumour tissues. These genes all show expression in the normal testis tissue, with no expression in any of the cancer samples tested here. The expression profile for *βACT* is shown as a positive control for the cDNA samples (top) and the expression profile of *MAGE-A1*, a known CT antigen gene, to show the expression profile of a CT antigen gene in normal tissue (top). These results appear to be reproducible as these PCRs were repeated at least three times.

No expression was observed in the cancer cell lines or tissues for these eight genes, therefore these genes have been classified as testis-restricted after validation. Although these genes were not found to display any expression in the cancer cell lines and tissues tested here, they were not dismissed as potential CT antigen candidate genes. Further screening of these genes may highlight expression in cancer cell lines and/or tissues not covered within the range tested here.

Five of the genes which appeared to fit the expression profile of a CT antigen in the normal tissues, were found to display expression in one or more of the cancer cell lines and/or tissues. The expression profiles for *c17orf98*, *DUSP21*, *MAS1*, *PSMA8* and *ZCCHC13* are shown in Figure 4.8.

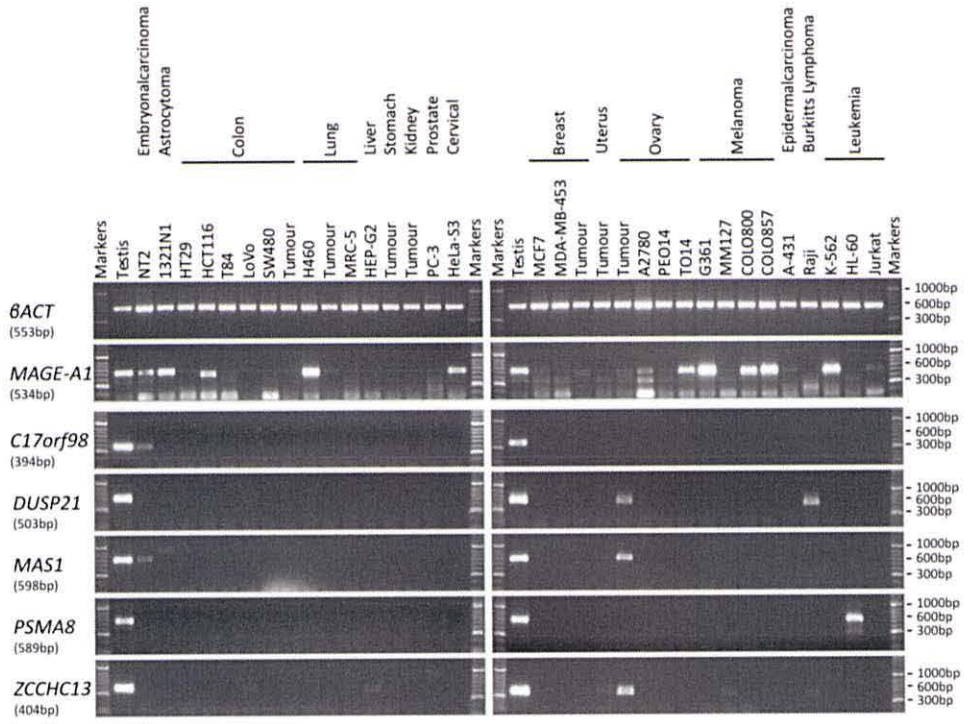

Figure 4.8. RT-PCR profiles for the potential CT antigen genes identified from the EST pipeline, with cancer cell lines and tissues. Agarose gels showing the RT-PCR profiles for the potential CT antigen genes, identified via the EST pipeline, which were positive for expression in the cancer cell lines and tissues (the expected PCR product size is shown in brackets). Expression of *c17orf98* was restricted to normal testis and NT2, an embryonalcarcinoma cell line, in the samples screened here, fitting the expected expression profile of a CT-restricted gene. *DUSP21* expression was shown in three cancer samples, two cell lines and one tumour tissue, fitting the expression profile of a testis-selective CT antigen gene. Expression was observed in one or more cancer cell line and/or tumour tissue for *MAS1*, *PSMA8* and *ZCCHC13*, therefore these genes appear to fit a CT/CNS-selective profile. The expression profile for *βACT* is shown as a positive control for the cDNA samples (top) and the expression profile of *MAGE-A1*, a known CT antigen gene, to show the expression profile of a CT antigen gene in normal tissue (top). These results appear to be reproducible as these PCRs were repeated at least three times.

Expression of *c17orf98* was restricted to the testes in the normal tissues, with additional expression also being shown in NT2 (an embryonalcarcinoma cell line) therefore fitting the expression profile of a potential CT-restricted CT antigen gene (see Table 4.4 for sequencing results). *C17orf98* was originally categorised in class I, according to the expression profile observed in the EST data, therefore these RT-PCR results appear to correspond to the expression profile found in the collated EST data.

DUSP21, *MAS1*, *PSMA8* and *ZCCHC13* were class 2 genes (testis-restricted) in the original classification according to the expression profiles observed in the EST data. However, RT-PCR analysis showed that the expression profiles of these four genes did not fit that of a testis-restricted gene. *DUSP21* was found to display a testis-selective expression profile, and *MAS1*, *PSMA8* and *ZCCHC13* were found to fit a testis/CNS-selective profile in the normal tissues. RT-PCR also showed *DUSP21* expression in a number of cancer samples; two cancer cell lines (LoVo and Raji) and one tumour tissue (uterus). Therefore *DUSP21* appears to fit the expression profile of a CT gene, with a CT-selective profile. Expression of *MAS1* was observed in two cell lines (NT2 and LoVo) and one tumour tissue (ovary), and expression of *PSMA8* was observed in one leukemia cell line (HL-60). *ZCCHC13* expression was shown in five cancer cell lines (LoVo, HEP-G2, PC-3, MM127 and Raji) and four tumour tissues (stomach, kidney, uterus and ovary). These results suggest that *MAS1*, *PSMA8* and *ZCCHC13* appear to fit the expression profile of a CT gene, with a CT/CNS-selective expression profile. The PCR products were purified and sequenced to ensure that the correct product was being amplified (see Table 4.4).

As the purpose for this screen was to identify potential new CT antigen genes, which in turn could potentially be used as a cancer marker and/or therapeutic target, stringent criteria was set for this gene screen, with the aim of identifying strict CT genes. Any genes found to display expression in more than two non-testis/CNS normal tissues were dismissed as candidate CT genes. Therefore *MAS1* and *PSMA8* were dismissed, even though expression was observed in multiple cancer cell lines and/or tissues.

These results suggest that three new CT genes were identified through the EST pipeline gene screen; *c17orf98*, *DUSP21* and *ZCCHC13*.

4.4 Summary of the sequencing results for the genes identified from the EST pipeline

The genes were classified according to their expression profile observed by RT-PCR, into one of seven categories:

i. Dismissed; genes which displayed expression in multiple normal tissues and did not fit the expression profile of a CT antigen gene in normal tissues.

ii. Testis-restricted; genes which displayed a testis-restricted expression profile in the normal tissues, but did not display expression in any of the cancer cell lines or tissues tested here.

iii. Testis/CNS-restricted; genes which display expression in the testis and CNS normal tissues, but did not display expression in any of the cancer cells.

iv. Testis/CNS-selective; genes which displayed expression in the testis and CNS normal tissues with additional expression in up to two non-testis/CNS tissues, but did not display expression in any of the cancer cells.

v. CT-restricted; genes whose expression was restricted to the testes in the normal tissues, but also displayed expression in one or more cancer cell line and/or tissue.

vi. CT-selective; genes which displayed a testis-selective expression profile in the normal tissues, but also showed expression in one or more cancer cell line and/or tissue.

vii. CT/CNS-selective; genes which displayed a testis/CNS-selective expression profile in the normal tissues, but also displayed expression in one or more cancer cell line and/or tissue.

The PCR products were purified and sequenced to ensure that the correct sequence was being amplified, the sequencing results and the gene classifications following validation by RT-PCR are summarised in Table 4.4. The original gene classifications from the EST pipeline data have also been included in the table below. The sequencing results for the two control genes, *βACT* and *MAGE-A1* (a known CT antigen gene), are shown also. *Italics* (and brackets) indicate the sequencing results which did not have a strong sequence identity with the expected sequence and therefore suggesting that an unexpected product was being amplified by the PCR.

Table 4.4. Summary of the sequencing results for the RT-PCR screen of the genes identified by the EST-based pipeline

Gene	Primers	Sequenced in Normal tissue	Sequenced in cancer sample	Sequence identity % *	Classification following validation
ACTB	F1 + R1	Testis	-	99.4	-
	F2 + R2	Testis	-	99.5	
MAGE-A1	F1 + R1	Testis	-	97.7	-
CLASS 1: Cancer/Testis-restricted					
C17orf98	F1 + R1	Testis	-	99.5	CT restricted gene
HSPB9	F1 + R1	Testis	-	96.0	Dismissed
(CT51)		Liver		95.1	
LRRC69*	F1 + R1	-	-	-	Dismissed
CLASS 2: Testis-restricted					
ARL13A	F1 + R1	Testis	-	99.5	Testis-specific gene
C1orf85	F1 + R1	Testis	-	99.4	Dismissed
C5orf47	F1 + R1	Testis	-	99.3	Testis-specific gene
C7orf72	F1 + R1	Testis	-	99.2	Testis-specific gene
		(Brain, cerebellum)		*(54.3)*	
		(Thymus (lower))		*(53.1)*	
C17orf105	F1 + R1	Testis		99.0	Dismissed
		Brain (cerebellum)		99.3	
			NT2	98.6	
CYLC1	F1 + R1	Testis	-	99.6	Testis-specific gene
DUSP21	F1 + R1	Testis	-	98.3	CT selective gene
		Bone marrow		98.4	
		Foetal liver		98.9	
EFCAB9	F1 + R1	Testis	-	98.1	Testis-specific gene
MAS1	F1 + R1	Brain (whole)	-	99.2	Dismissed
		Prostate		99.5	
		Bone marrow		99.5	
		Thymus		99.5	
		Uterus		100	
PSMA8	F1 + R1	Testis		97.9	Dismissed
		Brain (cerebellum)		97.9	
		Spinal cord		97.2	
		Thymus		95.2	
		Uterus		96.3	
			HL-60	100	
SLC25A2	F1 + R1	Testis	-	99.1	Dismissed
		Liver		87.1	
		Bone marrow		86.4	
SYCP3*		Chapter 3.0			Testis-restricted
ZCCHC13	F1 + R1	Testis	-	99.7	CT/CNS selective gene
		Spinal cord		98.3	
		Stomach		100	
CLASS 3: Cancer/Testis/CNS-restricted					
ADAD1	F1 + R1	Testis	-	99.7	Testis-specific gene
CATSPER1	F1 + R1	Testis	-	98.3	Testis-specific gene
SNTG1	F1 + R1a	Brain (cerebellum)	-	98.8	Dismissed
		Spinal cord		99.4	
		Spleen		99.1	
	F1 + R1b	Brain (cerebellum)		99.5	
		Spinal cord		98.3	
		Spleen		98.5	
SOX30	F1 + R1	Testis	-	99.8	Testis-specific gene

CLASS 4: Testis/CNS-restricted					
PTPN20A	F1 + R1	Testis	-	99.6	Dismissed
		Brain (cerebellum)		98.1	
		Foetal brain		97.5	

*The percentage of pairwise residues which are identical in the alignment, including gap versus non-gap residues, but excluding gap versus gap residues calculated using Geneious software.
**Genes identified and screened either the initial screen or the microarray analysis screen, but were also identified through the EST pipeline.

The sequences recovered from sequencing were aligned with the expected PCR product sequence using the Geneious software; see Appendix for the corresponding sequence alignments.

4.5 Discussion

4.5.1 Summary of RT-PCR expression profiles

The two bioinformatics screening approaches identified a much larger number of potential meiotic genes than the initial literature search, including a large number of previously uncharacterised genes. A significant number of these predicted meiotic genes were found to display expression in multiple non-testis normal tissues. The expression profiles observed for the predicted meiotic genes, identified through the microarray analysis and EST pipelines, in normal tissues and cancer samples are summarised in Figures 4.9 and 4.10 respectively.

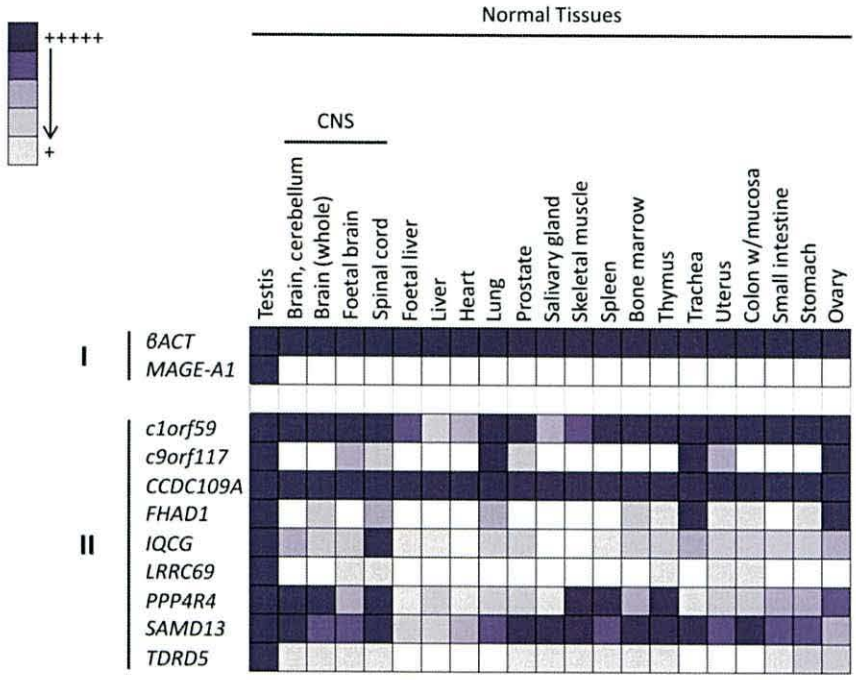

Figure 4.9. Chart summarising the gene expression profiles for the genes identified by the microarray analysis pipeline. The expression profile of each gene is represented by a row in the grid, with the columns corresponding to the normal human tissues used. The intensity of each PCR product viewed in an ethidium bromide stained agarose gel was ranked 1-5, which is represented in the grid with various shades of purple, thus giving a qualitative representation of the RT-PCR profiles relative to the intensity of the PCR product in the testis. The darkest shade of purple signifies PCR products ranked 5 (strong band), with lighter shades indicating fainter bands (see key, top left). **I.** The expression profiles of the control genes; *βACT* and *MAGEA1*. **II.** The expression profiles for the microarray analysis genes, these genes all showed expression in multiple normal tissues and were dismissed.

The microarray analysis pipeline identified 40 genes with a predicted meiosis-specific expression profile and 10 of these genes were randomly selected for screening here. A literature search revealed that *PLD6* was widely expressed (Kerkel *et al.*, 2010). This gene was therefore dismissed and not screened by RT-PCR, because this expression profile does not fit the expression profile of a CT antigen gene. RT-PCR analysis of the remaining nine genes showed expression in multiple normal tissues, with many of the genes being apparently widely expressed, thus not in line with a meiosis-specific expression profile. All nine genes were dismissed as candidate CT genes.

The EST pipeline identified 177 predicted meiosis-specific genes, and 23 of these genes were randomly selected for screening here. RT-PCR was unsuccessful for two of the genes; *MS4A13* and *USP50*; which therefore could not be analysed for expression in the normal tissues and/or the cancer cells. However, a role in mitosis has previously been suggested for

USP50 (Aressy *et al.*, 2010), therefore this gene would probably not have fitted a meiosis-specific expression profile had RT-PCR been successful. Another two of the genes identified by the EST pipeline; *SYCP3* and *LRRC69*; were also identified and screened during the initial screen (Chapter 3.0) and microarray analysis pipeline screen (Section 4.2) respectively. The expression profiles for the remaining 19 genes are shown in Figure 4.10.

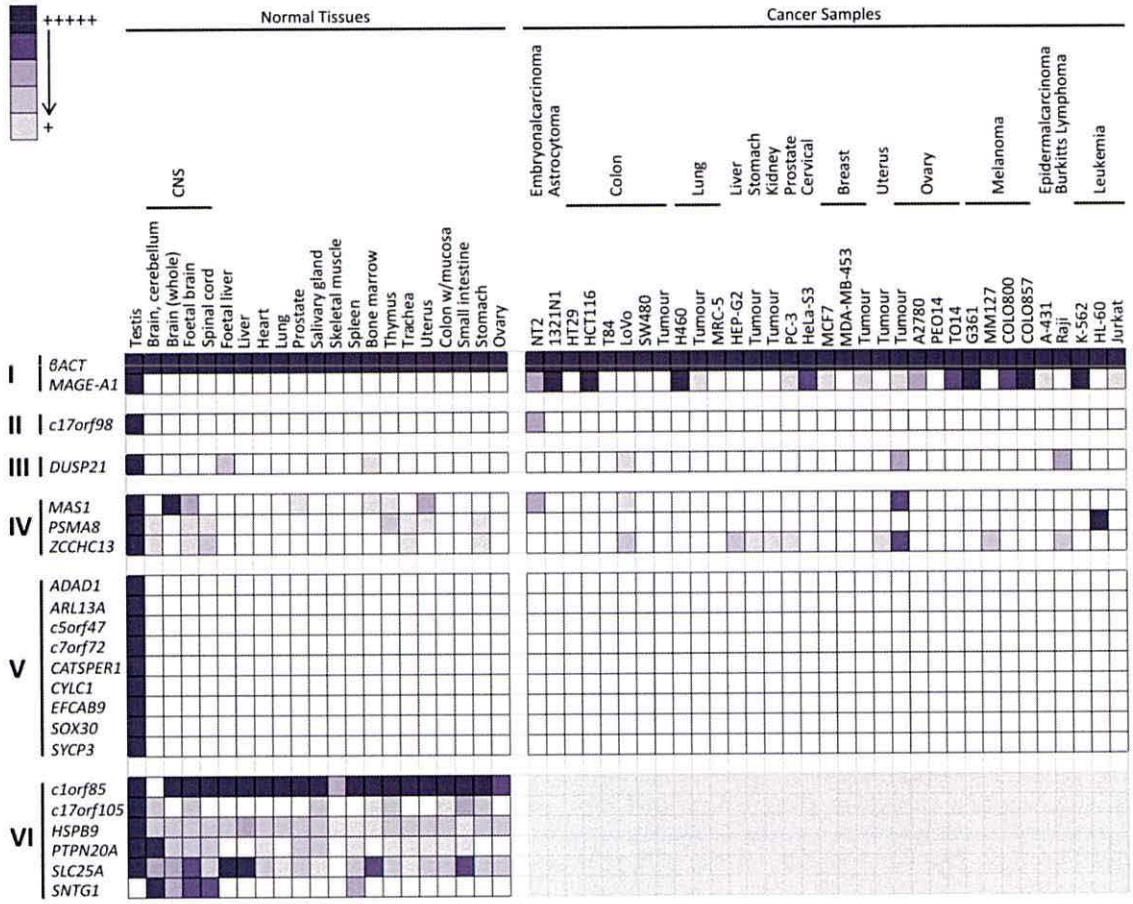

Figure 4.10. Chart summarising the gene expression profiles for the genes identified by the EST pipeline. The expression profile of each gene is represented by a row in the grid, with the columns corresponding to the tissues and cell lines used. The intensity of each PCR product viewed in an ethidium bromide stained agarose gel was ranked 1-5, giving a qualitative representation of the RT-PCR profiles relative to the intensity of the PCR product in the testis. Which is represented in the grid with various shades of purple; the darkest shade of purple signifies PCR products ranked 5 (strong band), with lighter shades indicating fainter bands (see key, top left). **I.** The expression profiles of the control genes; *βACT* and *MAGEA1*. **II.** CT-restricted gene; *c17orf98*. **III.** CT-selective gene; *DUSP21*. **IV.** CT/CNS-selective genes; *MAS1*, *PSMA8* and *ZCCHC13*. **V.** Testis-restricted genes. **VI.** Predicted meiosis-specific genes which were shown to display expression in multiple normal tissues.

This screen therefore identified 3 of the 23 genes as potential novel CT genes. These three genes have been characterised after validation as follows; *c17orf98* is a CT-restricted gene, *DUSP21* is a CT-selective gene and *ZCCHC13* is a CT/CNS-selective gene.

4.5.2 Dismissed genes

Six of the 19 predicted meiosis-specific genes (identified via the EST analysis pipeline) screened here were dismissed because their RT-PCR profiles did not fit that of a meiosis-specific gene and thereby a CT antigen gene. In a previous study, *HSPB9* was identified as a CT antigen gene, with testis-specific expression in a range of 30 normal tissues (De Wit *et al.*, 2004). However, here the RT-PCR results suggest that *HSPB9* is more widely expressed, showing expression in all of the normal tissues tested here. A high number of PCR cycles were used here, and therefore may have potentially identified low levels of *HSPB9* expression which were not detected in the De Wit *et al.*, study. The qualitative RT-PCR analysis (Figure 4.10) showed significantly weaker PCR bands for *HSPB9* in the somatic tissues in relation to that observed for the normal testis tissue. Consequently, differences in the expression profiles observed for *HSPB9* may be due to differences in RT-PCR sensitivity. The sequencing results indicated that the correct PCR product was being amplified by the primers however, qRT-PCR could be carried out to quantitatively establish the level of *HSPB9* expression in these normal tissues. In addition, another study reported *HSPB9* expression in lung and pancreas normal tissues, which supports the wider expression profile for *HSPB9* shown here (Vos *et al.*, 2009).

The De Wit *et al.*, (2004) study also presented immunohistochemical evidence for HSPB9 protein in several lung and colon cancer tissues, which was not detected in normal lung and colon tissues. Although the RT-PCR results shown here suggest that *HSPB9* expression is not as testis-specific in normal tissue as previously reported, this expression may not correlate to HSPB9 protein in these somatic cells. Further analysis to assess the potential HSPB9 protein abundance in normal tissues may cause HSPB9 to be re-assessed/re-classified as a CT antigen.

Intron-spanning primers could not be designed for *HSPB9* and therefore the possibility of genomic DNA contamination in the cDNA samples cannot be discounted. However, the total RNA prepared from the various tissue samples were purchased from two commercial sources (Clontech and Ambion) and thus were purified and quality control checked. Intron-spanning primers could also not be designed for another three genes identified from the EST pipeline; *DUSP21*, *MAS1* and *ZCCHC13*; and although these genes did display expression in a number of normal tissues, they were negative for the majority of the normal tissues tested

here. Also, the correct PCR product size was observed for the other genes screened, using intron-spanning primers. This may therefore suggest that genomic DNA contamination is unlikely.

Here we defined the testis-selective classification as those genes which show expression in up to two normal tissues in addition to the testis and CNS tissues. Therefore, despite expression in a number of cancer cells, *MAS1* and *PSMA8* were also dismissed because expression of these genes was shown in more than two non-testis/CNS normal tissues.

4.5.3 Novel CT-restricted gene

The RT-PCR profile of *c17orf98* showed expression in the normal testis and NT2 (an embryonalcarcinoma cell line) only, this expression profile might indicate a germ cell related-expression as NT2 is a germ line tumour. Germ cells give rise to gametes (oocytes and spermatocytes); in adult males this process occurs in the testis and an embryonalcarcinoma is a germ cell tumour. Interestingly, not all of the predicted meiosis-specific genes displayed expression in NT2, which may suggest that that this expression is not due to residual expression from the testis. However, this does not discount the possibility that *c17orf98* expression may be due to the embryonal gene expression profile rather than the carcinoma gene expression profile.

A recent study demonstrated that the transformation of germ cells into germ cell tumour cells in mice requires a series of key events. The germ cells fail to enter mitotic G_0 arrest, pluripotency is retained and genes associated with meiotic germ cell differentiation are prematurely expressed (Heaney *et al.*, 2012). Expression of *c17orf98* in NT2 may prove interesting because the expression of meiosis-specific genes has been shown to aid tumorigenesis in germ cell tumours (Heaney *et al.*, 2012).

4.5.4 CT-selective genes

Expression of *DUSP21* was shown in three normal tissues; testis, foetal liver and bone marrow. The expression observed in the foetal liver does not pose a problem for the potential use of DUSP21 as a diagnostic marker or an immunotherapy target, in adults. A study by Fujisaki *et al.*, (2011) identified the bone marrow microenvironment as a site of immune privilege. Haematopoietic stem cells (HSCs) are multipotent stem cells and are essential for the production of lymphoid and myeloid cells which are involved in a multitude

of physiological processes such as blood clotting, waste removal and oxygen delivery. The HSCs reside in discrete stem cell niches within the bone marrow and it is these niches which have been demonstrated to display immune privilege (Fujisaki *et al.*, 2011; Nwajei and Konopleva, 2013). This may make DUSP21 a more attractive target for use as a potential diagnostic marker and/or therapeutic target.

The CT/CNS-selective gene, *ZCCHC13,* displayed a wider expression profile in the normal tissues, with expression observed in the testis, brain (cerebellum), foetal brain, spinal cord, trachea and stomach. The testis and the CNS (cerebellum, foetal brain and spinal cord) tissues are immune privileged sites (Carson *et al.*, 2009) and therefore should not hinder potential use of ZCCHC13. However, the trachea and stomach do not appear to be immune privileged sites and therefore may seriously limit any potential use for ZCCHC13 as a therapeutic target.

Although CT antigen gene expression within the CNS tissues has been considered as acceptable here due to immune privilege in the CNS, it is also worth mentioning that the CNS is not isolated from the immune system by the BBB. The normal immune regulatory mechanisms of the CNS can be altered or rendered dysfunctional by several factors, including age, disease, pathogen exposure and neurodegeneration. As CNS immune privilege contributes to the function of the healthy brain and spinal cord, BBB dysfunction can decrease CNS protection (Carson *et al.*, 2009). This may limit the potential use of the testis/brain CT antigens as immunotherapeutic targets; however they may still be used for diagnostic purposes. The most ideal CT antigen gene candidates for potential use as targets in immunotherapeutic treatments are those genes found to display CT-restricted expression profiles in the normal tissues, such as *c17orf98* identified here.

4.5.5 Testis-restricted genes

Eight of the 19 genes were shown to have a testis-restricted expression profile in the normal tissues and displayed no apparent expression in the cancer cell lines and/or tissues. These genes were not dismissed however, because the cancer samples screened here only represent a relatively small number of cancer cells/tissues and further screening may potentially reveal expression in cancer. Meta-analysis was carried out on the testis-restricted genes, using the CancerMA online tool (http://www.cancerma.org.uk; Feichtinger

et al., 2012b), to assess any potential gene expression these genes may exhibit in cancer microarray data. The meta-analysis results did not show a statistically significant mean up-regulation or down-regulation for *ARL13A*, *c7orf72* and *EFCAB9* in the cancer array data. However, a mean up-regulation was identified for the expression of five of these testis-restricted genes (*ADAD1*, *c5orf74*, *CYLC1*, *SOX30* and *SYCP3*) in ovarian cancer array data. The meta-analysis results also identified a mean up-regulation for *CATSPER1* and *SYCP3* expression in renal cancer and leukemia array data respectively. The results from this meta-analysis is summarised in Figure 4.11.

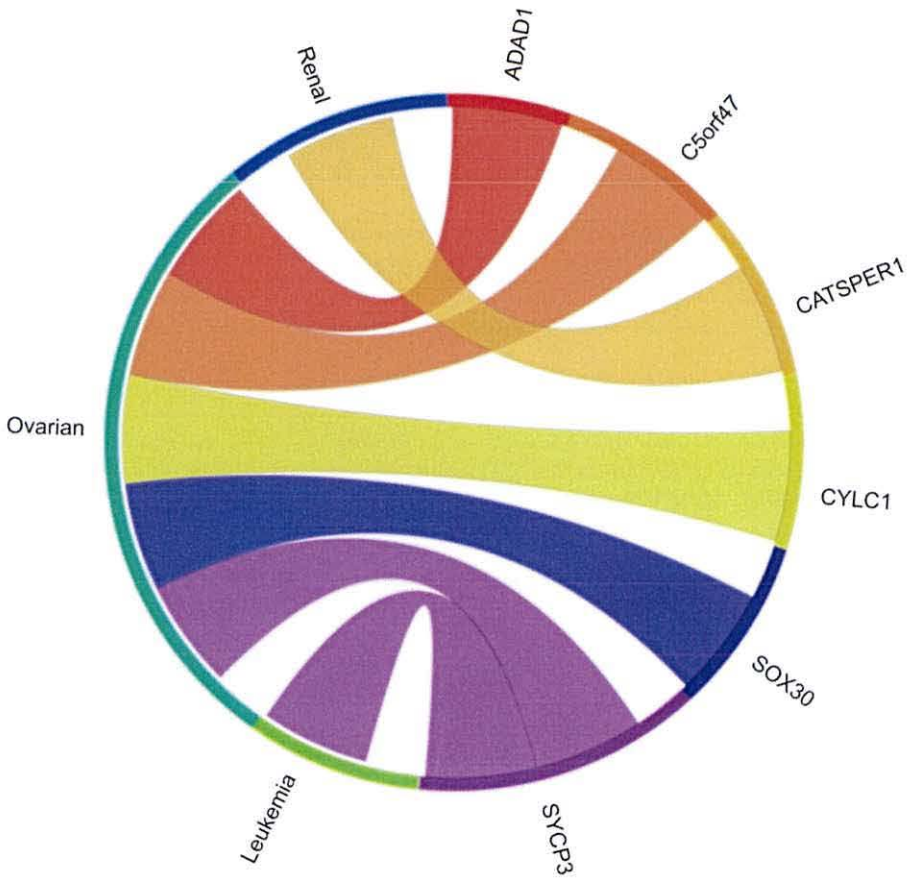

Figure 4.11. The Circos plot showing the meta-change in gene expression in relation to corresponding cancer types for the testis-restricted genes. The nine testis restricted genes were analysed using the CancerMA (http://www.cancerma.org.uk; Feichtinger *et al.*, 2012b) online tool; *ADAD1*, *ARL13A*, *c5orf47*, *c7orf72*, *CATSPER1*, *CYLC1*, *EFCAB9*, *SOX30* and *SYCP3*. Each connection between a gene and a cancer type indicates a statistically significant mean up-regulation for that type of cancer. The weight of each connection corresponds to the size of the meta-change in the gene expression. The CancerMA tool analysed the expression profiles of these nine genes using cancer array data from a number of combined array studies for cancer tissue *vs.* normal tissue.

A mean down-regulation was also identified for *CYLC1* expression in renal cancer and *SYCP3* expression in head and neck cancer array data. The results from the meta-analysis suggest that six of the nine testis-restricted genes identified here (and in Chapter 3.0) are expressed in clinically relevant material. Therefore this analysis has identified *ADAD1*, *c5orf47*, *CATSPER1*, *CYLC1*, *SOX30* and *SYCP3* as potential CT-restricted genes. *SYCP3* was found to have a testis-restricted expression profile in this screen (see Chapter 3.0), however it had previously been identified as a CT antigen gene. These meta-analysis results therefore provide further supporting evidence for *SYCP3* as a CT gene.

Interestingly, a large proportion of the CT genes identified here and in Feichtinger *et al.*, (2012a) appear to show a significant mean up-regulation in ovarian cancer array datasets. This may suggest that a high number of meiotic/CT genes are expressed or up-regulated in ovarian cancer. Ovarian cancer has previously been identified as have a high frequency of CT antigens (Caballero and Chen, 2009); therefore CT antigens may be potentially important for the development of diagnostic tools and/or treatments.

4.5.6 Validation of the bioinformatics pipeline

100% of the genes identified by the microarray analysis pipeline were dismissed, whereas only 43% of the genes identified by the EST pipeline were dismissed. These results suggest that the EST pipeline provides a more reliable tool for the identification of new CT genes than the microarray analysis pipeline. Although microarray analysis allows expression of thousands of genes to be surveyed in different populations of cells, it is limited by poor sensitivity and background noise which may result in false positives. This technique is also restricted by the lack of gene coverage on the array platforms and the number of high quality cancer microarrays available. Data collected from different microarray platforms cannot be accurately compared, making it difficult to collate data from multiple microarray datasets (Russo *et al.*, 2003). In comparison, the EST pipeline identified significantly fewer false positive genes. EST analysis appears to be a more sensitive approach, as a positive hit corresponds to positive gene expression. Every gene shown to give as few as one hit in the EST data analysis was screened (Feichtinger *et al.*, 2012a); thus giving rise to a highly stringent system. In contrast, the boundaries within a microarray analysis need to be defined, thus giving a trade off between background noise and signal.

ESTs are short, unedited, randomly selected, single pass DNA sequence reads derived from cDNA libraries, and are susceptible to errors because they are only sequenced once. Sequencing errors and differing error rates along each sequence may limit the EST analysis strategy. Contamination with DNA fragment, vector, linker, adaptor and chimeric sequences poses a problem in EST data construction. Sequencing artefacts and low quality sequences are frequently observed in ESTs, which can then lead to problems in the downstream analysis (Nagaraj *et al.*, 2006). Although the sensitivity of EST data analysis may be greater than that of microarray analysis, it is still limited by inherent problems in the construction of the cDNA libraries and the nature of ESTs, which may lead to redundancy, over-representation and under-representation of the selected host transcripts in the EST data (Nagaraj *et al.*, 2006). These limitations were highlighted in the RT-PCR results observed in this screen, because the gene classification based upon the expression profiles observed during the EST analysis did not match the gene classification after RT-PCR validation for many of the genes screened here. Also, as discussed in Chapter 3.0, there is evidence for microscopic cancers being present in healthy individuals, which remain dormant and asymptomatic (Naumov *et al.*, 2009). This might be why we miss/dismiss many candidates, as our 'normal' tissue may not be as normal as previously assumed.

Both microarray analysis and EST data analysis techniques have limitations; therefore validation of the bioinformatic pipelines was required. The results presented here suggest that the microarray analysis pipeline identified too many false positives, and is not a reliable tool for the identification of further genes. Validation of the EST-identified genes suggested that the EST pipeline is a powerful tool for gene identification and that meta-analysis is useful for the analysis of up-regulation of EST-based identified genes in tumour tissues. The results presented in Chapter 3.0 identified two novel CT genes, *RAD21L* and *SMC1β*; however these meiotic genes were not identified as candidate genes by the bioinformatics pipeline. This was probably due to the stringent criteria used for the bioinformatic pipeline approach and not the method.

In conclusion, three of the validated genes displayed a CT-restricted/selective expression profile and a further six of the testis-restricted genes show expression in cancer array datasets. Therefore, the systematic bioinformatic approach identified a larger number of genes to be screened, with many previously uncharacterised genes being highlighted. The

work presented here was undertaken as part of a larger CT gene screen undertaken by several members of the lab. The screen identified 42 genes which fit the expression profile of a CT antigen gene, results published in Feichtinger *et al.*, (2012a). These genes have been classified as meiCT genes as any possible antigenic potential is yet to be established. Further characterisation of these validated CT genes is required to establish the protein abundance (if any) of the corresponding gene products in cancer cells and in turn any potential antigenicity, or oncogenic function.

5.0 Characterisation of a potential CT antigen candidate in ovarian cancer cell lines

5.1 Introduction

Ovarian cancer is the fifth leading cause of death from cancer in women and causes more deaths than any other type of female reproductive cancer. In the USA there were 22,280 estimated new cases and 15,500 estimated deaths attributed to ovarian cancer in 2012 (Siegel *et al.*, 2012) with epithelial ovarian cancer accounting for the majority of ovarian cancers (Piek *et al.*, 2008; Zaman *et al.*, 2012). Ovarian cancer has been referred to as the 'silent killer' due to the non-specific nature of its presenting symptoms; for example, abdominal bloating, tiredness, back pain and pelvic pain. These ambiguous symptoms make an early diagnosis difficult and thus diagnosis often occurs during the advanced stages of the disease after regional or distant metastasis (Zaman *et al.*, 2012). The survival rates of ovarian cancer patients have barely improved over the past 40 years despite advances in chemotherapy. The five year survival rate for the advanced stage patients is less than 30% (Siegel *et al.*, 2012; Wright *et al.*, 2009).

Currently, diagnosis may involve a combination of the following; physical examination, transvaginal ultrasound and measurement of the serum glycoprotein CA-125 (Cancer Antigen 125). Elevated levels of CA-125 may also be indicative of other conditions, such as pregnancy, menstruation, endometriosis and other cancers, and has also been reported to detect less than 50% of early stage disease (Dodge *et al.*, 2012; Kan *et al.*, 2012). Using CA-125 as a marker for ovarian cancer diagnosis is less reliable than imaging using the transvaginal ultrasound; however this is a very invasive and expensive technique for routine diagnosis. High quality screening programmes have previously been shown to significantly reduce mortality rates, for example implementation of cervical cancer screening has been hugely successful in aiding early diagnosis (Siegel *et al.*, 2012). Numerous studies are therefore being carried out to identify a more reliable diagnostic marker for ovarian cancer with the aim of aiding early diagnosis.

The standard treatment for advanced ovarian cancer is cytoreductive surgery followed by platinum-based chemotherapy (Shih and Kurman, 2004; Zaman *et al.*, 2012). Recurrent ovarian cancer has been shown to respond initially to additional chemotherapy, but as chemo-resistance increases the progression-free interval shortens and eventually the disease becomes incurable (Zaman *et al.*, 2012).

Numerous treatment strategies for ovarian cancer are undergoing various stages of clinical trials, these include; antibody-based vaccines, cytokine vaccines, peptide-based vaccines, dendritic cell vaccines, heat shock protein vaccines and active immunisation using gene transduced whole tumour cells (Liu *et al.*, 2010). Peptide-based vaccines targeting a number of CT antigens, such as NY-ESO-1, are currently being tested. A high frequency of CT antigen gene expression has been shown in ovarian cancer, relative to other cancers (Caballero and Chen, 2009) and clinical trials have yielded positive results for CT antigen-based immunotherapy treatment of ovarian cancers (for example, Diefenbach *et al.*, 2008; Odunsi *et al.*, 2007). NY-ESO-1 is expressed in more than 40% of advanced epithelial ovarian cancers (Diefenbach *et al.*, 2008). A phase I clinical trial was carried out to assess the effects of vaccination with the HLA-A0201-restricted NY-ESO-1b peptide on epithelial ovarian cancer patients in high risk of remission. The results from this study suggested that vaccination with the HLA-A0201-restricted NY-ESO-1b peptide was safe and was shown to induce a T-cell immune response in NY-ESO-1 positive and negative patients (Diefenbach *et al.*, 2008).

Based on the evidence from previous studies, CT antigens may be good candidates from which to identify potential new targets for diagnostic tests and/or immunotherapeutic treatment of ovarian cancer. The results shown in Chapters 3.0 and 4.0 were a constituent part of a larger scale meiCT gene screen; the full results for the gene screen are detailed in Feichtinger *et al.*, (2012a). RT-PCR analysis identified 33 meiCT genes, 23 of which were shown to display expression in one or more of the ovarian cancer samples tested (three ovarian cancer cell lines and one ovarian tumour tissue). Meta-analysis was carried out on the RT-PCR validated meiCT candidate genes, using the CancerMA online tool (http://www.cancerma.org.uk; Feichtinger *et al.*, 2012b), to assess gene expression in cancer microarray data. A mean up-regulation was observed for many of the meiCT genes

in ovarian cancer, thus providing evidence that these meiCT genes are expressed in clinically relevant material (Feichtinger *et al.*, 2012a).

NUT (nuclear protein in testis) was identified and validated, by RT-PCR, as a meiCT gene in the CT gene screen detailed in Feichtinger *et al.*, (2012a). *NUT* expression was shown to be testis-restricted in the normal tissues, with additional expression in the ovarian tumour tissue, A2780 (epithelial ovarian cancer cell line) and HCT116 (colorectal cancer cell line). Meta-analysis also suggested a mean up-regulation of *NUT* in ovarian cancer (Feichtinger *et al.*, 2012a). *NUT* was therefore identified as a meiCT antigen gene which was shown to display expression in ovarian cancer cells. However, the relationship between gene expression and protein abundance is not always directly proportional. The correlation between changes in gene expression and protein abundance is effected by numerous post-transcriptional mechanisms including; translation, post-translational modification and degradation (Tan *et al.*, 2009; Waters *et al.*, 2006). Therefore, further characterisation is required to establish if the gene product is present in ovarian cancer cells and its potential for use as a diagnostic and/or therapeutic target.

The actual function of NUT is unknown; but a chromosomal aberration involving NUT is known to cause NUT midline carcinoma (NMC). NMC is a lethal cancer caused by the chromosome translocation mediated fusion of *NUT* (chromosome 15) to the 5' portions of *BRD4* (chromosome 19) or *BRD3* (chromosome 9) or other unknown genes. The presence of BRD-NUT fusion proteins arrest differentiation and contribute to the oncogenic progression of NMC (French *et al.*, 2003; Schwartz *et al.*, 2011; Yan *et al.*, 2011). These studies have shown NUT to have a clear role in cancer progression, albeit as a constituent of a fusion protein. Our study identified *NUT* as a CT gene by RT-PCR, and found expression in a broader range of cancers than previously described (Feichtinger *et al.*, 2012a). *NUT* was therefore selected for further characterisation in the ovarian cancer cell line, A2780.

5.2 Predicted nuclear export/import of NUT

The NUT protein sequence was analysed using a number of protein localisation prediction tools; NetNES 1.1 Server (http://www.cbs.dtu.dk/services/NetNES/; La Cour *et al.*, 2004),

NUCLEO (http://www.pprowler.itee.uq.edu.au; Hawkins *et al.*, 2007) and PredictProtein (http://www.predictprotein.org/; Rost *et al.*, 2004).

The NetNES 1.1 server predicts leucine-rich nuclear export signals (NES) in eukaryotic proteins (La Cour *et al.*, 2004) and identified a NES within the NUT sequence, which is highlighted in green in Figure 5.1, part A. The NUCLEO model was developed to identify nuclear proteins, including dual localisation proteins (Hawkins *et al.*, 2007), and predicted a nuclear localisation of NUT with a probability of 0.94.

The PredictProtein server tool searches up-to-date public sequence databases in order to create sequence alignments and predicts structural and functional aspects of the protein (Rost *et al.*, 2004). The results from the PredictProtein server analysis predicted that the NUT protein is localised in the nucleus. The NUT nuclear import and export sequences identified using these prediction tools are highlighted in red and green respectively in Figure 5.1, part A.

The NES score is calculated by combining the Artificial Neural Network (ANN) and Hidden Markov Model (HMM) scores, as described in La Cour *et al.*, (2004). The NetNES algorithm gives a theoretical scoring range of 0-2.1 for the NES score; the NES score threshold used by the NetNES prediction tool is set at 0.5 (La Cour *et al.*, 2004). The residues between positions 452 and 463 have a NES score above 0.5 and therefore these 12 residues were identified and highlighted as a NES within the NUT sequence (Figure 5.1, part B).

The PredictProtein server identified three potential NLS sequences within the NUT protein sequence, and cross-checked the cellular localisation of other proteins containing these NLS sequences. For example, the first motif was found in 193 proteins and 97.92% of these proteins were found to be nuclear (Figure 5.1, part C). This statistical data along with the NUCLEO prediction strongly suggests a nuclear localisation for NUT, but the presence of a NES sequence may suggest NUT is capable of export from the nucleus.

NUT has previously been found to contain nuclear localisation and export sequences which promote nuclear-cytoplasmic shuttling via a leptomycin-sensitive pathway (French *et al.*, 2008). Therefore these predictions are in line with the findings from the study by French *et al.*, (2008).

A

```
   1 MASDGASALP GPDMSMKPSA ALSPSPALPF LPPTSDPPDH PPREPPPQPI MPSVFSPDNP
  61 LMLSAFPSSL LVTGDGGPCL SGAGAGKVIV KVKTEGGSAE PSQTQNFILT QTALNSTAPG
 121 TPCGGLEGPA PPFVTASNVK TILPSKAVGV SQEGPPGLPP QPPPPVAQLV PIVPLEKAWP
 181 GPHGTTGEGG PVATLSKPSL GDRSKISKDV YENFRQWQRY KALARRHLSQ SPDTEALSCF
 241 LIPVLRSLAR LKPTMTLEEG LPLAVQEWEH TSNFDRMIFY EMAERFMEFE AEEMQIQNTQ
 301 LMNGSQGLSP ATPLKLDPLG PLASEVCQQP VYIPKKAASK TRAPRRRQRK AQRPPAPEAP
 361 KEIPPEAVKE YVDIMEWLVG THLATGESDG KQEEEGQQQE EEGMYPDPGL LSYINELCSQ
 421 KVFVSKVEAV IHPQFLADLL SPEKQRDPLA LIEELEQEEG LTLAQLVQKR LMALEEEEDA
 481 EAPPSFSGAQ LDSSPSGSVE DEDGDGRLRP SPGLQGAGGA ACLGKVSSSG KRAREVHGGQ
 541 EQALDSPRGM HRDGNTLPSP SSWDLQPELA APQGTPGPLG VERRGSGKVI NQVSLHQDGH
 601 LGGAGPPGHC LVADRTSEAL PLCWQGGFQP ESTPSLDAGL AELAPLQGQG LEKQVLGLQK
 661 GQQTGGRGVL PQGKEPLAVP WEGSSGAMWG DDRGTPMAQS YDQNPSPRAA GERDDVCLSP
 721 GVWLSSEMDA VGLELPVQIE EVIESFQVEK CVTEYQEGCQ GLGSRGNISL GPGETLVPGD
 781 TESSVIPCGG TVAAAALEKR NYCSLPGPLR ANSPPLRSKE NQEQSCETVG HPSDLWAEGC
 841 FPLLESGDST LGSSKETLPP TCQGNLLIMG TEDASSLPEA SQEAGSRGNS FSPLLETIEP
 901 VNILDVKDDC GLQLRVSEDT CPLNVHSYDP QGEGRVDPDL SKPKNLAPLQ ESQESYTTGT
 961 PKATSSHQGL GSTLPRRGTR NAIVPRETSV SKTHRSADRA KGKEKKKKEA EEEDEELSNF
1021 AYLLASKLSL SPREHPLSPH HASGGQGSQR ASHLLPAGAK GPSKLPYPVA KSGKRALAGG
1081 PAPTEKTPHS GAQLGVPREK PLALGVVRPS QPRKRRCDSF VTGRRKKRRR SQ
```

B

Sequence Position	Residue	NES Score
452	I	0.529
453	E	0.530
454	E	0.538
455	L	1.008
456	E	0.607
457	Q	0.582
458	E	0.583
459	E	0.590
460	G	0.591
461	L	0.535
462	T	0.522
463	L	0.973

C

Motif	No. with NLS	% Nuc	%NonNuc
[RK]{3,}?x{8,16}[RK]{4,}?	193	97.92	2.07
[KR][KR][KR][KR][KR][KR][KR]	74	100	0

NLS's found in NUT sequence:

- *RKRRCDSFVTGRRKKRRR* - 1113
- *RRKKRRR* - 1124

Figure 5.1. Summary of the predicted nuclear import and export sequences in the NUT protein sequence. **A.** The NUT nuclear export sequence (NES), predicted by NetNES 1.1 server is highlighted in green and the NUT nuclear localisation sequence (NLS), predicted by the PredictProtein server is highlighted in red. **B.** Table giving the NES scores for all of the residues in the predicted nuclear export sequence (NES), predicted by NetNES 1.1 server. **C.** NLS sequences identified for NUT (the number indicates the position of the motif) and a table summarising the statistical data for the predicted nuclear localisation signals in the NUT sequence, compared to other proteins with these NLS sequences. Motif abbreviations; [RK] represents R or K residue in this position; [RK]{3,}? represents 3 or more R or K residues; x {8,16} represents any amino acid residue can be present at this position, between 8 and 16 times.

5.3 Cellular localisation of NUT

NUT (nuclear protein in the testis) is a nuclear protein, and analysis using the protein localisation tools predicted nuclear localisation for NUT; therefore we initially predicted NUT would localise within the nucleus. The cellular localisation of NUT was analysed in A2780 (an ovarian carcinoma cell line) cells using western blot analysis and immunofluorescent staining of fixed cells. NT2 (an embryonal carcinoma cell line) and two ovarian adenocarcinoma cell lines, PEO14 and TO14, (from peritoneal ascites and solid metastasis respectively) were also used to assess NUT protein levels. The NUT protein was not expected to be detectable in the NT2, PEO14 and TO14 cell lines, because RT-PCR was negative for *NUT* expression (Feichtinger *et al.*, 2012a).

5.3.1 Western blot analysis

Nuclear and cytoplasmic protein fractions were prepared alongside WCEs for the A2780, PEO14, TO14 and NT2 cell lines, to assess the cellular localisation of NUT using anti-NUT (C52B1) (Cell Signaling Technology; 3625S). Chromatin association protein lysates were also prepared for A2780 to assess any potential NUT-chromosome association. These lysates were then analysed using western blot analysis, as shown in Figure 5.2.

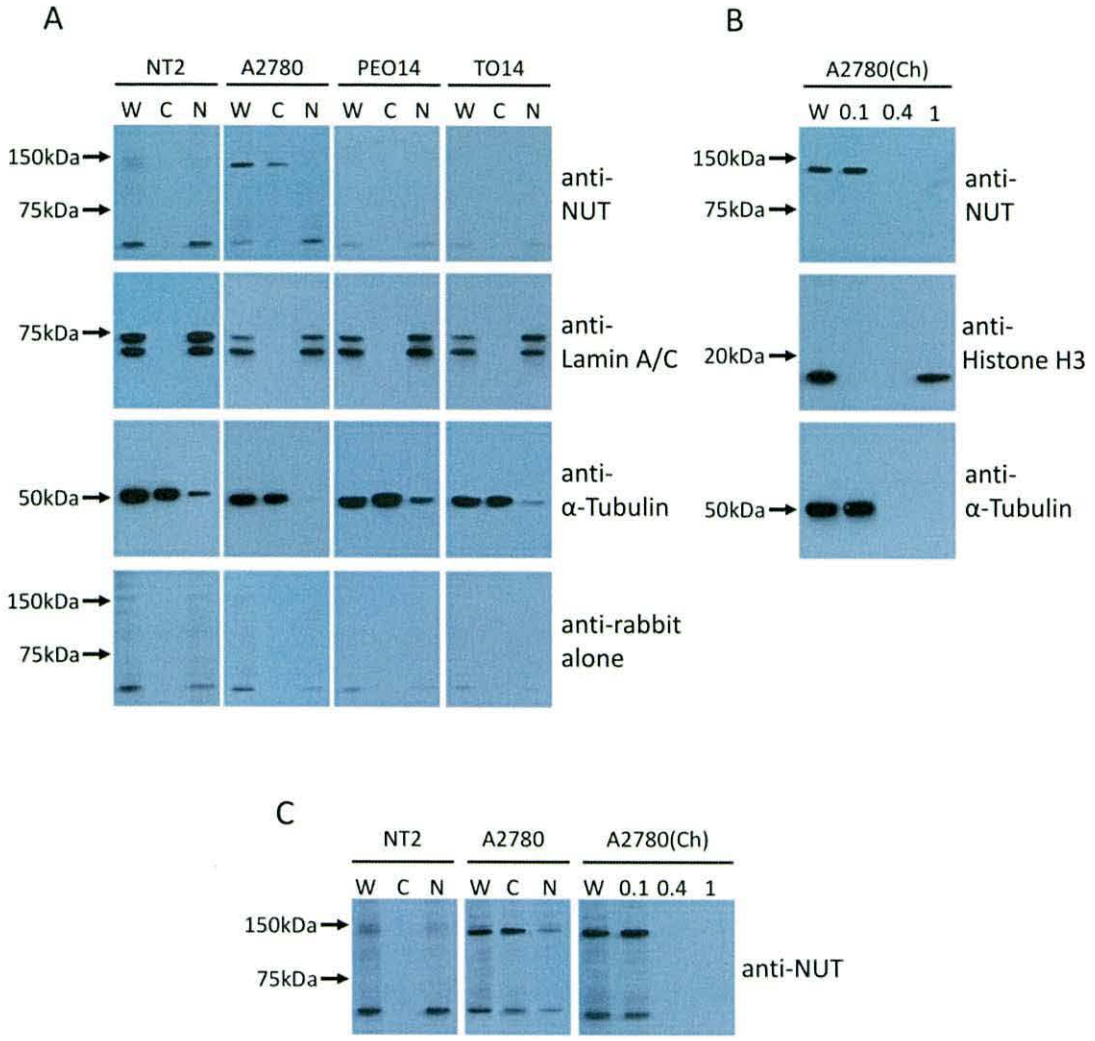

Figure 5.2. Western blot analysis for NUT in NT2, A2780, PEO14 and TO14 cell lines. A. Western blot analysis showing the cellular localisation of NUT in NT2, A2780, PEO14 and TO14 cell lines, using WCE (W), cytoplasmic lysate fraction (C) and nuclear lysate fraction (N). Antibodies against lamin A/C and α-tubulin were used as the positive controls (bottom), to check the efficiency of fractionation and the loading of the gel. The membranes were also probed with rabbit secondary antibody alone, as a negative control for anti-NUT (bottom). **B.** Western blot analysis using the chromatin association lysates to assess any potential chromatin association for NUT in A2780 cells. WCE (W) was loaded as a positive control and lysates with varying concentrations of salt were prepared to assess chromatin association; 0.1M (0.1), 0.4M (0.4) and 1M (1) NaCl. Antibodies against Histone H3 and α-tubulin were used as the positive controls (bottom). **C.** Overexposure of western blot analysis showing the cellular localisation of NUT in NT2 and A2780 cells, and also showing that NUT does not display any detectable chromatin association in A2780 cells. These results appear to be reproducible as this experiment was repeated at least two times.

Antibodies against lamin A/C and α-tubulin were used to control for the nuclear and cytoplasmic fractions respectively. The fractionation appears to be sufficient, although the α-tubulin results suggest some cytoplasmic protein present in the nuclear fractions for the NT2 and PEO14 cells.

The predicted band size for NUT using anti-NUT (C52B1) is approximately 150 kDa. A clear band can be observed just below 150 kDa in the A2780 cell line, therefore this band was believed to correspond to NUT. Interestingly, NUT appears to be predominately localised within the cytoplasm of the A2780 cells, but on overexposure of the western blot a band is apparent in the nuclear fraction also. A second prominent band was also observed below 75 kDa which was shown with varying degrees of intensity in all four of the cell lines used. This band appears to be a non-specific interaction arising from the secondary rabbit antibody, as it is clearly shown in the blots probed with anti-rabbit only (bottom row, Figure 5.2, part A).

The chromatin association assay (Ch) protein lysates were prepared consecutively with increasing concentrations of salt (NaCl). The 0.1 M Ch lysate corresponds to the proteins with no chromatin association, whereas the 0.4 M Ch lysate corresponds to proteins which display weak chromatin association and the 1 M Ch lysate to strongly chromatin associated proteins. Western blot analysis shows a band for the WCE and 0.1 M Ch lysates, but not the 0.4 M and 1 M Ch lysates, even on overexposure of the western blot. These results suggest that any NUT which may localise within the nucleus of the A2780 cells does not have any chromatin association. The antibodies against α-tubulin and histone-H3 showed the expected western blot profiles for no and strong chromatin associations respectively.

There is also a faint band at approximately the correct size in the NT2 cells; this band is observed in the WCE only. However, there is a relatively high level of background and it is not as clear as it is in the A2780 cells, therefore NUT protein presence in NT2 cells cannot be definitely concluded. NUT does not appear to be present in the PEO14 and TO14 ovarian cell lines, these results are in line with the expression profile observed for *NUT* in Feichtinger *et al.*, (2012a).

5.3.2 Immunofluorescent staining of fixed cells

Immunofluorescent staining was also carried out using the A2780, NT2 and PEO14 cell lines. The PEO14 cell line was used as a negative control for NUT staining, after the results shown from RT-PCR (Feichtinger *et al.*, 2012a) and western blot analysis suggested that NUT is not present in PEO14 cells (Figure 5.2). Figures 5.3, 5.4 and 5.5 show the results for immunofluorescent staining in the A2780, NT2 and PEO14 cell lines respectively.

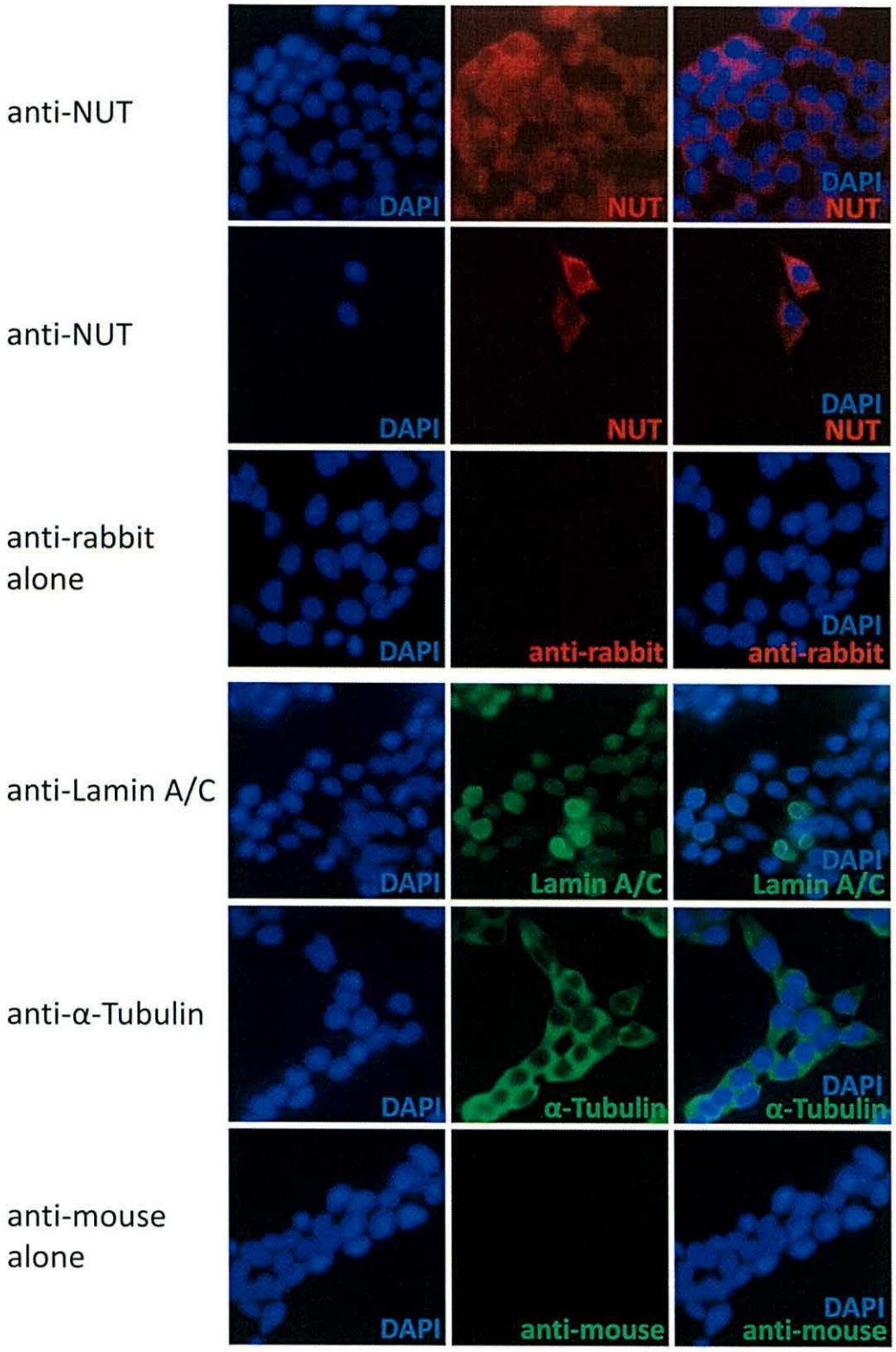

Figure 5.3. Immunofluorescent staining of fixed A2780 cells with anti-NUT. Images for immunofluorescent staining for NUT (red) in A2780 cells, viewed using a Zeiss Axioskop 2 fluorescent microscope (x100 lens). Staining with anti-lamin A/C (green) and anti-α-tubulin (green) was used as positive controls for nuclear and cytoplasmic staining of the cells respectively. Staining with the secondary antibodies only was used as the negative controls, anti-rabbit for the NUT-staining and anti-mouse for the anti-lamin A/C and anti-α-tubulin staining. (Experiment repeated more than three times).

The A2780 cells tend to clump together when growing, therefore making it difficult to get cells on a single plane for microscope analysis. Two pictures are shown for anti-NUT staining of A2780 cells; the upper row shows a typical spread of the cells, where they are overlapping and clumped together, whereas the lower row shows staining in only two cells. Both images suggest that NUT staining is predominantly concentrated in the cytoplasm of the A2780 cells.

The A2780 cells were stained with antibodies against lamin A/C and α-tubulin, to positively control for nuclear and cytoplasmic staining respectively. The cellular staining observed using the NUT antibody is most similar to the cytoplasmic staining with α-tubulin. The cytoplasmic region of the A2780 cells appear to be relatively small, but the apparent size and shape of the cytoplasmic region corresponds for the NUT and α-tubulin staining.

The anti-mouse and anti-rabbit secondary antibodies both appear to produce some non-specific background in the A2780 cells. The level of non-specific background interaction produced by the secondary antibodies appears to be insignificant compared to the staining with the primary antibodies. This may suggest that the staining observed for anti-NUT and the two positive controls (anti-lamin A/C and anti-α-tubulin) arises from primary antibody staining.

NT2 and PEO14 cells are comparatively larger than the A2780 cells, and staining with NUT was carried out alongside staining of the A2780 cells. The western blot results may have shown a faint band for NUT in the NT2 WCE, however due to the relatively high level of non-specific background observed, NUT presence could not be concluded. This observation appears to correspond to the results from immunostaining of NT2 cells, shown in Figure 5.4.

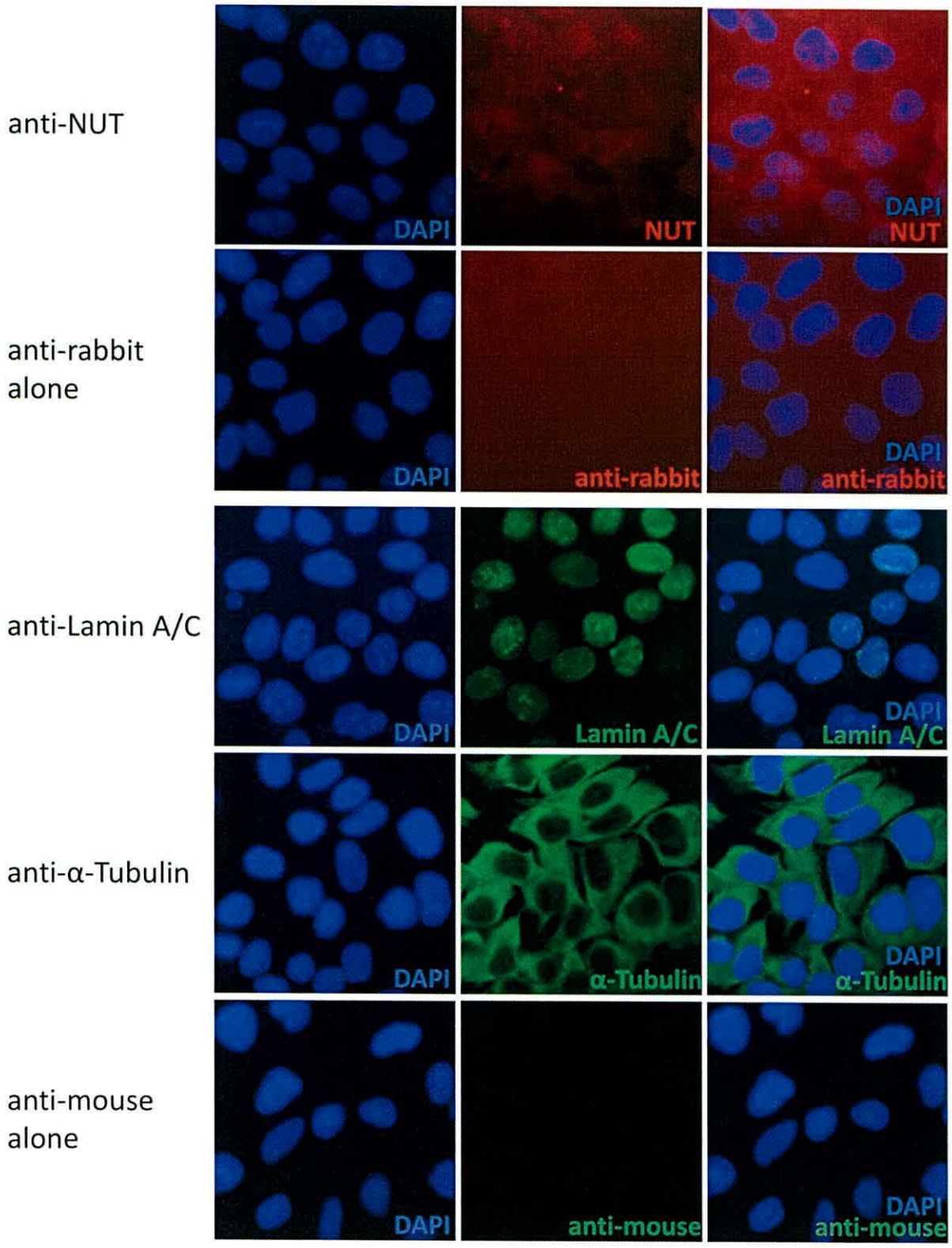

Figure 5.4. Immunofluorescent staining of fixed NT2 cells with anti-NUT. Images for immunofluorescent staining for NUT (red) in NT2 cells, viewed using a Zeiss Axioskop 2 fluorescent microscope (x100 lens). Staining with anti-lamin A/C (green) and anti-α-tubulin (green) was used as positive controls for nuclear and cytoplasmic staining of the cells. Staining with the secondary antibodies only was used as the negative controls, anti-rabbit for the NUT-staining and anti-mouse for the anti-lamin A/C and anti-α-tubulin staining. (Experiment repeated a minimum of three times).

Positive staining of the nucleus and cytoplasm with anti-lamin A/C and anti-α-tubulin respectively, shows a clear difference between nuclear and cytoplasmic staining in the NT2 cells. There also appears to be some weak NUT-staining in the NT2 cells, this staining appears to be cytoplasmic, however there does not appear to be a clear localisation to the staining as seen in the positive controls (or the NUT-staining observed in A2780 cells). There appears to be less background from the rabbit secondary antibody than that observed in the A2780 cells. This staining is not observed for the cells stained with anti-rabbit secondary antibody only, which may suggest that the staining is not non-specific background.

The western blot analysis results for NUT in NT2 cells were not conclusive, but a very faint band was observed in the WCE, and these immunofluorescent staining results appear to suggest some degree of cytoplasmic staining. This staining is not as clear as the staining observed in the A2780 cells, therefore if this is NUT-positive staining, and not background, this may suggest a very low level of NUT protein in the NT2 cells.

Immunofluorescent staining of PEO14 cells was also carried out, this cell line should be negative for NUT according to the results observed for RT-PCR (Feichtinger *et al.*, 2012a) and western blot analysis (Figure 5.2). The results for immunofluorescent staining of fixed PEO14 cells are shown in Figure 5.5.

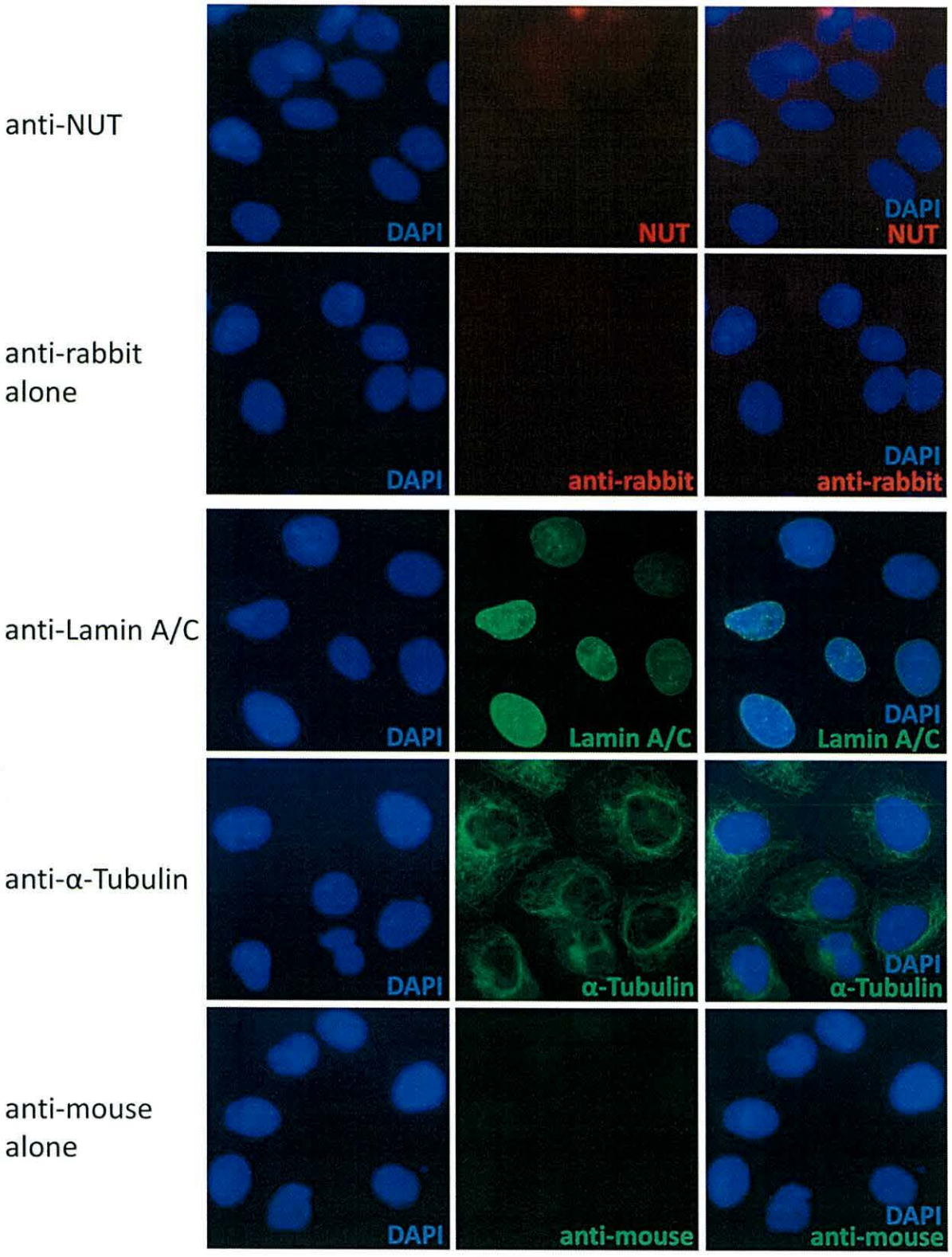

Figure 5.5. Immunofluorescent staining of fixed PEO14 cells with anti-NUT. Images for immunofluorescent staining for NUT (red) in PEO14 cells, viewed using a Zeiss Axioskop 2 fluorescent microscope (x100 lens). Staining with anti-lamin A/C (green) and anti-α-tubulin (green) was used as positive controls for nuclear and cytoplasmic staining of the cells. Staining with the secondary antibodies only was used as the negative controls, anti-rabbit for the NUT-staining and anti-mouse for the anti-lamin A/C and anti-α-tubulin staining. (Experiment repeated two times).

The signal observed with the NUT antibody in the PEO14 cells is comparable to the background signal coming from the rabbit secondary antibody. Thus suggesting that any signal observed in the NUT-stained PEO14 cells is non-specific. These results therefore suggest that there is no NUT staining in the PEO14 cells, and therefore NUT is not present at detectable levels in these cells.

PEO14 cell staining with the positive controls (anti-lamin A/C and anti-α-tubulin) was successful and clearly show a difference between nuclear and cytoplasmic staining. This suggests that the lack of NUT staining was not caused by a problem with the technique.

5.4 siRNA knockdown of NUT

Knockdown of NUT was attempted using siRNA in A2780 cells to determine any effect that knockdown of this protein may have on these cells and to also establish the specificity of the NUT antibody. WCEs were collected from the cells after siRNA treatment and analysed using western blot analysis, the results are shown in Figure 5.6.

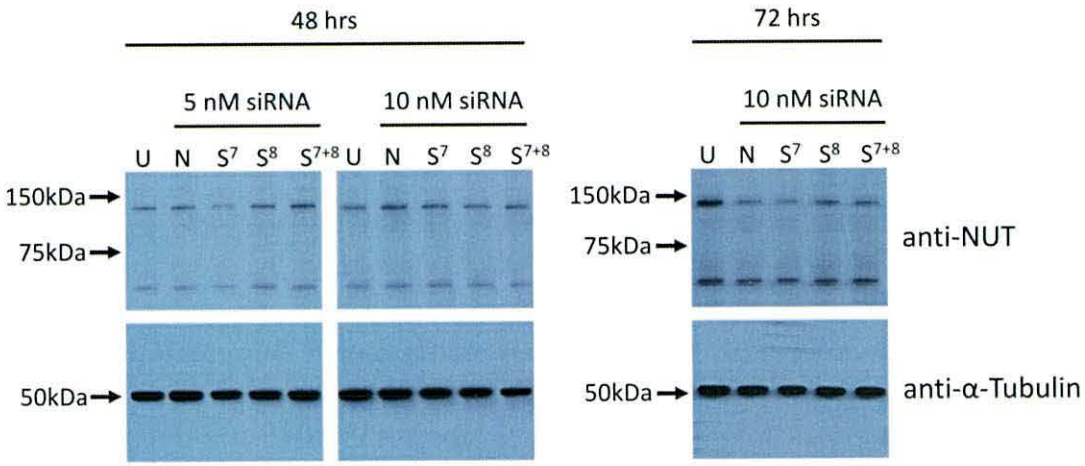

Figure 5.6. Western blot analysis for siRNA knockdown of NUT in A2780 cells. Untreated (U) A2780 cells and cells treated with non-interfering siRNA (N) were used as negative controls for the siRNA knockdown. Two different NUT specific siRNAs (from Qiagen) were tested; Hs_NUT_7 (S^7) and Hs_NUT_8 (S^8) and a combination of the two siRNAs was also used (S^{7+8}). The siRNA and transfection reagent were added to the cells upon seeding and then at 24 hr intervals (0, 24 and 48 hrs). 5 nM and 10 nM concentrations of siRNA were tested using the two "hit" method; wherein the cells collected 48 hrs after first treatment (described in Section 2.9). A three "hit" method was also tested for 10 nM siRNA; the cells were collected 72 hrs after the first treatment. Anti-α-tubulin was used as a loading control (bottom). The two "hit" siRNA strategy was repeated at least three times, and the three "hit" strategy was carried out once.

Several conditions were tested in an attempt to optimise any knockdown with siRNA treatment including; increasing the siRNA concentrations and the number of siRNA treatments ("hits").

The band thought to correspond to NUT appears fainter after 48 hrs treatment (2 "hits") with Hs_NUT_7 compared to the controls (untreated cells and cells treated with non-interfering siRNA), however this difference in signal intensity may be an artefact of the transfer, as the outline of a bubble is visible, or a difference in loading, as the α-tubulin appears to be slightly reduced compared to the untreated and non-interfering controls.

In the A2780 cells treated for 72 hrs (3 "hits") with 10 nM siRNA, the intensity of the band corresponding to NUT in the untreated cells appears to be greater than the treated cells, both non-interfering and the NUT-specific siRNA-treated; this is most likely due to a difference in the loading which is indicated by α-tubulin. However, when compared to the non-interfering control, there does not appear to be any NUT knockdown in the cells treated with 10 nM NUT-specific siRNA.

Increasing the siRNA concentrations and increasing the number of treatments, appeared to have no effect. No significant level of NUT knockdown is apparent from the results shown in Figure 5.6. However, the results from RT-PCR (Feichtinger *et al.*, 2012a), western blot analysis (Section 5.3.1) and immunofluorescent staining of fixed cells (Section 5.3.2) appear to correspond with each other.

5.5 Discussion

5.5.1 Novel CT gene

NUT was originally identified as a novel CT gene from the large scale meiCT gene screen undertaken by our lab. A mean up-regulation of *NUT* was observed in ovarian cancer samples after meta-analysis was carried out, thus providing evidence for *NUT* expression in clinically relevant ovarian cancer samples, results summarised in Feichtinger *et al.*, (2012a). Therefore NUT was selected for further characterisation in three ovarian cancer cell lines. The RT-PCR profile observed for *NUT*, in Feichtinger *et al.*, (2012a), showed expression was testis-restricted in the normal tissues, with additional expression in the ovarian tumour tissue and A2780 (ovarian carcinoma cell line). Further analysis and characterisation was

carried out for NUT using the NT2, A2780, PEO14 and TO14 cell lines. No *NUT* expression was observed in the two ovarian adenocarcinoma cancer cell lines (PEO14 and TO14) or in the embryonalcarcinoma cell line (NT2) (Feichtinger *et al.*, 2012a), therefore no NUT protein expression was expected for these cells. However, low levels of NUT protein were potentially detected in NT2 cells.

5.5.2 Cellular localisation of NUT in cancer cells

Both NES and NLS sequences were identified within the NUT sequence; however analysis using NUCLEO and PredictProtein predicted a nuclear localisation for NUT. Interestingly, the western blot analysis and immunofluorescent staining results shown here suggests that NUT is localised predominantly in the cytoplasm of A2780 cells. Correct subcellular localisation is essential for protein function and integration into functional biological networks. Aberrant protein localisation is a prominent feature of many human diseases, including cancer, and can arise from mutation, altered expression of cargo proteins and/or transport receptors (Hung and Link, 2011). Abnormalities in the subcellular localisation of a protein can prevent it from functioning correctly, for example the mis-localisation of several tumour suppressors has been shown to act as an inactivation mechanism in cancer. Deregulation of the spatiotemporal signalling dynamics has been shown to be involved in tumorigenesis, tumour growth and metastasis (Kau *et al.*, 2004; Wang and Hung, 2005). Therefore the cytoplasmic localisation of NUT in the A2780 cells could be the result of aberrant protein localisation observed in cancer cells.

Although the actual function of NUT is unknown, studies have shown NUT to have a clear role in disease progression in NMC, a lethal cancer. A chromosome translocation mediated fusion of *NUT* (chromosome 15) to the 5' portions of *BRD4* (chromosome 19) or *BRD3* (chromosome 9) or other unknown genes, gives rise to NUT-fusion proteins (French *et al.*, 2003; Schwartz *et al.*, 2011; Yan *et al.*, 2011). A study by French *et al.*, (2008) demonstrated that NUT contains nuclear localisation and nuclear export sequences which promote nuclear-cytoplasmic shuttling via a leptomycin-sensitive pathway. This therefore may suggest that the cytoplasmic localisation of NUT in A2780 cells is not due to an aberrant mis-localisation caused by deregulation of the spatiotemporal signalling dynamics in cancer cells. Conversely the NUT-fusion proteins, BRD3-NUT and BRD4-NUT, which have been shown to contribute to the oncogenic progression of NMC, are strictly nuclear (French *et al.*, 2008).

Although the primers used to identify *NUT* expression in Feichtinger *et al.*, (2012a) do not distinguish between *NUT* and *NUT*-fusion genes, the cytoplasmic localisation observed for NUT in the A2780 cells may suggest that the detectable levels of NUT do not comprise part of a BRD-NUT fusion protein. Also, the expected molecular weights of the NUT-fusion proteins are significantly greater than that of NUT (approximately 240 kDa for BRD4-NUT) and are known to bind to transcriptionally active chromatin (Haack *et al.*, 2009). Therefore providing further evidence to suggest that the western blot analysis and immunofluorescent staining of the fixed cells results observed were not detecting NUT-fusion proteins.

The apparent cytoplasmic localisation of NUT may suggest that NUT retains this shuttling capacity in the A2780 cells. Also, no chromatin association was observed for NUT in the A2780 cells, which is not surprising as it appears to localise predominantly within the cytoplasm. The BRD-NUT fusion proteins recruit histone acetyltransferases (HATs) via the NUT moiety which induces cycles of BRD-NUT/HAT recruitment, which leads to the formation of hyperacetylated foci. HAT sequestration to these foci results in a global hypoacetylation and transcriptional repression which thus turns off gene expression (Reynoird, *et al.*, 2010; Schwartz *et al.*, 2011; Yan *et al.*, 2011). There is also evidence to suggest that NUT alone does not induce the formation of hyperacetylated chromatin domains (Reynoird *et al.*, 2010). Therefore the subcellular localisation observed for NUT in the A2780 cells may be closely related to its subcellular localisation in normal testis cells. This indicates a possible difference in NUT-function within A2780 cells compared to the role of the NUT-fusion proteins in NMC progression. However, as the function of NUT in normal testis cells remains unknown, the function of NUT (if any) in the A2780 cells cannot be speculated.

NT2 cells were originally used as a negative control for NUT localisation; however western blot analysis showed a faint band in the WCE and immunofluorescent staining showed faint cytoplasmic staining. NT2 cells were negative for *NUT* expression (Feichtinger *et al.*, 2012a) yet these results may suggest a possible low level of NUT in the NT2 cells, which is significantly lower than that observed in A2780 cells. However, a weak signal was observed using anti-NUT for western blot analysis and immunofluorescent staining with a high level of non-specific background, therefore these results are not conclusive.

5.5.3 Further characterisation of NUT

siRNA knockdown of NUT in A2780 cells was unsuccessful, as no detectable levels of NUT knockdown were observed by western blot analysis, using two different siRNAs separately and in conjunction. These results could potentially indicate that the NUT antibody used is not specific for NUT. However, the circumstantial evidence from the RT-PCR, western blot analysis and immunofluorescent staining results suggest that the antibody is indeed identifying NUT. The unsuccessful NUT knockdown using siRNA may have been caused by a number of reasons, such as a failure in the technique, a highly stable NUT protein and/or an unstable mRNA encoding *NUT*. A more stable means of depleting NUT may be required to establish what effect NUT loss may have on the A2780 cells, such as *NUT* gene disruption using a TALEN (Transcription Activator-like Effector Nuclease)-based approach (methodology described in Cermak *et al.*, 2011).

RT-PCR showed *NUT* expression in the ovarian tumour tissue and meta-analysis indicated a mean up-regulation of *NUT* in ovarian cancer array data (Feichtinger *et al.*, 2012a). However, the results reported in this Chapter only show NUT protein in one of the three ovarian cancer cell lines tested here. The two NUT-negative cell lines were derived from the same patient (Langdon *et al.*, 1988). Although NUT appears to be an interesting candidate to analyse further, these results suggest that NUT will probably not provide a universal ovarian cancer antigen. Characterisation of *NUT* expression and protein localisation needs to be assessed in clinically relevant samples, such as ovarian cancer tissue with matched normal controls. Only further characterisation of NUT in clinically relevant ovarian cancer samples may validate or otherwise the potential use of NUT as a diagnostic target and/or immunotherapeutic target.

6.0 Biochemical analysis of REC8 and RAD21 in mitotic cells

6.1 Introduction

Mitosis occurs as part of the normal cell cycle and is required for tissue homeostasis and regeneration of damaged tissues in adults, whereas meiotic cell division is restricted to germ cells and is essential for the production of gametes (reviewed in Silkworth and Cimini, 2012). The process of mitosis involves one round of DNA replication followed by one round of chromosome segregation and produces two identical diploid daughter cells. In contrast, the process of meiosis involves one round of DNA replication followed by two successive rounds of chromosome segregation, and produces four genetically unique haploid daughter cells. During meiosis I, homologous chromosomes align on the metaphase plate and are pulled to opposite poles (reductional segregation) and during meiosis II, sister chromatids align on the metaphase plate and are pulled to opposite poles (equational segregation) (reviewed in Holt and Jones, 2009).

Accurate chromosome segregation is fundamental for cell division and occurs in a highly co-ordinated manner. Chromosome mis-segregation leads to progeny cells with an incorrect number of chromosomes, in a state known as aneuploidy. Aneuploidy gives rise to spontaneous abortion and genetic defects, and is a hallmark of cancer (Nicholson and Cimini, 2011; Silkworth and Cimini, 2012). Chromosome segregation in both meiosis and mitosis is co-ordinated by a protein complex known as cohesin. During mitosis, sister chromatids are held together by cohesin complexes along their arms. Arm cohesin dissociates from the sister chromatids during prophase via the prophase pathway. Centromeric cohesin remains and provides a source of tension when microtubule attachment occurs (reviewed in Holt and Jones, 2009; Nasmyth, 2011). The remaining cohesin is released upon chromosome segregation, when the α-kleisin is cleaved by separase (Uhlmann *et al.*, 1999; 2000).

In contrast, during meiosis I homologues are held together by crossovers and cohesin bonds along the sister chromatid arms, thus maintaining a bivalent structure. The crossover sites provide a source of tension when microtubule attachment occurs, with sister kinetochores

attached in a monopolar conformation. The sister chromatids remain physically linked by centromeric cohesin which is protected from degradation during meiosis I, until meiosis II. During meiosis II the sister centromeres revert to a bipolar conformation and attach to opposite poles, similar to mitosis (Holt and Jones, 2009).

Cohesin is a chromosome-associated multisubunit protein complex that is highly conserved in eukaryotes. The cohesin complex is a tripartite ring structure, consisting of two structural maintenance of chromosome (SMC) proteins and an α-kleisin subunit. This ring structure is thought to entrap the DNA, thus enabling intra- and inter-chromatid cohesion. In mammals the cohesin complex is formed by an SMC1-SMC3 heterodimer which associates with an α-kleisin subunit, which in turn recruits the SA (stromal antigen) and the cohesin accessory proteins (PDS5 and WAPL) (Nasmyth, 2011; Shintomi and Hirano, 2009). In mammals, there are two SMC1 subunits (SMC1α and SMC1β), three α-kleisins (RAD21, REC8 and RAD21L), three SA subunits (STAG1, STAG2 and STAG3) and two types of PDS5. There are 18 possible combinations of the cohesin complex and a number of these cohesin complexes are reported to be meiosis-specific. The following cohesin subunits are purported to be meiosis-specific in mammals; SMC1β, REC8, RAD21L and STAG3 (Nasmyth, 2011).

The principal mechanisms by which cohesion is mediated by the cohesin complex in eukaryotic cells is highly conserved, however there are differences between yeast and higher eukaryotes in how cohesin is regulated and distributed along the chromosomes (Peters *et al.*, 2008). Several studies have shown results which suggest that different cohesin complexes have different roles in chromosome segregation. For example, studies in mice have shown that RAD21L and REC8 display a mutually exclusive localisation pattern along the axial elements, during pachytene in spermatocytes and oocytes (Ishiguro *et al.*, 2011; Lee and Hirano, 2011). Also, centromeric cohesin until anaphase II, during meiosis, is established and maintained solely by the REC8-containing cohesin complex in mammals (Holt and Jones, 2009; Tachibana-Konwalski *et al.*, 2010). Tachibana-Konwalski *et al.*, (2010) reported a dramatic switch from REC8- to RAD21-containing cohesin complexes in the oocyte-zygote transition in mice. Prior to fertilization, sister chromatids are held together exclusively by REC8-containing cohesin and sister chromatid cohesin within the fertilised eggs (upon completion of meiosis) is established exclusively by RAD21-containing cohesin (Tachibana-Konwalski *et al.*, 2010).

The four reported meiosis-specific cohesin subunit genes (*RAD21L*, *REC8*, *SMC1β* and *STAG3*) were screened alongside their mitotic paralogues for expression in a range of normal tissues in Chapter 3.0. The RT-PCR and sequencing results presented in Chapter 3.0, showed testis-restricted expression profiles for *RAD21L* and *SMC1β* whereas *REC8* and *STAG3* expression was found in 21 normal human tissues including the testis and ovary. Several studies have shown that a number of meiosis-specific genes, including *REC8*, are constitutively transcribed in mitotic cells of the fission yeast, *S. pombe*. Post-transcriptional processing of the RNA ensures that the primary transcripts are not processed into mature mRNAs and are thus highly unstable. Changes in the RNA processing allow these meiotic genes to become functionally expressed when the cell enters meiosis (Chen *et al.*, 2011; Cremona *et al.*, 2011; Harigaya *et al.*, 2006; Yamanaka *et al.*, 2010).

Although the results presented in Chapter 3.0 were surprising, in that they may suggest that *REC8* and *STAG3* expression is not as tightly meiosis-specific in humans as previously reported, post-transcriptional mechanisms similar to that described in fission yeast may take place in human cells. Therefore this *REC8* and *STAG3* expression observed in the various mitotically dividing cells may not give rise to production of the REC8 and STAG3 proteins, and thus maintaining a meiosis-specific profile at the protein level. Therefore the potential protein abundance and cellular localisation of REC8 was investigated within mitotically dividing cells.

6.2 RT-PCR of *REC8* and *RAD21*

REC8 is believed to be a meiosis-specific cohesin subunit; however the RT-PCR results shown in Chapter 3.0 suggested that *REC8* is expressed in all of the normal human tissues tested. Expression of *REC8* in these normal tissues may be very interesting and may suggest that REC8 is not as meiosis-specific in humans as previously believed. RAD21 on the other hand is an essential component of the mitotic cohesin complex which has also been implicated in meiosis (Xu *et al.*, 2004). *RAD21* expression was also observed in all of the normal tissues tested in Chapter 3.0, as expected.

To determine whether cell lines could be used as a model system for addressing the presence of REC8 protein, the total RNA was extracted from 18 cancer cell lines, from a

range of histological origins, and cDNA was synthesised. RT-PCR was carried out, using intron-spanning primers, to assess *REC8* and *RAD21* expression in the cancer cell lines, the results are shown in Figure 6.1.

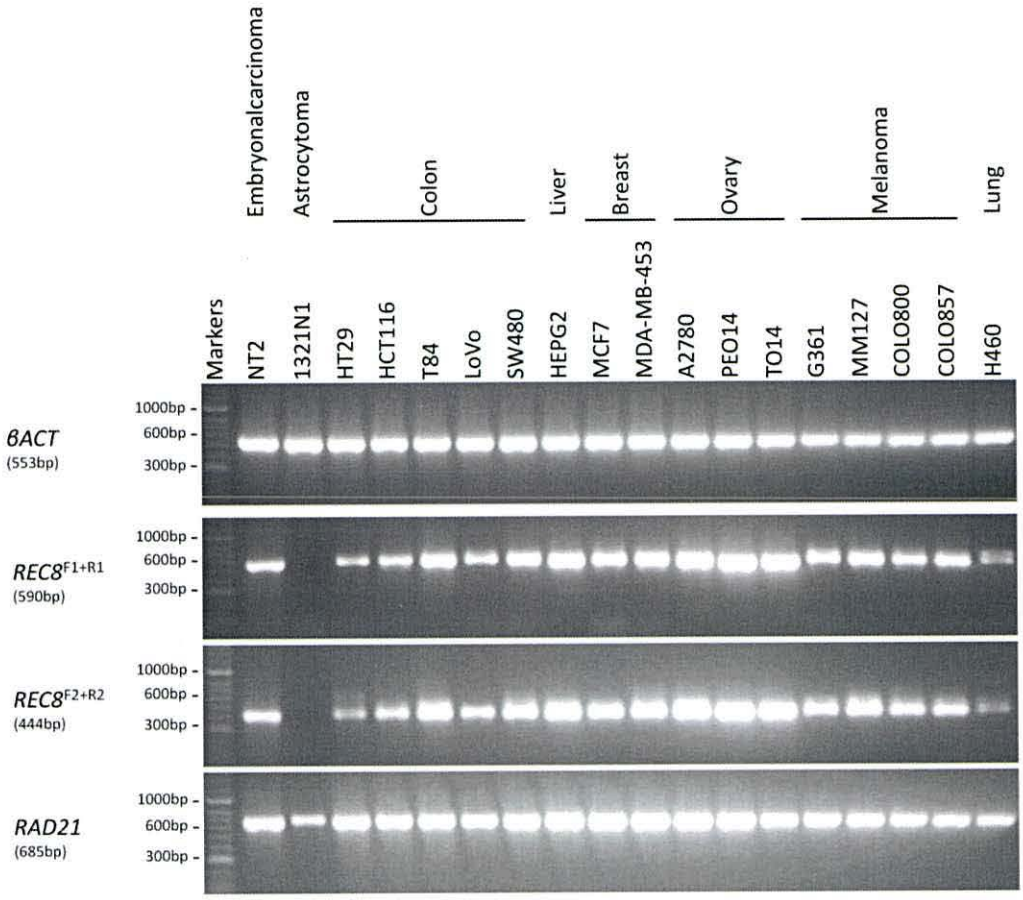

Figure 6.1. RT-PCR expression profiles for *REC8* and *RAD21* in the cancer cell lines. Agarose gels showing the expression of *REC8* and *RAD21* in 18 human cancer cell lines, from a range of histological origins (the expected PCR product size is shown in brackets). cDNA was generated from the total RNA extracted from the cancer cell lines. Two pairs of primers were used to assess *REC8* expression in the cancer cell lines. The expression profile for *βACT* is shown as a positive control for the cDNA samples (top). These results appear to be reproducible as these PCRs were repeated at least three times.

RAD21 expression was observed in all of the cell lines, this is in line with the current knowledge which states that RAD21 is an essential component of the mitotic cohesin complex (Nasmyth, 2011). The purported meiosis-specific gene *REC8* also appears to display expression in a wide range of cancer cells lines. Of the cell lines used here, only the brain cancer cell line (1321N1) did not show *REC8* expression. It is also interesting that the band observed for *RAD21* in the 1321N1 cell line is a lower intensity than that observed in the other cell lines, but the *βACT* expression appears to be relatively equal.

The cancer cell lines are mitotically dividing cells, therefore these results in conjunction with the results shown in Chapter 3.0 suggest that *REC8* is expressed in mitotically dividing cells, and that a number of cancer cell lines can be explored as models for studying the presence and function of the REC8 protein.

6.3 Cellular localisation of REC8 and RAD21

6.3.1 Western blot analysis

Numerous post-transcriptional mechanisms effect the correlation between gene expression and protein abundance (Tan *et al.*, 2009; Waters *et al.*, 2006). Therefore, these RT-PCR results showing *REC8* mRNA expression in a range of normal tissues and cancer cell lines do not guarantee that the REC8 protein is produced in these mitotic cells. The protein abundance and localisation of REC8 was assessed in a number of cancer cell lines.

Nuclear and cytoplasmic protein fractions were prepared alongside WCEs for five cell lines; NT2, HCT116, SW480, A2780 and HeLa T-REx. Western blot analysis was then carried out to assess REC8 protein cellular localisation; the results are shown in Figure 6.2.

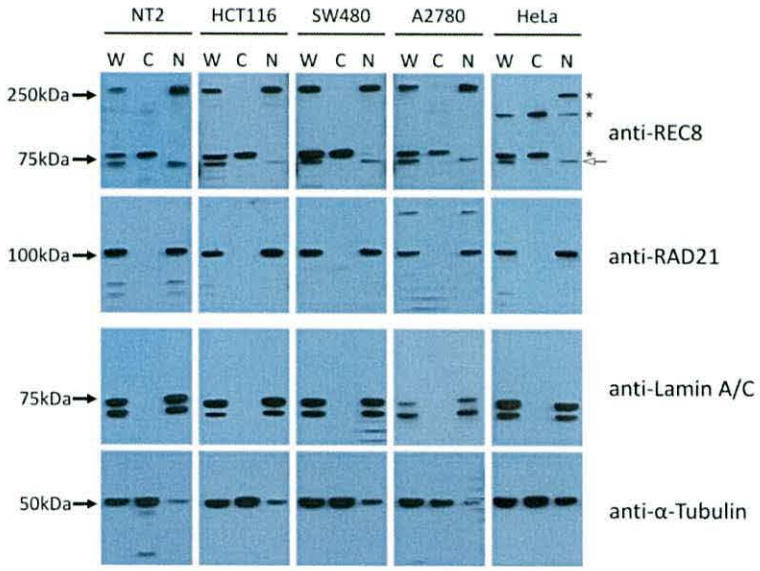

Figure 6.2. Western blot analysis for REC8 and RAD21 in cancer cell lines. Western blot analysis showing the cellular localisation of REC8 and RAD21 in the NT2, HCT116, SW480, A2780 and HeLa T-REx cell lines, using WCE (W), cytoplasmic lysate fraction (C) and nuclear lysate fraction (N). Antibodies against lamin A/C and α-tubulin were used as the positive controls, to check the efficiency of fractionation and the loading of the gel (bottom). These results appear to be reproducible as the fractionation was repeated at least three times.

The possible REC8-specific band, as per the results presented in Section 6.4, is indicated with an arrow (right). The likely non-specific bands are indicated by *.

Antibodies against lamin A/C and α-tubulin were used to control for the nuclear and cytoplasmic fractions respectively. The fractionation appears to be sufficient, although the α-tubulin results suggest some cytoplasmic protein present in the nuclear fraction.

The predicted molecular weight of REC8 is approximately 63 kDa, however two clear bands were observed using anti-REC8 antibodies at approximately 75kDa. The upper band appears to localise in the cytoplasm and the lower band appears to localise in the nucleus. These results could potentially suggest that the antibody recognises two forms of REC8 one of which appears to localise in the nucleus. The western blots were also probed using anti-RAD21 antibodies, which identified a strong band that appears to show strong nuclear localisation. The predicted molecular weight of RAD21 is approximately 72 kDa, however a band was observed just above 100 kDa using anti-RAD21. Both anti-REC8 and anti-RAD21 have identified bands significantly larger than the predicted size of the respective proteins, which may be due to post-translational modifications, such as phosphorylation.

Chromosome instability and aberrant gene expression is commonly observed in cancer cells, therefore *REC8* gene expression and REC8 protein localisation was assessed in fibroblast cells (NHDF). Protein lysates were also prepared from normal colon tissue (obtained from a patient at Ysbyty Gwynedd, by John Sammut) to assess REC8 protein localisation, the results are shown in Figure 6.3.

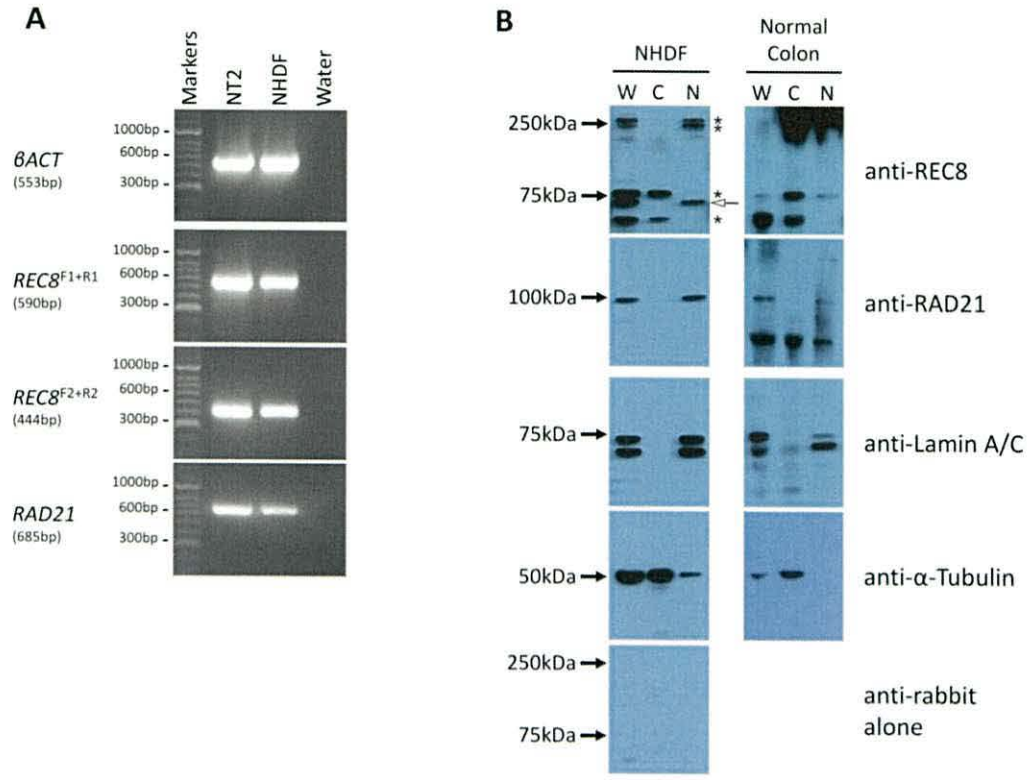

Figure 6.3. RT-PCR and Western blot analysis of REC8 and RAD21 in fibroblast cells. A. Agarose gels showing the expression of *REC8* and *RAD21* in NHDF cells. cDNA was generated from the total RNA extracted from NHDF cells. cDNA from the NT2 cell line was used as a positive control for *REC8* and *RAD21* expression. The expression of *βACT* is shown as a positive control for the cDNA samples (top). **B.** Western blot analysis showing the cellular localisation of REC8 and RAD21 in protein lysates prepared from NHDF cells and normal colon tissue. WCE (W), cytoplasmic lysate fraction (C) and nuclear lysate fraction (N). Antibodies against lamin A/C and α-tubulin were used as the positive controls, to check the efficiency of fractionation and the loading of the gel (bottom). (Experiment carried out only once).

The possible REC8-specific band (WB analysis), is indicated with an arrow, as per the results presented in Section 6.4. The likely non-specific bands are indicated by *.

As in the five cancer cell lines (shown in Figure 6.2), the anti-REC8 antibody appears to recognise two bands at approximately the predicted size in the fibroblast cells. In contrast, only a single band is observed for anti-REC8 in the normal colon tissue, which also appears to localise within the nucleus. The protein lysate preparation from the normal colon tissue does not appear to have been uniform or efficient (Figure 6.3, part B), which may be due to an incomplete homogenisation of the tissue samples. However the lamin A/C and α-tubulin controls suggest that fractionation was achieved, although it is not as clean as in the cancer cell lines.

These results suggest that *REC8* is expressed and its resultant protein is present in normal cells and localises in the nucleus, as observed in the cancer cells.

6.3.2 Immuno localisation of REC8

Immunofluorescent staining was also carried out for REC8 and RAD21 in the NT2 and SW480 cancer cell lines alongside the fibroblast cells, which were used as a normal control. The cells were fixed and then stained, the results for NT2, SW480 and NHDF cells are shown in Figures 6.4, 6.5 and 6.6 respectively.

The NT2 cells were stained with antibodies against lamin A/C and α-tubulin, to positively control for nuclear and cytoplasmic staining respectively. Staining for anti-RAD21 appears to demonstrate a strong nuclear staining, with limited cytoplasmic staining (Figure 6.4). These results correspond to the western blot results observed in Figure 6.2. Whereas anti-REC8 staining appears to be predominantly nuclear, with some staining in the cytoplasm which appears to be largely membrane associated (Figure 6.4). The cytoplasmic staining observed here may correspond to the upper band at approximately 75 kDa identified by western blot analysis in Figure 6.2. The nuclei exhibit a significant degree of punctate staining, for both anti-RAD21 and anti-REC8.

The anti-mouse and anti-rabbit secondary antibodies appear to produce some non-specific background in the NT2 cells. However, the level of non-specific background interaction produced by the secondary antibodies appears to be insignificant compared to the staining with the primary antibodies. This suggests that the staining observed for anti-RAD21 and anti-REC8 arises from primary antibody interaction.

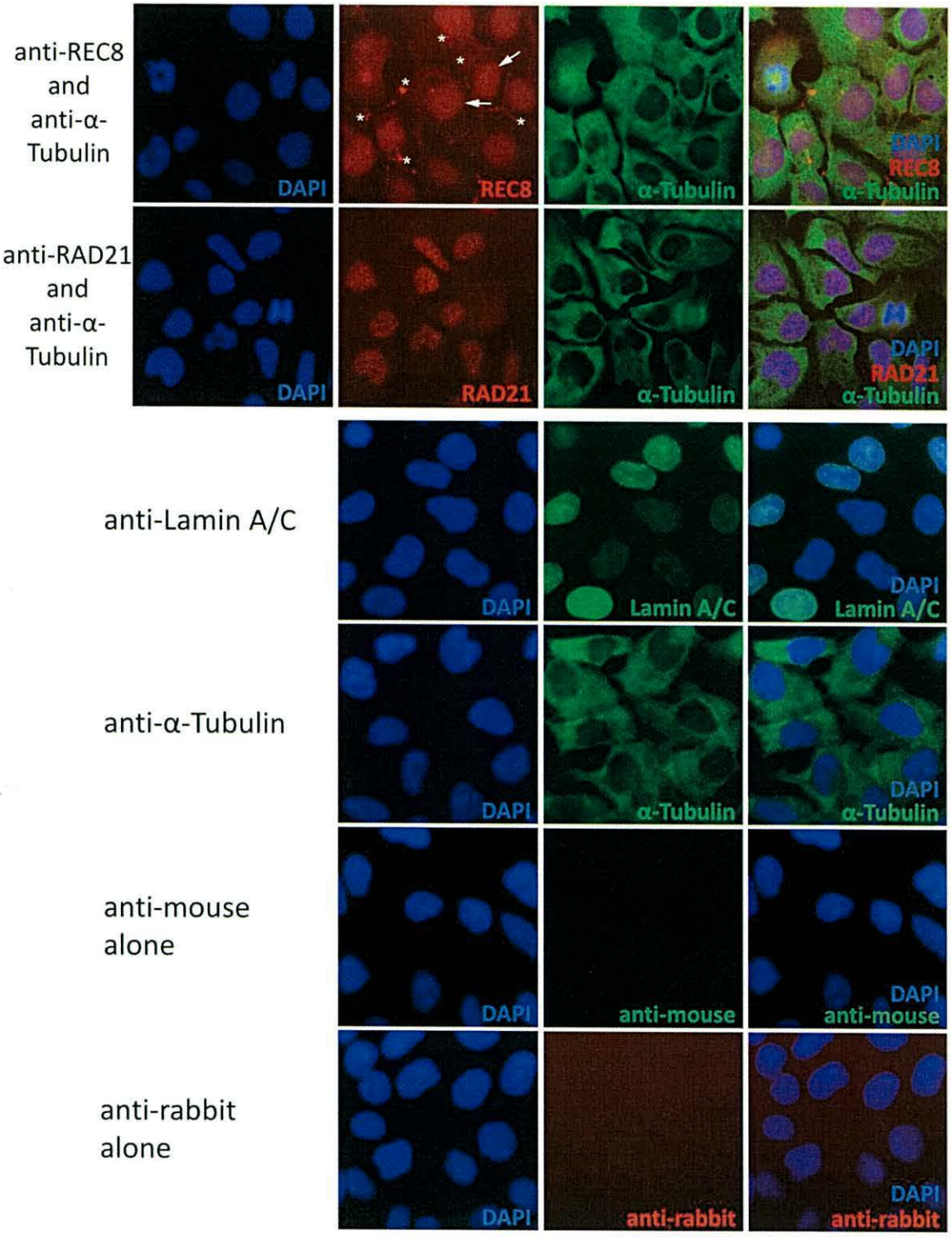

Figure 6.4. Immunofluorescent staining for REC8 and RAD21 in NT2 cells. Images for immunofluorescent staining for anti-REC8 (red) and anti-RAD21 (red) in NT2 cells, viewed using a Zeiss Axioskop 2 fluorescent microscope (x100 lens). Staining with anti-lamin A/C (green) and anti-α-tubulin (green) were used as positive controls for nuclear and cytoplasmic staining respectively. Staining with the secondary antibodies only were used as the negative controls, anti-rabbit for the anti-REC8 and anti-RAD21-staining and anti-mouse for the anti-lamin A/C and anti-α-tubulin staining. These results appear to be reproducible as this experiment was repeated more than three times.

The possible REC8-specific staining, as per the results presented in Section 6.4, is indicated with a white arrow. The likely non-specific bands are indicated by *.

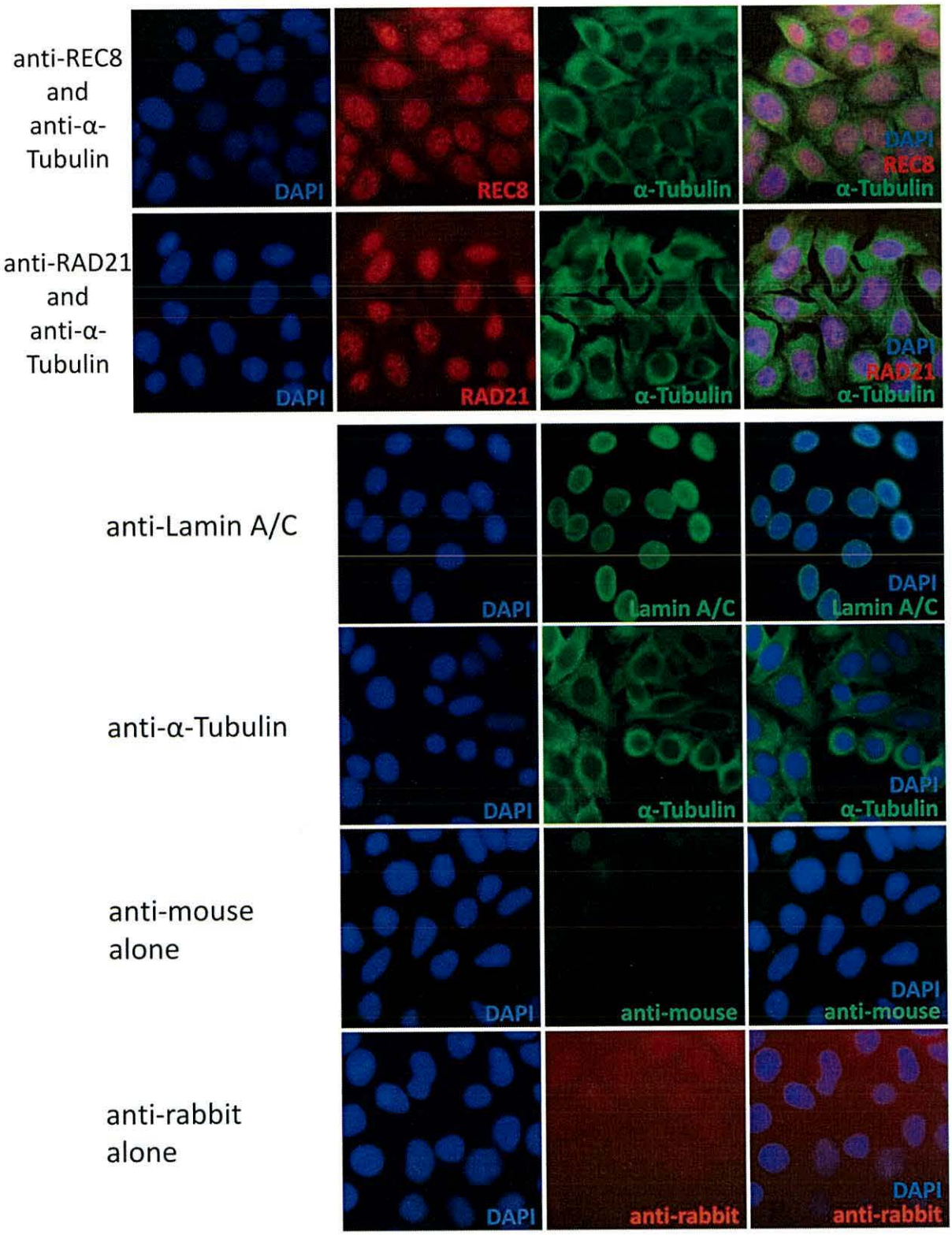

Figure 6.5. Immunofluorescent staining for REC8 and RAD21 in SW480 cells. Images for immunofluorescent staining for anti-REC8 (red) and anti-RAD21 (red) in SW480 cells, viewed using a Zeiss Axioskop 2 fluorescent microscope (x100 lens). Staining with anti-lamin A/C (green) and anti-α-tubulin (green) were used as positive controls for nuclear and cytoplasmic staining respectively. Staining with the secondary antibodies only were used as the negative controls, anti-rabbit for the anti-REC8 and anti-RAD21-staining and anti-mouse for the anti-lamin A/C and anti-α-tubulin staining. These results appear to be reproducible as this experiment was repeated three times.

The SW480 cells were also stained with antibodies against lamin A/C and α-tubulin, to positively control for nuclear and cytoplasmic staining respectively. As in the NT2 cells, staining with anti-RAD21 appears to be strongly nuclear, with little/no cytoplasmic staining (Figure 6.5). These results also correspond to the western blot results observed in Figure 6.2. Staining for anti-REC8 appears to be predominantly nuclear, with some staining in the cytoplasm (Figure 6.5). The anti-REC8 cytoplasmic staining in the SW480 cells appears to be weaker than the cytoplasmic staining observed in the NT2 cells. The immunofluorescent staining with anti-REC8 also appears to correspond with the results from the western blot analysis shown in Figure 6.2. As in the NT2 cells, the SW480 nuclei appear to exhibit a significant degree of punctate staining, for both anti-RAD21 and anti-REC8.

The anti-mouse secondary antibody also appears to produce a relatively high level of non-specific background in the SW480 cells, whereas the anti-rabbit secondary antibody does not. The level of non-specific background interaction produced by the secondary antibodies appears to be insignificant compared to the staining with the primary antibodies. This may therefore suggest that the staining observed for anti-RAD21 and anti-REC8 arises from primary antibody interaction.

Immunofluorescent staining was also carried out in fibroblast cells, to check if the same localisation pattern for REC8 and RAD21 is observed in normal cells, the results are shown in Figure 6.6.

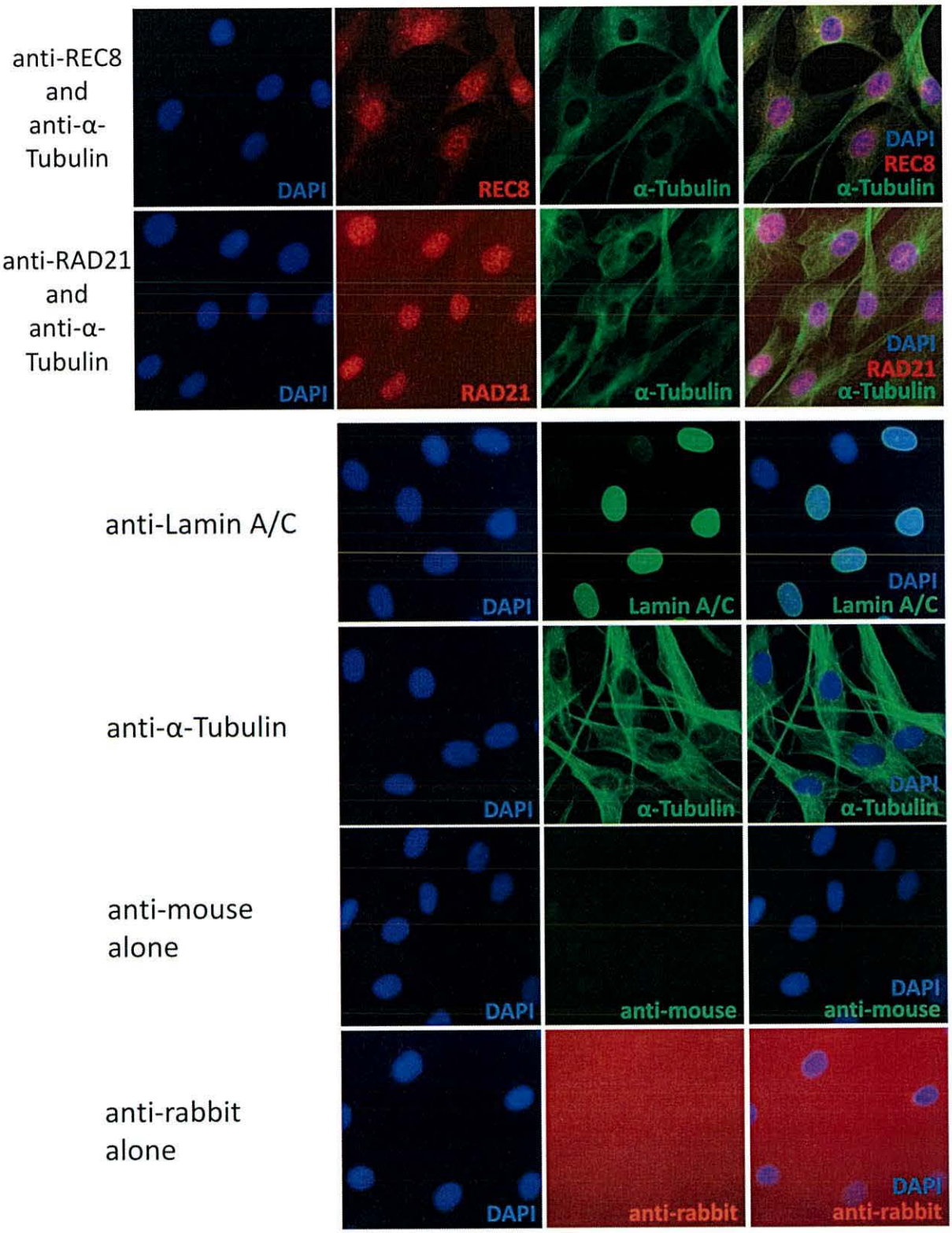

Figure 6.6. Immunofluorescent staining for REC8 and RAD21 in fibroblast cells. Images for immunofluorescent staining for anti-REC8 (red) and anti-RAD21 (red) in NHDF cells, viewed using a Zeiss Axioskop 2 fluorescent microscope (x100 lens). Staining with anti-lamin A/C (green) and anti-α-tubulin (green) were used as positive controls for nuclear and cytoplasmic staining respectively. Staining with the secondary antibodies only were used as the negative controls, anti-rabbit for the anti-REC8 and anti-RAD21-staining and anti-mouse for the anti-lamin A/C and anti-α-tubulin staining. This experiment was carried out once.

The NHDF cells were stained with antibodies against lamin A/C and α-tubulin, to positively control for nuclear and cytoplasmic staining respectively. Anti-RAD21 staining appears to be strongly nuclear, with little/no cytoplasmic staining, corresponding to the RAD21 localisation pattern observed in the NT2 and SW480 cells. Anti-REC8 staining appears to be predominantly nuclear, with some cytoplasmic staining. Western blot analysis identified two bands for anti-REC8 in the fibroblast cells, one nuclear and one cytoplasmic (Figure 6.3), which is in line with these immunofluorescent results. Punctate staining is observed for both anti-REC8 and anti-RAD21, in the NHDF nuclei, similar to that observed for NT2 and SW480 cells.

The anti-mouse and anti-rabbit secondary antibodies both appear to produce some non-specific background in the NHDF cells. The level of non-specific background interaction produced by the secondary antibodies appears to be insignificant compared to the staining with the primary antibodies. This suggests that the staining observed for anti-RAD21 and anti-REC8 arises from primary antibody interaction.

These results suggest that REC8 localises predominantly within the nucleus of the two cancer cell lines, NT2 and SW480, and the fibroblast cells. The nuclear localisation of REC8 may be potentially interesting, because the cohesin complex functions within the nucleus.

6.4 REC8 characterisation in the 1321N1 cell line

The RT-PCR results shown in Figure 6.1 showed *REC8* expression in 17 of the 18 cancer cell lines tested. The brain cancer cell line (1321N1) was negative for *REC8* expression, and although it displayed *RAD21* expression, the intensity of the PCR band was significantly fainter than that observed for the other cell lines tested. *REC8* expression and protein abundance was characterised within 1321N1 cells compared to NT2 cells.

6.4.1 qRT-PCR for *REC8* in 1321N1 cells

Commercial qRT-PCR primers (Qiagen) were used to carry out SYBR® Green-based real time RT-PCR for *REC8* and *RAD21* in 1321N1 cells compared to NT2 cells (as described in Section 2.7). The *REC8* and *RAD21* qRT-PCR results were normalised to the qRT-PCR results for *Lamin A* and *GAPDH* using the ΔΔCq method; the results are shown in Figure 6.7.

A

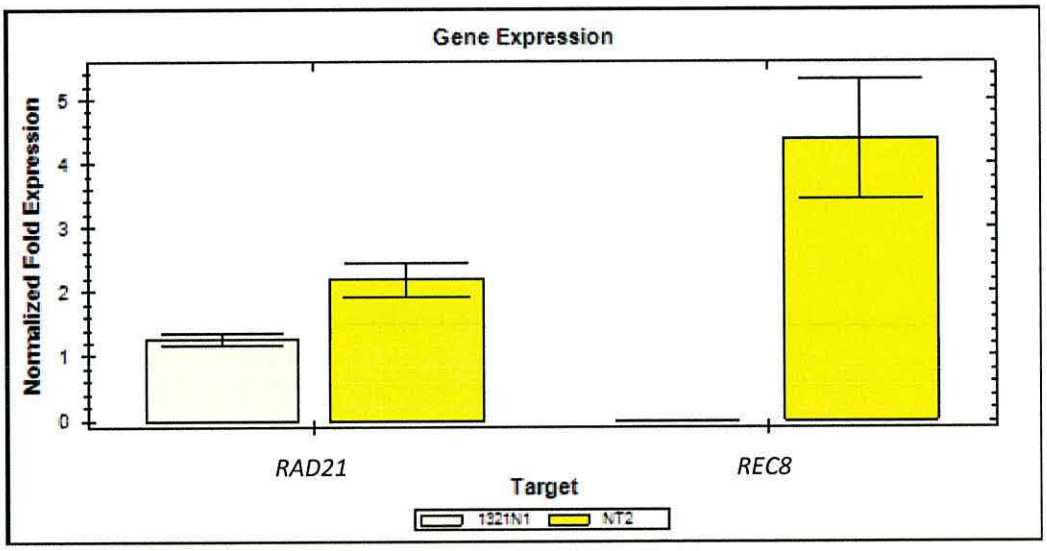

B

Target	Sample	Cq Reading 1	Cq Reading 2	Cq Reading 3	Cq Mean	Cq Std. Dev
REC8	NT2	38.59	38.04	38.02	38.22	0.323
RAD21	NT2	34.44	33.97	34.23	34.21	0.235
Lamin A	NT2	36.61	36.05	35.85	36.17	0.394
GAPDH	NT2	31.33	31.21	31.19	31.24	0.077
REC8	1321N1	N/A	N/A	N/A	0.00	0.000
RAD21	1321N1	33.03	33.29	33.31	33.21	0.155
Lamin A	1321N1	32.07	31.85	31.81	31.91	0.140
GAPDH	1321N1	32.00	31.76	31.93	31.90	0.124
Lamin A	NT2 (NRT)	N/A	N/A	N/A	0.00	0.000
GAPDH	NT2 (NRT)	N/A	N/A	N/A	0.00	0.000
REC8	NT2 (NRT)	N/A	N/A	N/A	0.00	0.000
RAD21	NT2 (NRT)	N/A	N/A	N/A	0.00	0.000
Lamin A	1321N1 (NRT)	N/A	N/A	N/A	0.00	0.000
GAPDH	1321N1 (NRT)	N/A	N/A	N/A	0.00	0.000
REC8	1321N1 (NRT)	N/A	N/A	N/A	0.00	0.000
RAD21	1321N1 (NRT)	N/A	N/A	N/A	0.00	0.000
Lamin A	NTC	N/A	N/A	N/A	0.00	0.000
GAPDH	NTC	N/A	N/A	N/A	0.00	0.000
REC8	NTC	N/A	N/A	N/A	0.00	0.000
RAD21	NTC	N/A	N/A	N/A	0.00	0.000

Figure 6.7. SYBR® Green-based real time RT-PCR for *REC8* and *RAD21* in 1321N1 cells compared to NT2 cells. A. Bar chart showing the gene expression results for *REC8* and *RAD21* in 1321N1 and NT2 cells, normalised to *Lamin A* and *GAPDH* expression using the ΔΔCq method. The data was analysed using the Bio-RAD CFX Manager. The error bars indicate the standard error for 3 repeats. **B.** Table showing the Cq (quantification cycle) readings and standard deviation for the *Lamin A*, *GAPDH*, *REC8* and *RAD21* readings. The Cq readings for the NRT (no reverse transcriptase) and NTC (no template control) negative controls are also shown in the table. These results appear to be reproducible as this experiment was carried out two times.

The relative expression of *Lamin A*, *GAPDH*, *REC8* and *RAD21* in 1321N1 and NT2 cells were calculated using the ΔCq method, the results are shown in the Appendix.

The NRT (no reverse transcriptase) and NTC (no template control) negative controls did not give a Cq (quantification cycle) reading, which suggests that there was no non-specific background and no genomic DNA contamination. These qRT-PCR results show a lower level of *RAD21* expression in the 1321N1 cells compared to the NT2 cells and also suggest that there is no/very little *REC8* gene expression in the 1321N1 cells. The RT-PCR results shown in Figure 6.1 suggested that the 1321N1 cell line was negative for *REC8* expression, and the intensity of the *RAD21* PCR band was fainter than that observed for the other cell lines. Therefore these qRT-PCR results correspond to the RT-PCR results previously observed (Figure 6.1). Interestingly, these results also appear to suggest a greater level of *REC8* expressed in the NT2 cells compared to *RAD21*.

Melting curve analysis was also carried out to establish if any non-specific amplicons were being produced by the primer assays. See Appendix for the corresponding melt curve graphs and the relative gene expression results for *GAPDH*, *Lamin A*, *REC8* and *RAD21* calculated using the ΔCq method.

6.4.2 Protein expression of REC8 in 1321N1 cells

As previously discussed (in Chapter 5.0) the correlation between gene expression and protein abundance is not directly proportional, and is effected by numerous post-transcriptional mechanisms (Tan *et al.*, 2009; Waters *et al.*, 2006). Therefore protein abundance and localisation of REC8 was assessed in 1321N1 cells compared to NT2 cells. WCEs were prepared for the 1321N1 and NT2 cell lines and subjected to western blot analysis; the results are shown in Figure 6.8.

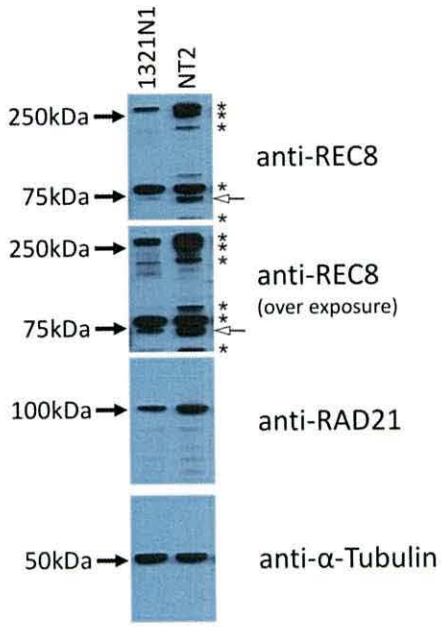

Figure 6.8. Western blot analysis for REC8 and RAD21 in 1321N1 cells. Western blot analysis showing the abundance of REC8 and RAD21 in 1321N1 cells compared to NT2 cells. WCEs were prepared and subjected to western blot analysis. Anti-α-tubulin was used as a loading control (bottom). This experiment was only carried out once.

The possible REC8-specific band is indicated with an arrow (right).
The likely non-specific bands are indicated by *.

The α-tubulin results suggest that the gel loading was relatively equal and therefore differences in band intensities are likely to be due to differences in protein abundance in the two cell lines. These western blot analysis results show a fainter band for RAD21 in the 1321N1 cells compared to the NT2 cells. The RT-PCR (Figure 6.1) and the qRT-PCR (Figure 6.7) results suggested a possible lower level of *RAD21* gene expression in the 1321N1 cells compared to the NT2 cells. Therefore, these western blot results appear to correspond with the gene expression results.

Western blot analysis using anti-REC8 identified two bands at approximately 75 kDa in the following cell lines; NT2, HCT116, SW480, A2780, HeLa T-REx and NHDF, and showed that the lower band localised in the nucleus and the upper band localised in the cytoplasm (Figures 6.2 and 6.3). These western blot results appear to show that the intensity of the upper band is approximately even in the 1321N1 and NT2 cells. However the lower band is significantly fainter in the 1321N1 cells compared to the NT2 cells. Also, the lower band observed for the 1321N1 cells may actually run slightly higher than the lower band observed in the NT2 cells. These western blot results in conjunction with the PCR results may suggest

that the upper band identified by anti-REC8 (at approximately 75 kDa) may not be specific to REC8.

Immunofluorescent staining for REC8 and RAD21 in fixed 1321N1 cells and NT2 cells was also carried out, to establish the cellular localisation and abundance of REC8 in the 1321N1 cells compared to NT2 cells. The results are shown in Figure 6.9.

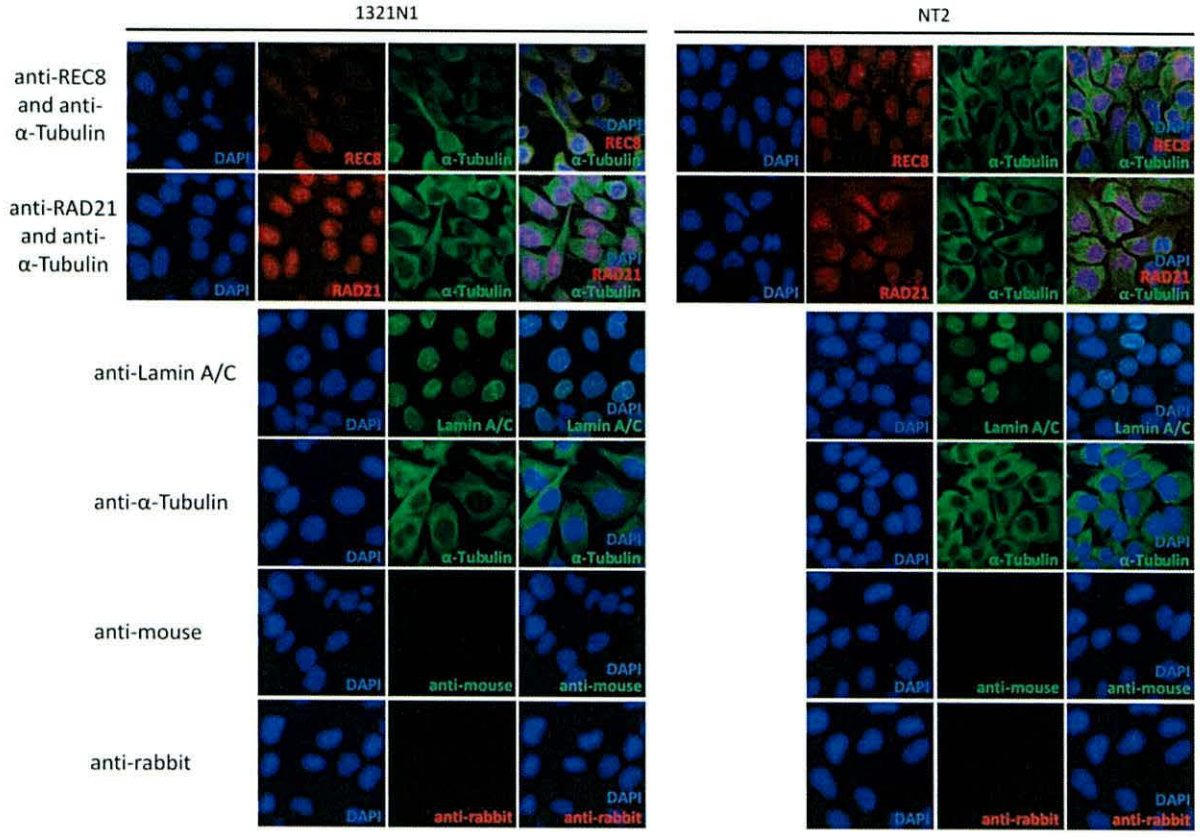

Figure 6.9. Immunofluorescent staining for REC8 and RAD21 in 1321N1 and NT2 cells. Images for immunofluorescent staining for anti-REC8 (red) and anti-RAD21 (red) in 1321N1 and NT2 cells, viewed using a Zeiss Axioskop 2 fluorescent microscope (x100 lens). Staining with anti-lamin A/C (green) and anti-α-tubulin (green) were used as positive controls for nuclear and cytoplasmic staining respectively. Staining with the secondary antibodies only were used as the negative controls, anti-rabbit for the anti-REC8 and anti-RAD21 staining and anti-mouse for the anti-lamin A/C and anti-α-tubulin staining. These results appear to be reproducible as the experiment was repeated two times.

The 1321N1 and NT2 cells were stained with antibodies against lamin A/C and α-tubulin, to positively control for nuclear and cytoplasmic staining respectively. Staining for anti-RAD21 appears to be strongly nuclear, with little/no cytoplasmic staining, for both cell lines. As previously shown in Figure 6.4, anti-REC8 staining appears to be predominantly nuclear, with some staining in the cytoplasm which appears to be membrane associated in the NT2

cells. However the anti-REC8 staining in the 1321N1 cells does not appear to show a clear nuclear localisation as it does in the NT2 cells. This appears to correspond with the western blot results, because the lower band was significantly fainter in the 1321N1 cells than in the NT2 cells, and may even correspond to a different protein size (Figure 6.8). Interestingly, a significant degree of nuclear punctate staining for anti-REC8 and anti-RAD21 was observed for the NT2, SW480 and NHDF cells (Figures 6.4-6.6); however the 1321N1 cells do not appear to exhibit this staining pattern for anti-REC8. Punctate staining is observed for anti-RAD21 in the 1321N1 nuclei, but not for anti-REC8.

Western blot analysis showed the upper band (around 75 kDa) to be localised in the cytoplasm (Figure 6.2), and the western blot analysis results shown in Figure 6.8 showed that the intensity of this upper band was relatively equal in the 1321N1 and NT2 cells. The immunofluorescent staining results appear to correspond to the western blot and PCR results, and suggest that the upper band at 75 kDa recognised by anti-REC8 may be non-specific.

The anti-rabbit secondary antibody appears to produce a relatively low level of non-specific background in the 1321N1 and NT2 cells. This suggests that the staining observed for anti-RAD21 and anti-REC8 arises from primary antibody interaction.

6.5 Chromatin association analysis of REC8

6.5.1 Chromatin association of REC8 and RAD21

Western blot analysis and immunofluorescent staining of fixed cells both suggest that RAD21 and REC8 localise in the nucleus. Although REC8 appears to localise within the nucleus of these cell lines, this does not specify a role in chromosome cohesion. Chromatin association (Ch) protein lysates were prepared for NT2, HCT116, SW480 and A2780 cells (as per Section 2.11.2) and any chromatin association displayed by REC8 was assessed by western blot. The cells were collected from asynchronous cultures and colcemid synchronised cultures for each cell line. The western blot results are shown in Figure 6.10.

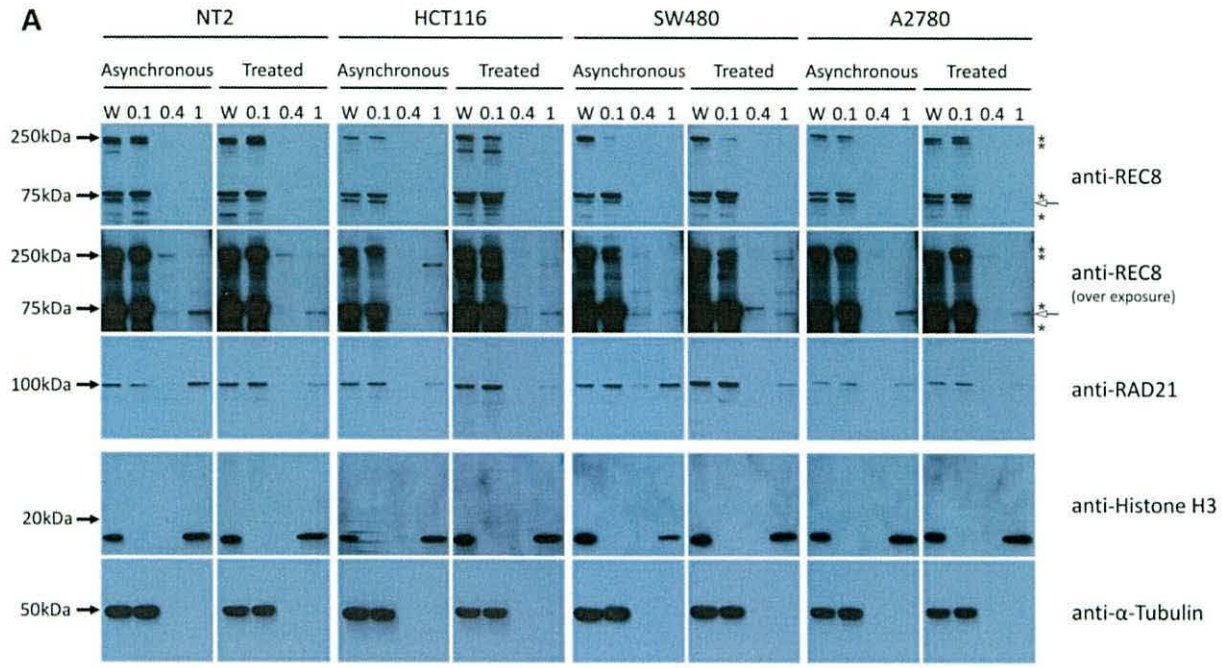

B

	NT2		HCT116		SW480		A2780	
	Async	Treated	Async	Treated	Async	Treated	Async	Treated
% Metaphase	0.99	66.99	0	65.49	2.44	71.89	0.50	70.33
% Not metaphase	99.01	33.01	100	34.51	97.56	28.11	99.50	29.67

Figure 6.10. Chromatin association of REC8 and RAD21 in NT2, HCT116, SW480 and A2780 cells. Cells were incubated with 0.1 μg/ml colcemid for 16 hrs to synchronise the cells at metaphase. Asynchronous cell cultures were compared to colcemid-synchronised cultures, to see if there is a difference in any chromatin association for REC8. **A.** Western blot analysis showing the chromatin association of REC8 and RAD21 in NT2, HCT116, SW480 and A2780 cell lines. WCE (W) was loaded as a positive control and lysates with varying concentrations of salt were prepared to assess chromatin association; 0.1 M (0.1), 0.4 M (0.4) and 1 M (1) NaCl. Antibodies against histone-H3 and α-tubulin were used as the positive controls (bottom). **B.** Metaphase spreads were carried out to establish the effectiveness of synchronisation. Table indicating the percentage of metaphase cells, from the metaphase spreads comparing the asynchronous and colemid-synchronised cell cultures. These results appear to be reproducible as this experiment was repeated two times.

The possible REC8-specific band, as per the results presented in Section 6.4, is indicated with an arrow (right). The likely non-specific bands are indicated by *.

Asynchronous cultures and colcemid-synchronised cultures were used to assess any changes in the chromatin association of REC8 and RAD21 at metaphase. The number of cells in metaphase appears to be significantly increased in the colcemid-treated culture compared to the asynchronous culture, for each cell line. The chromatin association assay (Ch) protein lysates were prepared consecutively with increasing concentrations of salt (NaCl) for the asynchronous and colcemid-synchronised cultures. The 0.1 M Ch lysate corresponds to the proteins with very weak or no chromatin association, whereas the 0.4 M Ch lysate

corresponds to proteins which display weak chromatin association and the 1 M Ch lysate to strongly chromatin associated proteins. Antibodies against histone-H3 and α-tubulin were used as positive controls to ensure the Ch lysates were prepared properly.

Western blot analysis shows a band for RAD21 in the 0.1 M and 1 M NaCl Ch lysates, therefore suggesting that RAD21 is strongly chromatin associated, but some RAD21 is either weakly associated or not associated. There also appears to be a possible reduction in the signal intensity observed in the 1 M NaCl Ch lysate for the colcemid-synchronised cells compared to the asynchronous cells.

A band for REC8 is also observed in the 0.1 M, 0.4 M and 1 M NaCl Ch lysates, which may suggest that REC8 is also strongly chromatin associated in these cells. However overexposure of the western blot was required to detect the band in the 1 M NaCl Ch lysate, which may suggest that significantly less REC8 is strongly chromatin associated than RAD21. The majority of the REC8 observed in these cells appears to be very weakly or not chromatin associated. Although it is not as clear as for RAD21, there appears to be a decrease in the signal intensity for REC8 in the 1 M NaCl Ch lysates for the colcemid-synchronised cells compared to the asynchronous cells for the NT2 and A2780 cell lines.

6.5.2 Chromatin association of REC8 and RAD21 with cell cycle analysis

Due to the potential differences observed for both RAD21 and REC8 for the metaphase-enriched cell cultures compared to the asynchronous cultures, we decided to assess chromatin association at different stages of the cell cycle. The cells were synchronised using thymidine and nocodazole as per Section 2.11 (methodology adapted from Bermudez *et al.*, 2012). The study by Bermudez *et al.*, (2012) carried out a cell cycle analysis using HeLa cells. The NT2, HCT116, SW480 and A2780 cell lines all display a similar doubling time to that observed in HeLa cells, therefore the same incubation times were used here. Cells were collected in the G_1, S, G_2 and M phases of the cell cycle and Ch protein lysates were prepared. Western blot analysis was used to assess RAD21 and REC8 chromatin association at different stages of the cell cycle. The results for NT2, HCT116, SW480 and A2780 cells are shown in Figures 6.11, 6.12, 6.13 and 6.14 respectively.

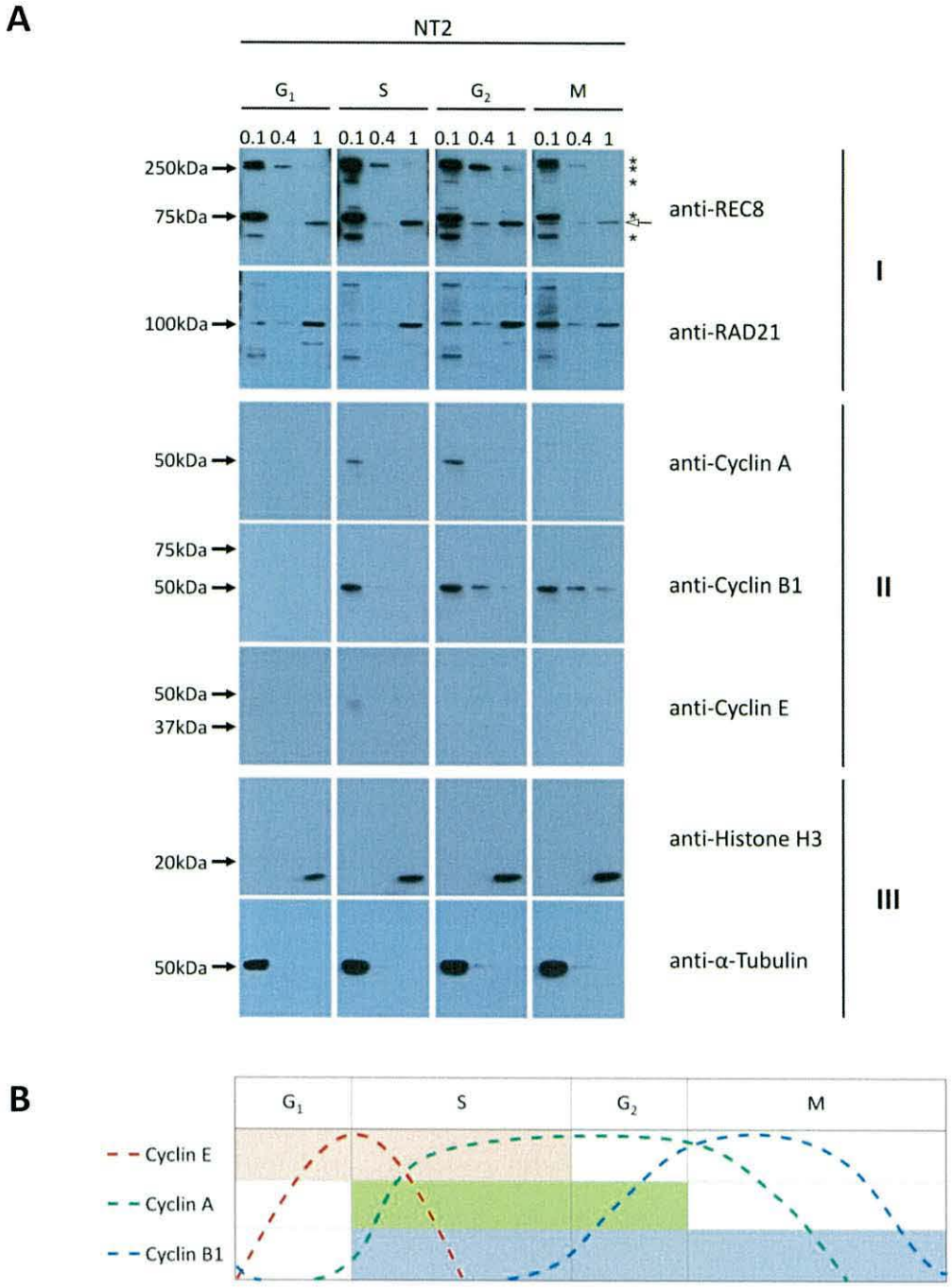

Figure 6.11. Chromatin association of REC8 and RAD21 with cell cycle analysis in NT2 cells. **A.** Western blot analysis showing the chromatin association of REC8 and RAD21 in NT2 cells, at the G_1, S, G_2 and M phases of the cell cycle. Protein lysates with varying concentrations of salt were prepared to assess chromatin association; 0.1 M (0.1), 0.4 M (0.4) and 1 M (1) NaCl. **I.** Chromatin association of REC8 and RAD21. **II.** Cell synchronisation at different stages of the cell cycle was assessed using antibodies against a number of cell cycle markers; cyclin A, cyclin B1 and cyclin E. **III.** Antibodies against histone-H3 and α-tubulin were used as the positive controls. **B.** A graphical representation of the expected cell cycle profile for cyclin A (green), cyclin E (red) and cyclin B1 (blue) (adapted from Bardin and Amon, 2001), is overlaid on a table which indicates which cell cycle stage each cyclin was observed for by western blot (part A). This experiment was carried out once only.

The possible REC8-specific band, as per the results presented in Section 6.4, is indicated with an arrow (right). The likely non-specific bands are indicated by *.

Antibodies against cyclin A, cyclin B1 and cyclin E were used to assess the cell cycle synchronisation efficiency in the NT2 cells. The western blot results for these antibodies were compared with the expected cell cycle profile (Figure 6.11, part B); cyclin E should be present during the G_1 and S stages of the cell cycle, which corresponds to the western blot analysis results observed for NT2 and cyclin B should be present from S phase to the end of M phase, which corresponds to the western blot analysis results observed for NT2. These results suggest that the cell cycle synchronisation was relatively successful in the NT2 cells.

Antibodies against histone-H3 and α-tubulin were also used to control for strong chromatin association and no chromatin association respectively. The controls display the expected western blot profiles, therefore changes observed in the western blot profiles for REC8 and RAD21 may be connected to changes in chromatin association during the cell cycle stages.

Western blot analysis shows a band for anti-RAD21 in the 0.4 M and 1 M NaCl Ch lysates at all four stages of the cell cycle. These results suggest that RAD21 is involved in both strong and weak chromatin association throughout the cell cycle. At M phase there appears to be a shift in signal intensity compared to the other cell cycle stages, the intensity of the band in the 0.1 M NaCl Ch lysate increases and the intensity of the band in the 1 M NaCl Ch lysate appears to decrease. These results may correspond to the release of cohesin from the sister chromatid arms during prophase (which corresponds to the start of M phase here) (Holt and Jones, 2009; Nasmyth, 2011).

REC8 also appears to display strong chromatin association at all four stages of the cell cycle, with a potential decrease in the band intensity observed at M phase.

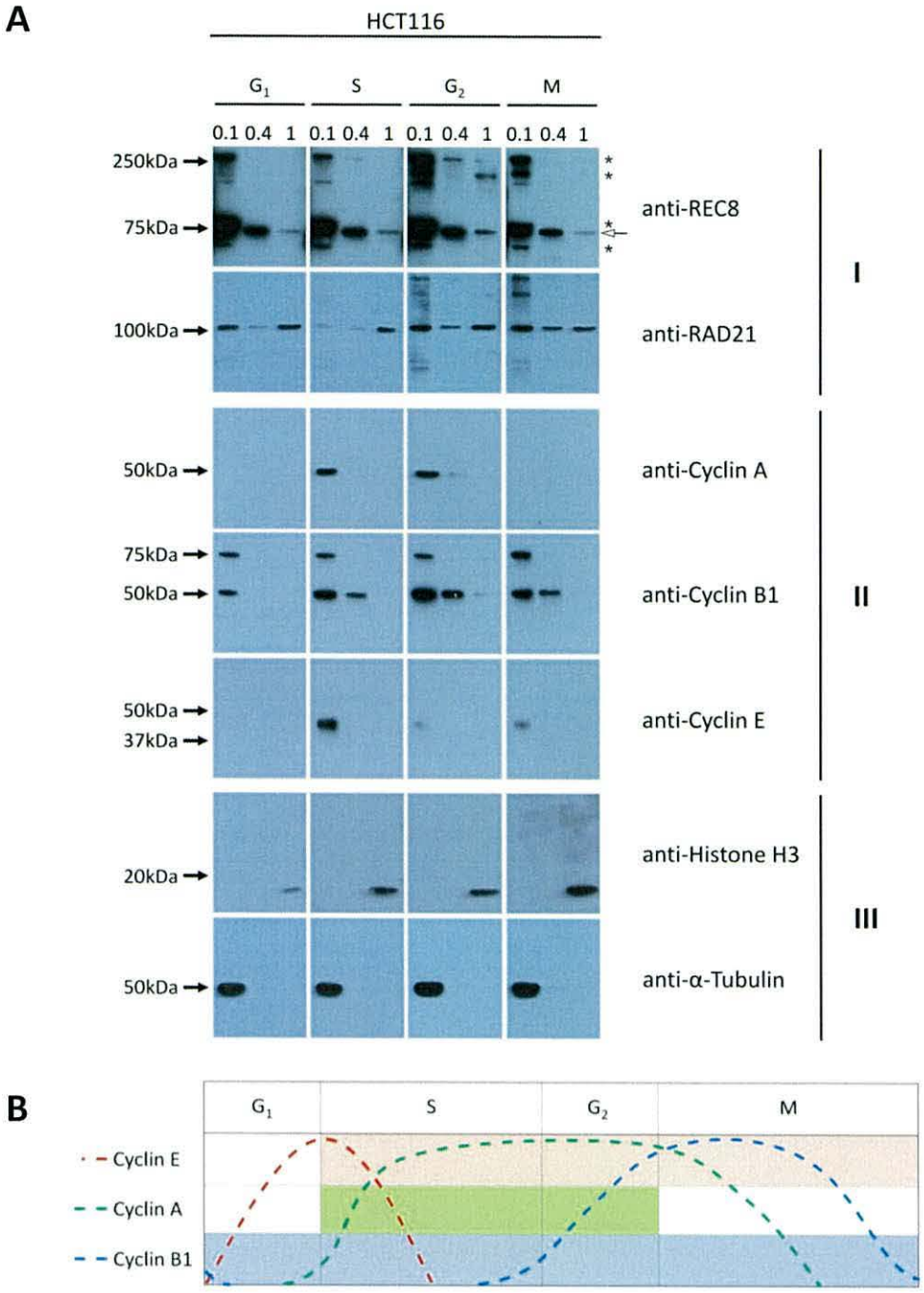

Figure 6.12. Chromatin association of REC8 and RAD21 with cell cycle analysis in HCT116 cells. **A.** Western blot analysis showing the chromatin association of REC8 and RAD21 in HCT116 cells, at the G_1, S, G_2 and M phases of the cell cycle. Protein lysates with varying concentrations of salt were prepared to assess chromatin association; 0.1 M (0.1), 0.4 M (0.4) and 1 M (1) NaCl. **I.** Chromatin association of REC8 and RAD21. **II.** Cell synchronisation at different stages of the cell cycle was assessed using antibodies against a number of cell cycle markers; cyclin A, cyclin B1 and cyclin E. **III.** Antibodies against histone-H3 and α-tubulin were used as the positive controls. **B.** A graphical representation of the expected cell cycle profile for cyclin A (green), cyclin E (red) and cyclin B1 (blue) (adapted from Bardin and Amon, 2001), is overlaid on a table which indicates which cell cycle stage each cyclin was observed for by western blot (part A). This experiment was carried out once only.

The possible REC8-specific band, as per the results presented in Section 6.4, is indicated with an arrow (right). The likely non-specific bands are indicated by *.

As for the NT2 cells, antibodies against cyclin A, cyclin B1 and cyclin E were used to assess the cell cycle synchronisation efficiency in the HCT116 cells. The western blot results for these antibodies were compared with the expected cell cycle profile (Figure 6.12, part B) and suggested that the cell cycle synchronisation was not successful for the HCT116 cells. Antibodies against histone-H3 and α-tubulin were also used to control for strong chromatin association and no chromatin association respectively. The positive controls show the expected western blot profiles, therefore any chromatin association observed for REC8 and RAD21 may be real, however any changes in their western blot profiles is unlikely to be connected to changes in chromatin association during the cell cycle stages.

Western blot analysis shows a band for anti-RAD21 in the 0.4 M and 1 M NaCl Ch lysates at all four stages of the cell cycle, which may suggest that RAD21 displays both strong and weak chromatin association throughout the cell cycle. The anti-RAD21 signal intensity does not appear to vary at the different stages of the cell cycle. As HCT116 cell cycle synchronisation was not as successful as for the NT2 cells, changes in chromatin association in relation to the cell cycle cannot be interpreted from these western blot results.

REC8 also appears to display strong chromatin association at all four stages of the cell cycle. Over exposure of the western blot was required to see the band in the 1 M NaCl Ch lysate, but the band in the 0.4 M NaCl Ch lysate appears to be quite strong. This may suggest that only a small amount of the REC8 protein is involved in strong chromatin association, and a much greater amount is involved in weak chromatin association.

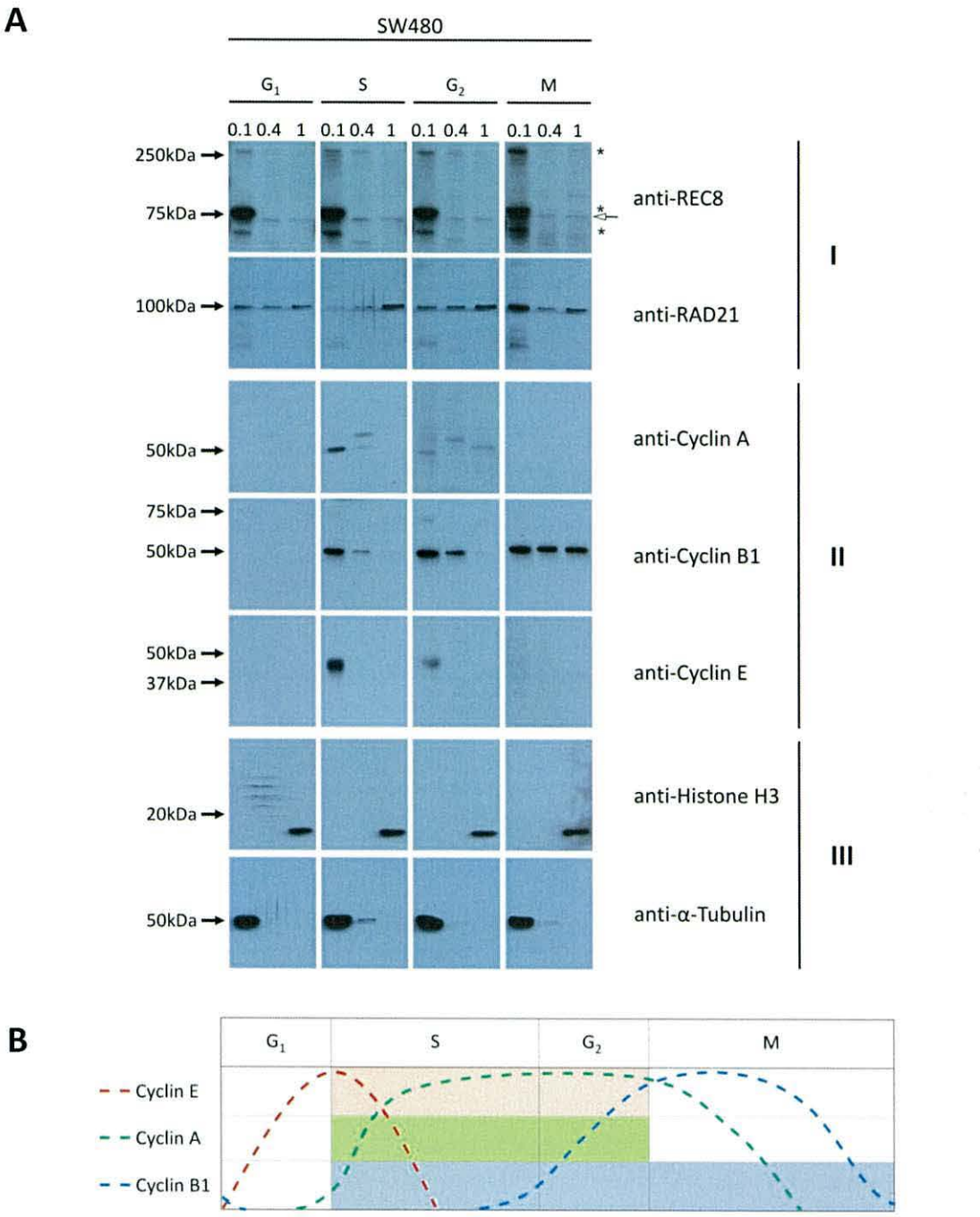

Figure 6.13. Chromatin association of REC8 and RAD21 with cell cycle analysis in SW480 cells. **A.** Western blot analysis showing the chromatin association of REC8 and RAD21 in SW480 cells, at the G_1, S, G_2 and M phases of the cell cycle. Protein lysates with varying concentrations of salt were prepared to assess chromatin association; 0.1 M (0.1), 0.4 M (0.4) and 1 M (1) NaCl. **I.** Chromatin association of REC8 and RAD21. **II.** Cell synchronisation at different stages of the cell cycle was assessed using antibodies against a number of cell cycle markers; cyclin A, cyclin B1 and cyclin E. **III.** Antibodies against histone-H3 and α-tubulin were used as the positive controls. **B.** A graphical representation of the expected cell cycle profile for cyclin A (green), cyclin E (red) and cyclin B1 (blue) (adapted from Bardin and Amon, 2001), is overlaid on a table which indicates which cell cycle stage each cyclin was observed for by western blot (part A). This experiment was carried out once only.

The possible REC8-specific band, as per the results presented in Section 6.4, is indicated with an arrow (right). The likely non-specific bands are indicated by *.

Antibodies against cyclin A, cyclin B1 and cyclin E were used to assess the cell cycle synchronisation efficiency in the SW480 cells. The western blot results for these antibodies were compared with the expected cell cycle profile (Figure 6.13, part B) and suggested that cell cycle synchronisation was relatively successful in the SW480 cells. Antibodies against histone-H3 and α-tubulin were also used to control for strong chromatin association and no chromatin association respectively. The controls display the expected western blot profiles, therefore changes observed in the western blot profiles for REC8 and RAD21 may be connected to changes in chromatin association during the cell cycle stages.

Western blot analysis shows a band for anti-RAD21 in the 0.4 M and 1 M NaCl Ch lysates at all four stages of the cell cycle. These results suggest that RAD21 is involved in both strong and weak chromatin association throughout the cell cycle. There may be a slight decrease in the anti-RAD21 signal intensity for the M phase 1 M NaCl Ch lysate compared to the S and G_2 cell cycle stage 1 M NaCl Ch lysates, which is paired with an increase in the intensity of the M phase 0.1 M NaCl Ch lysate. Although these results are not as clear as those observed for the NT2 cells, these results also appear to correspond to the release of cohesin from sister chromatid arms at prophase.

REC8 also appears to display strong and weak chromatin association at all four stages of the cell cycle. Overexposure of the western blot was required to observe the anti-REC8 band in the 0.4 M and 1 M NaCl Ch lysates, which may suggest a very small amount of REC8 is chromatin associated.

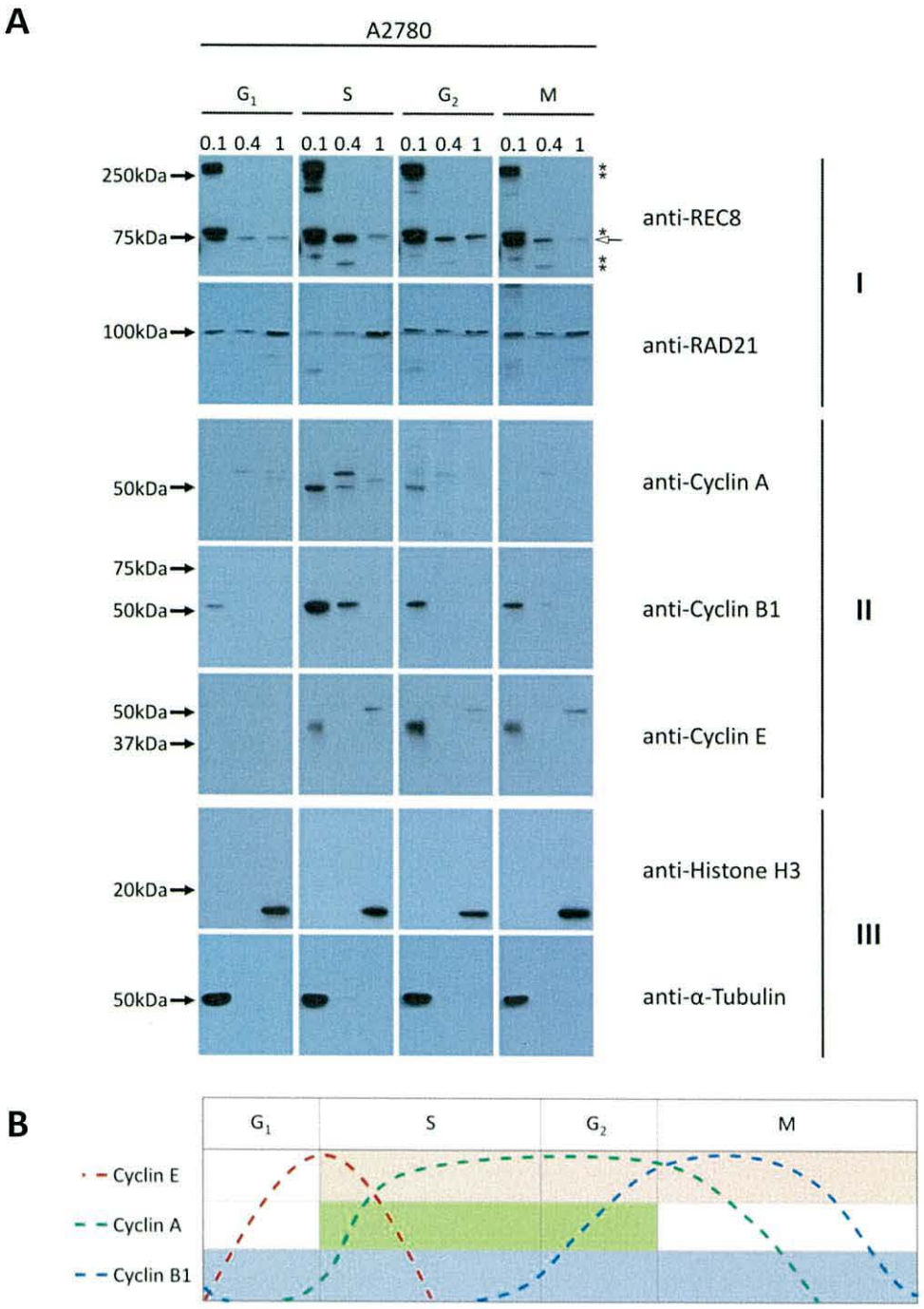

Figure 6.14. Chromatin association of REC8 and RAD21 with cell cycle analysis in A2780 cells. **A.** Western blot analysis showing the chromatin association of REC8 and RAD21 in A2780 cells, at the G_1, S, G_2 and M phases of the cell cycle. Protein lysates with varying concentrations of salt were prepared to assess chromatin association; 0.1 M (0.1), 0.4 M (0.4) and 1 M (1) NaCl. **I.** Chromatin association of REC8 and RAD21. **II.** Cell synchronisation at different stages of the cell cycle was assessed using antibodies against a number of cell cycle markers; cyclin A, cyclin B1 and cyclin E. **III.** Antibodies against histone-H3 and α-tubulin were used as the positive controls. **B.** A graphical representation of the expected cell cycle profile for cyclin A (green), cyclin E (red) and cyclin B1 (blue) (adapted from Bardin and Amon, 2001), is overlaid on a table which indicates which cell cycle stage each cyclin was observed for by western blot (part A). This experiment was carried out once only.

The possible REC8-specific band, as per the results presented in Section 6.4, is indicated with an arrow (right). The likely non-specific bands are indicated by *.

Western blot analysis using, antibodies against cyclin A, cyclin B1 and cyclin E, was used to assess the cell cycle synchronisation efficiency in the A2780 cells (Figure 6.14, part B). These results suggest that the cell cycle synchronisation was not successful for the A2780 cells.

Antibodies against histone-H3 and α-tubulin were also used to control for strong chromatin association and no chromatin association respectively. The positive controls show the expected western blot profiles, therefore any chromatin association observed for REC8 and RAD21 may be real, however any changes in their western blot profiles is unlikely to be connected to changes in chromatin association during the cell cycle stages.

Western blot analysis shows a band for anti-RAD21 in the 0.4 M and 1 M NaCl Ch lysates at all four stages of the cell cycle. These results suggest that RAD21 is involved in both strong and weak chromatin association throughout the cell cycle, with no apparent change in chromatin association strength. REC8 also appears to display strong chromatin association at all four stages of the cell cycle, with a potential decrease in the band intensity observed for the 1 M NaCl Ch lysate at the M phase. However, as A2780 cell cycle synchronisation was not as successful as for the NT2 and SW480 cells, no chromatin association pattern corresponding to the cell cycle stage can be interpreted from these western blot results. Overexposure of the western blot was required to observe the faint band for anti-REC8 in the 1 M NaCl Ch lysates, which may suggest a very small amount of REC8 is strongly associated with the chromatin.

Cell cycle synchronisation for the four cell lines was achieved with varying success, because western blot results suggested that the NT2 and SW480 cells were synchronised more successfully than the HCT116 and A2780 cells. These results suggest that REC8 and RAD21 display strong chromatin association at the G_1, S, G_2 and M phases of the cell cycle, with potentially a lower level of REC8 displaying strong chromatin association than RAD21.

Metaphase spreads were also carried out using these cancer cell lines to analyse REC8 and RAD21 binding to the metaphase chromosome. However, REC8 and RAD21 staining was negative for the metaphase spreads. An antibody against CENPA displayed positive staining for the metaphase spreads, which may suggest that the problem arose from the REC8 and RAD21 antibodies and not the technique.

6.5.3 Chromatin association of REC8 and RAD21 in NHDF cells

The western blot results for chromatin association in the cancer cell lines, suggest that REC8 may display strong and weak chromatin association in mitotically dividing cancer cells. Chromatin association protein lysates were also prepared for the fibroblast cells (asynchronous cell culture only), to establish if REC8 shows any chromatin association in normal (non-cancer) cells. Western blot analysis was carried out using the Ch lysates, the results are shown in Figure 6.15.

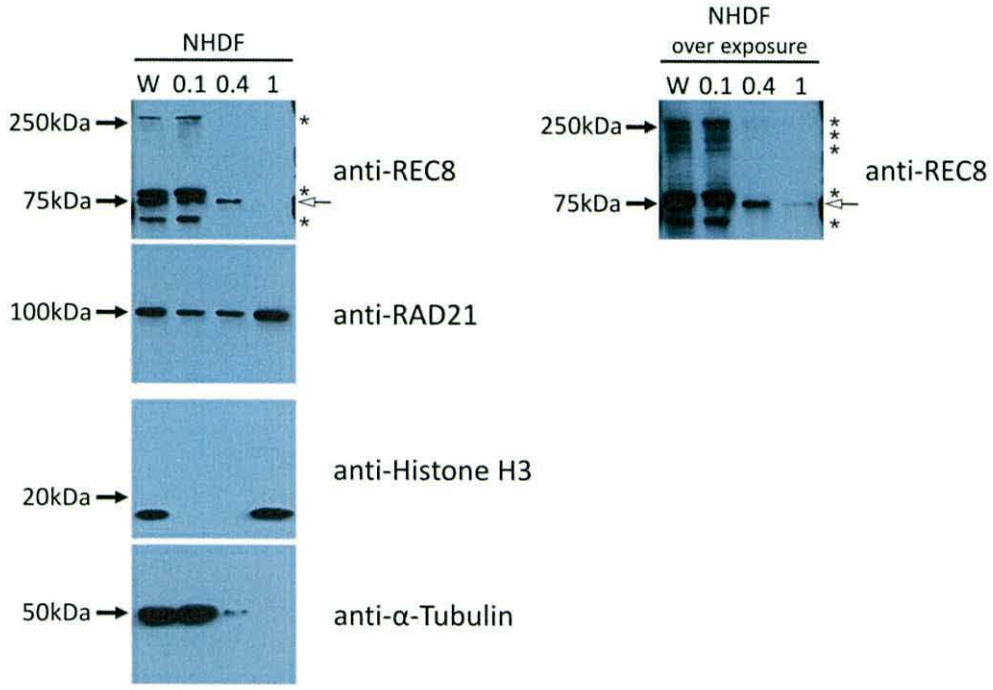

Figure 6.15. Chromatin association of REC8 and RAD21 in NHDF cells. Western blot analysis showing the chromatin association of REC8 and RAD21 in NHDF cells (asynchronous culture only). WCE (W) was loaded as a positive control and lysates with varying concentrations of salt were prepared to assess chromatin association; 0.1 M (0.1), 0.4 M (0.4) and 1 M (1) NaCl. Antibodies against histone-H3 and α-tubulin were used as the positive controls (bottom). This experiment was carried out once only.

The possible REC8-specific band, as per the results presented in Section 6.4, is indicated with an arrow (right). The likely non-specific bands are indicated by *.

Antibodies against histone-H3 and α-tubulin were also used to control for strong chromatin association and no chromatin association respectively. The positive controls show the expected western blot profiles, therefore any chromatin association observed for REC8 and RAD21 may be genuine.

The western blot results show a band for anti-RAD21 in the 0.1 M, 0.4 M and 1 M NaCl Ch lysates, which suggests that RAD21 displays weak and strong chromatin association in the

NHDF cells. This is in line with the western blot results for the four cancer cells lines (NT2, HCT116, SW480 and A2780), as expected, because RAD21 is reported to be an essential subunit of the mitotic cohesin complex.

A band is also shown for anti-REC8 in the 0.1 M, 0.4 M and 1 M NaCl Ch lysates, which suggests that REC8 also displays weak and strong chromatin association in the NHDF cells. Overexposure of the western blot was required to observe the faint band corresponding to anti-REC8 in the 1 M NaCl Ch lysate, which may indicate a very small amount of REC8 is strongly chromatin associated compared to the band intensity for weak or no chromatin association.

REC8 is reported to be a meiosis-specific protein, however these results suggest that it may be present in mitotically dividing cells and it displays a degree of strong chromatin association in the four cancer cell lines and the fibroblast cells tested.

6.6 Size fractionation

Although these results suggest that REC8 may be capable of strong and weak chromatin association in these mitotically dividing cells, there is no evidence to suggest that REC8 has a functional role or is associated with other cohesin subunits. WCEs were prepared for NT2 and NHDF cells and subjected to size exclusion chromatography (SEC) wherein the proteins/protein complexes are separated according to size. The fractions were then analysed using western blot analysis, the results are shown in Figure 6.16.

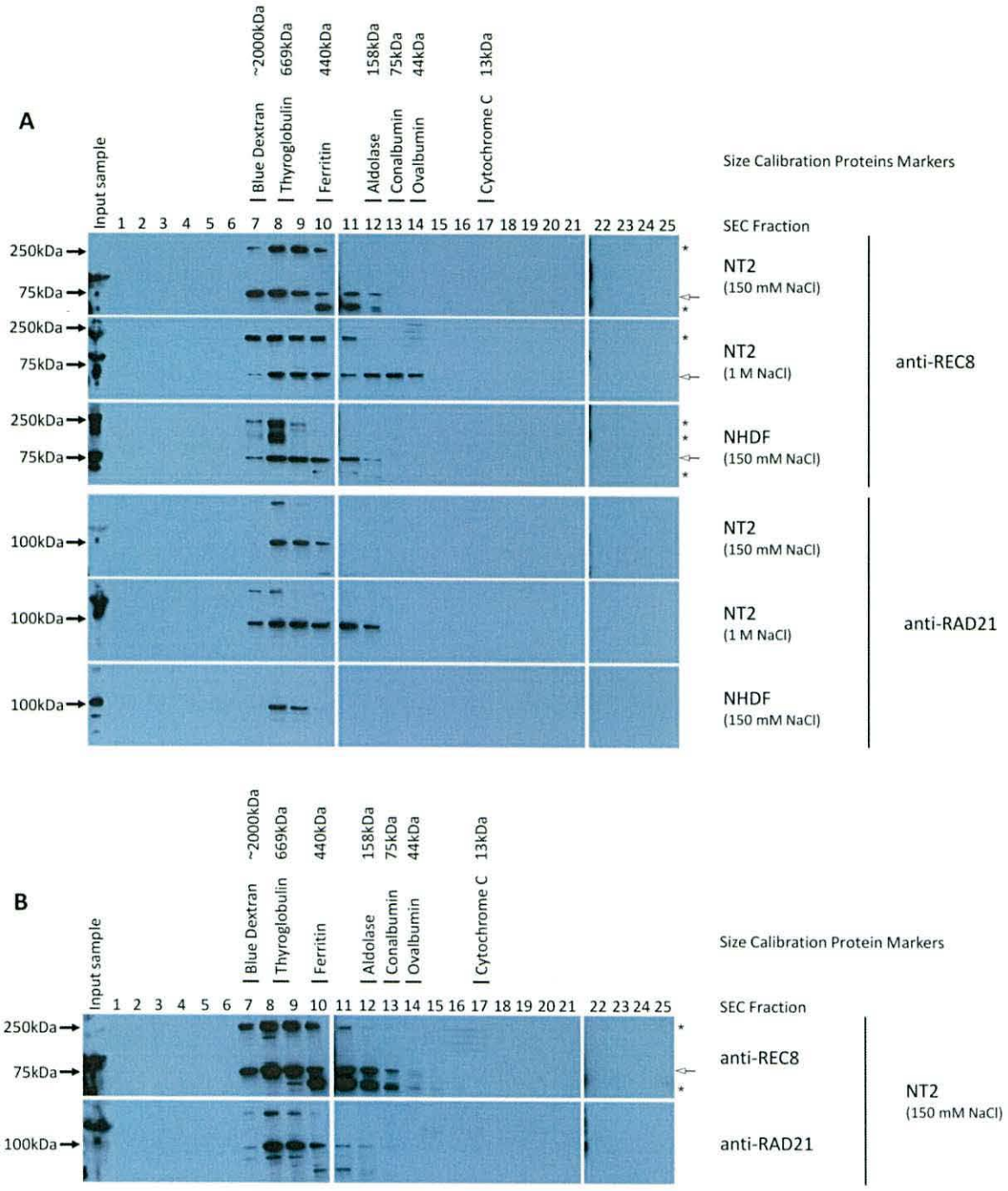

Figure 6.16. Western blot analysis for REC8 and RAD21 in SEC fractions 1-25. The SEC column was calibrated using the following standard proteins; blue dextran (approximately 2000 kDa), thyroglobulin (669 kDa), ferritin (440 kDa), aldolase (158 kDa), conalbumin (75 kDa), ovalbumin (44 kDa) and cytochrome C (13 kDa). The fraction in which elution of each standard protein peaked is indicated (top). **A.** Western blot analysis for REC8 and RAD21 in SEC fractions 1-25, for NT2 and NHDF cells with physiological salt (150 mM NaCl) and NT2 with high salt (1 M NaCl). An aliquot of the original input sample was run alongside the SEC fractions as a control; this sample is massively overloaded because the original input sample was very concentrated. **B.** Overexposure for anti-REC8 and anti-RAD21 for NT2 (150 mM NaCl) appears to show the monomer forms of both REC8 and RAD21. This experiment was carried out once only.

The possible REC8-specific band, as per the results presented in Section 6.4, is indicated with an arrow (right). The likely non-specific bands are indicated by *.

The western blot results appear to suggest that REC8 and RAD21 elute within a similar range of SEC fractions. The predicted molecular weights of REC8 and RAD21 are approximately 63 kDa and 72 kDa respectively, and the western blot bands observed for REC8 and RAD21 are approximately 75 kDa and 100 kDa respectively. These western blot results suggest that REC8 and RAD21 elution from the SEC column peaks in fraction 8. Elution of the standard protein thyroglobulin, which has a molecular weight of 669 kDa, peaked between fractions 8 and 9, therefore suggesting that both REC8 and RAD21 are eluting at a significantly higher molecular weight range than the predicted molecular weight of the monomeric proteins.

Two bands were previously identified by anti-REC8 using western blot analysis, for the cancer cell lines and the fibroblast cells. The band identified by anti-REC8 in the SEC fractions appears to correspond with the lower band (at approximately 75 kDa), which was shown to display nuclear localisation (Figures 6.2 and 6.3) and chromatin association (Figures 6.10-6.15). Anti-REC8 does not appear to recognise the upper band within the SEC fractions, which supports the suggestion that this band may correspond to a non-specific interaction.

RAD21 is known to be a component of the mitotic cohesin complex, which is a large multiprotein complex, and was therefore expected to elute at a high molecular weight. REC8 also appears to have eluted at a significantly higher molecular weight than that of the predicted molecular weight of monomeric protein, which may suggest that REC8 is also involved in a large protein complex. Interestingly, REC8 appears to have eluted in a similar range of SEC fractions as RAD21, which could potentially suggest that REC8 is involved in a cohesin complex structure within these mitotic cells. REC8 is known to be involved in the cohesin complex within meiotic cells; therefore we know it is capable of interacting with the other cohesin complex subunit proteins.

When the western blot membranes were overexposed, bands for anti-REC8 and anti-RAD21 were observed in fraction 13 for NT2 (150 mM NaCl); this is likely to correspond to the monomeric forms of the proteins. Elution of the standard protein conalbumi, which has a molecular weight of 75 kDa, peaked at fraction 13.

Also, when the NT2 protein extract was prepared using high salt (1 M NaCl) elution of REC8 and RAD21 appears to shift, and a greater amount of REC8 and RAD21 appears to elute at

lower molecular weights than observed for the physiological salt (150 mM NaCl). The high salt was used to disrupt protein-protein interactions and thus any potential protein complexes in which REC8 may be involved. Therefore these results suggest that REC8 may be involved in a protein complex similar to RAD21.

As these results suggest that REC8 may be involved in a protein complex, further analysis was carried out on these SEC fractions to assess the elution range of other cohesin complex subunit proteins. Western blot analysis was carried out using fractions 6-16 (the range of fractions containing the spread of signal observed in Figure 6.16. Antibodies against the following cohesin complex subunits were used; SMC1, SMC3, STAG1 and STAG2. These cohesin proteins are known to function within the mitotic cohesin complex. The western blot results are shown in Figure 6.17.

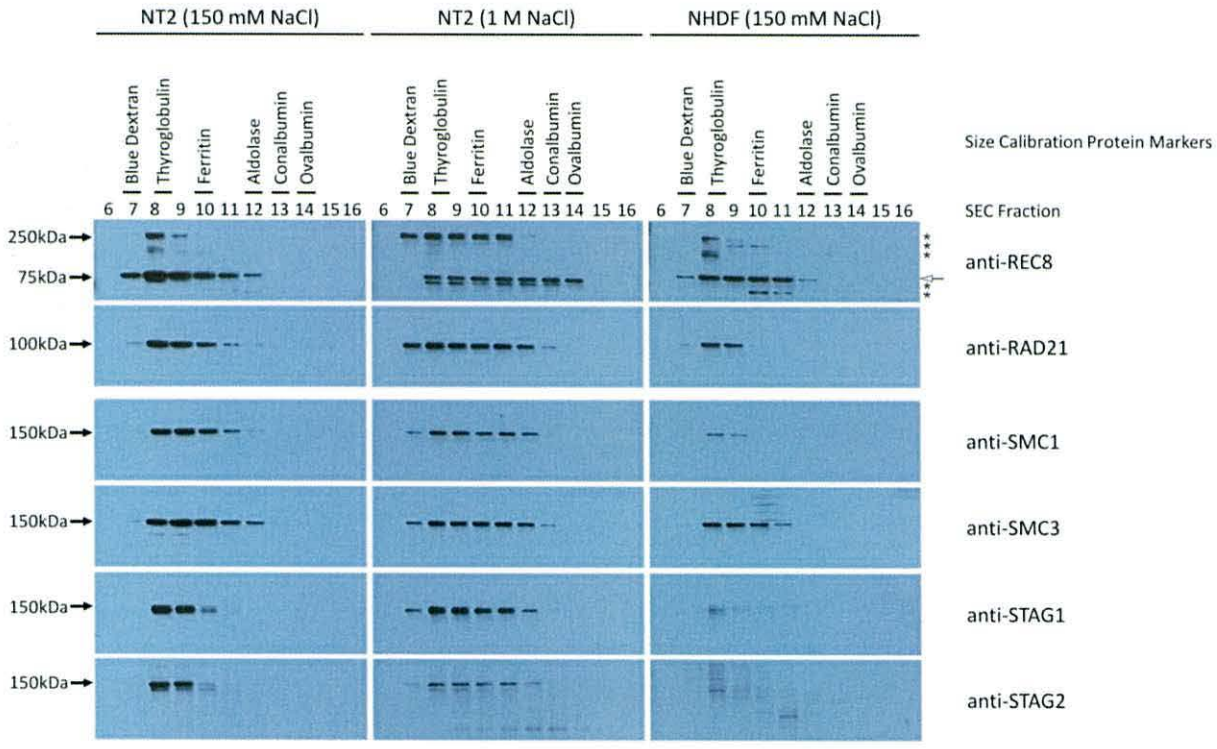

Figure 6.17. Western blot analysis for cohesin subunits in SEC fractions 6-16. Western blot analysis for REC8 and RAD21 in SEC fractions 6-16, for NT2 and NHDF cells with physiological salt (150 mM NaCl) and NT2 with high salt (1 M NaCl). The blots were also probed using antibodies against four cohesin complex proteins which are known to constitute the mitotic cohesin complex, SMC1, SMC3, STAG1 and STAG2. The SEC column was calibrated using the following standard proteins; blue dextran (approximately 2000 kDa), thyroglobulin (669 kDa), ferritin (440 kDa), aldolase (158 kDa), conalbumin (75 kDa) and ovalbumin (44 kDa). The fraction in which elution of each standard protein peaked is indicated (top). This experiment was carried out once only.

The possible REC8-specific band, as per the results presented in Section 6.4, is indicated with an arrow (right). The likely non-specific bands are indicated by *.

As shown in Figure 6.16, REC8 and RAD21 appear to elute in similar fractions, with elution peaking in fraction 8 under physiological salt conditions (150 mM NaCl). Western blot analysis using antibodies against SMC1, SMC3, STAG1 and STAG2 recognised bands in a similar range of fractions to that observed for REC8 and RAD21. The predicted molecular weights of SMC1, SMC3, STAG1 and STAG2 are 143 kDa, 141.5 kDa, 144 kDa and 146 kDa respectively. Therefore these proteins are eluting at a significantly higher molecular weight than the predicted molecular weight of the monomeric proteins.

The intensity of the western blot results do not appear to be as strong in the NHDF cells compared to the NT2 cells, and the results for anti-SMC1, anti-STAG1 and anti-STAG2 appear very faint. The input sample for the NHDF cells was not as concentrated as the input samples for the NT2 cells (with 150 mM and 1 M NaCl), this can be seen in Figure 6.16. Although the bands are fainter in the NHDF SEC fractions, the results suggest that these cohesin proteins elute in a similar range of fractions to that observed for REC8 and RAD21.

The elution of these proteins appears to tail off when the protein extract was prepared under high salt conditions (1 M NaCl). The high salt conditions may be disrupting any protein complexes that these proteins may be involved in, and thus causing a shift in the elution profile of the proteins. These results strongly suggest that REC8 may be involved in a large protein complex in these mitotic cells (NT2 and NHDF), which is in the same size range as the protein complexes involving RAD21, SMC1, SMC3, STAG1 and STAG2. However, these results do not indicate which proteins REC8 may be interacting with, therefore we cannot conclude that REC8 is a component of a cohesin complex structure in these mitotic cells.

The SEC UV elution profiles for the standard protein markers are provided in the Appendix.

6.7 Discussion

6.7.1 *REC8* gene expression and protein localisation in mitotic cells

Although *REC8* is a reported meiosis-specific gene, RT-PCR analysis found *REC8* expression in 21 normal tissues (Chapter 3.0) and 17/18 cancer cell lines (Figure 6.1) from a range of histological origins. These results show *REC8* expression in a range of mitotic cells, which suggests that *REC8* may not be as strictly meiotic in humans as previously reported. *REC8*

gene expression has been reported in *S. pombe* mitotic cells; however the primary transcripts are highly unstable due to post-transcriptional processing. This post-transcriptional processing mechanism prevents functional REC8 protein production in the mitotic fission yeast cells (Chen *et al.*, 2011; Cremona *et al.*, 2011; Harigaya *et al.*, 2006; Yamanaka *et al.*, 2010). Western blot analysis and immunofluorescent staining of fixed cells show REC8 staining within the nucleus of four cancer cell lines and fibroblast cells. These results suggest that an equivalent post-transcriptional processing of the *REC8* primary transcripts is unlikely to exist in human mitotic cells.

The RT-PCR and qRT-PCR results suggest no/little *REC8* expression in the brain cancer cell line, 1321N1. *REC8* expression was found in the two normal human brain cDNA samples (RT-PCR results shown in Figure 3.5), which may suggest that the reduced level of *REC8* expression may be a cell line-specific abnormality. Interestingly, the 1321N1 cell line also displayed a lower level of *RAD21* expression compared to the NT2 cell line. Therefore this brain cancer cell line may have adapted to survive with a reduced level of REC8 and RAD21.

REC8 has a predicted molecular weight of 63 kDa, whereas here western blot analysis with the anti-REC8 antibody identified two bands at approximately 75 kDa. The difference in the predicted and observed sizes may be caused by post-translational modifications. Previous studies have also shown western blot evidence that hRAD21 runs at a higher than predicted size (for example, Pati *et al.*, 2002). Many cohesin subunits are subjected to post-translational modifications, including SUMOylation, phosphorylation and acetylation (reviewed in Rudra and Skibbens, 2013). These post-translational modifications are thought to direct cohesins to participate in cell processes (Rudra and Skibbens, 2013). For example, RAD21 (Scc1) sumoylation and SMC3 (Smc3) acetylation are required for establishing stable cohesion in yeast and mammals (Almedawar *et al.*, 2012; Wu *et al.*, 2012). Studies have also shown that REC8 (Rec8) phosphorylation is required for efficient separase-mediated cleavage during meiosis, in yeast and mammals (Kitajma *et al.*, 2006; Llano *et al.*, 2008; Riedel *et al.*, 2006; Rumpf *et al.*, 2010).

Western blot analysis using nuclear and cytoplasmic fractions found the two anti-REC8 bands, observed at approximately 75 kDa, localised differently with the upper band shown in the cytoplasm and the lower band in the nucleus (Figures 6.2 and 6.3).

Immunofluorescent staining of fixed NT2, SW480 and NHDF cells also showed strong anti-REC8 staining in the nucleus and a lower level of staining in the cytoplasm (Figures 6.4-6.6). When western blot analysis was carried out using the 1321N1 cell line, the intensity of the lower band was significantly reduced compared to the NT2 cell line, whereas the upper band was of comparable intensity. The lower band observed in the 1321N1 cells may correspond to a different size than the lower (nuclear) band observed in the NT2 cells. Nuclear and cytoplasmic fractions for the 1321N1, may establish if the lower band corresponds to the nuclear-localised lower band observed in the NT2 cells or potentially a degradation product of the upper band. Although we cannot conclude that 1321N1 cells are REC8-negative, these results suggest that significantly less REC8 was observed in the 1321N1 compared to the other cancer cells lines (NT2, HCT116, SW480 and A2780).

The results presented here suggest that the cytoplasmic interaction displayed by the anti-REC8 antibody for western blot analysis and immunofluorescent staining may be the result of a non-specific interaction of the primary antibody. These results suggest that REC8 may localise within the nucleus of mitotic cells.

6.7.2 REC8 chromatin association

Western blot analysis was also used to demonstrate chromatin association of REC8 and RAD21 in four cancer cell lines. REC8 and RAD21 displayed both strong and weak chromatin association; however significantly less REC8 appears to be strongly chromatin associated than RAD21. Fibroblast cells (NHDF) were also used as a 'normal' control and the results presented here suggest that REC8 appears to behave similarly in fibroblast cells and cancer cells. This may suggest that REC8 protein production and localisation in the cancer cells is not the result of aberrant gene expression and protein production commonly observed in cancer.

Studies have provided evidence that cohesin binds to DNA with variable stability throughout the cell cycle. There is also evidence that cohesin cycles between soluble pools and weakly/tightly chromatin-associated complexes (Gause *et al.*, 2010; Gerlich *et al.*, 2006; McNairn and Gerton, 2008). This may explain the weak and strong chromatin associations observed for RAD21 and REC8 in the NT2, HCT116, SW480, A2780 and NHDF cells. During mitosis, cohesin is released from the DNA in two waves; the majority of cohesin is released

from the sister chromatid arms in the first wave, via the prophase pathway, and centromeric cohesin is protected from removal at this stage until its release at anaphase. Chromatin association with cell cycle analysis suggested a potential reduction in the amount of strongly chromatin associated REC8 and RAD21 in M phase compared to the other cell cycle stages for the NT2 and SW480 cell lines. This reduction may correspond to cohesin release from the chromatid arms during prophase, however metaphase spread analysis would determine this.

The chromatin association binding pattern of REC8 appears to mimic the chromatin association pattern of RAD21. Chromatin association of REC8 may indicate a potential role for this purported meiosis-specific protein in mitotic cells. Also, immunofluorescent staining of NT2, SW480 and NHDF cells revealed a nuclear punctate staining pattern for both anti-RAD21 and anti-REC8. These results therefore suggest that REC8 and RAD21 display a similar localisation within the nucleus. If REC8 localisation is mimicing the localisation pattern of RAD21 within the nuclei of mitotic cells, this may suggest that REC8 is behaving similarly to RAD21.

6.7.3 REC8 involvement in a protein complex?

SEC does not give an accurate indication of the actual molecular weight of the proteins; western blot analysis suggests that protein elution is spread over a range of fractions. The SEC column was calibrated using seven standard protein markers; blue dextran, thyroglobulin, ferritin, aldolase, conalbumin, ovalbumin and cytochrome C. These standard size markers are globular proteins whereas the cohesin subunit proteins such as SMC proteins are rod-shaped and therefore may behave differently and elute differently from the column. Therefore the SEC results may give a broad indication of protein complex size, but is not accurate.

Western blot analysis using the SEC fractions found that REC8 was eluted in the same range of SEC fractions as RAD21. Calibration of the size exclusion column suggested that REC8 eluted at a significantly higher molecular weight than that of the monomeric protein. SEC was also carried out using a protein lysate prepared with a high salt lysis buffer (1 M NaCl) to establish REC8s potential involvement in a protein complex. High salt concentrations are known to interfere with protein-protein interactions and can therefore disrupt protein

complexes. Western blot analysis using the high salt SEC fractions showed a shift in the elution profiles of both REC8 and RAD21. REC8 and RAD21 both appear to elute in a larger range of SEC fractions, with elution peaking in a fraction corresponding to a lower molecular weight. These results suggest that REC8 may be involved in a large protein complex within these mitotic cells, and the protein complex is partially disrupted with a high salt concentration.

These results suggest that REC8 is involved in a large protein complex similar to the protein complex containing RAD21. Another four mitotic cohesin complex proteins were also found to elute in the same range of SEC fractions as the REC8 and RAD21; SMC1, SMC3, STAG1 and STAG2. These results suggest that these six cohesin proteins are all involved in large protein complexes of approximately the same molecular weight. Although these results do not confirm which proteins REC8 forms a protein complex with, they suggest that REC8 is behaving in a similar way to these five mitotic cohesin proteins in mitotic cells.

These results provide strong circumstantial evidence to suggest that REC8 may be participating in a cohesin-like protein complex however these results do not identify which proteins are interacting with REC8. Co-immunoprecipitation experiments may be able to establish if REC8 is interacting with other cohesin proteins and if so, which ones. This further analysis would establish REC8s potential involvement in a cohesin protein complex in mitotic cells. If REC8 is found to interact with other cohesin subunit proteins, it may be assumed that REC8 is participating in a cohesin complex which may potentially have a functional role within mitosis.

Several studies have reported depletion of chromatid cohesion and aberrant anaphases after RAD21 depletion in human cells (Losada *et al.*, 2005; Toyoda and Yanagida, 2006). RAD21 depletion causes an uncoordinated loss of cohesion during anaphase but does not result in the complete failure to establish cohesion (Díaz-Martínez *et al.*, 2007). RAD21 depleted human cells have been shown to retain centromeric cohesion until metaphase or anaphase. Díaz-Martínez *et al.*, (2008) suggests that additional factors may be working alongside the cohesin complex to establish cohesion between sister chromatids, for example; DNA catenation which is the physical intertwining of sister chromatids formed as a byproduct of DNA replication. There is some evidence to indicate that catenation-mediated

cohesion is sufficient for cohesin-independent sister chromatid cohesion (Díaz-Martínez *et al.*, 2006; Toyoda and Yanagida, 2006; Vagnarelli *et al.*, 2004). However, centromeric catenation is thought to be maintained by cohesin (Bauer *et al.*, 2012) and a study by Tachibana-Konwalski *et al.*, (2010) demonstrated that cohesin alone is responsible for sister chromatid cohesion. Interestingly, cohesion is maintained at the centromeres after RAD21 depletion. If REC8 is able to participate in a cohesin complex within mitotic cells, it may potentially be capable of maintaining chromosome cohesion in RAD21 depleted cells.

Western blot analysis appears to suggest that there is significantly less strongly chromatin associated-REC8, than strongly chromatin associated-RAD21. This may suggest that if REC8 does have a function within mitotic cells, it may not have the same functional role as RAD21. Previous studies have shown the RAD21L-, REC8- and RAD21-containing cohesin complexes to localise along the chromosomes in a mutually exclusive manner during meiosis in mice, therefore suggesting different functional roles for the different cohesin complexes (Ishiguro *et al.*, 2011; Lee and Hirano, 2011). The cohesin complex has been implicated in a wide range of functions in addition to chromosome cohesion, including transcriptional control in yeast and mammals (Lin *et al.*, 2011a; Parelho *et al.*, 2008). Lin *et al.*, (2011a) identified a cohesin-mediated feedback loop responsible for regulating transcription of *REC8* in yeast, wherein Rec8-containing cohesin is required for full activation of the *REC8* promoter via Scc2 association. Further analysis may establish a potential role for REC8 in transcriptional control in these human mitotic cells.

Interestingly, *REC8* does not appear to be as widely expressed in mouse normal tissue compared to human normal tissue (Chapter 3.0). As discussed in Chapter 3.0, there may be a greater dissimilarity in the meiotic programs of mouse and human that previously presumed. A study by Xu *et al.*, (2005) demonstrated germ cell failure in *REC8* null mice and therefore concluded that REC8 is essential for the completion of meiosis. Interestingly, this study also reported a high mortality rate and reduced growth for the *REC8* null mice, therefore Xu and colleagues (2005) suggested a possible role for REC8 in one or more non-meiotic process. As REC8 appears to be more widely expressed in human tissues, this may also suggest a potential non-meiotic role for REC8 in human cells. Therefore further analysis may establish a potential role for REC8 in human mitotic cells (explored further in Chapter 7.0).

In summary, biochemical analysis suggests that REC8 localises within the nucleus, displays chromatin association and may be involved in a large protein complex in mitotic cells. If REC8 is involved in a cohesin-like complex, these results may indicate a potential role for REC8 in mitotic cell division. However functional analysis is required to establish a potential role for REC8 in mitotic cell division and chromosome segregation.

7.0 Functional analysis of REC8 and RAD21 in mitotic cells

7.1 Introduction

The cohesin multi-protein complex has been implicated in a wide range of functions in addition to its role in chromosome segregation. These functions include; homologous chromosome pairing during meiosis (Thomas *et al.*, 2005); double-strand break (DSB) formation and repair in meiotic and mitotic cells (Kim *et al.*, 2010; Sjogren and Nasmyth, 2001); assembly of replication factories during S-phase (Guillou *et al.*, 2010); axial element assembly in the formation of the synaptonemal complex during meiotic prophase (Kim *et al.*, 2010); sister kinetochore co-orientation during the first meiotic division (Sakuno *et al.*, 2009); and transcriptional control in yeast, trypanosomes, flies, fish and mammals (reviewed in Nasmyth, 2011). A variety of cohesin complexes are known to exist, which are composed of different combinations of cohesin proteins, however the particular functions of the individual cohesin complexes remain poorly understood (Murdoch *et al.*, 2013; Nasmyth, 2011).

The α-kleisin subunit plays an important structural and functional role within the mitotic and meiotic cohesin complex, as it acts as the only physical link between the SMC1-SMC3 heterodimer and the STAG subunit. The integrity of the α-kleisin subunit regulates the association and disassociation of functional cohesin with sister chromatids (Deardorff *et al.*, 2012; Nasmyth, 2011). Three α-kleisin subunit proteins have been identified in mammals to date; RAD21, RAD21L and REC8. REC8 and RAD21L are reported to be meiosis-specific and RAD21 is known to function in meiosis and mitosis (Ishiguro *et al.*, 2011; Lee and Hirano, 2011, Nasmyth, 2011).

Rad21 is essential for cell viability in fission yeast (Tomonaga *et al.*, 2000), and SCC1 (RAD21) has been shown to be essential for chromosome cohesion during interphase and mitosis in vertebrates (Morrison *et al.*, 2003). In a study using DT40 chicken cells, Scc1 deficient cells frequently failed to complete metaphase chromosome alignment and showed chromosome segregation defects (Sonoda *et al.*, 2001). Loss of chromosome cohesion also impedes homologous recombination repair of DNA damage (Sonoda *et al.*, 2001). In human cells

RAD21 is required for the timely separation of chromosomes and completion of mitosis (Díaz-Martínez *et al.*, 2007). RAD21 depleted cells displayed an un-coordinated loss of cohesion and aberrant anaphases, however cells were able to achieve mitosis with chromatids separating in an asynchronous manner. Interestingly, centromeric cohesion was observed in the RAD21 depleted cells, therefore it was proposed that RAD21-containing cohesin is important for sister arm separation but not centromeric separation (Díaz-Martínez *et al.*, 2007). In this study, RAD21 depletion was achieved to less than 10% of the endogenous level of RAD21 using RNAi (Díaz-Martínez *et al.*, 2007) therefore the possibility that the residual RAD21 preferentially localises to the centromeres cannot be excluded. In contrast, several studies have shown that REC8-containing cohesin is essential for completion of meiosis (Holt and Jones, 2009; Tachibana-Konwalski *et al.*, 2010). A study by Xu *et al.*, (2005) demonstrated that *REC8* null mice which reached sexual maturity displayed germ cell failure and were sterile, thus suggesting that REC8 is essential for the completion of meiosis. This study also reported a high mortality rate and reduced growth for the *REC8* null mice, therefore suggesting a possible role for REC8 in one or more non-meiotic process (Xu *et al.*, 2005), however these results also suggest that REC8 is not essential for somatic cells in mice.

The results from these studies suggest that the role of RAD21 (SCC1) in establishing chromosome cohesion is highly conserved; however there are distinct differences between different species. This may reflect the differing requirements for sister chromatid interactions during DNA compaction and progression through mitosis (Sonoda *et al.*, 2001).

Cohesin is essential for the accurate segregation of chromosomes during both meiotic and mitotic cell division; therefore disruption of normal cohesin function could contribute to genome instability. Mutations in the cohesin subunit genes have been associated with developmental syndromes (such as Cornelia de Lange syndrome (CdLS) and Roberts syndrome) and tumorigenesis (Deardorff *et al.*, 2012; Rhodes *et al.*, 2011). The study by Deardoff and colleagues (2012) demonstrated that RAD21 mutations can result in human congenital disorder, which can cause growth retardation and minor skeletal abnormalities. Several studies have also reported changes in the expression of cohesin subunits in different types of cancer. For example, *RAD21* over-expression has been reported in breast cancer (cell lines and primary tumour samples) (Oishi *et al.*, 2007; Rhodes *et al.*, 2011; Xu *et al.*,

2011), mutations in *SMC1β* and *STAG3* have been shown in primary colorectal tumours (Barber *et al.*, 2008), and increased *SMC3* expression was observed in colon cancer cell lines and primary tumours (Ghiselli and Iozzo, 2000). *RAD21* and *STAG2* gene deletions have also been reported in myeloid leukemia cells; a small heterozygous deletion was reported at chromosome location 8q24, this region contains *RAD21* (Rocquain *et al.*, 2010).

The results presented in Chapter 6.0 suggested that REC8 may be involved in a large proteinaceous complex and displays strong chromatin association in human mitotic cells. Given the importance of the α-kleisin subunit within the cohesin complex and the results presented in Chapter 6.0, we wanted to assess any potential functional role which REC8 may have in these mitotic cells.

7.2 RAD21 knockdown

Knockdown of RAD21 was carried out using siRNA in NT2 cells to determine the effect that RAD21 knockdown may have on these cells and to establish the specificity of the RAD21 antibody. WCEs were collected from the cells after siRNA treatment and analysed using western blot analysis, the results are shown in Figure 7.1.

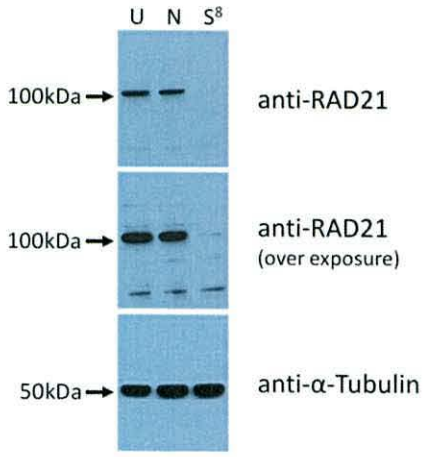

Figure 7.1. Western blot analysis showing siRNA knockdown of RAD21 in NT2 cells. Untreated (U) NT2 cells and cells treated with non-interfering siRNA (N) were used as negative controls for the siRNA knockdown. Knockdown was carried out using a RAD21-specific siRNA from Qiagen; Hs_RAD21_8 (S). The 5 nM siRNA and transfection reagent were added to the cells upon seeding and then again after 24 hrs (the two "hit" method as described in Section 2.9) and the cells were collected at 48 hrs. Anti-α-tubulin was used as a loading control (bottom). This result was reproducible, as this experiment was repeated a minimum of ten times.

Western blot analysis shows a significant difference for anti-RAD21 in the lysate prepared from the cells treated with the RAD21-specific siRNA (Hs_RAD21_8), compared to the negative controls (untreated cells and the cells treated with the non-interfering siRNA). When the western blot was over-exposed a faint band was observed for the cells treated with RAD21-specific siRNA. The α-tubulin appears to be relatively equal, which suggests that this difference is due to a successful RAD21 knockdown.

RAD21 has an essential role in accurate and co-ordinated chromosome segregation (Nasmyth, 2011) therefore we predicted that RAD21 knockdown would have a significant effect on cell survival. RAD21 knockdown was carried out in NT2 cells using the one "hit" and two "hit" strategies, and cell viability counts were carried out using trypan blue stain (Figure 7.2). Incubation with the HiPerfect transfection reagent appears to have had a significant effect on the total cell number; the number of cells was approximately halved after incubation with HiPerfect compared to untreated cells after 24 hrs and 48 hrs (Figure 7.2, part A). This may suggest that the HiPerfect transfection reagent is having a toxic effect on the NT2 cells. Although the cell count is lowered, the treatment with the transfection reagent does not show any effect on the RAD21 knockdown by western blot (Figure 7.2, part B). The cell viability counts for the cells treated with the non-interfering siRNA are comparable to the cell viability counts for cells treated with the HiPerfect reagent after 24 hrs, and slightly decreased after 48 hrs. Therefore suggesting that the decrease in cell number compared to the untreated cells is primarily due to the transfection reagent.

The western blot results show a significant level of knockdown after 24 hrs (one "hit"), with a greater level of knockdown after 48 hrs (two "hits") (Figure 7.2, part B). The α-tubulin appears to be relatively equal, thus suggesting that the gel loading is comparatively even. The cells treated with the RAD21-specific siRNA do not appear to show a significant decrease in cell number or cell viability compared to the cells treated with the transfection reagent only and the non-interfering siRNA (Figure 7.2). This is interesting because previous studies have shown that RAD21 (SCC1) is required for timely separation of chromosomes and completion of mitosis in human cells (Díaz-Martínez *et al.*, 2007).

A

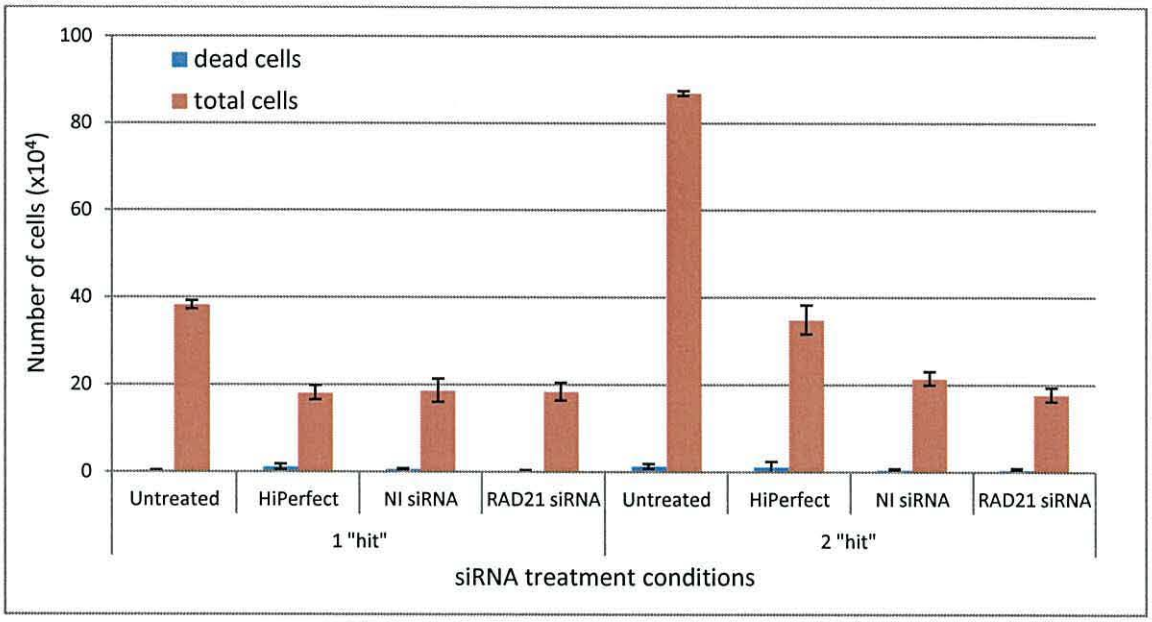

B

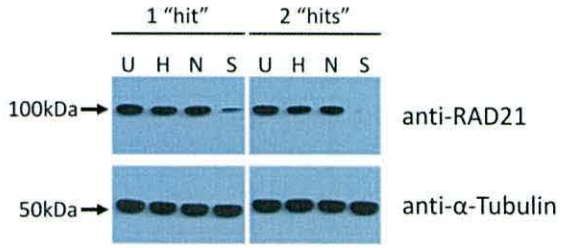

C

Treatment	*t*-test	*P*-value
1 "hit"	Untreated *vs* HiPerfect	0.000436
	Untreated *vs* NI siRNA	0.002324
	Untreated *vs* RAD21 siRNA	0.000879
	NI siRNA *vs* RAD21 siRNA	**0.940365**
2 "hit"	Untreated *vs* HiPerfect	0.000103
	Untreated *vs* NI siRNA	0.000002
	Untreated *vs* RAD21 siRNA	0.000002
	NI siRNA *vs* RAD21 siRNA	**0.164789**

Figure 7.2. NT2 cell viability after siRNA knockdown of RAD21. Untreated NT2 cells, cells treated with HiPerfect transfection reagent (Qiagen) only and non-interfering (NI) siRNA were used as negative controls for the siRNA knockdown. Knockdown was carried out using a RAD21-specific siRNA from Qiagen; Hs_RAD21_8. 5 nM siRNA and transfection reagent were added to the cells upon seeding and then the cells were either collected after 24 hrs (one "hit") or a second siRNA treatment was added (two "hits") and the cells were collected at 48 hrs. **A.** Trypan blue stain was used to assess cell viability, by counting the total number of cells and the number of dead cells after one and two siRNA "hits". The error bars represent the standard error calculated from three repeats for each treatment condition. **B.** WCEs were prepared for each condition after the cell viability counts and western blot analysis was carried out to ensure a successful RAD21 knockdown was achieved. Anti-α-tubulin was used as a loading control for the western blot analysis (bottom). **C.** Student's *t*-test *P*-values for two tailed comparisons of the total cell counts for RAD21 knockdown against untreated cells and NI siRNA-treated cells. This experiment was repeated two times.

These western blot results suggest that the level of RAD21 knockdown was considerable, but 100% knockdown was not achieved. Therefore the remaining RAD21 which was not knocked down may have been sufficient for RAD21 to function properly. An alternate

possibility is that another protein may be mediating cohesin function. The results shown in Chapter 6.0 suggest that REC8 may be involved in a protein complex and was found to display some strong chromatin association in mitotic cells. Therefore a potential function that is redundant with RAD21 was proposed for REC8 in the mitotic cells. Therefore, to establish a potential functional role for REC8 in mitotic human cells, we aimed to carry out a double knockdown of REC8 and RAD21.

7.3 REC8 knockdown

7.3.1 siRNA knockdown of REC8

Knockdown of REC8 was attempted using siRNA in NT2 cells to determine any effect that knockdown of this protein may have on these cells and to also establish the specificity of the REC8 antibody. WCEs were collected from the cells after siRNA treatment and analysed using western blot analysis, the results are shown in Figure 7.3.

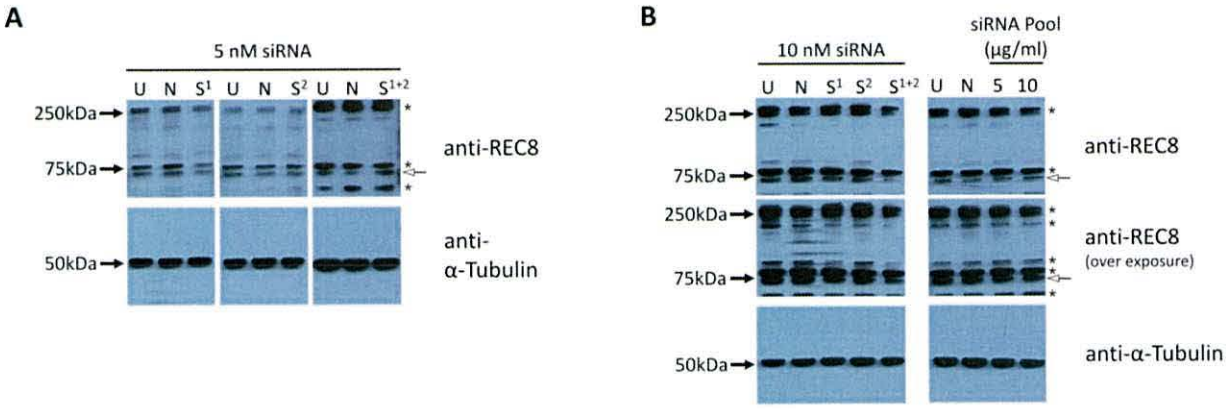

Figure 7.3. Western blot analysis showing siRNA knockdown of REC8 in NT2 cells. Untreated (U) NT2 cells and cells treated with non-interfering siRNA (N) were used as negative controls for the REC8-siRNA knockdown. Two different REC8-specific siRNAs (from Qiagen) were tested; Hs_REC8_1 (S^1) and Hs_REC8_2 (S^2) and a combination of the two siRNAs was also used (S^{1+2}). 5 nM (**A**) and 10 nM (**B**) concentrations of siRNA were tested using the two "hit" strategy (described in Section 2.9); the siRNA and transfection reagent were added to the cells upon seeding and after 24 hrs, then collected after 48 hrs. **C.** siRNA knockdown of REC8 was also attempted using a Dharmacon smart pool (Thermo Scientific), which contains four different REC8-specific siRNAs. 5 nM and 10 nM concentrations of the siRNA smart pool were tested using the two "hit" method. Anti-α-tubulin was used as a loading control (bottom). These experiments were repeated a minimum of three times.

The possible REC8-specific band, as per the results presented in Chapter 6.0, is indicated with an arrow (right). The likely non-specific bands are indicated by *.

Several conditions were tested in an attempt to optimise any REC8 knockdown with siRNA treatment. REC8 knockdown was attempted using; two individual REC8-specific siRNAs (Qiagen) and a pool of four REC8-specific siRNAs (Thermo Scientific). Anti-REC8 appears to identify two bands at approximately 75 kDa, as previously described in Chapter 6.0. The lower band at approximately 75 kDa appears to be fainter after treatment with 10 nM Hs_REC8_1 and Hs_REC8_2 together (Figure 7.3, part B), which may indicate a degree of REC8 knockdown. However on over exposure of the western blot, the intensity of the lower band appears comparable to that of the controls (untreated cells and cells treated with non-interfering siRNA). Therefore, the western blot results do not appear to show any significant knockdown of REC8.

REC8 knockdown was also attempted using a combination of four REC8-specific siRNAs (Dharmacon smart pool) (Figure 7.3, part C). The western blot results do not appear to show a difference in the intensity of the two bands, at approximately 75 kDa, in the siRNA-treated cells compared to the negative controls. Therefore suggesting that REC8 knockdown using the REC8-specific Dharmacon smart pool was unsuccessful.

7.3.2 miRNA (Bangor University)

As REC8 knockdown using siRNA was not successful, REC8 knockdown was attempted using miRNA. A HeLa T-REx cell line containing an miRNA construct directed at REC8, which was stably integrated under the control of a tetracycline repressor was gifted by Prof. Alistair Goldman, University of Sheffield. The miRNA construct and regulatory sequences were inserted into the pcDNA5/FRT/TO vector (Invitrogen) in a site specific manner, because the original cell line contained a single Flp recombination target site. This cell line had been previously used to successfully knockdown REC8 by Adam Croucher (University of Sheffield), results shown in Figure 7.4, part A. REC8 knockdown is induced through the addition of 1 µg/ml tetracycline to the cells.

REC8 knockdown was attempted using this HeLa T-REx cell line, with the aim of reproducing the level of knockdown observed by Adam Croucher (A. Croucher, Ph.D. thesis, Sheffield University). WCEs were prepared for each condition and western blot analysis was used to assess any knockdown, the results are shown in Figure 7.4.

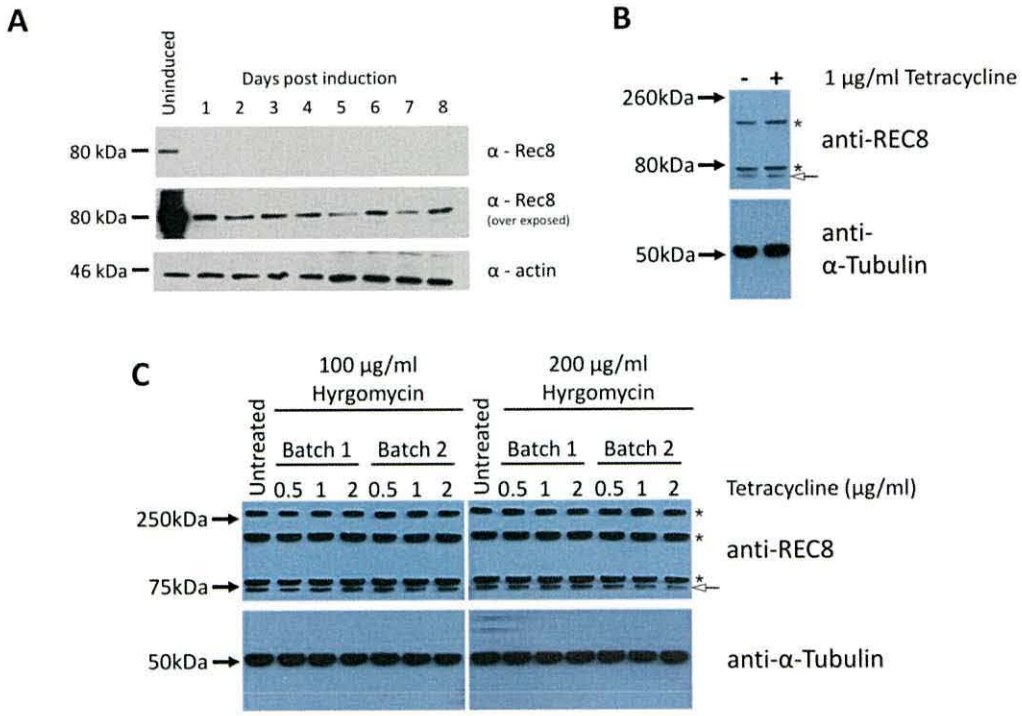

Figure 7.4. Western blot analysis showing REC8 knockdown in the HeLa T-REx cell line. **A.** REC8 knockdown was induced overnight using 1 µg/ml tetracycline and the cells were harvested every 24 hrs for 8 days. The cells were lysed and subjected to western blot analysis. Anti-α-actin was used as a loading control (bottom) (A. Croucher, Ph.D. thesis, Sheffield University). **B.** REC8 knockdown was induced using 1 µg/ml tetracycline and the cells were collected after 48 hrs, replicating the induction conditions used by Adam Croucher. **C.** Three concentrations of tetracycline (from two separate batches) were used to induce REC8 knockdown; 0.5, 1 and 2 µg/ml. The cells were also maintained at two concentrations of hygromycin, 100 and 200 µg/ml. Anti-α-tubulin was used as a loading control in parts **B** and **C** (bottom).

The possible REC8-specific band, as per the results presented in Chapter 6.0, is indicated with an arrow (right). The likely non-specific bands are indicated by *.

Significant REC8 knockdown was observed one day after induction and appeared to have a long lasting effect in the subsequent days with no additional tetracycline induction (A. Croucher, Ph.D. thesis, Sheffield University) (Figure 7.4, part A). However, when a direct repeat was attempted using the same induction conditions, no REC8 knockdown was observed (Figure 7.4, part B). Therefore different induction conditions were tested; three concentrations of tetracycline (0.5, 1 and 2 µg/ml) and two concentrations of hygromycin (100 and 200 µg/ml). Hygromycin was used to maintain the miRNA construct within the HeLa T-REx cell line.

Two separate batches of tetracycline were tested, to rule out the possibility that the lack of induction was not caused by a problem with the tetracycline. However, no REC8 knockdown was observed for any of the induction conditions tested. Therefore, RT-PCR was

carried out to establish if the HeLa T-REx cells had retained the miRNA construct. The forward primer was designed within the tetracycline operator site, which was used in conjunction with two reverse primers; one specific to the miRNA sequence and one specific to the BGH (bovine growth hormone) polyadenylation signal. The BGH-specific reverse primer was used as a positive control, because this PCR should work in the absence of the REC8 miRNA construct. The PCR products were purified and sequenced; the results are shown in Figure 7.5.

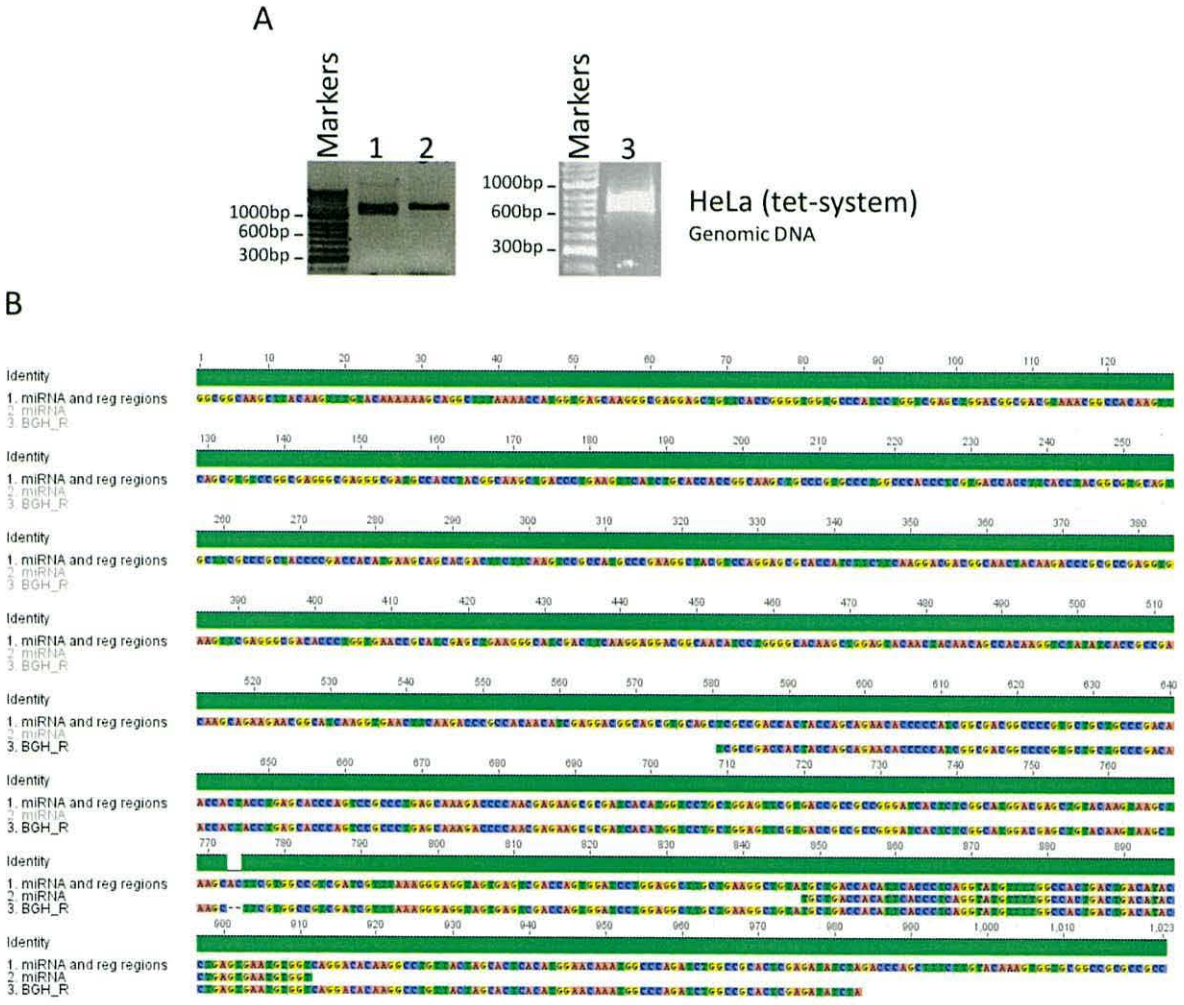

Figure 7.5. RT-PCR and sequencing results for the HeLa T-REx cells. A. Agarose gels showing the RT-PCR for the miRNA construct using genomic DNA extracted from the HeLa T-REx cells. Lane 1; RT-PCR using TetO_F + miRNA_R primers, lane 2; RT-PCR using TetO_F + BGH_R primers and lane 3; control RT-PCR using ACTB F2 + R2. **B.** Multialignment diagram showing the sequencing results for the RT-PCR products corresponding to lanes 1 and 2 (part A) with the expected sequence for the miRNA and regulatory regions. The sequences were aligned using the Geneious software and the sequence identity was calculated. The sequencing results for the TetO_F + miRNA_R PCR product showed 100% sequence identity* and the sequencing results for the TetO_F + BGH_R PCR product showed 99.5% sequence identity* to the expected sequence.

*The percentage of pair wise residues which are identical in the alignment, including gap versus non-gap residues, but excluding gap versus gap residues; calculated using Geneious software.

Sequencing results for the TetO_F + miRNA_R PCR product showed 100% sequence identity and the sequencing results for the TetO_F + BGH_R PCR product showed 99.5% sequence identity to the expected sequences (Figure 7.5, part B). Therefore these sequencing results confirm that the HeLa T-REx cells contain the REC8-specific miRNA construct. This may suggest that the lack of REC8 knockdown is caused by the induction conditions or protocol being used, or the cells are turning off the REC8 miRNA expression via epigenetic shut off (such as DNA methylation).

The original plasmid containing the REC8 miRNA, which was used to construct the HeLa T-REx cell line, was also gifted by Prof. Alistair Goldman (University of Sheffield). NT2 cells were transfected with the plasmid DNA, using Lipofectamine 2000 (Invitrogen), WCEs were then prepared and subjected to western blot analysis; the results are shown in Figure 7.6.

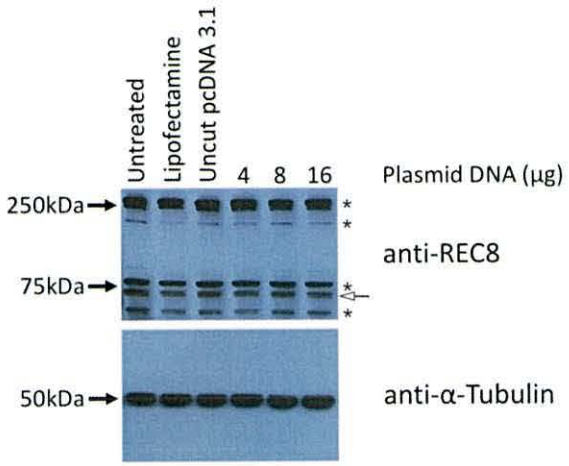

Figure 7.6. NT2 cells transfected with plasmid DNA containing the REC8 miRNA construct. The following negative controls were used; untreated NT2 cells, cells treated with Lipofectamine 2000 only and cells transfected with an empty uncut pcDNA 3.1 plasmid. The NT2 cells were transfected using 4, 8 and 16 µg of the plasmid, containing the REC8 miRNA construct. Anti-α-tubulin was used as a loading control (bottom).

The possible REC8-specific band, as per the results presented in Chapter 6.0, is indicated with an arrow (right). The likely non-specific bands are indicated by *.

These western blot results do not appear to show a significant difference in the intensity of the two bands identified by anti-REC8, at approximately 75 kDa, after the cells were transfected with the plasmid. The α-tubulin appears to be relatively even, suggesting equal loading of the gel. Therefore the lack of REC8 knockdown is probably due to an unsuccessful transfection of the cells or inefficient action of miRNA construct.

No significant REC8 knockdown was observed for NT2 cells transfected with REC8-specific siRNAs and miRNA. The lack of REC8 knockdown may be caused by a number of things, for example the nascent stability of the REC8 protein and/or *REC8* mRNA, or a problem with the knockdown technique. RAD21 knockdown was successful, which may suggest that the unsuccessful knockdown of REC8 is unlikely to be due to a problem with the siRNA knockdown procedure. Although the RT-PCR results showed that the HeLa T-REx cells contained the miRNA construct, no/insignificant REC8 knockdown was observed in the HeLa T-REx cells when a range of tetracycline concentrations were used. A significant level of REC8 knockdown was observed by Adam Croucher (results shown in Figure 7.4, part A), which may suggest that there is a problem with the induction conditions.

7.3.3 miRNA (University of Sheffield)

Significant REC8 knockdown was achieved using this HeLa T-REx cell line by Adam Croucher, at the University of Sheffield. I was given the opportunity to work with Dr. Helen Bryant and Prof. Alistair Goldman in the Institute for Cancer Studies, University of Sheffield. The stock of HeLa T-REx cells previously used (Figures 7.4 and 7.5) were late passage cells, these cells were taken to Sheffield and used alongside early passage cells. Induction was compared in early and late passage HeLa T-REx cells, to establish if the lack of REC8 knockdown was caused due to the late passage number of the cells being used. The same reagents used by Adam Croucher were then used to reproduce the REC8 knockdown, WCEs were prepared and western blot was carried out, the results are shown in Figure 7.7.

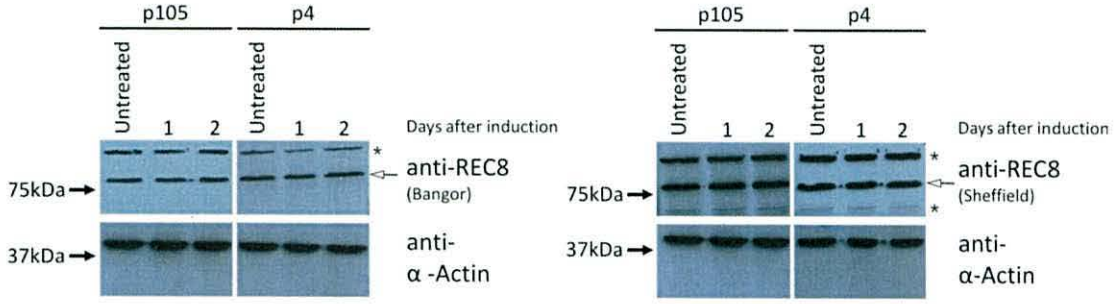

Figure 7.7. Western blot analysis showing REC8 knockdown in early and late passage HeLa T-REx cells. REC8 knockdown was induced overnight using 1 µg/ml tetracycline and the cells were harvested after 24 hrs and 48 hrs. Late passage cells (p105) and early passage cells (p4) were induced alongside one another. WCEs were prepared and subjected to western blot analysis; both the Bangor and Sheffield anti-REC8 stocks were used (Proteintech; 10793-1-AP). The lysates were separated on a 10% SDS-PAGE gel. Anti-α-actin was used as a loading control (bottom).

The possible REC8-specific band, as per the results presented in Chapter 6.0, is indicated with an arrow (right). The likely non-specific bands are indicated by *.

The western blot analysis results presented in Chapter 6.0 and Sections 7.3.1 and 7.3.2 showed that two clear bands, at approximately 75 kDa, were observed using anti-REC8 (predicted molecular weight of REC8 is approximately 63 kDa). However, the western blot results shown here, identified one clear band above 75 kDa, which is in line with the protein size observed by Adam Croucher (results shown in Figure 7.4, part A). This difference in the size identified by anti-REC8 may have been the result of differences in the western blot conditions and reagents used in the Bangor and Sheffield university laboratories. Two separate batches of the anti-REC8 antibody, with different lot numbers, were used also (the second lot was the one used by Adam Croucher, University of Sheffield). Western blot analysis using the two batches of REC8 antibody appear to show the same interaction profiles for the early and late passage HeLa T-REx cells. Thus suggesting that the lack of REC8 knockdown observed previously was not caused by a difference in the REC8-specific interaction of the two batches of antibody. Western blot analysis does not appear to show a difference between the early and late passage cells, with no REC8 knockdown 24 hrs or 48 hrs after induction.

As no REC8 knockdown was observed when using the same induction conditions used by Adam Croucher, a number of different conditions were tested using the early and late passage cells. Induction was attempted using three separate batches of tetracycline, at a range of concentrations; 1, 2, 4 and 10 µg/ml. WCEs were prepared and subjected to western blot analysis; the results are shown in Figure 7.8.

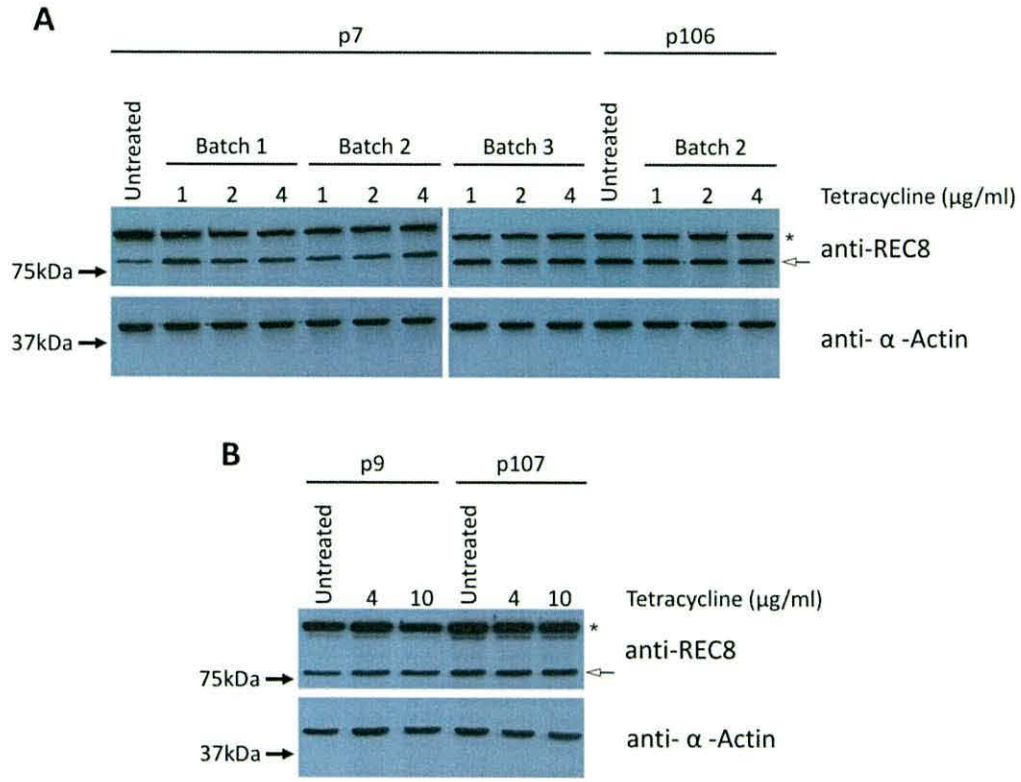

Figure 7.8. Western blot analysis showing REC8 knockdown induced using a range of tetracycline concentrations in early and late passage HeLa T-REx cells. A. Three separate batches of tetracycline were used to induce REC8 knockdown in the early passage cells (p9) and batch 2 was used to induce REC8 knockdown in the late passage cells (p107). Three concentrations of tetracycline were used; 1, 2 and 4 µg/ml. **B.** A higher concentration of tetracyline batch 2 (10 µg/ml) was used to induce the REC8 knockdown in early and late passage cells. The cells were harvested 48 hrs after induction and WCEs were prepared and subjected to western blot analysis in both cases. The lysates were separated on a 10% SDS-PAGE gel. Anti-α-actin was used as the loading control (bottom).

The possible REC8-specific band, as per the results presented in Chapter 6.0, is indicated with an arrow (right). The likely non-specific band is indicated by *.

The α-actin suggests that the gel loading was equal, therefore suggesting that any difference in band intensity may be caused by the different induction conditions. The intensity of the band at approximately 75 kDa does not appear to change after tetracycline induction, thus suggesting no REC8 knockdown. A range of tetracycline concentrations were tested, ranging from 1-10 µg/ml and no significant difference was observed by western blot analysis. Although Adam Croucher showed significant REC8 knockdown was induced with 1 µg/ml tetracycline, no knockdown was observed here when the cells were induced using 10 µg/ml tetracycline. Induction was also attempted using three separate batches of tetracycline; however western blot analysis showed no significant difference for the cells induced with the different stocks of tetracycline. This may therefore suggest that the lack of REC8 knockdown was probably not caused by degradation of the tetracycline.

As no REC8 knockdown was achieved after the HeLa T-REx cells were induced using 10 µg/ml tetracycline, induction was attempted using 100 µg/ml tetracycline. To rule out the possibility that tetracycline degradation was preventing REC8 knockdown, the cells were induced using multiple additions of tetracycline. Adam Croucher found that one addition of 1 µg/ml tetracycline was sufficient for significant knockdown for eight days following induction (Figure 7.4, part A). Induction was also attempted using doxycycline, a more stable member of the tetracycline antibiotics family. WCEs were prepared and subjected to western blot analysis, to assess REC8 knockdown; the results are shown in Figure 7.9.

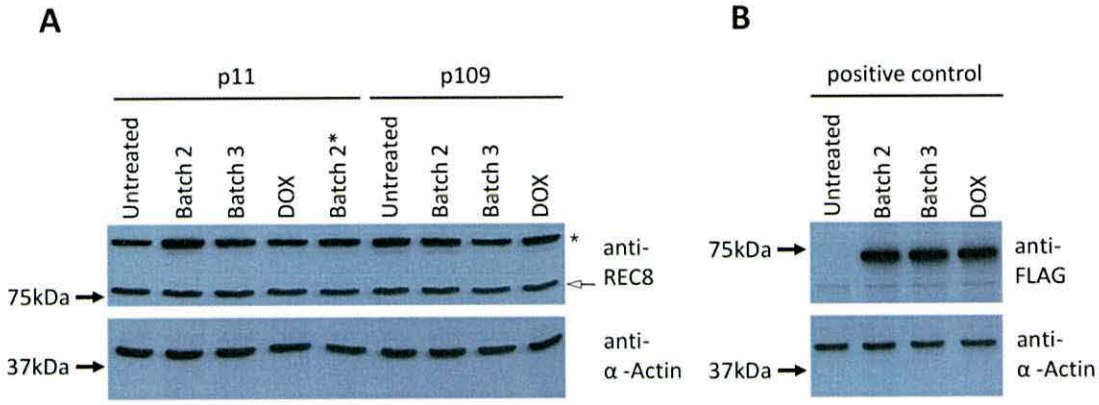

Figure 7.9. Western blot analysis showing REC8 knockdown induced using multiple tetracycline treatments, in early and late passage HeLa T-REx cells. **A.** Two separate batches of tetracycline were used to induce REC8 knockdown, in the early (p11) and late passage (p109) cells, at a concentration of 1 µg/ml. The lane labelled; Batch 2* corresponds to cells induced using 100 µg/ml tetracycline batch 2. Induction was also attempted using 1 µg/ml doxycycline (DOX), which is a more stable member of the tetracycline antibiotics family. The cells were induced upon seeding, with two additional tetracycline/doxycycline treatments (after approximately 24 and 30 hrs). **B.** Another HeLa T-REx cell line with tetracycline induced expression was used as a positive control. Two separate batches of tetracycline and the doxycycline were used at a concentration of 1 µg/ml. The cells were induced with one tetracycline/doxycycline treatment and the cells were harvested 48 hrs after induction. WCEs were prepared in both cases and subjected to western blot analysis. The lysates were separated on an 8% SDS-PAGE gel. Anti-α-actin was used as the loading control (bottom).

The possible REC8-specific band, as per the results presented in Chapter 6.0, is indicated with an arrow (right). The likely non-specific band is indicated by *.

No REC8 knockdown was observed when the cells were induced using 100 µg/ml tetracycline or the re-additions of 1 µg/ml tetracycline or doxycycline (Figure 7.9, part A). The doxycycline is more stable than tetracycline and unlikely to degrade over 48 hrs.

Another HeLa T-REx cell line being used in the laboratory, in which expression of the desired protein is switched on after tetracycline induction. This HeLa T-REx cell line was used as a

positive control for the tetracycline induction system and treated alongside the HeLa T-REx cell line containing the REC8 miRNA construct. The western blot results show a significant induction in the cells induced with both tetracycline (two separate batches) and doxycycline (Figure 7.9, part B). These results suggest that the induction technique and reagents are working, and possibly indicate a potential problem with the HeLa T-REx cell line containing the REC8 miRNA construct.

7.3.4 Western blot analysis for REC8

A number of different lysate buffers have been used to prepare protein lysates for western blot analysis. Depending on which lysate buffer, one or two bands were observed around 75 kDa by western blot analysis using anti-REC8. The western blot results are summarised in Table 7.1.

Table 7.1. Summary of the western blot results for REC8 using lysates prepared with the various lysis buffers

Lysate Preparation	Lysate buffer(s)	Description of Results	Figure(s)
WCE (BU)	Lysis buffer A (Section 2.8.1)	Two bands around 75 kDa	Figures 6.2 and 6.3
Crude fractionation (BU)	Hypotonic buffer, lysis buffer C and lysis buffer N (Section 2.8.3)	Two bands around 75 kDa; the upper band was cytoplasmic and the lower band was nuclear	Figures 6.2 and 6.3
Chromatin association (BU)	0.1 M, 0.4 M and 1 M NaCl Ch lysis buffers (Section 2.11.2)	Two bands around 75 kDa; the upper band displayed no chromatin association and the lower band displayed weak and strong chromatin association	Figures 6.10-6.15
SEC physiological salt buffer (BU)	SEC (150 mM NaCl) (Section 2.12)	One band at approximately 75 kDa in SEC fractions 7-12	Figures 6.16 and 6.17
SEC high salt buffer (BU)	SEC (1 M NaCl) (Section 2.12)	Two bands around 75 kDa in SEC fractions 8-13	Figures 6.16 and 6.17
WCE (SU)	RIPA buffer (Section 2.8.2)	One band above 75 kDa, which appears to correspond to the upper band observed for the BU lysates	Figures 7.7, 7.8 and 7.9

Bangor University (BU), University of Sheffield (SU)

Anti-REC8 identified two bands at approximately 75 kDa for the cancer cell lines (Chapter 6.0), and the western blot results for the 1321N1 cells suggested that the upper band is likely to be the result of a non-specific interaction (Figure 6.8). Western blot analysis with the SEC fractions suggested that REC8 may be involved in a large protein complex which is in the same size range as the protein complex in which several cohesin proteins are involved. As discussed in Chapter 6.0, the band identified by anti-REC8 in the same fractions as RAD21

appears to correspond to the lower band. However, in fractions 8-13 using the high salt lysis buffer (1 M NaCl) anti-REC8 appears identify another band below the 'lower' band, which may correspond to a degradation product of the lower band.

Two bands were observed with western blot analysis for the anti-REC8 antibody for all of the lysate preparation techniques except for the WCE prepared using RIPA buffer (University of Sheffield). The composition of the different lysis buffers do not differ significantly, however different protease inhibitors were used during the different lysate preparation techniques (Section 2.8). Lysates were prepared using the different lysis buffers and were then treated with alkaline phosphatase to see if the double band is the result of protein phosphorylation; the results are shown in Figure 7.10.

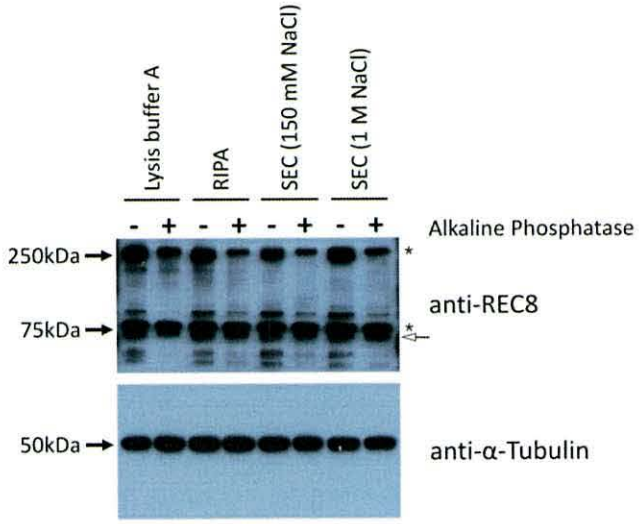

Figure 7.10. Alkaline Phosphatase treatment of NT2 protein lysates prepared with different lysis buffers. Protein lysates were prepared for NT2 cells, using four different lysis buffers; lysis buffer A, RIPA buffer, SEC physiological salt (150 mM NaCl) buffer and SEC high salt (1 M NaCl) buffer. After the lysates were prepared they were incubated with alkaline phosphatase (1 unit/µg of protein) and no phosphatase inhibitors were added to the lysates treated with alkaline phosphatase. The treated and untreated lysates were incubated at 37°C for 1 hr before the addition of Laemmli buffer. Anti-α-tubulin was used as a loading control. This experiment was only carried out once.

The possible REC8-specific band, as per the results presented in Chapter 6.0, is indicated with an arrow (right). The likely non-specific bands are indicated by *.

Treatment with the alkaline phosphatase does not appear to have had an effect on the presence of the two bands identified by anti-REC8, at approximately 75 kDa. These results may suggest that the upper band is not the result of protein phosphorylation. The two bands at approximately 75 kDa were observed in the NT2 lysates prepared with the four different lysis buffers. Therefore these western blot results do not correspond to the

western blot results observed when the cell lysates were prepared in Sheffield. The differences observed in the western blot results may be due to differences in the western blot methodologies and/or reagents used in Bangor and Sheffield university laboratories, for example differences in the membrane blocking conditions.

7.4 1321N1 growth curve

The results from RT-PCR, qRT-PCR, western blot analysis and immunofluorescent staining of fixed cells suggests that REC8 is significantly less abundant in the 1321N1 cells compared to the NT2 cells (Chapter 6.0). Cell growth rate was measured using cell viability counts every 24 hrs over four days, to establish if the reduced level of REC8 in the 1321N1 cells effected cell growth rate compared to NT2 cells. The 1321N1 and NT2 growth curves are shown in Figure 7.11.

The growth curves representing the total number of cells appear to show the 1321N1 and NT2 cells growing at a similar rate over four days. The images displaying cell density over the four days also suggest a similar growth rate for the 1321N1 and NT2 cell lines. These results therefore suggest that the reduced level of REC8 and RAD21 found in 1321N1 cells does not affect the cellular growth rate of these cells compared to NT2 cells.

Interestingly, RT-PCR found that *REC8* was expressed in the normal human whole brain and cerebellum cDNA (Figure 3.5). This may therefore suggest that the difference observed for REC8 and RAD21 abundance is due to abnormalities in the 13221N1 cancer cell line. If this is the case, then the 1321N1 cell line may have adapted to survive with the reduced levels of REC8 and RAD21.

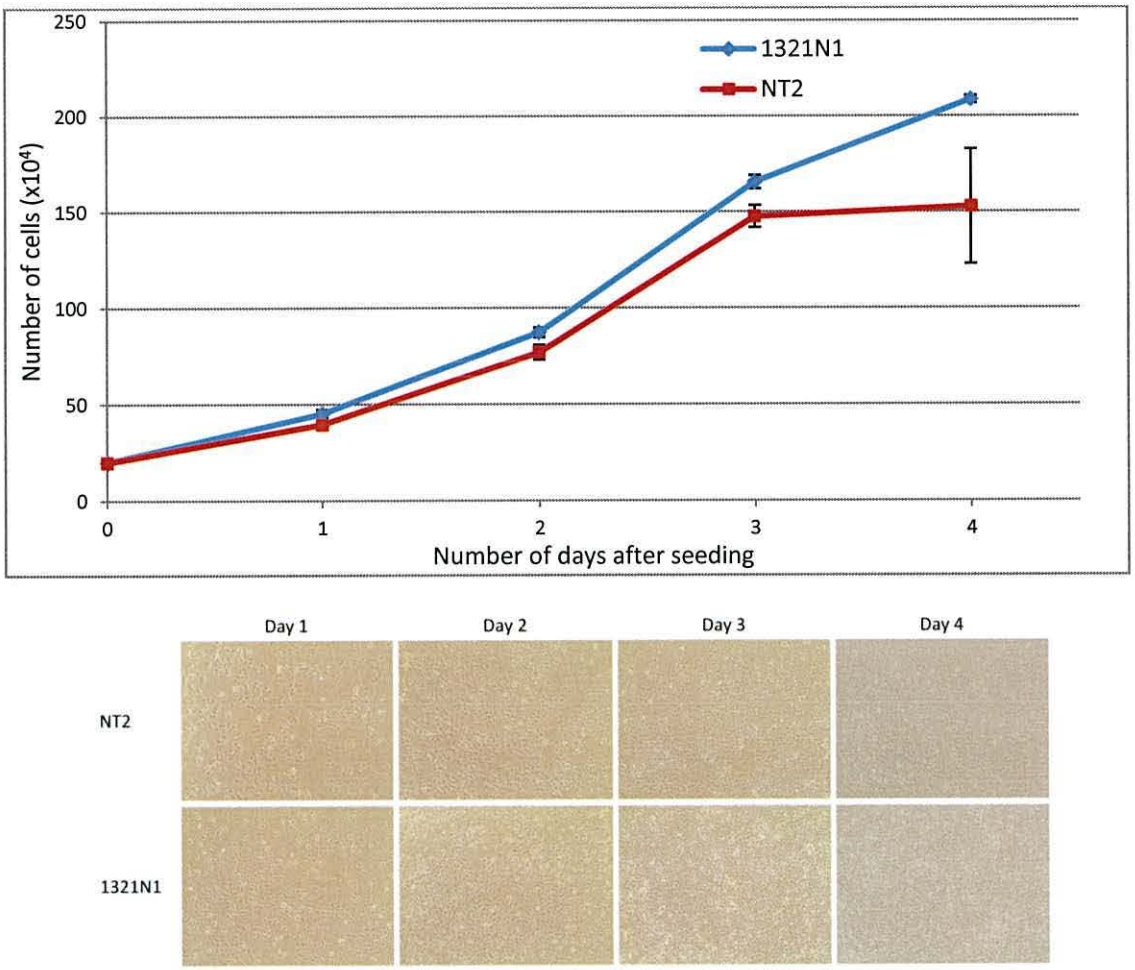

Figure 7.11. Cell growth curve for 1321N1 cells compared to NT2 cells. Graph showing the total number of cells counted at 24 hr intervals over four days. The cells were seeded at $2x10^5$ cells per well in a 6 well plate and the cells were counted using trypan blue stain. The error bars represent the standard error for the total number of cells, calculated for three repeats. Images of the cells were taken before trypsinisation to assess cell density at each time point. This experiment was carried out one time only.

7.5 Characterisation of RAD21 knockdown

RAD21 knockdown using siRNA did not appear to show a significant effect on NT2 cell viability (results shown in Figure 7.2). This is potentially interesting because previous studies have shown that RAD21 (SCC1) is required for timely separation of chromosomes and completion of mitosis in human cells (Díaz-Martínez *et al.*, 2007). Therefore we wanted to assess the effect of RAD21 knockdown when the cells are under genotoxic stress.

7.5.1 RAD21 knockdown with phleomycin treatment

RAD21 was knocked down in NT2 cells using siRNA, and then the cells were treated with the DNA damaging reagent phleomycin. Cells were harvested 24 and 48 hrs after phleomycin treatment, and cell viability counts were carried out using trypan blue stain (Figure 7.12).

The cells received the first siRNA "hit" upon seeding and the second siRNA "hit" after phleomycin addition. WCEs were prepared after the cell viability counts and subjected to western blot analysis, to ensure sufficient RAD21 knockdown was achieved. When the cells were harvested and counted 48 hrs after phleomycin treatment, there were not a sufficient number of cells to prepare WCEs for these conditions; therefore they are not shown in the western blot analysis results (Figure 7.12, part C). The western blot results suggest that significant RAD21 knockdown was achieved. Interestingly, the RAD21 knockdown appears to be less efficient with increasing phleomycin incubation time, which may suggest that there is an enrichment of cells in which RAD21 knockdown was unsuccessful.

Two tailed Student's *t*-test analysis was carried out for RAD21 siRNA knockdown total cell counts against the total cell counts for untreated and NI siRNA-treated cells, the *P*-values are shown in Table 7.2.

Table 7.2. Student's *t*-test *P*-values for two tailed comparisons of the total cell number for RAD21 siRNA knockdown against untreated and NI siRNA-treated cells

Phleomycin Treatment	*t*-test	24 hrs after Phleomycin Treatment	48 hrs after Phleomycin Treatment
Control	Untreated *vs* HiPerfect	0.000426	0.000028
	Untreated *vs* NI siRNA	0.000197	0.000020
	Untreated *vs* RAD21 siRNA	0.000196	0.000018
	NI siRNA *vs* RAD21 siRNA	**0.60805**	**0.142892**
15 s	Untreated *vs* HiPerfect	0.000110	0.000119
	Untreated *vs* NI siRNA	0.000050	0.000098
	Untreated *vs* RAD21 siRNA	0.000056	0.000094
	NI siRNA *vs* RAD21 siRNA	**0.065196**	**0.221001**
1 hr	Untreated *vs* HiPerfect	0.000048	0.000657
	Untreated *vs* NI siRNA	0.000257	0.000612
	Untreated *vs* RAD21 siRNA	0.000016	0.000751
	NI siRNA *vs* RAD21 siRNA	**0.482618**	**0.561438**
3 hrs	Untreated *vs* HiPerfect	0.000111	0.000607
	Untreated *vs* NI siRNA	0.000146	0.000706
	Untreated *vs* RAD21 siRNA	0.000111	0.000505
	NI siRNA *vs* RAD21 siRNA	**0.260745**	**0.404088**
8 hrs	Untreated *vs* HiPerfect	0.008221	0.002523
	Untreated *vs* NI siRNA	0.002814	0.001780
	Untreated *vs* RAD21 siRNA	0.002416	0.001738
	NI siRNA *vs* RAD21 siRNA	**0.664038**	**0.814902**

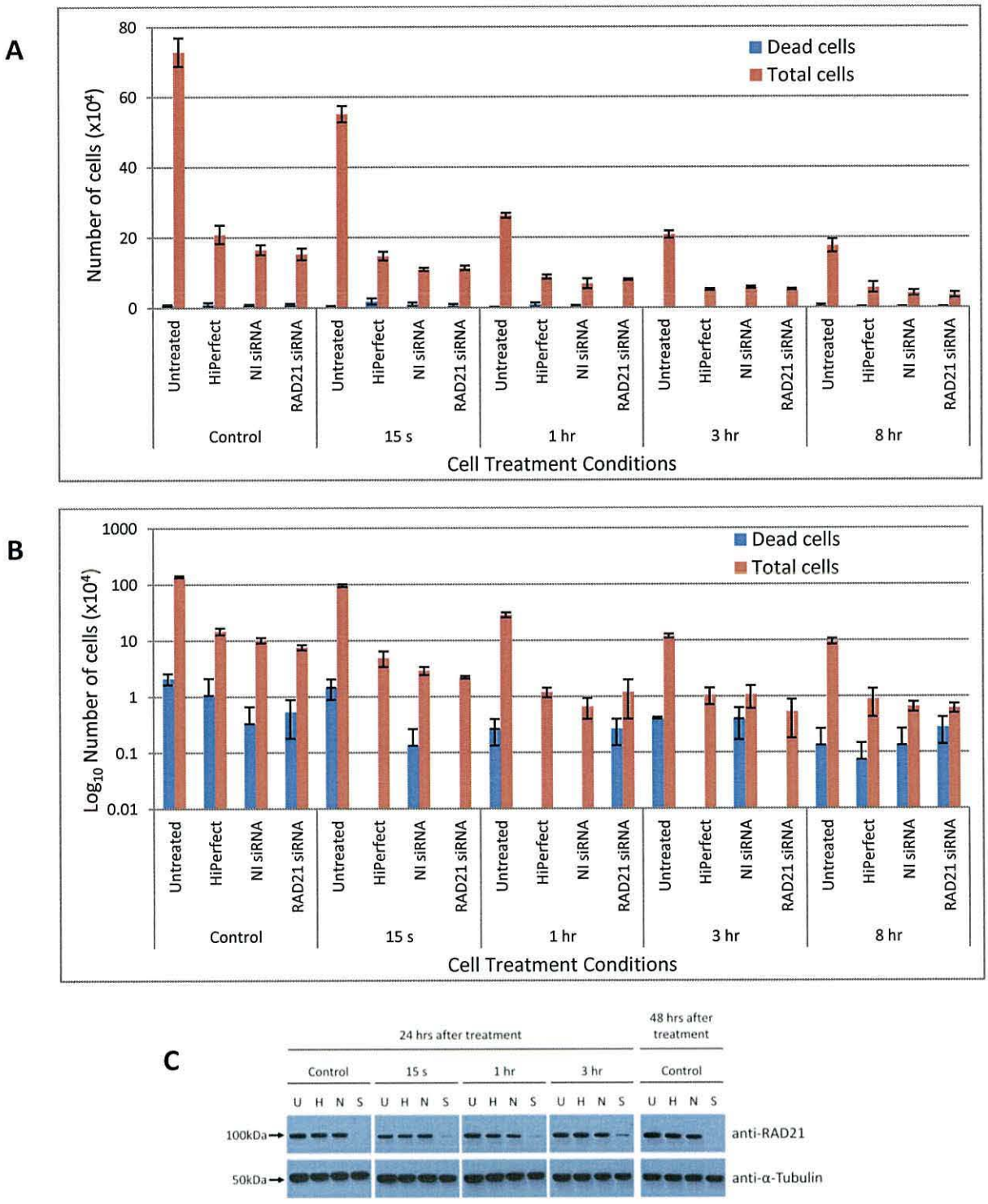

Figure 7.12. NT2 cell viability after siRNA knockdown of RAD21 and phleomycin treatment. Knockdown was carried out using a RAD21-specific siRNA from Qiagen; Hs_RAD21_8. Untreated NT2 cells, cells treated with HiPerfect transfection reagent (Qiagen) only and non-interfering (NI) siRNA were used as negative controls for the siRNA knockdown. The cells were incubated with 100 µg/ml phleomycin 24 hrs after receiving the first siRNA "hit" for 15 s, 1 hr, 3 hrs and 8 hrs. **A.** Cell viability of NT2 cells 24 hrs after phleomycin treatment. **B.** Cell viability of NT2 cells 48 hrs after phleomycin treatment. The error bars represent the standard error for the cell counts from the three repeats. **C.** WCEs were prepared for each condition after the cell viability counts and western blot analysis was carried out to ensure a successful RAD21 knockdown was achieved. Anti-α-tubulin was used as a loading control (bottom). Experiment repeated two times.

The cell viability counts (Figure 7.12) and the *P*-values from the Student's *t*-test (Table 7.2) suggest that treatment with the HiPerfect transfection reagent produces a significant reduction in the total cell number compared to the untreated cells, for all of the phleomycin treatment conditions tested. The results also show no significant reduction in the total number of cells after RAD21 knockdown compared to the total number of cells treated with non-interfering siRNA, even after phleomycin treatment. RAD21 knockdown does not appear to make the NT2 cells more sensitive to phleomycin treatment, and does not appear to have affected the number of dead cells.

7.5.2 Clonogenic survival assay

Aberrant *RAD21* expression has previously been associated with breast cancer and has been shown to confer poor prognosis and resistance to chemotherapy. Suppression of RAD21 expression has also been reported to decrease cell growth and increase sensitivity to chemotherapeutic agents (Atienza *et al.*, 2005; Xu *et al.*, 2011). Therefore the effect of RAD21 knockdown on cell survival was assessed in the breast cancer cell line, MCF7, alongside the NT2 cell line. The effect of RAD21 knockdown was assessed using a clonogenic survival assay for the NT2 and MCF7 cell lines. Table 7.3 shows the survival fraction calculated from the clonogenic survival assays for NT2 and MCF7 cell lines after RAD21 knockdown and their associated *P*-values.

Table 7.3. Survival fraction for NT2 and MCF7 cells after RAD21 knockdown

Cell Line	Survival Fraction	*P*-value
NT2	0.048	0.00095
MCF7	0.037	0.00002

Student's *t*-test *P*-values for two tailed comparisons of RAD21 siRNA knockdown survival against NI siRNA survival.

The survival fraction was calculated as the fraction of colonies formed from cells after RAD21 knockdown compared to the number of colonies formed from cells treated with NI siRNA. Therefore the survival fraction for the NI siRNA treated cells was set as 1, and the survival fractions for RAD21 siRNA treated cells was 0.048 (4.8%) and 0.037 (3.7%) for NT2 and MCF7 respectively. The *P*-values show that the survival fractions for the NT2 and MCF7 cells are statistically significant.

We found that the colonies formed by the NT2 cell line during the clonogenic survival assay were not as good as those formed by the MCF7 cells (Table 7.3), and the NT2 cells also

appeared to be very sensitive to ionising radiation (IR) (Figure 7.13). Therefore only the MCF7 cells were used to assess any phenotypic change that RAD21 knockdown may induce with genotoxic insult. Clonogenic survival assays were carried out for MCF7 cells after RAD21 knockdown and genotoxic insult, using IR, the results are shown in Figure 7.13.

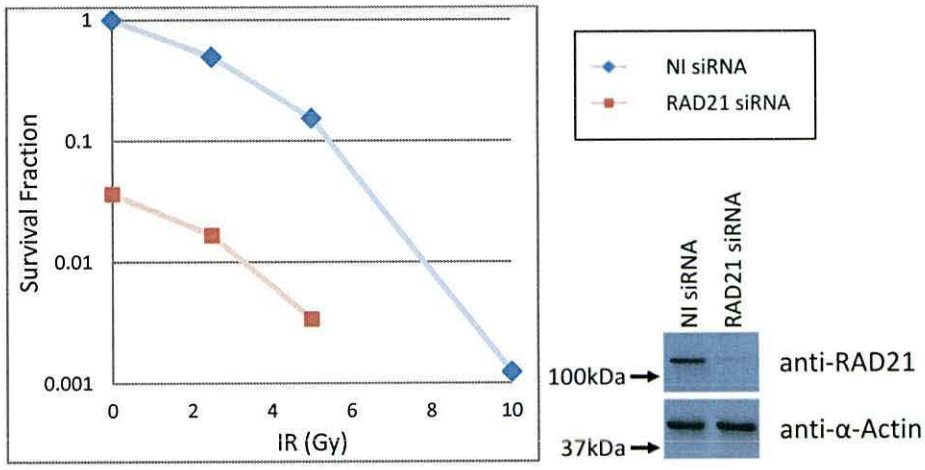

Figure 7.13. Clonogenic survival assay for RAD21 knockdown after genotoxic insult using IR. The clonogenic survival fractions were calculated for the NI (non-interfering) siRNA and the RAD21 knockdown (RAD21 siRNA) cells with 0, 2, 5 and 10 Gy IR. The survival fraction of the NI siRNA treated cells with 0 Gy was set as 1, and the other survival fractions were calculated compared to this. No error bars are shown on the graphs, because this experiment was only repeated two times. Western blot analysis was carried out to ensure RAD21 knockdown was successful, when the cells were plated for the clonogenic survival assay. The lysates were separated on an 8% SDS-PAGE gel and anti-α-actin was used as a loading control.

The western blot results show a successful RAD21 knockdown in the MCF7 cells before genotoxic insult. These survival fractions suggest that RAD21 knockdown does not appear to increase the sensitivity of the MCF7 cells to genotoxic insult with IR.

7.5.3 Cell growth after RAD21 knockdown

Clonogenic survival assays show a significant decrease in survival after RAD21 knockdown. Previously cell viability counts were carried out after 24 hrs and 48 hrs siRNA treatment (1 "hit" and 2 "hits" respectively). RAD21 was knocked down in NT2 cells and MCF7 cells, using the 2 siRNA "hit" method, and a cell viability count was done after 48 hrs siRNA treatment (this is the 0 day point). Fresh media was added to the cells and cell viability counts were carried out at regular time points during the following 8 days. WCEs were prepared for the cells after the cell viability counts, and then subjected to western blot analysis, to ensure RAD21 knockdown was sufficient in the cells. The cell survival counts for MCF7 and NT2 after RAD21 knockdown are shown in Figures 7.14 and 7.15 respectively.

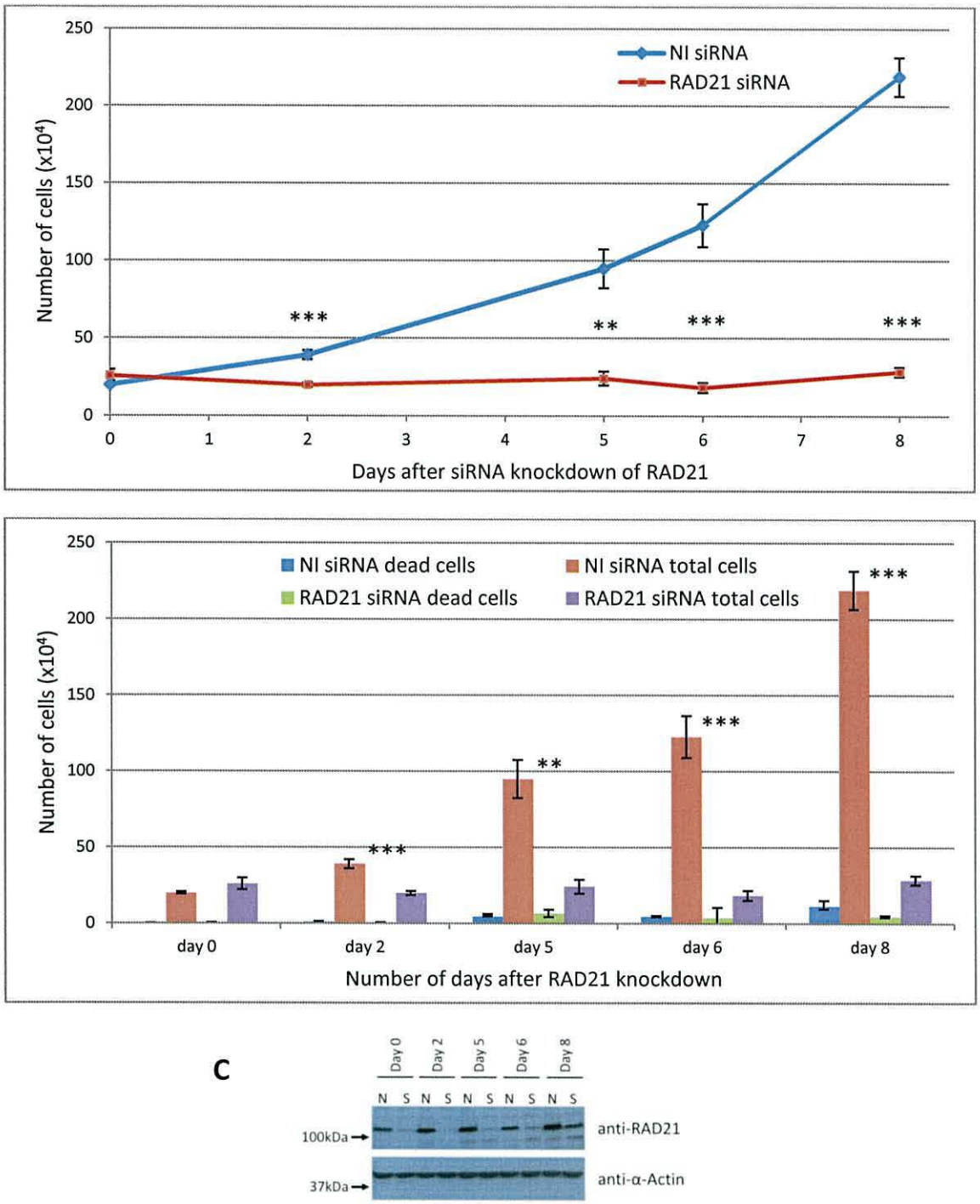

Figure 7.14. MCF7 cell growth after RAD21 Knockdown. Knockdown was carried out using a RAD21-specific siRNA from Qiagen; Hs_RAD21_8. Cells treated with non-interfering (NI) siRNA were used as the negative control for the RAD21 siRNA knockdown. The MCF7 cells were subjected to two siRNA "hits", and the first cell viability count was done after 48 hrs siRNA treatment, which is referred to as day 0, and subsequent counts were conducted on days 2, 5, 6 and 8. **A.** Total number of MCF7 cells over eight days following RAD21 knockdown. **B.** Cell viability of MCF7 cells over eight days following RAD21 knockdown. The error bars represent the standard error calculated for three independent repeats. **C.** WCEs were prepared after the cell viability counts and western blot analysis was carried out to ensure a successful RAD21 knockdown was achieved, using an 8% SDS-PAGE gel. Anti-α-actin was used as a loading control (bottom). Experiment carried out one time.

Student's *t*-test *P*-values for two tailed comparisons of NI siRNA treated *vs.* RAD21 siRNA (*P<0.05, **P<0.01, ***P<0.005).

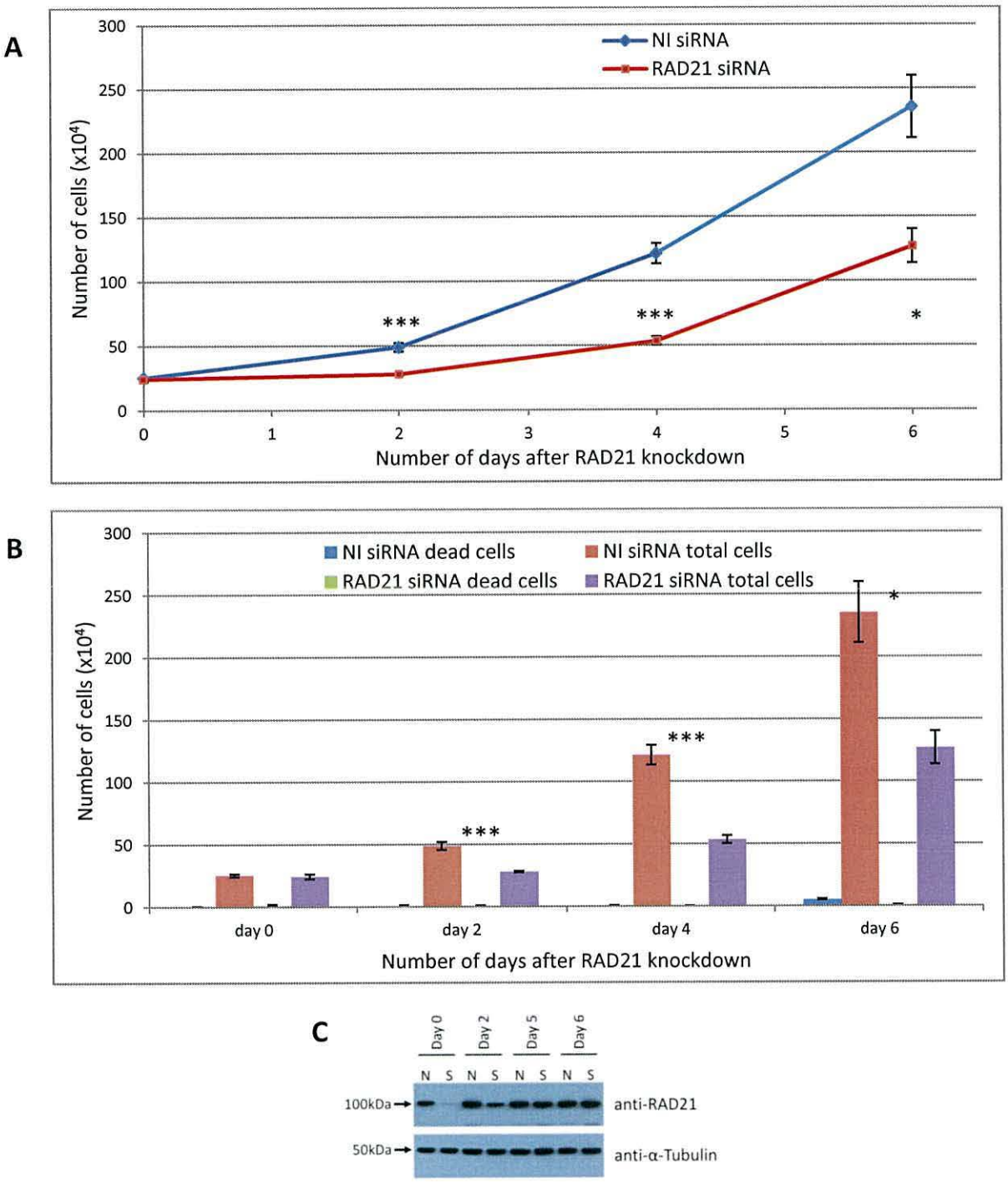

Figure 7.15. NT2 cell growth after RAD21 Knockdown. Knockdown was carried out using a RAD21-specific siRNA from Qiagen; Hs_RAD21_8. Cells treated with non-interfering (NI) siRNA were used as the negative control for the RAD21 siRNA knockdown. The NT2 cells were subjected to two siRNA "hits", and the first cell viability count was done after 48 hrs siRNA treatment, which is referred to as day 0, and subsequent counts were conducted on days 2, 4 and 6. **A.** Total number of NT2 cells over six days following RAD21 knockdown. **B.** Cell viability of NT2 cells over six days following RAD21 knockdown. The error bars represent the standard error calculated for three independent repeats. **C.** WCEs were prepared after the cell viability counts and western blot analysis was carried out to ensure a successful RAD21 knockdown was achieved. Anti-α-tubulin was used as a loading control (bottom). This experiment was carried out one time only.

Student's *t*-test *P*-values for two tailed comparisons of NI siRNA treated *vs.* RAD21 siRNA (*P<0.05, **P<0.01, ***P<0.005).

The western blot results appear to show significant RAD21 knockdown in the MCF 7 cells on days 0, 2, 5 and 6, with less knockdown shown for day 8 (Figure 7.14, part C). These results may suggest that the MCF7 cells may be recovering after RAD21 knockdown. The MCF7 cells treated with the non-interfering siRNA appear to grow at a steady rate, whereas the total number of cells does not appear to change significantly after RAD21 knockdown (Figure 7.14). The MCF7 cell viability counts do not appear to show a significant increase in the number of dead cells in the RAD21 knockdown cells compared to the cells treated with non-interfering siRNA. These cell viability counts may suggest that RAD21 knockdown does not cause cell death, but may potentially arrest the cells and thus cause the total cell number to remain relatively static.

The western blot results also appear to show a significant level of RAD21 knockdown in the NT2 cells on days 0 and 2, however the NT2 cells appear to be recovering normal levels of RAD21 on days 4 and 6 (Figure 7.15, part C). These cell viability counts may suggest that RAD21 knockdown does not cause cell death in the NT2 cells. The total number of cells appears not to change significantly between days 0 and 2, similar to the results observed for MCF7 cells, but begin to increase at a steady rate after day 2 (Figure 7.15). This increase in the total cell number coincides with the return of normal RAD21 levels in the NT2 cells treated with siRNA, as shown by the western blot results (Figure 7.15, part C).

The RAD21 knockdown appears not to be as long lasting in the NT2 cells compared to the MCF7 cells, however both cell lines appear to show a decrease in the total number of cells after RAD21 knockdown compared to the cells treated with non-interfering siRNA.

7.5.4 Flow cytometry analysis

The cell viability counts for MCF7 and NT2 cell survival after RAD21 knockdown showed a significant difference in the total number of cells for RAD21 siRNA treated cells compared to cells treated with non-interfering siRNA 2 days after RAD21 knockdown. Untreated cells and cells treated with non-interfering siRNA and RAD21-specific siRNA were collected 2 days after RAD21 knockdown and stained using propidium iodide. The stained cells were then subjected to flow cytometry analysis to establish if RAD21 knockdown cause cell cycle arrest in the MCF7 and NT2 cells. WCEs were prepared for the cells 2 days after RAD21 knockdown, to confirm RAD21 knockdown before flow cytometry analysis. The cell cycle

analysis results for RAD21 knockdown in MCF7 and NT2 cells are shown in Figures 7.16 and 7.17 respectively.

A

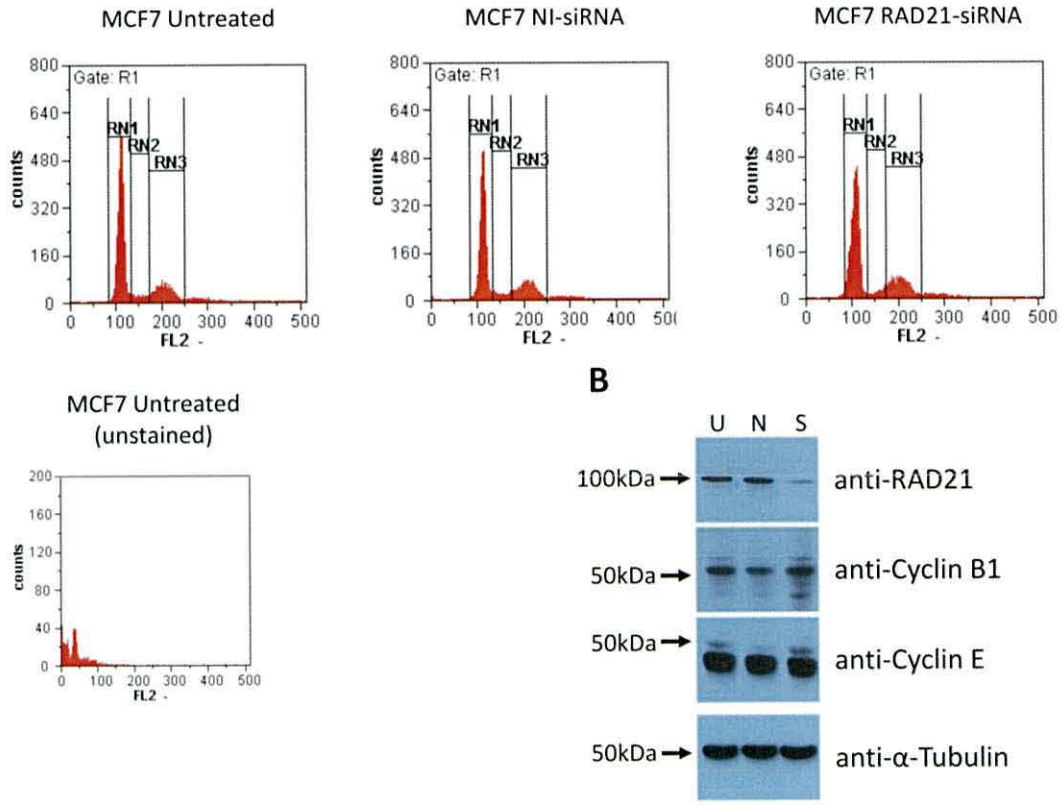

C

Cell Condition	Gate	Corresponding Cell Cycle Phase	% cells	Mean –x	CV-x%
Untreated	RN1	G_1	61.37	112.32	6.01
	RN2	S	6.39	152.41	7.75
	RN3	G_2	20.97	206.70	8.79
NI siRNA	RN1	G_1	57.45	112.28	6.31
	RN2	S	6.71	151.86	7.97
	RN3	G_2	23.00	207.98	8.52
RAD21 siRNA	RN1	G_1	58.67	107.89	7.90
	RN2	S	6.00	156.80	7.33
	RN3	G_2	22.57	204.19	8.89

Figure 7.16. Flow cytometry analysis results for RAD21 knockdown in MCF7 cells. A. Cell cycle profiles for propidium iodide-stained untreated cells and cells treated with non-interfering siRNA and RAD21-specific siRNA. The cell cycle profile is also shown for untreated (unstained) NT2 cells, which suggests a low level of non-specific background. **B.** WCEs were prepared also, to ensure sufficient RAD21 knockdown was achieved. Antibodies against cyclins B1 and E were used to establish any potential arrest in G_2 and G_1 cell cycle phases respectively. Anti-α-tubulin was used as a loading control (bottom). **C.** Table detailing the percentage of cells (% cells) in each cell cycle phase, the centre of the peak (Mean-x) and the coefficient of variation (CV-x%), as calculated by the Partec PAS III flow cytometer. The coefficient of variation is calculated as standard deviation/mean. This experiment was carried out one time only.

A

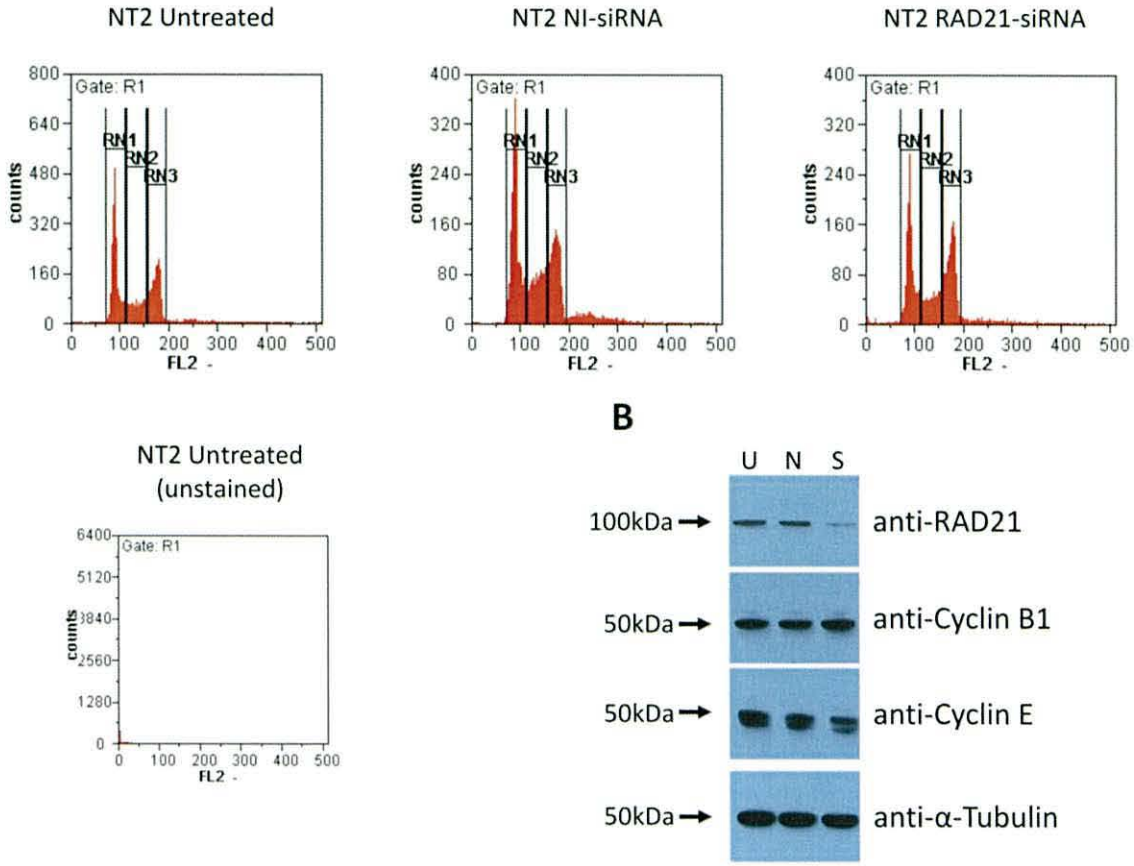

B

C

Cell Condition	Gate	Corresponding Cell Cycle Phase	% cells	Mean –x	CV-x%
Untreated	RN1	G_1	39.25	92.33	7.52
	RN2	S	18.44	135.72	8.63
	RN3	G_2	30.08	173.54	4.67
NI siRNA	RN1	G_1	39.15	91.62	8.66
	RN2	S	20.18	136.53	8.39
	RN3	G_2	26.32	172.48	4.92
RAD21 siRNA	RN1	G_1	33.46	92.40	8.44
	RN2	S	17.16	135.87	8.56
	RN3	G_2	34.50	174.10	4.87

Figure 7.17. Flow cytometry analysis results for RAD21 knockdown in NT2 cells. A. Cell cycle profiles for propidium iodide-stained untreated cells and cells treated with non-interfering siRNA and RAD21-specific siRNA. The cell cycle profile is also shown for untreated (unstained) NT2 cells, which suggests very little non-specific background. **B.** WCEs were prepared also, to ensure sufficient RAD21 knockdown was achieved. Antibodies against cyclins B1 and E were used to establish any potential arrest in G_2 and G_1 cell cycle phases respectively. Anti-α-tubulin was used as a loading control (bottom). **C.** Table detailing the percentage of cells (% cells) in each cell cycle phase, the centre of the peak (Mean-x) and the coefficient of variation (CV-x%), as calculated by the Partec PAS III flow cytometer. The coefficient of variation is calculated as standard deviation/mean. This experiment was carried out one time only.

The western blot analysis results show a significant level of RAD21 knockdown when the MCF7 cells were collected for flow cytometry analysis (Figure 7.16, part B). Antibodies against cyclin B1 and cyclin E were also used to probe the western blots, to assess any potential cell cycle arrest in G_2 and G_1 phases respectively. The cell cycle profile for the unstained, untreated MCF7 cells does not show any significant cell staining, thus showing a low level of non-specific background staining. The flow cytometry results in conjunction with the western blot results suggest that the MCF7 cells do not arrest in the G_1 or G_2 phases after RAD21 knockdown (Figure 7.16).

The western blot analysis results also show a significant level of RAD21 knockdown when the NT2 cells were collected for flow cytometry analysis (Figure 7.17, part B). The flow cytometry results in conjunction with the western blot results suggest that the NT2 cells do not arrest in the G_1 or G_2 phases after RAD21 knockdown (Figure 7.17).

The results shown in Figures 7.16 and 7.17 represent preliminary results, which suggest that RAD21 knockdown does not cause any significant cell cycle arrest in the MCF7 and NT2 cell lines. The flow cytometry results show a change in the NT2 cell profile for the cells treated with the non-interfering siRNA compared to the untreated cells. This may suggest that the HiPerfect transfection reagent has a toxic effect on the NT2 cells, which corresponds with the previous cell viability counts (Figure 7.2). The HiPerfect transfection reagent does not appear to be as toxic in the MCF7 cells.

7.6 Discussion

7.6.1 REC8 functional analysis

Different functional roles have been suggested for the different cohesin complexes, however the particular functions of the individual cohesin complexes remain poorly understood (Murdoch *et al.*, 2013; Nasmyth, 2011). During meiosis RAD21-, RAD21L- and REC8-containing cohesin complexes were found to display mutually exclusive localisation along the axial elements, in mice. RAD21L localises along the axial elements prior to REC8 localisation during leptotene and RAD21 transiently localises to the axial elements after REC8 and RAD21L dissociation in late pachytene (Ishiguro *et al.*, 2011). Centromeric cohesion is established and maintained solely by REC8-containing cohesin until anaphase II

(Holt and Jones, 2009; Tachibana-Konwalski *et al.*, 2010). Mounting evidence suggests different roles for the different cohesin complexes within both meiotic and mitotic cell division. REC8 knockdown was unsuccessful and therefore a potential functional role could not be established for REC8 in the human mitotic cells.

No significant level of REC8 knockdown was achieved using siRNA in the NT2 cells or the HeLa T-REx cells containing the REC8 miRNA construct. Although RT-PCR was used to confirm the presence of the miRNA construct within the cells, we cannot be sure that the cell line was still expressing the REC8 miRNA. However, it may be unlikely that both early and late passage HeLa T-REx cells simultaneously stopped expressing the miRNA construct. Interestingly, the qRT-PCR results presented in Chapter 6.0 suggested that the NT2 cell line displays a greater level of *REC8* expression than *RAD21* expression. The abundance of *REC8* mRNA within these cells may have rendered a significant level siRNA knockdown unlikely. A degree of knockdown may have been achieved which was insufficient to show any significant knockdown at the protein level. Therefore qRT-PCR may be used to assess the level of REC8 knockdown achieved (if any) using the REC8-specific siRNAs.

Survival assay results presented by Adam Croucher suggested that REC8 knockdown did not produce any phenotypic change in the HeLa T-REx cell line (A. Croucher, Ph.D. thesis, Sheffield University). However a complete REC8 knockdown was not achieved, therefore the low level of REC8 remaining after induction may have been efficient to fulfil any functional role that REC8 may have in these mitotic cells. The results presented in Chapter 6.0, showed strong circumstantial evidence that REC8 is involved in a large protein complex and displays strong chromatin association in human mitotic cells, however a functional role for REC8 in these cells cannot be concluded. Evidence has been reported which suggests a possible functional role for REC8 within mouse somatic cells, however, this study also suggests that REC8 is not essential for somatic cells in mice (Xu *et al.*, 2005).

A potential functional role for REC8 needs to be established and characterized in human mitotic cells. REC8 knockdown is essential to carry out REC8 functional analysis within these mitotic cells; however the siRNA and miRNA protocols used here were unsuccessful. Further techniques can be used to assess REC8s potential function for example; a TALEN-

based technique may be used to create a stable cell line with a *REC8* knockout (methodology described in Cermak *et al.*, 2011).

7.6.2 RAD21 functional analysis

A significant level of RAD21 knockdown was achieved using siRNA in NT2 cells and MCF7 cells, which may suggest that the lack of REC8 knockdown observed in the NT2 cells was a REC8-specific problem and not a problem with the knockdown technique. Initial cell viability counts suggested that RAD21 knockdown had no effect on NT2 cell viability or sensitivity to phleomycin, after 48 hrs of siRNA treatment. However, cell survival assays wherein cell viability counts were carried out for a week after 48 hrs siRNA treatment suggested that RAD21 knockdown had an effect on cell proliferation. A significant difference was observed in the total cell number after RAD21 knockdown compared to the cells treated with non-interfering siRNA, for both MCF7 and NT2 cells. The NT2 cells appeared to recover normal levels of RAD21 quicker than the MCF7 cells, which was reflected in the cell growth. Previous studies have reported an enhanced level of *RAD21* expression in the MCF7 cell line (Kao *et al.*, 2009; Xu *et al.*, 2011). Therefore it is probable that the MCF7 cells have adapted to require an enhanced level of RAD21, which may account for the differences observed for NT2 and MCF7 cells after RAD21 knockdown.

Clonogenic survival assays showed a significant difference in cell survival after RAD21 knockdown compared to that of the cells treated with non-interfering siRNA, for both NT2 and MCF7 cells. These results may suggest that RAD21 is an essential protein for cell survival, although previous studies using human cells have suggested that RAD21 knockdown does not cause cell death and cells are able to complete mitosis (Deardorff *et al.*, 2012; Díaz-Martínez *et al.*, 2007). Clonogenic survival assays also suggested that RAD21 knockdown did not appear to cause an increased sensitivity of MCF7 cells to genotoxic insult with ionising radiation. These results however do not correspond to the findings of previous studies; RAD21 suppression has previously been linked with increased sensitivity to genotoxic insult (Atienza *et al.*, 2005; Deardorff *et al.*, 2012; Xu *et al.*, 2011). RAD21 has been shown to play a central role in mediating an ionising radiation response and DNA-damage repair in yeast (Birkenbihl and Subramani, 1992; Sjogren and Nasmyth, 2001) and vertebrates (Sonoda *et al.*, 2001; Xu *et al.*, 2010).

The cell survival assay using cell viability counts suggest that RAD21 knockdown massively reduced the cell growth rate; therefore the cells with successful RAD21 knockdown may not have been dividing quickly enough to form colonies during the clonogenic survival assay. Western blot analysis showed that RAD21 knockdown was not complete, and thus the colonies observed in the clonogenic survival assay after RAD21 knockdown may represent the survival of the cells in which RAD21 knockdown was unsuccessful/insufficient. Therefore, although the results presented here do not represent the effect of RAD21 knockdown with genotoxic insult, they do confirm that RAD21 knockdown has a significant effect on cell division and potentially the cell proliferation rate. Cell survival assays, using cell viability counts, may be used to assess the effect of RAD21 knockdown when the cells are subjected to genotoxic insult.

The cell survival assay, using cell viability counts, also showed a significant decrease in the total number of cells after RAD21 knockdown compared to the cells treated with non-interfering siRNA, with no significant increase in the number of dead cells. Preliminary results from flow cytometry analysis however showed no change in the NT2 and MCF7 cell cycle profiles after RAD21 knockdown. No cell cycle arrest after RAD21 knockdown was apparent, which may suggest that the cells are progressing through the cell cycle at a massively reduced rate, or the cells are arrested at the cell cycle point which they were at when RAD21 was knocked down. Studies in DT40 chicken cells have shown that the cells accumulate in G_2/M with extensive cell death observed later, after Scc1 depletion (Sonoda *et al.*, 2001). A small number of Scc1 depleted DT40 cells were able to complete mitosis however these cells consistently show chromosome mis-segregation (Sonoda *et al.*, 2001). These results provide further evidence to suggest that the functional role/necessity of RAD21 (SCC1) differs between different species.

Rad21 is essential for cell viability in fission yeast (Tomonaga *et al.*, 2000), and SCC1 is essential for chromosome cohesion during interphase and mitosis in vertebrates (Morrison *et al.*, 2003). In a study using DT40 chicken cells, Scc1 deficient cells frequently failed to complete metaphase chromosome alignment and showed chromosome segregation defects (Sonoda *et al.*, 2001). In DT40 chicken cells, the absence of functional Scc1, sister chromatids remain in close proximity in most cells, however the mechanism underlying this association is unknown (Sonoda *et al.*, 2001). A study by Xu *et al.*, (2010) showed that a

biallelic deletion of *RAD21* in mice resulted in early embryonic death, and heterozygous *RAD21* mutants were defective in homologous recombination DNA damage repair, therefore providing evidence that RAD21 is essential in mice.

Previous studies have shown that human cells are able to complete mitosis after RAD21 knockdown, but display un-coordinated loss of cohesion and aberrant anaphases (Losada *et al.*, 2005; Toyoda and Yanagida, 2006). Asynchronous chromatid separation was also observed for cells after RAD21 knockdown (Díaz-Martínez *et al.*, 2007). However, this study did not state if the cells were capable of undergoing a second round of mitotic cell division after RAD21 depletion. Un-coordinated chromosome segregation may result in a slower cell cycle progression than that observed for RAD21-containing cells, or if the cells were unable to undergo a second round of cell division, this would not result in cell cycle arrest and thus correspond with the preliminary flow cytometry results here.

Deardoff *et al.*, (2012) demonstrated that *RAD21* mutations, which alter RAD21 activity, can result in human congenital disorder, which can cause growth retardation and minor skeletal abnormalities. If RAD21 depletion significantly decreases the rate at which a cell can undergo cell division, this may potentially be linked to growth retardation in patients with RAD21 mutations. In contrast, enhanced *RAD21* expression was identified in undifferentiated cancers which displayed aggressive *in vitro* or clinical courses. Undifferentiated cancers fail to recapitulate the normal architecture associated with the tissue from which they arose, but maintain a disordered state and display increased cell proliferation and invasion of surrounding tissue (Rhodes *et al.*, 2004). This may suggest that the level of RAD21 expression is directly related to the cell proliferation speed.

In summary, RAD21 knockdown appears to significantly reduce the cell proliferation rate of NT2 and MCF7 cells. To establish a potential functional role for REC8 in mitotic cells a successful REC8 knockdown is essential. REC8-containing cohesin is essential for the completion of meiosis (Xu *et al.*, 2005), and if found to behave similarly in mitotic cells a complete knockdown may result in cell death. However, if REC8 depleted cells are capable of cell division, a double knockdown of REC8 and RAD21 may be required to render the cells incapable of completing mitosis. Although this was the original aim for this study, this was not achieved due to a lack of successful REC8 knockdown in the cancer cell lines.

8.0 General discussion

8.1 Screening meiotic genes

RT-PCR screening of the purported meiosis-specific genes and predicted meiotic genes, identified by the bioinformatics pipeline, in Chapters 3.0 and 4.0 found that a large number of the candidate genes were widely expressed. Surprisingly, of the nine reported meiosis-specific genes screened in Chapter 3.0, only three genes displayed a testis-restricted expression profile in the normal human tissues. The two well characterised meiotic genes *REC8* and *STAG3* displayed expression in all of the normal human tissues tested. Although *STAG3* expression was observed in all the normal mouse and human tissues screened, *REC8* expression was found to be more widely expressed in human tissues than in mouse tissues. The meiosis-specificity of REC8, and its orthologues, has previously been reported to be widely conserved from yeast to humans (Parisi *et al.*, 1999). Therefore the gene expression profiles identified during this study do not agree with the previous studies. This lack of correspondence with the previously published work may be due to the high number of PCR cycles identifying low levels of gene expression.

Studies in fission yeast have demonstrated that meiotic genes are expressed in mitotic cells, but a post-transcriptional processing mechanism ensures that the meiotic genes are not functionally expressed until the onset of meiosis (Chen *et al.*, 2011; Cremona *et al.*, 2011; Harigaya *et al.*, 2006; Yamanaka *et al.*, 2010). Western blot analysis and immunofluorescent staining using a commercial antibody against REC8, suggested that REC8 localises within the nucleus of mitotically dividing human cells. This may therefore suggest that the primary transcripts of meiotic genes, in human mitotic cells, are not degraded via a post-transcriptional mechanism similar to that described for fission yeast.

Securin is an inhibitory chaperone protein which inactivates separase and orthologues have been identified in yeast and mammals, securin (mice and human), Pds1 in budding yeast and Cut2 fission yeast (Mei *et al.*, 2001). Cut2 is essential in fission yeast, whereas studies have shown that Pds1 is not essential in budding yeast, but loss of Pds1 causes genome instability (Yamamoto *et al.*, 1996). Studies have also shown that securin is not essential in mouse (Mei *et al.*, 2001) and human (Pfleghaar *et al.*, 2005) cells. These studies provide

evidence that the securin/separase pathway has diversified during evolution and represents different strategies controlling the metaphase-anaphase transition, used by various organisms (Mei *et al.*, 2001; Pfleghaar *et al.*, 2005). Phosphorylation of separase has also been shown to mediate separase inhibition in vertebrate cells (Stemmann *et al.*, 2001) and this inhibitory phosphorylation functions in the absence of securin (Huang *et al.*, 2005). This may suggest that other mechanisms during mitosis could have diversified during evolution, which may give rise to the differences observed in Chapter 3.0 for meiotic gene expression profiles in mouse and human normal tissues.

A greater number of different cohesin subunits have been identified in mammalian meiocytes than in the meiotic cells of lower eukaryotes. For example a second SMC1-type protein (SMC1β) and a second meiosis-specific α-kleisin protein (RAD21L) have been identified in vertebrates, but not in invertebrate species (Ishiguro *et al.*, 2011; Lee and Hirano, 2011; Revenkova *et al.*, 2010). There is mounting evidence for significant differences between the meiotic programs of different species and the results from this study may highlight greater differences, than previously reported, in the control and regulation of meiotic genes and/or proteins within different species.

In budding yeast, Scc3 (SA/STAG in mammals) has been shown to play a specific role in maintaining a normal level of Rec8 by regulating *REC8* gene expression during meiosis (Lin *et al.*, 2011b). Evidence was also presented which suggests that Scc3 is required for Rec8 chromosome association in budding yeast (Lin *et al.*, 2011b). Studies in mice have shown that REC8 preferentially associates with STAG3 rather than STAG1 or STAG2 (Lee and Hirano, 2011). This may be potentially interesting because the RT-PCR results presented here suggest that *STAG3* and *REC8* are both widely expressed in the normal human tissues. *STAG3* gene expression was observed in a wide range of human and mouse normal tissues, however western blot analysis using commercially available antibodies against human STAG3 was unsuccessful. Therefore biochemical analysis of STAG3 production within the human cancer cell lines was unsuccessful. Further characterisation needs to be carried out to firstly establish any STAG3 protein production in human and mouse mitotically dividing cells. If the STAG3 protein is found in mitotic cells, biochemical and functional analyses should be carried out, and if a functional role is identified for STAG3 in mitotic cells then this

may cause STAG3 to be re-assessed as a meiosis-specific protein within humans and/or mice.

8.2 Further characterisation of novel CT genes

CT antigen genes display highly tissue restricted expression profiles in normal tissues, and therefore we proposed that meiotic genes may provide a good source from which to identify new CT antigen genes. The RT-PCR results presented in Chapters 3.0 and 4.0 identified five potential CT antigen genes; three CT-restricted genes, one CT-selective gene and one CT/CNS-selective gene. Additionally, six of the nine testis-restricted genes (after RT-PCR validation) were found to display expression in clinically relevant cancer samples after meta-analysis (www.cancerma.org.uk; Feichtinger *et al.*, 2012b). Therefore taken altogether, these results suggest that this study identified eleven CT genes from the 37 genes screened here. These results represent part of a larger study (detailed in Feichtinger *et al.*, 2012a), which identified 42 meiCT genes. Thus supporting the original hypothesis, that meiotic genes provide a good source for the identification of further novel CT genes. Interestingly, RT-PCR analysis and meta-analysis found that a large number of the meiCT genes displayed expression in the ovarian cancer cells lines and/or clinical samples. Clinical trials have yielded positive results for CT antigen-based immunotherapy treatment of ovarian cancers (for example, Diefenbach *et al.*, 2008; Odunsi *et al.*, 2007). Therefore CT antigens appear to be good candidates from which to identify potential new targets for diagnostic tests and/or immunotherapeutic treatment of ovarian cancer.

My project funding was geared towards identifying markers of ovarian cancer therefore *NUT*, which was identified as a novel CT gene in the larger gene screen (Feichtinger *et al.*, 2012a), was selected for biochemical analysis within ovarian cancer cell lines. *NUT* expression was observed in HCT116 (human colorectal cancer cell line), A2780 (ovarian cancer cell line) and the ovarian tumour tissue (Feichtinger *et al.*, 2012a). Therefore further analysis was carried out for *NUT* because expression had been observed in ovarian cancer cells and commercial antibodies against NUT were available. Western blot analysis and immunofluorescent staining results suggested that NUT was primarily localised in the cytoplasm of A2780 cells. Although low levels of NUT appeared to localise in the nucleus of the A2780 cells, no chromatin association was observed. Biochemical analysis also

suggested that NUT may be produced at very low levels in NT2 cells, thus implying that *NUT* may be more widely expressed in cancer cells than RT-PCR initially suggested. Further characterisation is required to establish if NUT has a functional role within the cancer cells, any potential antigenicity conferred by NUT and if NUT is produced in clinically relevant samples.

A significant number of the meiCT genes identified in the CT gene screen (Feichtinger *et* al., 2012a) were found to show expression in the ovarian cancer cells. Ten ovarian cancers with matched normal tissue FFPE (formalin fixed paraffin embedded) blocks were purchased from Proteogenex. Total RNA could be extracted from these FFPE tissue blocks using an RNeasy FFPE kit (Qiagen; 73504) and RT-PCR could be carried out to screen for the expression of the meiCT genes (found to be up-regulated in ovarian cancer cells) in these ovarian cancer samples. Immunohistochemistry could also be carried out for NUT using these FFPE tissue blocks, to establish the protein localisation observed in the cell lines represents that in the patient tissue.

Further studies are also required to establish if the protein products of the CT genes identified here are produced in the cancer cells and if so, their cellular localisation and potential function within the cancer cells. The potential antigenicity of the protein products of the meiCT genes identified in this study also needs to be established before these genes can be classified as novel CT antigens. Commercial antibodies were not available against the protein products of the novel CT genes identified here, therefore these CT genes could not be characterised at the protein level. As CT-restricted expression profiles were observed for *RAD21L*, *SMC1β* and *c17orf98* these may represent more ideal candidates, than the CT-selective genes, for potential CT antigens. Therefore antibodies against RAD21L, SMC1β and c17orf98 could be produced which would allow further characterisation of these meiotic proteins within cancer cells.

8.3 Meiotic proteins in cancer

Links have been established between cancer and gametogenesis, because there is evidence to suggest a common evolutionary pathway between meiotic ploidy cycles and polyploidy in tumour cells (Kalejs and Erenpreisa, 2005; Old, 2001). A highly variable expression pattern

has been observed for CT antigen genes. It remains unclear whether the up-regulation of CT antigen genes is the result of genomic instability commonly observed in cancer cells or whether they are activated to elicit a survival advantage thus enabling tumorigenesis (Kalejs and Erenpreisa, 2005). For example, homologous recombination has been shown to confer anti-apoptotic effects in tumour cells (Raderschall *et al.*, 2002).

Several CT antigens identified in previous studies have a known role in normal gamete development, such as SPO11, SYCP1 (Türeci *et al.*, 1998) and SYCP3 (Mobasheri *et al.*, 2007; Simpson *et al.*, 2005). The up-regulation of meiotic proteins in mitotically dividing cells may induce a meiotic-like cell division program, which in turn could cause oncogenic genetic changes. Up-regulation of meiosis-specific proteins in cancer cells may facilitate and/or promote inappropriate non-allelic intra- and/or inter-chromosomal recombination and inter-homologue recombination (Caballero and Chen, 2009).

Interestingly, several of the SC component proteins are capable of self-assembly when over-expressed in cells (Zickler and Kleckner, 1999). When up-regulated in cancer cells, are these proteins able to form meiotic-like structures and/or complexes? Studies could be carried out to establish a potential functional role for CT antigens within cancer cells and if any of the meiotic genes are co-expressed in cancer cells. If the meiotic proteins are able to form meiotic-like structures/complexes in mitotically dividing cancer cells, does this aid aneuploidy and genomic instability and/or provide a survival advantage? The mammalian AE proteins have also been implicated in inter-homologue bias during meiotic recombination, and SYCP3 has been shown to form a complex with BRCA2 in cancer cells which therefore inhibits the mitotic recombination DNA repair pathway and induces chromosome instability (Hosoya *et al.*, 2012). This may suggest that SYCP3 promotes inter-homologue recombination during meiosis, by inhibiting inter-sister recombination.

In mouse meiotic cells, RAD21L localises along the AEs/LEs and disappears at mid-pachytene, which corresponds with the completion of DNA DSB repair and CO formation (Lee and Hirano, 2011). The results from the study by Lee and Hirano, (2011) suggest that RAD21L-containing cohesin may be involved in synapsis initiation and crossover recombination between homologous chromosomes. Another study using mice has also shown that SMC1β is essential for maintaining meiotic sister chromatid cohesion and

chiasmata (Revenkova *et al.*, 2010). *SMC1β*$^{-/-}$ oocytes and spermatocytes show incomplete synapsis (Revenkova *et al.*, 2010). Functional analysis studies should be carried out to determine any potential functional role(s) for the products of these CT genes in cancer cells, and if this potential functional role resembles their function during meiosis. If RAD21L and SMC1β are found to be functionally active cohesins in cancer cells they could potentially be used as drug targets for cancer treatment. For example, blocking RAD21L and SMC1β functions may inhibit cell proliferation of the tumour cells in a tumour cell-specific manner, as they are testis-specific in normal human tissues.

8.4 REC8 and RAD21

REC8 is essential for the completion of meiosis and faithful chromosome segregation, with a range of functional roles, including; sister chromatid cohesion, AE formation and SC initiation (Eijpe *et al.*, 2003; Klein *et al.*, 1999), HR partner bias (Kim *et al.*, 2010), monopolar kinetochore orientation (Yokobayashi *et al.*, 2003). REC8 orthologues have been identified in many species (from yeast to humans) and has previously been reported to be meiosis-specific (Parisi *et al.*, 1999). However, the RT-PCR results presented here displayed *REC8* gene expression in a wide range of normal human tissues and cancer cell lines. The results from western blot analysis and immunofluorescent staining suggested that the REC8 protein was detected in human mitotic cells and was found to display a nuclear localisation. The results presented here also suggest that REC8 may be involved in a large protein complex and displayed strong chromatin association in human mitotic cells. However, REC8 knockdown was unsuccessful therefore no functional role could be determined for REC8 in the human cancer cell lines.

RAD21 knockdown in MCF7 and NT2 cells suggested that RAD21-deficient cells were unable to proliferate normally. These results correspond with the findings from previous studies, which suggested that RAD21 is required for the timely separation of chromosomes and completion of mitosis in human cells (Díaz-Martínez *et al.*, 2007).

Single and double REC8 and RAD21 knockdowns should be carried out in the cancer cell lines, to establish any potential effect on cell division and/or cell viability. Stable cell lines could be created with *REC8* and *RAD21* knockouts could be created using a TALEN-based

technique (methodology described in Cermak *et al.*, 2011) which may aid functional analysis of REC8 in mitotic cells compared RAD21. As previous studies have demonstrated evidence that REC8 is essential during meiosis and is responsible for a range of functions, a potential functional role (if any) should be established for REC8 in human mitotic cells. For example, does REC8-containing cohesin mediate chromosome cohesion in mitotic cells, or have a non-chromosomal cohesion role such as a role within transcriptional control? If a functional role is identified for REC8 in mitotic cells, this may cause REC8 to be re-assessed as a meiosis-specific protein within humans. Metaphase spread analysis could also be used to characterise RAD21 and REC8 localisation along the chromosomes, to establish if they co-localise or display mutually exclusive localisation, as seen previously during mouse meiosis (Ishiguro *et al.*, 2011; Lee and Hirano, 2011).

8.5 Conclusions and Future Research

In conclusion, RT-PCR screening of meiotic genes using a range of normal tissues and cancer cells identified five novel CT genes (*RAD21L*, *SMC1β*, *c17orf98*, *DUSP21*, and *ZCCHC13*) and meta-analysis of the validated testis-restricted genes identified an additional six CT genes (*ADAD1*, *c5orf47*, *CATSPER1*, *CYLC1*, *SOX30* and *SYCP3* as shown in Figure 4.11). These results therefore support the original hypothesis that meiotic genes may provide a good source for identifying potential novel CT antigen genes. If the products of these genes are produced in cancer cells they may provide tumour-specific targets. The results presented here also provide evidence to suggest that there are greater differences, than previously proposed, in the control and regulation of meiotic genes and/or proteins within different species.

A number of experiments could be carried out to continue the research presented here, including:

- Antibodies could be created against the proteins encoded by the potential novel CT genes identified by the CT gene screen. Thereby allowing biochemical characterisation of these proteins to establish their potential as possible CT antigens.

- Biochemical analysis of NUT in HCT116 cells and compare with the A2780 cells, and immunohistochemical analysis of NUT in ovarian cancer tissue samples with matched normal controls (using normal testis tissue as a positive control).
- To determine the specificity of the anti-REC8 antibody a number of techniques could be used:
    i. Immunoprecipitation using anti-REC8 and mass spectrometry to identify the protein with which anti-REC8 is binding.
    ii. A REC8-tagged cell line could be created, which would alter the size at which REC8 runs on a SDS-PAGE gel.
- If the specificity of anti-REC8 is proven, then CoIP could be used to determine which (if any) proteins REC8 binds to in human mitotic cells.
- REC8 knockdown could be carried out to determine if REC8 has a functional role in mitotically dividing human cells.

9.0 References

AGARWAL, S. AND ROEDER, G.S. 2000. Zip3 provides a link between recombination enzymes and synaptonemal complex proteins. *Cell*, **102**, 245-255.

ALMEDAWAR, S., COLOMINA, N., BERMUDEZ-LOPEZ, M., POCINO-MERINO, I. AND TORRES-ROSELL, J. 2012. A SUMO-dependent step during establishment of sister chromatid cohesion. *Current Biology*, **22**, 1576-1581.

ALMEIDA, L.G., SAKABE, N.J., DE OLIVEIRA, A.R., SILVA, M.C., MUNDSTEIN, A.S., COHEN, T., CHEN, Y.T., CHUA, R., GURUNG, S., GNJATIC, S., JUNGBLUTH, A.A., CABALLERO, O.L., BAIROCH, A., KIESLER, E., WHITE, S.L., SIMPSON, A.J., OLD, L.J., CAMARGO, A.A. AND VASCONCELOS, A.T. 2009. CTdatabase: A knowledge-base of high throughput and curated data on cancer-testis antigens. *Nucleic Acids Research*, **37**, D816-D819.

ANVERSA, P., KAJSTURA, J., LERI, A. AND BOLLI, R. 2006. Life and death of cardiac stem cells: a paradigm shift in cardiac biology. *Circulation*, **113**, 1451-1463.

ARESSY, B., JULLIEN, D., CAZALES, M., MARCELLIN, M., BUGLER, B., BURLET-SCHILTZ, O. AND DUCOMMUN, B. 2010. A screen for deubiquitinating enzymes involved in the G2/M checkpoint identifies USP50 as a regulator of HSP90-dependent Wee1 stability. *Cell Cycle*, **9**, 3815-3822.

ATIENZA, J.M., ROTH, R.B., ROSETTE, C., SMYLIE, K.J., KAMMERER, S., REHBOCK, J., EKBLOM, J. AND DENISSENKO, M.F. 2005. Suppression of *RAD21* gene expression decreases cell growth and enhances cytotoxicity of etoposide and bleomycin in human breast cancer cells. *Molecular Cancer Therapeutics*, **4**, 361-368.

BARBER, T.D., MCMANUS, K., YUEN, K.W., REIS, M., PARMIGIANI, G., SHEN, D., BARRETT, I., NOUHI, Y., SPENCER, F., MARKOWITZ, S., VELCULESCU, V.E, KINZLER, K.W., VOGELSTEIN, B., LENGAUER, C. AND HIETER, P. 2008. Chromatid cohesion defects may underlie chromosome instability in human colorectal cancers. *PNAS USA*, **105**, 3443-3448.

BARDHAN, A. 2010. Many functions of the meiotic cohesin. *Chromosome Research*, **18**, 909-924.

BARDIN, A.J. AND AMON, A. 2001. Men and sin: what's the difference? *Nature Reviews, Molecular Cell Biology*, **2**, 815-826.

BAUDAT, F., BUARD, J., GREY, C., FLEDEL-ALON, A., OBER, C., PRZEWORSKI, M., COOP, G. AND DE MASSY, B. 2010. PRDM9 is a major determinant of meiotic recombination hotspots in humans and mice. *Science*, **327**, 836-840.

BAUER, D.L., MARIE, R., RASMUSSEN, K.H., KRISTENSEN, A. AND MIR, K.U. 2012. DNA catenation maintains structure of human metaphase chromosomes. *Nucleic Acids Research*, **40**, 11428-11434.

BEAUDOUIN, J., GERLICH, D., DAIGLE, N., EILS, R. AND ELLENBERG, J. 2002. Nuclear envelope breakdown proceeds by microtubule-induced tearing of the lamina. *Cell*, **108**, 83-96.

BEN-SHAHAR, T.R., HEEGER, S., LEHANE, C., EAST, P., FLYNN, H., SKEHEL, M. AND UHLMANN, F. 2008. Eco1-dependent cohesin acetylayion during establishment of sister chromatid cohesion. *Science*, **321**, 563-566.

BERGER, S.L. 2007. The complex language of chromatin regulation during transcription. *Nature*, **447**, 407-412.

BERGERAT, A., DE MASSY, B., GADELLE, D., VAROUTAS, P.C., NICOLAS, A. AND FORTERRE, P. 1997. An atypical topoisomerase II from Archaea with implications for meiotic recombination. *Nature*, **386**, 414-417.

BERMUDEZ, V.P., FARINA, A., HIGASHI, T.L., DU, F., TAPPIN, I., TAKAHASHI, T.S. AND HURWITZ, J. 2012. In vitro loading of human cohesin on DNA by the human Scc2-Scc4 loader complex. *PNAS*, **109**, 9366-9371.

BERNSTEIN, S.L., GUO, Y., PETERSON, K. AND WISTOW, G. 2009. Expressed sequence tag analysis of adult human optic nerve for NEIBank: identification of cell type and tissue markers. *BMC Neuroscience*, **10**, 121-131.

BHALLA, N. AND DERNBURG, A.F. 2008. Prelude to a division. *Annual Review of Cell and Developmental Biology*, **24**, 397-424.

BIRKENBIHL, R.P. AND SUBRAMANI, S. 1992. Cloning and characterization of rad21 an essential gene of Schizosaccharomyces pombe involved in DNA double-strand-break repair. *Nucleic Acids Research*, **20**, 6605-6611.

BISHOP, D.K. AND ZICKLER, D. 2004. Early decision; meiotic crossover interference prior to stable strand exchange and synapsis. *Cell*, **117**, 9-15.

BOLCUN-FILAS, E., COSTA, Y., SPEED, R., TAGGART, M., BENAVENTE, R., DE ROOIJ, D.G. AND COOKE, H.J. 2007. SYCE2 is required for synaptonemal complex assembly, double strand break repair, and homologous recombination. *The Journal of Cell Biology*, **176**, 741-747.

BOLCUN-FILAS, E., SPEED, R., TAGGART, M., GREY, C., DE MASSY, B., BENAVENTE, R. AND COOKE, H.J. 2009. Mutation of the mouse *Syce1* gene disrupts synapsis and suggests a link between synaptonemal complex structural components and DNA repair. *PLoS Genetics*, **5**, e1000393.

BORNER, G.V., KLECKNER, N. AND HUNTER, N. 2004. Crossover/noncrossover differentiation, synaptonemal complex formation, and regulatory surveillance at the leptotene/zygotene transition of meiosis. *Cell*, **117**, 29-45.

BUHEITEL, J. AND STEMMANN, O. 2013. Prophase pathway-dependent removal of cohesin from human chromosomes requires opening of the Smc3-Scc1 gate. *The EMBO Journal*, **32**, 666-676.

BUONOMO, S.B., CLYNE, R.K., FUCHS, J., LOIDL, J., UHLMANN, F. AND NASMYTH, K. 2000. Disjunction of homologous chromosomes in meiosis I depends on proteolytic cleavage of the meiotic cohesin Rec8 by separin. *Cell*, **103**, 387-398.

CABALLERO, O.L. AND CHEN, Y.T. 2009. Cancer/testis (CT) antigens: potential targets for immunotherapy. *Cancer Science*, **100**, 2014-2021.

CALLENDER, T.L. AND HOLLINGSWORTH, N.M. 2010. Mek1 suppression of meiotic double-strand break repair is specific to sister chromatids, chromosome autonomous and independent of Rec8 cohesin complexes. *Genetics*, **185**, 771-782.

CAMACHO, J.A., RIOSECO-CAMACHO, N., ANDRADE, D., PORTER, J. AND KONG, J. 2003. Cloning and characterization of human ORNT2: a second mitochondrial ornithine transporter that can rescue a defective ORNT1 in patients with the hyperornithinemia-hyperammonemia-homocitrullinuria syndrome, a urea cycle disorder. *Molecular Genetics and Metabolism*, **79**, 257-271.

CANALS, M., JENKINS, L., KELLETT, E. AND MILLIGAN, G. 2006. Up-regulation of the angiotensin II type 1 receptor by the *MAS* proto-oncogene is due to constitutive activation of Gq/G11 by MAS. *The Journal of Biological Chemistry*, **281**, 16757-16767.

CANUDAS, S. AND SMITH, S. 2009. Differential regulation of telomere and centromere cohesion by the Scc3 homologues SA1 and SA2, respectively, in human cells. *The Journal of Cell Biology*, **187**, 165-173.

CARSON, M.J., DOOSE, J.M., MELCHOIR, B., SCHMID, C.D. AND PLOIX, C.C. 2009. CNS immune privilege: hiding in plain sight. *Immunological Reviews*, **213**, 48-65.

CERMAK, T., DOYLE, E.L., CHRISTIAN, M., WANG, L., ZHANG, Y., SCHMIDT, C., BALLER, J.A., SOMIA, N.V., BOGDANOVE, A.J. AND VOYTAS, D.F. 2011. Efficient design and assembly of custom TALEN and other TAL effector-based constructs for DNA targeting. *Nucleic Acids Research*, **39**, e82.

CHALMEL, F., ROLLAND, A. D., NIEDERHAUSER-WIEDERKEHR, C., CHUNG, S. S., DEMOUGIN, P., GATTIKER, A., MOORE, J., PATARD, J.J., WOLGEMUTH, D.J., JÉQOU, B. AND PRIMIG, M. 2007. The conserved transcriptome in human and rodent male gametogenesis. *PNAS USA*, **104**, 8346-8351.

CHAMPION, M.D. AND HAWLEY, R.S. 2002. Playing for half the deck: the molecular biology of meiosis. *Nature Cell Biology*, **4**, s50-S56.

CHAN, K.L., ROIG, M.B., HU, B., BECKOUËT, F., METSON, J. AND NASMYTH, K. 2012. Cohesin's DNA exit gate is distinct from its entrance gate and is regulated by acetylation. *Cell*, **150**, 961-974.

CHEN, H.M., FUTCHER, B. AND LEATHERWOOD, J. 2011. The fission yeast RNA binding protein Mmi1 regulates meiotic gene by controlling intron specific splicing and polyadenylation coupled RNA turnover. *PLoS One*, **6**, e26804.

CHEN, Y.T., SCANLAN, M.J., SAHIN, U., TÜRECI, O., GURE, A.O., TSANG, S., WILLIAMSON, B., STOCKERT, E., PFREUNDSCHUH, M. AND OLD, L.J. 1997. A testicular antigen aberrantly expressed in human cancers detected by autologous antibody screening. *PNAS*, **94**, 1914-1918.

CHEN, S.Y., TSUBOUCHI, T., ROCKMILL, B., SANDLER, J.S., RICHARDS, D.R., VADER, G., HOCHWAGEN, A., ROEDER, G.S. AND FUNG, J. 2008. Global analysis of the meiotic crossover landscape. *Developmental Cell*, **15** 401-415.

CHEN, Y.T., VENDITTI, C.A., THEILER, G., STEVENSON, B.J., ISELI, C., GURE, A.O., JONGENEEL, C.V., OLD, L.J. AND SIMPSON, A.J. 2005. Identification of CT46/HORMAD1, an immunogenic cancer/testis antigen encoding a putative meiosis-related protein. *Cancer Immunity*, **5**, 9-16.

CHENG, Y.H., WONG, E.W. AND CHENG, C.Y. 2011. Cancer/testis (CT) antigens, carcinogenesis and spermatogenesis. *Spermatogenesis*, **1**, 209-220.

CHERVONA, Y. AND COSTA, M. 2012. Histone modifications and cancer: biomarkers of prognosis? *American Journal of Cancer Research*, **2**, 589-597.

CHEUNG, V.G., SHERMAN, S.L. AND FEINGOLD, E. 2010. Genetics. Genetic control of hotspots. *Science*, **327**, 791-792.

CHO, B., LEE, H., JEONG, S., BANG, Y.J., LEE, H.J., HWANG, K.S., KIM, H.Y., LEE, Y.S., KANG, G.H. AND JEOUNG, D.I. 2003. Promoter hypomethylation of a novel cancer/testis antigen gene CAGE is correlated with its aberrant expression and is seen in premalignant stage of gastric carcinoma. *Biochemical and Biophysical Research Communications*, **307**, 52-63.

CHOW, J.C., YEN, Z., ZIESCHE, S.M. AND BROWN, C.J. 2005. Silencing of the mammalian X-chromosome. *Annual Review of Genomics and Human Genetics*, **6**, 69-92.

CHUA, P.R. AND ROEDER, G.S. 1998. Zip2, a meiosis-specific protein required for the initiation of chromosome synapsis. *Cell*, **93**, 349-359.

CIMINI, D., CAMERON, L.A. AND SALMON, E.D. 2004. Anaphase spindle mechanics prevent mis-segregation of merotelically oriented chromosomes. *Current Biology*, **14**, 2149-2155.

CIMINI, D., WAN, X., HIREL, C.B. AND SALMON, E.D. 2006. Aurora kinase promotes turnover of kinetochore microtubules to reduce chromosome segregation errors. *Current Biology*, **16**, 1711-1718.

CIOSK, R., SHIRAYAMA, M., SHEVCHENKO, A., TANAKA, T., TOTH, A., SHEVCHENKO, A. AND NASMYTH, K. 2000. Cohesin's binding to chromosomes depends on a separate complex consisting of Scc2 and Scc4 proteins. *Molecular Cell*, **5**, 243-254.

CLIFT, D. AND MARSTON, A.L. 2011. The role of Shugoshin in meiotic chromosome segregation. *Cytogenetic and Genome Research*, **133**, 234-242.

CLIFT, D., BIZZARI, F. AND MARSTON, A.L. 2009. Shugoshin prevents cohesin cleavage by $PP2A^{Cdc55}$-dependent inhibition of separase. *Genes and Development*, **23**, 766-780.

COSTA, F.F., LE BLANC, K. AND BRODIN, B. 2007. Concise review: cancer/testis antigens, stem cells and cancer. *Stem Cells*, **25**, 707-711.

COSTA, Y., SPEED, R., OLLINGER, R., ALSHEIMER, M., SEMPLE, C.A., GAUTIER, P., MARATOU, K., NOVAK, I., HOOG, C., BENAVENTE, R. AND COOKE, H.J. 2005. Two novel proteins recruited by synaptonemal complex protein 1 (SYCP1) are at the centre of meiosis. *Journal of Cell Science*, **118**, 2755-2762.

CREMONA, N., POTTER, K. AND WISE, J.A. 2011. A meiotic gene regulatory cascade driven by alternative fates for newly synthesized transcripts. *Molecular Biology of the Cell*, **22**, 66-77.

CROMIE, G. AND SMITH, G.R. 2008. Meiotic recombination in *Schizosaccharomyces pombe*: A paradigm for genetic and molecular analysis. *Genome Dynamics and Stability*, **3**, 195.

CRONWRIGHT, G., LE BLANC, K., GOTHERSTROM, C., DARCY, P., EHNMAN, M. AND BRODIN, B. 2005. Cancer/testis antigen expression in human mesenchymal stem cells: down-regulation of *SSX* impairs cells migration and matrix metalloproteinase 2 expression. *Cancer Research*, **65**, 2207-2215.

CSORDÁS, G., VÁRNAI, P., GOLENÁR, T., SHEU, S.S. AND HAJNÓCZKY, G. 2012. Calcium transport across the inner mitochondrial membrane: molecular mechanisms and pharmacology. *Molecular and Cellular Endocrinology*, **353**, 109-113.

CT DATABASE (online). http://www.cta.lncc.br/

DANIEL, K., LANGE, J., HACHED, K., FU, J., ANASTASSIADIS, K., ROIG, I., COOKE, H.J., STEWART, A.F., WASSMANN, K., JASIN, M., KEENEY, S. AND TOTH, A. 2011. Meiotic homologue alignment and its quality surveillance are controlled by mouse HORMAD1. *Nature Cell Biology*, **13**, 599-610.

DARWICHE, N., FREEMAN, L.A. AND STRUNNIKOV, A. 1999. Characterization of the components of the putative mammalian sister chromatid cohesin complex. *Gene*, **233**, 39-47.

DAVIES, O.R., MAMAN, J.D. AND PELLEGRINI, L. 2012. Structural analysis of the human SYCE2-TEX12 complex provides molecular insights into synaptonemal complex assembly. *Open Biology*, **2**, 120099.

DEARDORFF, M.A., WILDE, J.J., ALBRECHT, M., DICKINSON, E., TENNSTEDT, S., BRAUNHOLZ, D., MONNICH, M., YAN, Y., XU, W., GIL-RODRÍGUEZ, M.C., CLARK, D., HAKONARSON, H., HALBACH, S., MICHELIS, L.D., RAMPURIA, A., ROSSIER, E., SPRANGER, S., VAN MALDERGEM, L., LYNCH, S.A., GILLESSEN-KAESBACH, G., LUDECKE, H.J., RAMSAY, R.G., MCKAY, M.J., KRANTZ, I.D., XU, H., HORSFIELD, J.A. AND KAISER, F.J. 2012. RAD21 mutations cause a human cohesinopathy. *American Journal of Human Genetics*, **90**, 1014-1027.

DE BOER, E. AND HEYTING, C. 2006. The diverse roles of transverse filaments of synaptonemal complexes in meiosis. *Chromosoma*, **115**, 220-234.

DE CARVALHO, D.D., YOU, J.S. AND JONES, P.A. 2010. DNA methylation and cellular reprogramming. *TRENDS in Cell Biology*, **20**, 609-617.

DE SMET, C., DE BACKER, O., FARAONI, I., LURQUIN, C., BRASSEUR, F. AND BOON, T. 1996. The activation of human gene MAGE-1 in tumour cells is correlated with genome-wide demethylation. *PNAS USA*, **93**, 7149-7153.

DE SMET, C., LURQUIN, C., LETHÉ, B., MARTELANGE, V. AND BOON, T. 1999. DNA methylation is the primary silencing mechanism for a set of germ line- and tumour-specific genes with a CpG-rich promoter. *Molecular and Cellular Biology*, **19**, 7327-7335.

DE SOUZA, C.P. AND OSMANI, S.A. 2007. Mitosis, not just open or closed. *Eukaryotic Cell*, **6**, 1521-1527.

DE VRIES, F.A., DE BOER, E., VAN DEN BOSCH, M., BAARENDS, W.M., OOMS, M., YUAN, L., LIU, J.G., VAN ZEELAND, A., HEYTING, C. AND PASTINK, A. 2005. Mouse *Sycp1* functions in synaptonemal complex assembly, meiotic recombination, and XY body formation. *Genes and Development*, **19**, 1376-1389.

DE WIT, N.J., VERSCHUURE, P., KAPPÉ, G., KING, S.M., DE JONG, W.W., VAN MUIJEN, G.N. AND BOELENS, W.C. 2004. Testis-specific human small heat shock protein HSPB9 is a cancer/testis antigen and potentially interacts with the dynein subunit TCTEL1. *European Journal of Cell Biology*, **83**, 337-345.

DÍAZ-MARTÍNEZ, L.A., GIMÉNEZ-ABIÁN, J.F., AZUMA, Y., GUACCI, V., GIMÉNEZ-MARTÍN, G., LANIER, L.M. AND CLARKE, D.J. 2006. PIASgamma is required for faithful chromosome segregation in human cells. *PLoS ONE*, **1**, e53.

DÍAZ-MARTÍNEZ, L.A., GIMÉNEZ-ABIÁN, J.F. AND CLARKE, D.J. 2007. Cohesin is dispensable for centromere cohesion in human cells. *PLoS ONE*, **2**, e318.

DÍAZ-MARTÍNEZ, L.A., GIMÉNEZ-ABIÁN, J.F. AND CLARKE, D.J. 2008. Chromosome cohesion – rings, knots, orcs and fellowship. *Journal of Cell Science*, **121**, 2107-2114.

DIEFENBACH, C.S., GNJATIC, S., SABBATINI, P., AGHAJANIAN, C., HENSLEY, M.L., SPRIGGS, D.R., IASONOS, A., LEE, H., DUPONT, B., PEZZULLI, S., JUNGBLUTH, A.A., OLD, L.J. AND DUPONT, J. 2008. Safety and immunogenicity study of NY-ESO-1b peptide and montanide ISA-51 vaccination of patients with epithelial ovarian cancer in high-risk first remission. *Clinical Cancer Research*, **14**, 2740-2748.

DODGE, J.E., COVENS, A.L., LACCHETTI, C., ELIT, L.M., LE, T., DEVRIES-ABOUD, M. AND FUNG-KEE-FUNG, M. 2012. Preoperative identification of a suspicious adnexal mass: a systematic review and meta-analysis. *Gynecologic Oncology*, **126**, 157-166.

DRAY, E., DUNLOP, M.H., KAUPPI, L., SAN FILIPPO, J., WIESE, C., TSAI, M.S., BEGOVIC, S., SCHILD, D., JASIN, M., KEENEY, S. AND SUNG, P. 2011. Molecular basis for enhancement of the meiotic DMC1 recombinase by RAD51 associated protein 1 (RAD51AP1). *PNAS USA*, **108**, 3560-3565.

EGGER, G., LIANG, G., APARICIO, A. AND JONES, P.A. 2004. Epigenetics in human disease and prospects for epigenetic therapy. *Nature*, **429**, 457-463.

EIJPE, M., HEYTING, C., GROSS, B. AND JESSBERGER, R. 2000. Association of mammalian SMC1 and SMC3 proteins with meiotic chromosomes and synaptonemal complexes. *Journal of Cell Science*, **113**, 673-682.

EIJPE, M., OFFENBERG, H., JESSBERGER, R., REVENKOVA, E. AND HEYTING, C. 2003. Meiotic cohesin REC8 marks the axial elements of rat synaptonemal complexes before cohesins SMC1β and SMC3. *The Journal of Cell Biology*, **160**, 657-670.

ERENPREISA, J., CRAGG, M.S., SALMINA, K., HAUSMANN, M. AND SCHERTHAN, H. 2009. The role of meiotic cohesin REC8 in chromosome segregation in γ irradiation-induced endopolyploid tumour cells. *Experimental Cell Research*, **315**, 2593-2603.

FATEMI, M., PAO, M.M. JEONG, S., GAL-YAM, E.N., EGGER, G., WEISENBERGER, D.J. AND JONES, P.A. 2005. Footprinting of mammalian promoters: use of a CpG DNA methyltransferase revealing nucleosome positions at a single molecule level. *Nucleic Acids Research*, **33**, e176.

FEICHTINGER, J., ALDEAILEJ, I., ANDERSON, R., ALMUTAIRI, M., ALMATRAFI, A., ALSIWIEHRI, N., GRIFFITHS, K., STUART, N., WAKEMAN, J., LARCOMBE, L. AND MCFARLANE, R. 2012a. Meta-analysis of clinical data using human meiotic genes identifies a novel cohort of highly restricted cancer-specific marker genes. *Oncotarget*, **3**, 843-853.

FEICHTINGER, J., MCFARLANE, R.J. AND LARCOMBE, L.D. 2012b. CancerMA: a web-based tool for automatic meta-analysis of public cancer microarray data. *Database* doi: 10.1093/database/bas055.

FEICHTINGER, J., MCFARLANE, R.J. AND LARCOMBE, L.D. 2012. CancerMA, (online). http://www.cancerma.org.uk Accessed January 2013.

FIJAK, M. AND MEINHARDT, A. 2006. The testis in immune privilege. *Immunological Reviews*, **213**, 66-81.

FISZER, D. AND KURPISZ, M. 1998. Major histocompatibility complex expression on human, male germ cells: a review. *American Journal of reproductive Immunology*, **40**, 172-176.

FODERO-TAVOLETTI, M.T., HARDY, M.P., CORNELL, B., KATSIS, F., SADEK, C.M., MITCHELL, C.A., KEMP, B.E. AND TIGANIS, T. 2005. Protein tyrosine phosphatase hPTPN20a is targeted to sites of actin polymerization. *The Biochemical Journal*, **389**, 343-354.

FRATTA, E., CORAL, S., COVRE, A., PARISI, G., COLIZZI, F., DANIELLI, R., NICOLAY, H.J., SIGALOTTI, L. AND MAIO, M. 2011. The biology of cancer testis antigens: putative function, regulation and therapeutic potential. *Molecular Oncology*, **5**, 164-182.

FRENCH, C.A., MIYOSHI, I., KUBONISHI, I., GRIER, H.E., PEREZ-ATAYDE, A.R. AND FLETCHER, J.A. 2003. *BRD4-NUT* fusion oncogene: a novel mechanism in aggressive carcinoma. *Cancer Research*, **63**, 304-307.

FRENCH, C.A., RAMIREZ, C.L., KOLMAKOVA, J., HICKMAN, T.T., CAMERON, M.J., THYNE, M.E., KUTOK, J.L., TORETSKY, J.A., TADAVARTHY, A.K., KEES, U.R., FLETCHER, J.A. AND ASTER, J.C. 2008. BRD-NUT oncoproteins: a family of closely related nuclear proteins that block epithelial differentiation and maintain the growth of carcinoma cells. *Oncogene*, **27**, 2237-2242.

FUJISAKI, J., WU, J., CARLSON, A.L., SILBERSTEIN, L., PUTHETI, P., LAROCCA, R., GAO, W., SAITO, T.I., LO CELSO, C., TSUYUZAKI, H., SATO, T., CÔTÉ, D., SYKES, M., STROM, T.B., SCADDEN, D.T. AND LIN, C.P. 2011. *In vivo* imaging of Treg cells providing immune privilege to the haematopoietic stem-cell niche. *Nature*, **474**, 216-219.

FUKUDA, T., DANIEL, K., WOJTASZ, L., TOTH, A. AND HOOG, C. 2010. A novel mammalian HORMA domain-containing protein, HORMAD1, preferentially associates with unsynapsed meiotic chromosomes. *Experimental Cell Research*, **316**, 158-171.

FUNG, J.C., ROCKMILL, B., ODELL, M. AND ROEDER, G.S. 2004. Imposition of crossover interference through the nonrandom distribution of synapsis initiation complexes. *Cell*, **116**, 795-802.

GARDINER-GARDEN, M. AND FROMMER, M. 1987. CpG islands in vertebrate genomes. *Journal of Molecular Biology*, **196**, 261-282.

GAUSE, M., MISULOVIN, Z., BILYEU, A. AND DORSETT, D. 2010. Dosage-sensitive regulation of cohesin chromosome binding and dynamics by Nipped-B, Pds5, and Wapl. *Molecular and Cellular Biology*, **30**, 4940-4951.

GERLICH, D., KOCH, B., DUPEUX, F., PETERS, J.M. AND ELLENBERG, J. 2006. Live-cell imaging reveals a stable cohesin-chromatin interaction after but not before DNA replication. *Current Biology*, **16**, 1571-1578.

GERTON, J.L. AND HAWLEY, R.S. 2005. Homologous chromosome interactions in meiosis: diversity amidst conservation. *Nature Reviews. Genetics*, **6**, 477-487.

GHAFOURI-FARD, S. AND MODARRESSI, M.H. 2009. Cancer-testis antigens: Potential targets for cancer immunotherapy. *Archives of Iranian Medicine*, **12**, 395-404.

GHISELLI, G. AND IOZZO, R.V. 2000. Overexpression of bamacan/SMC3 causes transformation. *The Journal of Biological Chemistry*, **275**, 20235-20238.

GIBSON, G. 2003. Microarray analysis: genome-scale hypothesis scanning. *PLoS Biology*, **1**, 28-29.

GIMENÉZ-ABIÁN, J.F., DÍAZ-MARTÍNEZ, L.A., BEAUCHENE, N.A., HSU, W.S., TSAI, H.J. AND CLARKE, D.J. 2010. Determinants of Rad21 localization at the centrosome in human cells. *Cell Cycle*, **9**, 1759-1763.

GREGAN, J., POLAKOVA, S., ZHANG, L., TOLIC-NORRELYKKE, I.M. AND CIMINI, D. 2011. Merotelic kinetochore attachment: causes and effects. *TRENDS in Cell Biology*, **21**, 374-381.

GRUBER, S., ARUMUGAM, P., KATOU, Y., KUGLITSCH, D., HELMHART, W., SHIRAHIGE, K. AND NASMYTH, K. 2006. Evidence that loading of cohesin onto chromosomes involves opening of its SMC hinge. *Cell*, **127**, 523-537.

GRUBER, S., HAERING, C.H. AND NASMYTH, K. 2003. Chromosomal cohesin forms a ring. *Cell*, **112**, 765-777.

GUACCI, V., KOSHLAND, D. AND STRUNNIKOV, A. 1997. A direct link between sister chromatid cohesion and chromosome condensation revealed through the analysis of MCD1 in *S. cerevisiae*. *Cell*, **91**, 47-57.

GUILLOU, E., IBARRA, A., COULON, V., CASADO-VELA, J., RICO, D., CASAL, I., SCHWOB, E., LOSADA, A. AND MÉNDEZ, J. 2010. Cohesin organizes chromatin loops at DNA replication factories. *Genes and Development*, **24**, 2812-2822.

GUTIÉRREZ-CABALLERO, C., HERRÁN, Y., SÁNCHEZ-MARTÍN, M., SUJA, J.A., BARBERO, J.L., LLANO, E. AND PENDÁS, A.M. 2011. Identification and molecular characterization of the mammalian α-kleisin RAD21L. *Cell Cycle*, **10**, 1477-1487.

HAACK, H., JOHNSON, L.A., FRY, C.J., CROSBY, K., POLAKIEWICZ, R.D., STELOW, E.B., HONG, S.M., SCHWARTZ, B.E., CAMERON, M.J., RUBIN, M.A., CHANG, M.C., ASTER, J.C. AND FRENCH, C.A. 2009. Diagnosis of NUT midline carcinoma using a NUT-specific monoclonal antibody. *The American Journal of Surgical Pathology*, **33**, 984-991.

HAERING, C.H., FARCAS, A.M., ARUMUGAM, P., METSON, J. AND NASMYTH, K. 2008. The cohesin ring concatenates sister DNA molecules. *Nature*, **454**, 297-301.

HAMER, G., GELL, K., KOUZNETSOVA, A., NOVAK, I., BENAVENTE, R. AND HOOK, C. 2006. Characterization of a novel meiosis-specific protein within the central element of the synaptonemal complex. *Journal of Cell Science*, **119**, 4025-4032.

HAMER, G., WANG, H., BOLCUN-FILAS, E., COOKE, H.J., BENAVENTE, R. AND HOOG, C. 2008. Progression of meiotic recombination requires structural maturation of the central element of the synaptonemal complex. *Journal of Cell Science*, **121**, 2445-2451.

HAN, F., WANG, Z., WU, F., LIU, Z., HUANG, B. AND WANG, D. 2010. Characterization, phylogeny, alternative splicing and expression of Sox30 gene. *BMC Molecular Biology*, **11**, 98-108.

HANAHAN, D. AND WEINBERG, R.A. 2011. Hallmarks of cancer: the next generation. *Cell*, **144**, 646-674.

HANDEL, M.A. 2004. The XY body: a specialized meiotic chromatin domain. *Experimental Cell Research*, **296**, 57-63.

HANDEL, M.A. AND SCHIMENTI, J.C. 2010. Genetics of mammalian meiosis: regulation, dynamics and impact on fertility. *Nature Reviews Genetics*, **11**, 124-136.

HARIGAYA, Y., TANAKA, H., YAMANAKA, S., TANAKA, K., WATANABE, Y., TSUTSUMI, C., CHIKASHIGE, Y., HIRAOKA, Y., YAMASHITA, A. AND YAMAMOTO, M. 2006. Selective elimination of messenger RNA prevents an incidence of untimely meiosis. *Nature*, **442**, 45-50.

HARTSUIKER, E., MIZUNO, K., MOLNAR, M., KOHLI, J., OHTA, K., CARR, A.M. 2009. Ctp1CtIP and Rad32Mre11 nuclease activity are required for Rec12Spo11 removal, but Rec12Spo11 removal is dispensable for other MRN-dependent meiotic functions. *Molecular and Cellular Biology*, **29**, 1671-1681.

HASSLER, M.R. AND EGGER, G. 2012. Epigenomics of cancer – emerging new concepts. *Biochimie*, **94**, 2219-2230.

HASSOLD, T. AND HUNT, P. 2001. To err (meiotically) is human: the genesis of human aneuploidy. *Nature Reviews. Genetic*, **2**, 280-291.

HASSOLD, T., HALL, H. AND HUNT, P. 2007. The origin of human aneuploidy: where we have been, where we are going. *Human Molecular Genetics*, **16**, R203-R208.

HAUF, S., ROITINGER, E., KOCH, B., DITTRICH, C.M., MECHTLER, K. AND PETERS, J.M. 2005. Dissociation of cohesin from chromosome arms and loss of arm cohesion during early mitosis depends on phosphorylation of SA2. *PLoS Biology*, **3**, e69.

HAUF, S. AND WATANABE, Y. 2004. Kinetochore orientation in mitosis and meiosis. *Cell*, **119**, 317-327.

HAWKINS, J., DAVIS, L. AND BODÉN, M. 2007. Predicting nuclear localization. *Journal of Proteome Research*, **6**, 1402-1409.

HAYASHI, M., MLYNARCZYK-EVANS, S. AND VILLENEUVE, A.M. 2010. The synaptonemal complex shapes the crossover landscape through cooperative assembly, crossover promotion and crossover inhibition during *Caenorhabditis elegans* meiosis. *Genetics*, **186**, 45-58.

HEANEY, J.D., ANDERSON, E.L., MICHELSON, M.V., ZECHEL, J.L., CONRAD, P.A., PAGE, D.C. AND NADEAU, J.H. 2012. Germ cell pluripotency, premature differentiation and susceptibility to testicular teratomas in mice. *Development*, **139**, 1577-1586.

HENDERSON, K.A. AND KEENEY, S. 2005. Synaptonemal complex formation: where does it start? *Bioessays*, **27**, 995-998.

HILLERS, K.J. 2004. Crossover interference. *Current Biology*, **14**, R1036-R1037.

HIROSE, Y., SUZUKI, R., OHBA, T., HINOHARA, Y., MATSUHARA, H., YOSHIDA, M., ITABASHI, Y., MURAKAMI, H. AND YAMAMOTO, A. 2011. Chiasmata promote monopolar attachment of sister chromatids and their co-segregation toward the proper pole during meiosis I. *PLoS Genetics*, **7**, e1001329.

HOFMANN, O., CABALLERO, O.L., STEVENSON, B.J., CHEN, Y.T., COHEN, T., CHUA, R., MAHER, C.A., PANJI, S., SCHAEFER, U., KRUGER, A., LEHVASLAIHO, M., CARNINCI, P., HAYASHIZAKI, Y., JONGENEEL, C.V., SIMPSON, A.J., OLD, L.J. AND HIDE, W. 2008. Genome-wide analysis of cencer/testis gene expression. *PNAS*, **105**, 20422-20427.

HOLT, J.E. AND JONES, K.T. 2009. Control of homologous chromosome division in the mammalian oocyte. *Molecular Human Reproduction*, **15**, 139-147.

HOOD, K.L., TOBIN, J.F. AND YOON, C. 2002. Identification and characterization of two novel low-molecular-weight dual specificity phosphatases. *Biochemical and Biophysical Research Communications*, **298**, 545-551.

HORSFIELD, J.A., ANAGNOSTOU, S.H., HU, J.K., CHO, K.H., GEISLER, R., LIESCHKE, G., CROSIER, K.E. AND CROSIER, P.S. 2007. Cohesin-dependent regulation of *Runx* genes. *Development*, **134**, 2639-2649.

HORSFIELD, J.A., PRINT, C.G. AND MONNICH, M. 2012. Diverse developmental disorders from the One Ring: distinct molecular pathways underlie the cohesinopathies. *Frontiers in Genetics*, **3**, 171.

HOSOYA, N., OKAJIMA, M., KINOMURA, A., FUJII, Y., HIYAMA, T., SUN, J., TASHIRO, S. AND MIYAGAWA, K. 2012. Synaptonemal complex protein SYCP3 impairs mitotic recombination by interfering with BRCA2. *EMBO Reports*, **13**, 44-51.

HU, B., ITOH, T., MISHRA, A., KATOH, Y., CHAN, K.L., UPCHER, W., GODLEE, C., ROIG, M.B., SHIRAHIGE, K. AND NASMYTH, K. 2011. ATP hydrolysis is required for relocating cohesin from sites occupied by its Scc2/4 loading complex. *Current Biology*, **21**, 12-24.

HUANG, X., HATCHER, R., YORK, J.P. AND ZHANG, P. 2005. Securin and separase phosphorylation act redundantly to maintain sister chromatid cohesion in mammalian cells. *Molecular Biology of the Cell*, **16**, 4725-4732.

HUNG, M.C. AND LINK, W. 2011. Protein localization in disease and therapy. *Journal of Cell Science*, **124**, 3381-3392.

HUNT, P.A. AND HASSOLD, T.J. 2002. Sex matters in meiosis. *Science*, **296**, 2181-2183.

HYPPA, R.W. AND SMITH, G.R. 2010. Crossover invariance determined by partner choice for meiotic DNA break repair. *Cell*, **142**, 243-255.

ILLINGWORTH, R.S. AND BIRD, A.P. 2009. CpG islands – 'a rough guide'. *FEBS Letters*, **583**, 1713-1720.

INAGAKI, A., SCHOENMAKERS, S. AND BAARENDS, W.M. 2010. DNA double strand break repair, chromosome synapsis and transcriptional silencing in meiosis. *Epigenetics*, **5**, 255-266.

IOANNONI, R., BEAUDOIN, J., LOPEZ-MAURY, L., CODLIN, S., BAHLER, J. AND LABBE, S. 2012. Cuf2 is a novel meiosis-specific regulatory factor of meiosis maturation. *PLoS One*, **7**, e36338.

IRIZARRY, R.A., LADD-ACOSTA, C., WEN, B., WU, Z., MONTANO, C., ONYANGO, P., CUI, H., GABO, K., RONGIONE, M., WEBSTER, M., JI, H., POTASH, J., SABUNCIYAN, S. AND FEINBERG, A.P. 2009. Genome-wide methylation analysis of human colon cancer reveals similar hypo- and hypermethylation at conserved tissue-specific CpG island shores. *Nature Genetics*, **41**, 178-186.

ISHIGURO, K., KIM, J., FUJIYAMA-NAKAMURA, S., KATO, S. AND WATANABE, Y. 2011. A new meiosis-specific cohesin complex implicated in the cohesin code for homologous pairing. *The European Molecular Biology Organization Reports*, **12**, 267-275.

JEMAL, A., BRAY, F., CENTER, M.M., FERLAY, J., WARD, E. AND FORMAN, D. 2011. Global cancer statistics. *CA: A Cancer Journal for Clinicians*, **61**, 69-90.

JONES, G.H. AND FRANKLIN, F.C.H. 2006. Meiotic crossing-over: obligation and interference. *Cell*, **126**, 246-248.

JUDIS, L., CHAN, E.R., SCHWARTZ, S., SEFTEL, A. AND HASSOLD, T. 2004. Meiosis I arrest and azoospermia in an infertile male explained by failure of formation of a component of the synaptonemal complex. *Fertility and Sterility*, **81**, 205-209.

KAGEY, M.H., NEWMAN, J.J., BILODEAU, S., ZHAN, Y., ORLANDO, D.A., VAN BERKUM, N.L., EBMEIER, C.C., GOOSSENS, J., RAHL, P.B., LEVINE, S.S., TAATJES, D.J., DEKKER, J. AND YOUNG, R.A. 2010. Mediator and cohesin connect gene expression and chromatin architecture. *Nature*, **467**, 430-435.

KALEJS, M. AND ERENPREISA, J. 2005. Cancer/testis antigens and gametogenesis: a review and "brain-storming" session. *Cancer Cell International*, **5**, 4-14.

KALEJS, M., IVANOV, A., PLAKHINS, G., CRAGG, M.S., EMZINSH, D., ILLIDGE, T.M. AND ERENPREISA, J. 2006. Upregulation of meiosis-specific genes in lymphoma cell lines following genotoxic insult and induction of mitotic catastrophe. *BMC Cancer*, **6**, 6-15.

KAN, C.W., HAHN, M.A., GARD, G.B., MAIDENS, J., HUH, J.Y., MARSH, D.J. AND HOWELL, V.M. 2012. Elevated levels of circulating microRNA-200 family members correlate with serous epithelial ovarian cancer. *BMC Cancer*, **12**, 627-635.

KAN, F., DAVIDSON, M.K. AND WAHLS, W.P. 2011. Meiotic recombination protein Rec12: functional conservation, crossover homeostasis and early crossover/non-crossover decision. *Nucleic Acids Research*, **39**, 1460-1472.

KAO, J., SALARI, K., BOCANEGRA, M., CHOI, Y.L., GIRARD, L., GANDHI, J., KWEI, K.A., HERNANDEZ-BOUSSARD, T., WANG, P., GAZDAR, A.F., MINNA, J.D. AND POLLACK, J.R. 2009. Molecular profiling of breast cancer cell lines defines relevant tumour models and provides a resource for cancer gene discovery. *PLoS ONE*, **4**, e6146.

KATIS, V.L., GALOVA, M., RABITSCH, K.P., GREGAN, J. AND NASMYTH, K. 2004. Maintenance of cohesin at centromeres after meiosis I in budding yeast requires a kinetochore-associated protein related to MEI-S332. *Current Biology*, **14**, 560-572.

KATIS, V.L., LIPP, J.J., IMRE, R., BOGDANOVA, A., OKAZ, E., HABERMANN, B., MECHTLER, K., NASMYTH, K. AND ZACHARIAE, W. 2010. Rec8 phosphorylation by casein kinase 1 and Cdc7-Dbf4 Kinase regulates cohesin cleavage by separase during meiosis. *Developmental Cell*, **18**, 397-409.

KAU, T.R., WAY, J.C. AND SILVER, P.A. 2004. Nuclear transport and cancer: from mechanism to intervention. *Nature Reviews. Cancer*, **4**, 106-117.

KAWASHIMA, S.A., TSUKAHARA, T., LANGEGGER, M., HAUF, S., KITAJIMA, T.S. AND WATANABE, Y. 2007. Shugoshin enables tension-generating attachment of kinetochores by loading Aurora to centromeres. *Genes and Development*, **21**, 420-435.

KEENEY, S. GIROUX, C.N. AND KLECKNER, N. 1997. Meiosis-specific DNA double-strand breaks are catalyzed by Spo11, a member of a widely conserved protein family. *Cell*, **88**, 375-384.

KERKEL, K., SCHUPF, N., HATTA, K., PANG, D., SALAS, M., KRATZ, A., MINDEN, M., MURTY, V., ZIGMAN, W.B., MAYEUX, R.P., JENKINS, E.C., TORKAMANI, A., SCHORK, N.J., SILVERMAN, W., CROY, B.A. AND TYCKO, B. 2010. Altered DNA methylation in leukocytes with trisomy 21. *PLoS Genetics*, **6**, e1001212.

KIBURZ, B.M., AMON, A. AND MARSTON, A.L. 2008. Shugoshin promotes sister kinetochore biorientation in *Saccharomyces cerevisiae*. *Molecular Biology of the Cell*, **19**, 1199-1209.

KIM, K.P., WEINER, B.M., ZHANG, L., JORDAN, A., DEKKER, J. AND KLECKNER, N. 2010. Sister cohesion and structural axis components mediate homolog bias of meiotic recombination. *Cell*, **143**, 924-937.

KIRONMAI, K.M., MUNIYAPPA, K., FRIEDMAN, D.B., HOLLINGSWORTH, N.M. AND BYERS, B. 1998. DNA-binding activities of Hop1 protein, a synaptonemal complex component from *Saccharomyces cerevisiae*. *Molecular and Cellular Biology*, **18**, 1424-1435.

KITAJIMA, T.S., KAWASHIMA, S.A. AND WATANABE, Y. 2004. The conserved kinetochore protein shugoshin protects centromeric cohesion during meiosis. *Nature*, **427**, 510-517.

KITAJIMA, T.S., SAKUNO, T., ISHIGURO, K., IEMURA, S., NATSUME, T., KAWASHIMA, S.A. AND WATANABE, Y. 2006. Shugoshin collaborates with protein phosphatase 2A to protect cohesin. *Nature*, **441**, 46-52.

KLECKNER, N. 1996. Meiosis: how could it work? *PNAS USA*, **93**, 8167-8174.

KLECKNER, N. 2006. Chiasma formation: chromatin/axis interplay and the role(s) of the synaptonemal complex. *Chromosoma*, **115**, 175-194.

KLECKNER, N., STORLAZZI, A. AND ZICKLER, D. 2003. Coordinate variation in meiotic pachytene SC length and total crossover/chiasma frequency under conditions of constant DNA length. *TRENDS in Genetics*, **19**, 623-628.

KLECKNER, N., ZICKLER, D., JONES, G.H., DEKKER, J., PADMORE, R., HENLE, J. AND HUTCHINSON, J. 2004. A mechanical basis for chromosome function. *PNAS USA*, **101**, 12592-12597.

KLEIN, F., MAHR, P., GALOVA, M., BUONOMO, S.B., MICHAELIS, C., NAIRZ, K. AND NASMYTH, K. 1999. A central role for cohesins in sister chromatid cohesion, formation of axial elements, and recombination during yeast meiosis. *Cell*, **98**, 91-103.

KNOWLTON, A.L., LAN, W. AND STUKENBERG, P.T. 2006. Aurora B is enriched at merotelic attachment sites, where it regulates MCAK. *Current Biology*, **16**, 1705-1710.

KOSTENIS, E., MILLIGAN, G., CHRISTOPOULOS, A., SANCHEZ-FERRER, C.F., HERINGER-WALTHER, S., SAXTON, P.M., GEMBARDT, F., KELLETT, E., MARTINI, L., VANDERHEYDEN, P., SCHULTHEISS, H.P. AND WALTHER, T. 2005. G-protein-coupled receptor Mas is a physiologicalantagonist of the angiotensin II type 1 receptor. *Circulation*, **111**, 1806-1813.

KOSZUL, R. AND KLECKNER, N. 2009. Dynamic chromosome movements during meiosis: a way to eliminate unwanted connections? *TRENDS in Cell Biology*, **19**, 716-724.

KOUZNETSOVA, A., NOVAK, I., JESSBERGER, R. AND HOOG, C. 2005. SYCP2 and SYCP3 are required for cohesin core integrity at diplotene but not for centromere cohesion at the first meiotic division. *Journal of Cell Science*, **118**, 2271-2278.

KRONJA, I. AND ORR-WEAVER, T.L. 2011. Translational regulation of the cell cycle: when, where, how and why? *Philosophical Transactions of the Royal Society B: Biological Sciences*, **366**, 3638-3652.

KUDO, N.R., WASSMANN, K., ANGER, M., SCHUH, M., WIRTH, K.G., XU, H., HELMHART, W., KUDO, H., MCKAY, M., MARO, B., ELLENBERG, J., DE BOER, P. AND NASMYTH, K. 2006. Resolution of chiasmata in oocytes requires separase-mediated proteolysis. *Cell*, **126**, 135-146.

KUNDA, P. AND BAUM, B. 2009. The actin cytoskeleton in spindle assembly and positioning. *TRENDS in Cell Biology*, **19**, 174-179.

KWON, M., GODINHO, S.A., CHANDHOK, N.S., GANEM, N.J., AZIOUNE, A., THERY, M. AND PELLMAN, D. 2008. Mechanisms to suppress multipolar divisions in cancer cells with extra centrosomes. *Genes and Development*, **22**, 2189-2203.

LA COUR, T., KIEMER, L., MØLGAARD, A., GUPTA, R., SKRIVER, K. AND BRUNAK, S. 2004. Analysis and prediction of leucine-rich nuclear export signals. *Protein Engineering, Design and Selection*, **17**, 527-536.

LANDEIRA, D., BART, J.M., VAN TYNE, D. AND NAVARRO, M. 2009. Cohesin regulates VSG monoallelic expression in trypanosomes. *Journal of Cell Biology*, **186**, 243-254.

LANGDON, S.P., LAWRIE, S.S., HAY, F.G., HAWKES, M.M., MCDONALD, A., HAYWARD, I.P., SCHOL, D.J., HILGERS, J., LEONARD, R.C. AND SMYTH, J.F. 1988. Characterization and properties of nine human ovarian adenocarcinoma cell lines. *Cancer Research*, **48**, 6166-6172.

LATYPOV, V., ROTHENBERG, M., LORENZ, A., OCTOBRE, G., CSUTAK, O., LEHMANN, E., LOIDL, J. AND KOHLI, J. 2010. Roles of Hop1 and Mek1 in meiotic chromosome pairing and recombination partner choice in *Schizosaccharomyces pombe*. *Molecular and Cellular Biology*, **30**, 1570-1581.

LEE, B. AND AMON, A. 2001. Meiosis: how to create a specialized cell cycle. *Current Opinion in Cell Biology*, **13**, 770-777.

LEE, J. AND HIRANO, T. 2011. RAD21L, a novel cohesin subunit implicated in linking homologous chromosomes in mammalian meiosis. *The Journal of Cell Biology*, **192**, 263-276.

LEE, J.Y. AND ORR-WEAVER, T.L. 2001. The molecular basis of sister-chromatid cohesion. *Annual Review of Cell and Developmental Biology*, **17**, 753-777.

LEE, J., KITAJIMA, T., TANNO, Y., YOSHIDA, K., MORITA, T., MIYANO, T., MIYAKE, M. AND WATANABE, Y. 2008. Unified mode of centromeric protection by shugoshin in mammalian oocytes and somatic cells. *Nature Cell Biology*, **10**, 42-52.

LEMAIRE-ADKINS, R., RADKE, K. AND HUNT, P.A. 1997. Lack of checkpoint control at the metaphase/anaphase transition: a mechanism of meiotic nondisjunction in mammalian females. *The Journal of Cell Biology*, **139**, 1611-1619.

LENGRONNE, A., MCINTYRE, J., KATOU, Y., KANOH, Y., HOPFNER, K.P., SHIRAHIGE, K. AND UHLMANN, F. 2006. Establishment of sister chromatid cohesion at the *S. cerevisiae* replication fork. *Molecular Cell*, **23**, 787-799.

LI, X.C., BOLCUN-FILAS, E. AND SCHIMENTI, J.C. 2011. Genetic evidence that synaptonemal complex axial elements govern recombination pathway choice in mice. *Genetics*, **189**, 71-82.

LI, H.G., LIAO, A.H., DING, X.F., ZHOU, H. AND XIONG, C.L. 2006. The expression and significance of CATSPER1 in human testis and ejaculated spermatozoa. *Asian Journal of Andrology*, **8**, 301-306.

LIEBE, B., ALSHEIMER, M., HOOG, C., BENAVENTE, R. AND SCHERTHAN, H. 2004. Telomere attachment, meiotic chromosome condensation, pairing, and bouquet stage duration are modified in spermatocytes lacking axial elements. *Molecular Biology of the Cell*, **15**, 827-837.

LIM, S.H., ZHANG, Y. AND ZHANG, J. 2012. Cancer-testis antigens: the current status on antigen regulation and potential clinical use. *American Journal of Blood Research*, **2**, 29-35.

LIMBO, O., CHAHWAN, C., YAMADA, Y., DE BRUIN, R.A. WITTENBERG, C. AND RUSSELL, P. 2007. Ctp1 is a cell-cycle-regulated protein that functions with Mre11 complex to control double-strand break repair by homologous recombination. *Molecular Cell*, **28**, 134-146.

LIN, W., JIN, H., LIU, X., HAMPTON, K. AND YU, H.G. 2011a. Scc2 regulates gene expression by recruiting cohesin to the chromosome as a transcriptional activator during yeast meiosis. *Molecular Biology of the Cell*, **22**, 1985-1996.

LIN, W., WANG, M., JIN, H. AND YU, H.G. 2011b. Cohesin plays a dual role in gene regulation and sister-chromatid cohesion during meiosis in *Saccharomyces cerevisiae*. *Genetics*, **187**, 1041-1051.

LINK, P.A., GANGISETTY, O., JAMES, S.R., WOLOSZYNSKA-READ, A., TACHIBANA, M., SHINKAI, Y. AND KARPF, A.R. 2009. Distant roles for histone methyltransferases G9a and GLP in cancer germ-line antigen gene regulation in human cancer cells and murine embryonic stem cells. *Molecular Cancer Research*, **7**, 851-862.

LIPPINCOTT-SCHWARTZ, J. 2002. Ripping up the nuclear envelope. *Nature*, **416**, 31-32.

LISBY, M., BARLOW, J.H. BURGESS, R.C. AND ROTHSTEIN, R. 2004. Choreography of the DNA damage response: spatiotemporal relationships among checkpoints and repair proteins. *Cell*, **118**, 699-713.

LIU, B., NASH, J., RUNOWICZ, C., SWEDE, H., STEVENS, R. AND LI, Z. 2010. Ovarian cancer immunotherapy: opportunities, progresses and challenges. *Journal of Hematology and Oncology*, **3**, 7-17.

LIU, H., RANKIN, S. AND YU, H. 2013. Phosphorylation-enabled binding of SGO1-PP2A to cohesin protects sororin and centromeric cohesion during mitosis. *Nature Cell Biology*, **15**, 40-49.

LIU, J.G., YUAN, L., BRUNDELL, E., BJORKROTH, B., DANEHOLT, B. AND HOOG, C. 1996. Localization of the N-terminus of SCP1 to the central element of the synaptonemal complex and evidence for direct interactions between the N-termini of SCP1 molecules organized head-to-head. *Experimental Cell Research*, **226**, 11-19.

LLANO, E., GÓMEZ, R., GUTIÉRREZ-CABALLERO, C., HERRÁN, Y., SÁNCHEZ-MARTÍN, M., VÁZQUEZ-QUINONES, L., HERNÁNDEZ, T., DE ÁLAVA, E., CUADRADO, A., BARBERO, J.L., SUJA, J.A. AND PENDÁS, A.M. 2008. Shugoshin-2 is essential for the completion of meiosis but not for mitotic cell division in mice. *Genes and Development*, **22**, 2400-2413.

LONGHESE, M.P., BONETTI, D., GUERINI, I., MANFRINI, N. AND CLERICI, M. 2009. DNA double-strand breaks in meiosis: Checking their formation, processing and repair. *DNA Repair*, **8**, 1127-1138.

LONGHESE, M.P. BONETTI, D., MANFRINI, N. AND CLERICI, M. 2010. Mechanisms and regulation of DNA end resection. *EMBO Journal*, **29**, 2864-2874.

LONGHESE, M.P. GUERINI, I., BALDO. V. AND CLERICI. M. 2008. Surveillance mechanisms monitoring chromosome breaks during mitosis and meiosis. *DNA Repair*, **7**, 545-557.

LOSADA, A., YOKOCHI, T. AND HIRANO, T. 2005. Functional contribution of Pds5 to cohesin-mediated cohesion in human cells and *Xenopus* egg extracts. *Journal of Cell Science*, **118**, 2133-2141.

LYNN, A., SOUCEK, R. AND BORNER, G.V. 2007. ZMM proteins during meiosis: crossover artists at work. *Chromosome Research*, **15**, 591-605.

MACQUEEN, A.J., COLAIACOVO, M.P., MCDONALD, K., VILLENEUVE, A.M. 2002. Synapsis-dependent and -independent mechanisms stabilize homolg pairing during meiotic prophase in *C. elegans*. *Genes and Development*, **16**, 2428-2442.

MACQUEEN, A.J. AND ROEDER, G.S. 2009. Fpr3 and Zip3 ensure that initiation of meiotic recombination precedes chromosome synapsis in budding yeast. *Current Biology*, **19**, 1519-1526.

MALMANCHE, N., MAIA, A. AND SUNKEL, C.E. 2006. The spindle assembly checkpoint: preventing chromosome mis-segregation during mitosis and meiosis. *FEBS Letters*, **580**, 2888-2895.

MARSTON, A. AND AMON, A. 2004. Meiosis: cell-cycle controls shuffle and deal. *Nature Reviews. Molecular Cell Biology*, **5**, 983-997.

MARSTON, A., THAM, W.H., SHAH, H. AND AMON, A. 2004. A genome-wide screen identifies genes required for centromeric cohesion. *Science*, **303**, 1367-1370.

MARTINI, E., DIAZ, R.L., HUNTER, N. AND KEENEY, S. 2006. Crossover homeostatsis in yeast meiosis. *Cell*, **126**, 285-295.

MCKIM, K.S., JANG, J.K. AND MANHEIM, E.A. 2002. Meiotic recombination and chromosome segregation in *Drosophila* females. *Annual Review of Genetics*, **36**, 205-232.

MCNAIRN, A.J. AND GERTON, J.L. 2008. The chromosome glue gets a little stickier. *TRENDS in genetics*, **24**, 382-389.

MEI, J., HUANG, X. AND ZHANG, P. 2001. Securin is not required for cellular viability, but is required for normal growth of mouse embryonic fibroblasts. *Current Biology*, **11**, 1197-1201.

MERLO, L.M., PEPPER, J.W., REID, B.J. AND MALEY, C.C. 2006. Cancer as an evolutionary and ecological process. *Nature Reviews Cancer*, **6**, 924-935.

MICHAELIS, C., CIOSK, R. AND NASMYTH, K. 1997. Cohesins: chromosomal proteins that prevent premature separation of sister chromatids. *Cell*, **91**, 35-45.

MIHOLA, O., TRACHTULEC, Z., VLCEK, C., SCHIMENTI, J.C. AND FOREJT, J. 2009. A mouse speciation gene encodes a meiotic histone H3 methyltransferase. *Science*, **323**, 373-375.

MIKESKA, T., BOCK, C., DO, H. AND DOBROVIC, A. 2012. DNA methylation biomarkers in cancer: progress towards clinical implementation. *Expert Review of Molecular Diagnostics*, **12**, 473-487.

MIKLOS, G.L. AND MALESZKA, R. 2004. Microarray reality checks in the context of a complex disease. *Nature Biotechnology*, **22**, 615-621.

MitoCheck consortium. 2010. MitoCheck (online). http://www.mitocheck.org

MITRUS, I., BRYNDZA, E., SOCHANIK, A. AND SZALA, S. 2012. Evolving models of tumor origin and progression. *Tumor Biology*, **33**, 911-917.

MOBASHERI, M.B., JAHANZAD, I., MOHAGHEGHI, M.A., AARABI, M., FARZAN, S. AND MODARRESSI, M.H. 2007. Expression of two testis-specific genes, TSGA10 and SYCP3, in different cancers regarding to their pathological features. *Cancer Detection and Prevention*, **31**, 296-302.

MORRISON, C., VAGNARELLI, P., SONODA, E., TAKEDA, S. AND EARNSHAW, W.C. 2003. Sister chromatid cohesion and genome stability in vertebrate cells. *Biochemical Society Transactions*, **31**, 263-265.

MRUK, D.D. AND CHENG, C.Y. 2010. Tight junctions in the testis: new perspectives. *Philosophical transactions of the Royal Society of London. Series B, Biological Sciences*, **365**, 1621-1635.

MUNZ, P. 1994. An analysis of interference in fission yeast *Schizosaccharomyces pombe*. *Genetics*, **137**, 701-707.

MURAYAMA, Y. AND UHLMANN, F. 2013. Chromosome segregation: how to open cohesin without cutting the ring? *The EMBO Journal*, **32**, 614-616.

MURDOCH, B., OWEN, N., STEVENSE, M., SMITH, H., NAGAOKA, S., HASSOLD, T., MCKAY, M., XU, H., FU, J., REVENKOVA, E., JESSBERGER, R. AND HUNT, P. 2013. Altered cohesin gene dosage affects mammalian meiotic chromosome structure and behaviour. *PLoS Genetics*, **9**, e1003241.

MYERS, S., BOTTOLO, L., FREEMAN, C., MCVEAN, G. AND DONNELLY, P. 2005. A fine-scale map of recombination rates and hotspots across the human genome. *Science*, **310**, 321-324.

MYERS, S., BOWDEN, R., TUMIAN, A., BONTROP, R.E., FREEMAN, C., MACFIE, T.S., MCVEAN, G. AND DONNELLY, P. 2010. Drive against hotspot motifs in primates implicates the *PRDM9* gene in meiotic recombination. *Science*, **327**, 876-879.

NAGARAJ, S.H., GASSER, R.B. AND RANGANATHAN, S. 2006. A hitchhiker's guide to expressed sequence tag (EST) analysis. *Briefings in Bioinformatics*, **8**, 6-21.

NASMYTH, K. 2001. Disseminating the genome: joining, resolving, and separating sister chromatids during mitosis and meiosis. *Annual Review of Genetics*, **35**, 673-745.

NASMYTH, K. 2011. Cohesin: a catenase with separate entry and exit gates? *Nature Cell Biology*, **13**, 1170-1177.

NASMYTH, K. AND HAERING, C.H. 2005. The structure and function of SMC and kleisin complexes. *Annual Review of Biochemistry*, **74**, 595-648.

NAUMOV, G.N., FOLKMAN, J. AND STRAUME, O. 2009. Tumour dormancy due to failure of angiogenesis: role of the microenvironment. *Clinical and Experimental Metastasis*, **26**, 51-60.

NEALE, M.J. AND KEENEY, S. 2006. Clarifying the mechanics of DNA strand exchange in meiotic recombination. *Nature*, **442**, 153-158.

NEALE, M.J., PAN, J. AND KEENEY, S., 2005. Endonucleolytic processing of covalent protein-linked DNA double-strand breaks. *Nature*, **436**, 1053-1057.

NetNES 1.1 Server (online). http://www.cbs.dtu.dk/services/NetNES/ Accessed February 2013.

NEUMANN, B., WALTER, T., HÉRICHE, J.K., BULKESCHER, J., ERFLE, H., CONRAD, C., ROGERS, P., POSER, I., HELD, M., LIEBEL, U., CETIN, C., SIECKMANN, F., PAU, G., KABBE, R., WUNSCHE, A., SATAGOPAM, V., SCHMITZ, M.H., CHAPUIS, C., GERLICH, D.W., SCHNEIDER, R., EILS, R., HUBER, W., PETERS, J.M., HYMAN, A.A., DURBIN, R., PEPPERKOK, R. AND ELLENBERG, J. 2010. Phenotypic profiling of the human genome by time-lapse microscopy reveals cell division genes. *Nature*, **464**, 721-727.

NEZI, L. AND MUSACCHIO, A. 2009. Sister chromatid tension and the spindle assembly checkpoint. *Current Opinion in Cell Biology*, **21**, 785-795.

NICHOLSON, J.M. AND CIMINI, D. 2011. How mitotic errors contribute to karyotypic diversity in cancer. *Advances in Cancer Research*, **112**, 43-75.

NIEMEYER, P., TURECI, O., EBERLE, T., GRAF, N., PFREUNDSCHUH, M. AND SAHIN, U. 2003. Expression of serologically identified tumour antigens in acute leukemias. *Leukemia Research*, **27**, 655-660.

NISHIYAMA, T., LADURNER, R., SCHMITZ, J., KREIDL, E., SCHLEIFFER, A., BHASKARA, V., BANDO, M., SHIRAHIGE, K., HYMAN, A.A., MECHTLER, K. AND PETERS, J.M. 2010. Sororin mediates sister chromatid cohesion by antagonizing Wapl. *Cell*, **143**, 737-749.

NIU, H., LI, X., JOB, E., PARK, C., MOAZED, D., GYGI, S.P. AND HOLLINGSWORTH, N.M. 2007. Mek1 kinase is regulated to suppress double-strand break repair between sister chromatids during budding yeast meiosis. *Molecular and Cell Biology*, **27**, 5456-5467.

NIU, H., WAN, L., BAUMGARTNER, B., SCHAEFER, D., LOIDL, J. AND HOLLINGSWORTH, N.M. 2005. Partner choice during meiosis is regulated by Hop1-promoted dimerization of Mek1. *Molecular Biology of the Cell*, **16**, 5804-5818.

NUCLEO (online). http://www.pprowler.itee.uq.edu.au Accessed February 2013.

NWAJEI, F. AND KONOPLEVA, M. 2013. The bone marrow microenvironments as niche retreats for hematopoietic and leukemic stem cells. *Advances in Hematoology*, **2013**, 953982.

OBESO, D. AND DAWSON, D.S. 2010. Temporal characterization of homology-independent centromere coupling in meiotic prophase. *PLoS ONE*, **5**, e10336.

ODUNSI, K., QIAN, F., MATSUZAKI, J., MHAWECH-FAUCEGLIA, P., ANDREWS, C., HOFFMANN, E.W., PAN, L., RITTER, G., VILLELLA, J., THOMAS, B., RODABAUGH, K., LELE, S., SHRIKANT, P., OLD, L.J. AND GNJATIC, S. 2007. Vaccination with an NY-ESO-1 peptide of HLA class I/II specificities induces integrated humoral and T cell responses in ovarian cancer. *PNAS USA*, **104**, 12837-12842.

O'FARRELL, P.H. 2011. Quiescence: early evolutionary origins and universality do not imply uniformity. *Philosophical Transactions of the Royal Society of London. Series B, Biological Sciences*, **366**, 3498-3507.

OFFENBERG, H.H., SCHALK, J.A.C., MEUWISSEN, R.L.J., VAN AALDEREN, M., KESTER, H.A., DIETRICH, A.J.J. AND HEYTING, C. 1998. SCP2: a major protein component of the axial elements of synaptonemal complexes of the rat. *Nucleic Acids Research*, **26**, 2572–2579.

OISHI, Y., NAGASAKI, K., MIYATA, S., MATSUURA, M., NISHIMURA, S., AKIYAMA, F., IWAI, T. AND MIKI, Y. 2007. Functional pathway characterized by gene expression analysis of supraclavicular lymph node metastasis positive breast cancer. *Journal of Human Genetics*, **52**, 271-279.

OLD, L.J. 2001. Cancer/testis (CT) antigens – a new link between gametogenesis and cancer. *Cancer Immunity*, **1**, 1-7.

OLLINGER, R., ALSHEIMER, M. AND BENAVENTE, R. 2005. Mammalian protein SCP1 forms synaptonemal complex-like structures in the absence of meiotic chromosomes. *Molecular Biology of the Cell*, **16**, 212-217.

OSAKI, E., NISHINA, Y., INAZAWA, J., COPELAND, N.G., GILBERT, D.J., JENKINS, N.A., OHSUGI, M., TEZUKA, T., YOSHIDA, M. AND SEMBA, K. 1999. Identification of a novel Sry-related gene and its germ cell-specific expression. *Nucleic Acids Research*, **27**, 2503-2510.

PAGE, S.L. AND HAWLEY, R.S. 2004. The genetics and molecular biology of the synaptonemal complex. *Annual Review of Cell and Developmental Biology*, **20**, 525-558.

PARELHO, V., HADJUR, S., SPIVAKOV, M., LELEU, M., SAUER, S., GREGSON, H.C., JARMUZ, A., CANZONETTA, C., WEBSTER, Z., NESTEROVA, T., COBB, B.S., YOKOMORI, K., DILLON, N., ARAGON, L., FISHER, A.G. AND MERKENSCHLAGER, M. 2008. Cohesins functionally associate with CTCF on mammalian chromosome arms. *Cell*, **132**, 422-433.

PARISI, S., MCKAY, M.J., MOLNAR, M., THOMPSON, M.A., VAN DER SPEK, P.J., VAN DRUNEN-SCHOENMAKER, E., KANAAR, R., LEHMANN, E., HOEIJMAKERS, J.H. AND KOHLU, J. 1999. Rec8p, a meiotic recombination and sister chromatid chesion phosphoprotein of the Rad21p family conserved from fission yeast to humans. *Molecular and Cellular Biology*, **19**, 3515-3528.

PARMIGIANI, R.B., BETTONI, F., VIBRANOVSKI, M.D., LOPES, M.H., MARTINS, W.K., CUNHA, I.W., SOARES, F.A., SIMPSON, A.J.G., DE SOUZA, S.J. AND CAMARGO, A.A. 2006. Characterization of cancer/testis (CT) antigen gene family capable of eliciting humoral response in cancer patients. *PNAS*, **103**, 18066-18071.

PATI, D., ZHANG, N. AND PLON, S.E. 2002. Linking sister chromatid cohesion and apoptosis: role of Rad21. *Molecular and Cell Biology*, **22**, 8267-8277.

PAULI, A., ALTHOFF, F., OLIVEIRA, R.A., HEIDMANN, S., SCHULDINER, O., LEHNER, C.F., DICKSON, B.J. AND NASMYTH, K. 2008. Cell-type-specific TEV protease cleavage reveals cohesion functions in *Drosophila* neurons. *Developing Cell*, **14**, 239-251.

PAULI, A., VAN BEMMEL, J.G., OLIVEIRA, R.A., ITOH, T., SHIRAHIGE, K., VAN STEENSEL, B. AND NASMYTH, K. 2010. A direct role for cohesin in gene regulation and ecdysone response in *Drosophila* salivary glands. *Current Biology*, **20**, 1787-1798.

PELTTARI, J., HOJA, M.R., YUAN, L., LIU, J.G., BRUNDELL, E., MOENS, P., SANTUCCI-DARMANIN, S., JESSBERGER, R., BARBERO, J.L., HEYTING, C. AND HOOG, C. 2001. A meiotic chromosomal core consisting of cohesin complex proteins recruits DNA recombination proteins and promotes synapsis in the absence of an axial element in mammalian meiotic cells. *Molecular and Cellular Biology*, **21**, 5667-5677.

PETERS. J.M., TEDESCHI, A. AND SCHMITZ, J. 2008. The cohesin complex and its roles in chromosome biology. *Genes and Development*, **22**, 3089-3114.

PETRONCZKI, M., SIOMOS, M.F. AND NASMYTH, K. 2003. Un ménage à quatre: the molecular biology of chromosome segregation in meiosis. *Cell*, **112**, 423-440.

PFLEGHAAR, K., HEUBES, S., COX, J., STEMMANN, O. AND SPEICHER, M.R. 2005. Securin is not required for chromosomal stability in human cells. *PLoS Biology*, **3**, e416.

PIEK, J.M., VAN DIEST, P.J. AND VERHEIJEN, R.H. 2008. Ovarian carcinogenesis: an alternative hypothesis. *Advances in Experimental Medicine and Biology*, **622**, 79-87.

PILUSO, G., MIRABELLA, M., RICCI, E., BELSITO, A., ABBONDANZA, C., SERVIDEI, S., PUCA, A.A., TONALI, P., PUCA, G.A. AND NIGRO, V. 2000. γ1- and γ2-syntrophins, two novel dystrophin-binding proteins localized in neuronal cells. *The Journal of Biological Chemistry*, **276**, 15851-15860.

PINSKY, B.A. AND BIGGINS, S. 2005. The spindle checkpoint: tension versus attachment. *TRENDS in Cell Biology*, **15**, 486-493.

PredictProtein server (online). http://www.predictprotein.org/ Accessed February 2013

PRIETO, I., SUJA, J.A., PEZZI, N., KREMER, L., MARTINEZ, A.C., RUFAS, J.S. AND BARBERO, J.L. 2001. Mammalian STAG3 is a cohesin specific to sister chromatid arms in meiosis I. *Nature Cell Biology*, **3**, 761-766.

QIAO, H., CHEN, J. K., REYNOLDS, A., HOOG, C., PADDY, M. AND HUNTER, N. 2012. Interplay between synaptonemal complex, homologous recombination, and centromeres during mammalian meiosis. *PLoS Genetics*, **8**, e1002790.

RABITSCH, K.P., GREGAN, J., SCHLEIFFER, A., JAVERZAT, J.P., EISENHABER, F. AND NASMYTH, K. 2004. Two fission yeast homologs of *Drosophila* Mei-S332 are required for chromosome segregation during meiosis I and II. *Current Biology*, **14**, 287-301.

RADERSCHALL, E., STOUT, K., FREIER, S., SUCKOW, V., SCHWEIGER, S. AND HAFF, T. 2002. Elevated levels of Rad51 recombination protein in tumor cells. *Cancer Research*, **62**, 219-225.

RANKIN, S., AYAD, N.G. AND KIRSCHNER, M.W. 2005. Sororin, a substrate of the anaphase-promoting complex, is required for sister chromatid cohesion in vertebrates. *Molecular Cell*, **18**, 185-200.

REVENKOVA, E., EIJPE, M., HEYTING, C., GROSS, B. AND JESSBERGER, R. 2001. Novel meiosis-specific isoform of mammalian SMC1. *Molecular and Celular Biology*, **21**, 6984-6998.

REYNOIRD, N., SCHWARTZ, B.E., DELVECCHIO, M., SADOUL, K., MEYERS, D., MUKHERIEE, C., CARON, C., KIMURA, H., ROUSSEAUX, S., COLE, P.A., PANNE, D., FRENCH, C.A. AND KHOCHBIN, S. 2010. Oncogenesis by sequestration of CBP/p300 in transcriptionally inactive hyperacetylated chromatin domains. *EMBO Journal*, **29**, 2943-2952.

RHODES, D.R., YU, J., SHANKER, K., DESHPANDE, N., VARAMBALLY, R., GHOSH, D., BARRETTE, T., PANDEY, A. AND CHINNAIYAN, A.M. 2004. Large-scale meta-analysis of cancer microarray data identifies common transcriptional profiles of meoplastic transformation and progression. *PNAS USA*, **101**, 9309-9314.

RHODES, J.M., MCEWAN, M. AND HORSFIELD, J.A. 2011. Gene regulation by cohesin in cancer: is the ring an unexpected party to proliferation? *Molecular Cancer Research*, **9**, 1587-1607.

RICHARDSON, C., HORIKOSHI, N. AND PANDITA, T.K. 2004. The role of the DNA double-strand break response network in meiosis. *DNA Repair*, **3**, 1149-1164.

RIEDEL, C.G., KATIS, V.L., KATOU, Y., MORI, S., ITOH, T., HELMHART, W., GÁLOVÁ, M., PETRONCZKI, M., GREGAN, J., CETIN, B., MUDRAK, I., OGRIS, E., MECHTLER, K., PELLETIER, L., BUCHHOLZ, F., SHIRAHIGE, K. AND NASMYTH, K. 2006. Protein phosphatase 2A protects centromeric sister chromatid cohesion during meiosis I. *Nature*, **441**, 53-61.

ROCQUAIN, J., GELSI-BOYER, V., ADÉLAIDE, J., MURATI, A., CARBUCCIA, N., VEY, N., BIRNBAUM, D., MOZZICONACCI, M.J., CHAFFANET, M. 2010. Alteration of cohesin genes in myeloid disease. *American Journal of Hematology*, **85**, 717-719.

ROST, B., YACHDAV, G. AND LIU, J. 2004. The PredictProtein server. *Nucleic Acids Research*, **32** (Web Server issue), W321-326.

RUDRA, S. AND SKIBBENS, R.V. 2013. Cohesin codes – interpreting chromatin architecture and the many facets of cohesin function. *Journal of Cell Science*, **26**, 31-41.

RUMPF, C., CIPAK, L., DUDAS, A., BENKO, Z., POZGAJOVA, M., RIEDEL, C.G., AMMERER, G., MECHTLER, K. AND GREGAN, J. 2010. Casein kinase 1 is required for efficient removal of Rec8 during meiosis I. *Cell Cycle*, **9**, 2657-2662.

RUSSO, G., ZEGAR, C. AND GIORDANO, A. 2003. Advantages and limitations of microarray technology in human cancer. *Oncogene*, **22**, 6497-6507.

SAKUNO, T., TADA, K. AND WATANABE, Y. 2009. Kinetochore geometry defined by cohesion within the centromere. *Nature*, **458**, 852-858.

SALINA, D., BODOOR, K., ECKLEY, D.M., SCHROER, T.A., RATTNER, J.B. AND BURKE, B. 2002. Cytoplasmic dynein as a facilitator of nuclear envelope breakdown. *Cell*, **108**, 97-107.

SAN FILIPPO, J., SUNG, P. AND KLEIN, H. 2008. Mechanism of eukaryotic homologous recombination. *Annual Review of Biochemistry*, **77**, 229-257.

SARTORI, A.A. LUKAS, C., COATES, J., MISTRIK, M., FU, S., BARTEK, J., BAER, R., LUKAS, J. AND JACKSON, S.P. 2007. Human CtIP promotes DNA resection. *Nature*, **450**, 509-514.

SAXONOV, S., BERG, P. AND BRUTLAG, D.L. 2005. A genome-wide analysis of CpG dinucleotides in the human genome distinguishes two distinct classes of promoters. *PNAS*, **103**, 1412-1417.

SCHALK, J.A., DIETRICH, A.J., VINK, A.C., OFFENBURG, H.H., VAN AALDEREN, M. AND HEYTING, C. 1998. Localization of SCP2 and SCP3 protein molecules within synaptonemal complexes of the rat. *Chromosoma*, **107**, 540-548.

SCHMEKEL, K., MEUWISSEN, R.L., DIETRICH, A.J., VINK, A.C., VAN MARLE, J., VAN VEEN, H. AND HEYTING, C. 1996. Organization of SCP1 protein molecules within synaptonemal complexes of the rat. *Experimental Cell Research*, **226**, 20-30.

SCHMITZ, J., WATRIN, E., LÉNÁRT, P., MECHTLER, K. AND PETERS, J.M. 2007. Sororin is required for stable binding of cohesin to chromatin and for sister chromatid cohesion in interphase. *Current Biology*, **17**, 630-636.

SCHRAMM, S., FRAUNE, J., NAUMANN, R., HERNANDEZ-HERNANDEZ, A., HOOG, C., COOKE, H.J., ALSHEIMER, M. AND BENAVENTE, R. 2011. A novel mouse synaptonemal complex protein is essential for loading of central element proteins, recombination, and fertility. *PLoS Genetics*, **7**, e1002088.

SCHWARTZ, B.E., HOFER, M.D., LEMIEUX, M.E., BAUER, D.E., CAMERON, M.J., WEST, N.H., AGOSTON, E.S., REYNOIRD, N., KHOCHBIN, S., INCE, T.A., CHRISTIE, A., JANEWAY, K.A., VARGAS, S.O., PEREZ-ATAYDE, A.R., ASTER, J.C., SALLAN, S.E., KUNG, A.L., BRADNER, J.E. AND FRENCH, C.A. 2011. Differentiation of NUT midline carcinoma by epigenomic reprogramming. *Cancer Research*, **71**, 2686-2696.

SHIH, IE.M. AND KURMAN, R.J. 2004. Ovarian tumorigenesis: a proposed model based on morphological and molecular genetic analysis. *The American Journal of Pathology*, **164**, 1511-1518.

SHIN, Y.H., CHOI, Y., ERDIN, S.U., YATSENKO, S.A., KLOC, M., YANG, F., WANG, P.J., MEISTRICH, M.L. AND RAJKOVIC, A. 2010. *Hormad1* mutation disrupts synaptonemal complex formation, recombination, and chromosome segregation in mammalian meiosis. *PLoS Genetics*, **6**, e1001190.

SHINTOMI, K. AND HIRANO, T. 2009. Releasing cohesin from chromosome arms in early mitosis: opposing actions of Wapl-Pds5 and Sgo1. *Genes and Development*, **23**, 2224-2236.

SIDDIQUI, R.A., SAUERMANN, U., ALTMULLER, J., FRITZER, E., NOTHNAGEL, M., DALIBOR, N., FELLAY, J., KAUP, F.J., STAHL-HENNIG, C., NÜRNBERG, P., KRAWCZAK, M. AND PLATZER, M. 2009. X chromosomal variation is associated with slow progression to AIDS in HIV-1-infected women. *American Journal of Human Genetics*, **85**, 228-239.

SIEGEL, R., NAISHADAM, D. AND JEMAL, A. 2012. Cancer statistics, 2012. *CA: A Cancer Journal for Clinicians*, **62**, 10-29.

SILKWORTH, W.T. AND CIMINI, D. 2012. Transient defects of mitotic spindle geometry and chromosome segregation errors. *Cell Division*, **7**, 19-26.

SILKWORTH, W.T., NARDI, I.K., SCHOLL, L.M. AND CIMINI, D. 2009. Multipolar spindle pole coalescence is a major source of kinetochore mis-attachment and chromosome mis-segregation in cancer cells. *PLoS One*, **4**, e6564.

SIMPSON, A.J., CABALLERO, O.L., JUNGBLUTH, A., CHEN, Y.T. AND OLD, L.J. 2005. Cancer/testis antigens, gametogenesis and cancer. *Nature Reviews Cancer*, **5**, 615-625.

SJOGREN, C. AND NASMYTH, K. 2001. Sister chromatid cohesion is required for postreplicative double-strand break repair in *Saccharomyces cerevisiae*. *Current Biology*, **11**, 991-995.

SJOGREN, C. AND STROM, L. 2010. S-phase and DNA damage activated establishment of sister chromatid cohesion: importance for DNA repair. *Experimental Cell Research*, **316**, 1445-1453.

SMITH, A.V. AND ROEDER, G.S. 1997. The yeast Red1 protein localizes to the cores of meiotic chromosomes. *Journal of Cell Biology*, **136**, 957-967.

SONODA, E., MATSUSAKA, T., MORRISON, C., VAGNARELLI, P., HOSHI, O., USHIKI, T., NOJIMA, K., FUKAGAWA, T., WAIZENEGGER, I.C., PETERS, J.M., EARNSHAW, W.C. AND TAKEDA, S. 2001. Scc1/Rad21/Mcd1 is required for sister chromatid cohesion and kinetochores function in vertebrate cells. *Developmental Cell*, **1**, 759-770.

STEMMANN, O., ZOU, H., GERBER, S.A., GYGI, S.P. AND KIRSCHNER, M.W. 2001. Dual inhibition of sister chromatid separation at metaphase. *Cell*, **107**, 715-726.

STORLAZZI, A., TESSÉ, S., GARGANO, S., JAMES, F., KLECKNER, N. AND ZICKLER, D. 2003. Meiotic double-strand breaks at the interference of chromosome movement, chromosome remodelling, and reductional division. *Genes and Development*, **17** 2675-2687.

SVETLANOV, A. AND COHEN, P.E. 2004. Mismatch repair proteins, meiosis, and mice: understanding the complexities of mammalian meiosis. *Experimental Cell Research*, **296**, 71-79.

SYM, M. AND ROEDER, G.S. 1994. Crossover interference is abolished in the absence of a synaptonemal complex protein. *Cell*, **79**, 283-292.

SYM, M., ENGEBRECHT, J.A. AND ROEDER, G.S. 1993. ZIP1 is a synaptonemal complex protein required for meiotic chromosome synapsis. *Cell*, **72**, 365-378.

SYM, M. AND ROEDER, G.S. 1995. Zip1-induced changes in synaptonemal complex structure and polycomplex assembly. *Journal of Cell Biology*, **128**, 455-466.

TACHIBANA-KONWALSKI, K., GODWIN, J., VAN DER WEYDEN, L., CHAMPION, L., KUDO, N.R., ADAMS, D.J. AND NASMYTH, K. 2010. Rec8-containing cohesin maintains bivalents without turnover during the growing phase of mouse oocytes. *Genes and Development*, **24**, 2505-2516.

TAN, C.S., SALIM, A., PLONER, A., LEHTIÖ, J., CHIA, K.S. AND PAWITAN, Y. 2009. Correlating gene and protein expression data using Correlated Factor Analysis. *BMC Bioinformatics*, **10**, 272-284.

TANKIMANOVA, M., HULTÉN, M.A. AND TEASE, C. 2004. The initiation of homologous chromosome synapsis in mouse fetal oocytes is not directly driven by centromere and telomere clustering in the bouquet formation. *Cytogenetic and Genome Research*, **105**, 172-181.

TARSOUNAS, M., MORITA, T., PEARLMAN, R.E. AND MOENS, P.B. 1999. RAD51 and DMC1 form mixed complexes associated with mouse meiotic chromosome cores and synaptonemal complexes. *Journal of Cell Biology*, **147**, 207-220.

TEASE, C. AND HULTÉN, M.A. 2004. Inter-sex variation in synaptonemal complex lengths largely determine the different recombination rates in male and female germ cells. *Cytogenetic and Genome Research*, **107**, 208-215.

TERRET, M.E., WASSMANN, K., WAIZENEGGER, I., MARO, B., PETERS, J.M. AND VERLHAC, M.H. 2003. The meiosis I-to-meiosis II transition in mouse oocytes requires separase activity. *Current Biology*, **13**, 1797-1802.

THOMAS, S.E., SOLTANI-BEJNOOD, M., ROTH, P., DORN, R., LOGSDON, J.M. JR AND MCKEE, B.D. 2005. Identification of two proteins required for conjunction and regular segregation of achiasmate homologs in Drosphila male meiosis. *Cell*, **123**, 555-568.

TOMITA, K. AND COOPER, J.P. 2007. The telomere bouquet controls the meiotic spindle. *Cell*, **130**, 113-126.

TOMONAGA, T., NAGAO, K., KAWASAKI, Y., FURUYA, K., MURAKAMI, A., MORISHITA, J., YUASA, T., SUTANI, T., KEARSEY, S.E., UHLMANN, F., NASMYTH, K. AND YANAGIDA, M. 2000. Characterisation of fission yeast cohesin: essential anaphase proteolysis of Rad21 phosphorylated in the S phase. *Gene and Development*, **14**, 2757-2770.

TOYODA, Y. AND YANAGIDA, M. 2006. Coordinated requirements of human topo II and cohesin for metaphase centromere alignment under Mad2-dependent spindle checkpoint surveillance. *Molecular Biology of the Cell*, **17**, 2287-2302.

TSAI, J.H. AND MCKEE, B.D. 2011. Homologous pairing and the role of pairing centers in meiosis. *Journal of Cell Science*, **124**, 1955-1963.

TSUBOUCHI, T. AND ROEDER, G.S. 2005. A synaptonemal complex protein promotes homology-independent centromere coupling. *Science*, **308**, 870-873.

TSUBOUCHI, T., MACQUEEN, A.J. AND ROEDER, G.S. 2008. Initiation of meiotic chromosome synapsis at centromeres in budding yeast. *Genes and Development*, **22**, 3217-3226.

TSUBOUCHI, T., ZHAO, H. AND ROEDER, G.S. 2006. The meiosis-specific zip4 protein regulates crossover distribution by promoting synaptonemal complex formation together with zip2. *Developing Cell*, **10**, 809-819.

TURECI, O., SAHIN, U., ZWICK, C., KOSLOWSKI, M., SEITZ, G. AND PFREUNDSCHUH, M. 1998. Identification of a meiosis-specific protein as a member of the class of cancer/testis antigens. *PNAS*, **95**, 5211-5216.

TURNER, J.M. 2007. Meiotic sex chromosome inactivation. *Development*, **134**, 1823-1831.

UCSC Genome Bioinformatics (online). http://www.genome.ucsc.edu Accessed March 2013.

UHLMANN, F., BOUCHOUX, C. AND LÓPEZ-AVILÉS, S. 2011. A quantitative model for cyclin-dependent kinase control of the cell cycle: revisited. *Philosophical Transactions of the Royal Society of London. Series B, Biological Sciences*, **366**, 3572-3583.

UHLMANN, F., LOTTSPEICH, F. AND NASMYTH, K. 1999. Sister chromatid separation at anaphase onset is promoted by cleavage of the cohesin subunit Scc1p. *Nature*, **400**, 37-42.

UHLMANN, F., WERNIC, D., POUPART, M.A., KOONIN, E. AND NASMYTH, K. 2000. Cleavage of cohesin by the CD clan protease separin triggers anaphase in yeast. *Cell*, **103**, 375-386.

VAGNARELLI, P., MORRISON, C., DODSON, H., SONODA, E., TAKEDA, S. AND EARNSHAW, W.C. 2004. Analysis of Scc1-deficient cells defines a key metaphase role of vertebrate cohesin in linking sister kinetochores. *EMBO reports*, **5**, 167-171.

VALLENTE, R.U., CHENG, E.Y. AND HASSOLD, T.J. 2006. The synaptonemal complex and meiotic recombination in humans: new approaches to old questions. *Chromosoma*, **115**, 241-249.

VANOOSTHUYSE, V., PRYKHOZHIJ, S. AND HARDWICK, K.G. 2007. Shugoshin 2 regulates localisation of the chromosomal passenger proteins in fission yeast mitosis. *Molecular Biology of the Cell*, **18**, 1657-1669.

VAUR, S., CUBIZOLLES, F., PLANE, G., GENIER, S., RABITSCH, P.K., GREGAN, J., NASMYTH, K., VANOOSTHUYSE, V., HARDWICK, K.G. AND JAVERZAT, J.P. 2005. Control of shugoshin function during fission-yeast meiosis. *Current Biology*, **15**, 2263-2270.

VAZQUEZ, J., BEOLMONT, A.S. AND SEDAT, J.W. 2002. The dynamics of homologous chromosome pairing during male *Drosophila* meiosis. *Current Biology*, **12**, 1473-1483.

VOS, M.J., KANON, B. AND KAMPINGA, H.H. 2009. HSPB7 is a SC35 speckle resident small heat shock protein. *Biochimica et Biophysica Acta*, **1793**, 1343—1353.

WANG, S.C. AND HUNG, M.C. 2005. Cytoplasmic/nuclear shuttling and tumour progression. *Annals of the New York Academy of Sciences*, **1059**, 11-15.

WATANABE, Y. 2005. Sister chromatid cohesion along arms and at centromeres. *TRENDS in Genetics*, **21**, 405-412.

WATERS, K.M., POUNDS, J.G. AND THRALL, B.D. 2006. Data merging for integrated microarray and proteomic analysis. *Briefings in Functional Genomics and Proteomics*, **5**, 261-272.

WEAVER, B.A. AND CLEVELAND, D.W. 2006. Does aneuploidy cause cancer? *Current Opinion in Cell Biology*, **18**, 658-667.

WEBER, J., SALGALLER, M., SAMID, D., JOHNSON, B., HERLYN, M., LASSAM, N., TREISMAN, J. AND ROSENBERG, S.A. 1994. Expression of the MAGE-1 tumour antigen is up-regulated by the demethylating agent 5-aza-2'-deoxycytidine. *Cancer Research*, **54**, 1766-1771.

WILLIAMS, R.S., MONCALIAN, G., WILLIAMS, J.S., YAMADA, Y., LIMBO, O., SHIN, D.S., GROOCOCK, L.M., CAHILL, D., HITOMI, C., GUENTHER, G., MOIANI, D., CARNEY, J.P., RUSSELL, P. AND TAINER, J.A. 2008. Mre11 dimers coordinate DNA end bridging and nuclease processing in double-strand break repair. *Cell*, **135**, 97-109.

WOJTASZ, L., DANIEL, K., ROIG, I., BOLCUN-FILAS, E., XU, H., BOONSANAY, V., ECKMANN, C.R., COOKE, H.J., JASIN, M., KEENEY, S., MCKAY, M.J. AND TOTH, A. 2009. Mouse HORMAD1 and HORMAD2, two conserved meiotic chromosomal proteins, are depleted from synapsed chromosome axes with the help of TRIP13 AAA-ATPase. *PLoS Genetics*, **5**, e1000702.

WOJTASZ, L., CLOUTIER, J.M., BAUMANN, M., DANIEL, K., VARGA, J., FU, J., ANASTASSIADIS, K., STEWART, A.F., REMÉNYI, A., TURNER, J.M.A. AND TOTH, A. 2012. Meiotic DNA double-strand breaks and chromosome asynapsis in mice are monitored by distinct HORMAD2-independent and -dependent mechanisms. *Genes and Development*, **26**, 958-973.

WRIGHT, J.D., SHAH, M., MATHEW, L., BURKE, W.M., CULHANE, N., SCHIFF, P.B. AND HERZOG, T.J. 2009. Fertility preservation in young women with epithelial ovarian cancer. *Cancer*, **115**, 4118-4126.

WU, N., KONG, X., JI, Z., ZENG, W., POTTS, P.R., YOKOMORI, K. AND YU, H. 2012. Scc1 sumoylation by Mms21 promotes sister chromatid recombination through counteracting Wapl. *Genes and Development*, **26**, 1473-1485.

XU, H., BALAKRISHNAN, K., MALATERRE, J., BEASLEY, M., YAN, Y., ESSERS, J., APPELDOORN, E., TOMASZEWSKI, J.M., VAZQUEZ, M., VERSCHOOR, S., LAVIN, M.F., BERTONCELLO, I., RAMSAY, R.G. AND MCKAY, M.J. 2010. Rad21-cohesin haploinsufficiency impedes DNA repair and enhances gastrointestinal radiosensitivity in mice. *PLoS ONE*, **5**, e12112.

XU, H., BEASLEY, M., VERSCHOOR, S., INSELMAN, A., HANDEL, M.A. AND MCKAY, M.J. 2004. A new role for the mitotic RAD21/SCC1 cohesin in meiotic chromosome cohesion and segregation in the mouse. *EMBO Reports*, **5**, 378-384.

XU, H., BEASLEY, M.D., WARREN, W.D., VAN DER HORST, G.T.J. AND MCKAY, M.J. 2005. Absence of mouse REC8 cohesin promotes synapsis of sister chromatids in meiosis. *Developmental Cell*, **8**, 949-961.

XU, H., TOMASZEWSKI, J.M. AND MCKAY, M.J. 2011. Can corruption of chromosome cohesion create a conduit to cancer? *Nature Reviews. Cancer*, **11**, 199-210.

XU, Z., CETIN, B., ANGER, M., CHO, U.S., HELMHART, W., NASMYTH, K. AND XU, W. 2009. Structure and function of the PP2A-shugoshin interaction. *Molecular Cell*, **35**, 426-441.

YABUTA, Y., OHTA, H., ABE, T., KURIMOTO, K., CHUMA, S. AND SAITOU, M. 2011. TDRD5 is required for retrotransposon silencing, chromatoid body assembly, and spermiogenesis in mice. *The Journal of Cell Biology*, **192**, 781-795.

YAMAMOTO, A., GUACCI, V. AND KOSHLAND, D. 1996. Pds1p, an inhibitor of anaphase in budding yeast, plays a critical role in APC and checkpoint pathway(s). *Cell Biology*, **133**, 99-110.

YAMANAKA, S., YAMASHITA, A., HARIGAYA, Y., IWATA, R. AND YAMAMOTO, M. 2010. Importance of polyadenylation in the selective elimination of meiotic mRNAs in growing *S. pombe* cells. *The EMBO Journal*, **29**, 2173-2181.

YAN, J., DIAZ, J., JIAO, J., WANG, R. AND YOU, J. 2011. Perturbation of BRD4 protein function by BRD4-NUT protein abrogates cellular differentiation in NUT midline carcinoma. *The Journal of Biological Chemistry*, **286**, 27663-27675.

YANG, F., DE LA FUENTE, R., LEU, N.A., BAUMANN, C., MCLAUGHLIN, K.J. AND WANG, P.J. 2006. Mouse SYCP2 is required for synaptonemal complex assembly and chromosomal synapsis during male meiosis. *Journal of Cell Biology*, **173**, 497-507.

YOKOBAYASHI, S., YAMAMOTO, M. AND WATANABE, Y. 2003. Cohesins determine the attachment manner of kinetochores to spindle microtubules at meiosis I in fission yeast. *Molecular and Cellular Biology*, **23**, 3965-3973.

YUAN, L., LIU, J.G., HOJA, M.R., WILBERTZ, J., NORDQVIST, K. AND HOOG, C. 2002. Female germ cell aneuploidy and embryo death in mice lacking the meiosis-specific protein SCP3. *Science*, **296**, 1115-1118.

YUAN, L., LIU, J.G., ZHAO, J., BRUNDELL, E., DANEHOLT, B. AND HOOG, C. 2000. The murine *SCP3* gene is required for synaptonemal complex assembly, chromosome synapsis, and male fertility. *Molecular Cell*, **5**, 73-83.

YUAN, L., PELTTARI, J., BRUNDELL, E., BJöRKROTH, B., ZHAO, J., LIU, J.G., BRISMAR, H., DANEHOLT, B. AND HOOG, C. 1998. The synaptonemal complex protein SCP3 can form multistranded cross-striated fibers in vivo. *Journal of Cell Biology*, **142**, 331-139.

ZAMAN, M.S., MAHER, D.M., KHAN, S., JAGGI, M., CHAUHAN, S.C. 2012. Current status and implications of microRNAs in ovarian cancer diagnosis and therapy. *Journal of Ovarian Research*, **5**, 44. doi: 10.1186/1757-2215-5-44.

ZICKLER, D. AND KLECKNER, N. 1998. The leptotene-zygotene transition of meiosis. *Annual Review of Genetics*, **32**, 619-697.

ZICKLER, D. AND KLECKNER, N. 1999. Meiotic chromosomes: integrating structure and function. *Annual Review of Genetics*, **33**, 603-754.

Appendix

List of Contents

Appendix A: Sequencing results (Chapters 3.0 and 4.0)

Appendix B: qRT-PCR (Chapter 6.0)

Appendix C: SEC standard protein elusion profiles (Chapter 6.0)

Appendix A: Sequencing results

The PCR products observed in the CT gene screen presented in Chapters 3.0 and 4.0 were purified and sequenced to ensure that the correct sequences were being amplified. The sequencing results were aligned against the expected amplification sequences (specific to each pair of primers), using the Geneious software. The sequence alignment for the *ACTB* PCR product, using primers F1 + R1, is shown in Figure 1.

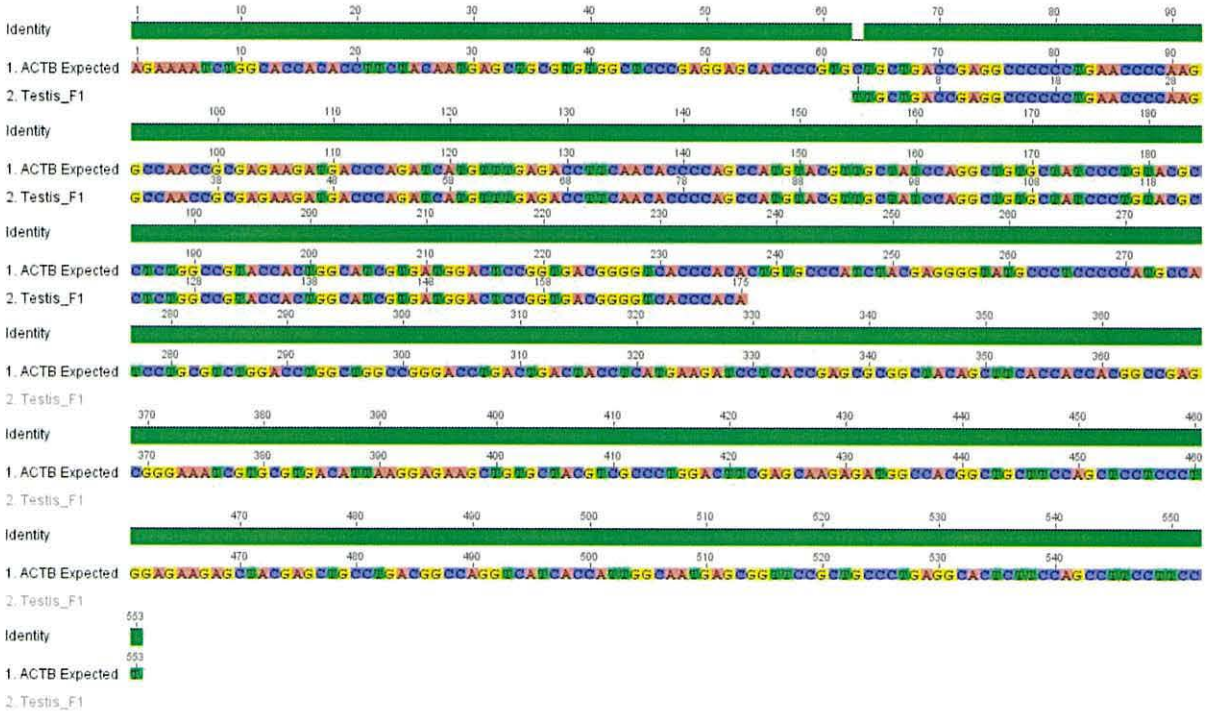

Figure 1. Sequence alignment for showing the *βACT* sequencing result for F1+R1. This sequence alignment shows the sequencing results obtained for the *ACTB* F1 + R1 primers in the normal testis, using the forward primer. The PCR product from the testes normal cDNA was sequenced using the forward primer; Testis_F1 (row 2), and the expected sequence is labelled as; ACTB expected (row 1). The sequences were aligned using the Geneious software. The solid green bar above the sequences represents the sequence identity, and gaps in the green bar represent differences in the sequences.

The sequence alignments for the other genes screened in Chapters 3.0 and 4.0 have been included on a CD. Tables 1 and 2 summarise the sequence alignment details for all of the PCR products. A positive match has been indicated when the sequencing results displayed a high sequence identity to the expected sequence (shown in Tables 3.2, 4.2 and 4.4). All of the sequence alignments follow the same format as the *βACT* alignment shown above (Figure 1).

Table 1. Summary table for the sequence alignments for Chapter 3.0.

File Name	Gene	Primers	Normal tissue	Cancer sample	Positive or Negative match?
Figure 1	*ACTB*	F1 + R1	Testis	-	Positive
Figure 2	*ACTB*	F2 + R2	Testis	-	Positive
Figure 3	*MAGEA1*	F1 + R1	Testis	-	Positive
			MEIOTIC GENES FROM THE LITERATURE		
Figure 4	*HORMAD1*	F1 + R1	Testis, Brain (whole)	-	Positive
Figure 5	*RAD21*	F1 + R1	Testis, Brain (cerebellum)	-	Positive
Figure 6	*mRAD21*	F + R	Testis	-	Positive
Figure 7	*RAD21L*	F1a + R1	Testis	NT2, A2780	Positive
Figure 8	*RAD21L*	F1b + R1	Testis	NT2, MDA-MB-453	Positive
Figure 9	*RAD21L*	F1b + R1	Testis (lower band)	-	Negative
Figure 10	*mRAD21L*	F + R	Testis	-	Positive
Figure 11	*REC8*	F1 + R1	Testis, Spinal cord, Heart, Thymus, Trachea	-	Positive
Figure 12	*REC8*	F2 + R2	Testis, Brain (cerebellum), Thymus	-	Positive
Figure 13	*mREC8*	F + R	Testis, Kidney	-	Positive
Figure 14	*SMC1α*	F1 + R1	Testis, Brain (cerebellum)	-	Positive
Figure 15	*SMC1β*	F1a + R1	Testis	MDA-MB-453	Positive
Figure 16	*SMC1β*	F1a + R1	-	NT2, MCF7	Negative
Figure 17	*SMC1β*	F1b + R1	Testis	MDA-MB-453	Positive
Figure 18	*SMC1β*	F1b + R1	-	Stomach tumour	Negative
Figure 19	*mSMC1β*	F + R	Testis	-	Positive
Figure 20	*SMC3*	F1 + R1	Brain (cerebellum) Ovary	-	Positive
Figure 21	*STAG1*	F1 + R1	Brain (cerebellum) Ovary	-	Positive
Figure 22	*STAG2A*	F1 + R1a	Brain (cerebellum) Ovary	-	Positive
Figure 23	*STAG2B*	F1 + R1b	Brain (cerebellum) Ovary	-	Positive
Figure 24	*STAG3*	F1 + R1	Testis	-	Positive
Figure 25	*STAG3*	F2 + R2	Testis	-	Positive
Figure 26	*mSTAG3*	F + R	Testis, Heart, Spleen, Embryo (days 11 and 17)	-	Positive
Figure 27	*SYCE2*	F1 + R1	Testis, Brain (cerebellum), Foetal brain, Spinal cord	-	Positive
Figure 28	*SYCP2*	F1 + R1	Brain (cerebellum), Spinal cord, Bone marrow	-	Positive
Figure 29	*SYCP3*	F1 + R1	Testis	-	Positive
Figure 30	*SYCP3*	F2 + R2	Testis	-	Positive
Figure 31	*SYCP3*	F2 + R2	Brain (cerebellum), Spinal cord, thymus	-	Negative
Figure 32	*SYCP3*	F2 + R2	-	NT2, Brain tumour	Negative
Figure 33	*SYCP3*	F3 + R3	Testis	-	Positive
Figure 34	*SYCP3*	F4 + R4	Testis	-	Positive
Figure 35	*SYCP3*	F4 + R4	Brain (cerebellum), Brain (whole)	-	Negative
Figure 36	*SYCP3*	F4 + R4	-	A2780, NT2, Leukemia	Negative
Figure 37	*TEX12*	F1 + R1	Testis, Spinal cord, Spleen, Small Intestine	-	Positive

Table 2. Summary table for the sequence alignments for Chapter 4.0.

File Name	Gene	Primers	Normal tissue	Cancer sample	Positive or Negative match?
Figure 1	*ACTB*	F1 + R1	Testis	-	Positive
Figure 2	*ACTB*	F2 + R2	Testis	-	Positive
Figure 3	*MAGEA1*	F1 + R1	Testis	-	Positive
			MICROARRAY ANALYSIS GENES		
Figure 38	*C1orf59*	F1 + R1	Lung, Ovary	-	Positive
Figure 39	*C9orf117*	F1 + R1	Testis, Lung, Trachea, Ovary	-	Positive
Figure 40	*CCDC109A*	F1 + R1	Lung, Ovary	-	Positive
Figure 41	*FHAD1*	F1 + R1	Testis, Lung, Ovary	-	Positive
Figure 42	*IQCG*	F1 + R1	Lung, Ovary	-	Positive
Figure 43	*LRRC69*	F1 + R1	Testis (upper + lower), Spinal cord, Spleen (upper), Thymus (upper)	-	Positive
Figure 44	*LRRC69*	F1 + R1	Brain (cerebellum)	-	Negative
Figure 45	*PPP4R4*	F1 + R1a	Lung, Ovary	-	Positive
Figure 46	*PPP4R4*	F1 + R1b	Lung, Ovary	-	Positive
Figure 47	*SAMD13*	F1 + R1	Ovary	-	Positive
Figure 48	*TDRD5*	F1 + R1	Testis, Stomach, Ovary	-	Positive
			EST ANALYSIS GENES		
Figure 49	*C17orf98*	F1 + R1	Testis	-	Positive
Figure 50	*HSPB9*	F1 + R1	Testis, Liver	-	Positive
Figure 51	*ARL13A*	F1 + R1	Testis	-	Positive
Figure 52	*C1orf85*	F1 + R1	Testis	-	Positive
Figure 53	*C5orf47*	F1 + R1	Testis	-	Positive
Figure 54	*C7orf72*	F1 + R1	Testis	-	Positive
Figure 55	*Corf72*	F1 + R1	Brain (cerebellum), Thymus (lower)	-	Negative
Figure 56	*C17orf105*	F1 + R1	Testis, Brain (cerebellum)	NT2	Positive
Figure 57	*CYLC1*	F1 + R1	Testis	-	Positive
Figure 58	*DUSP21*	F1 + R1	Testis, Bone marrow, Foetal liver	-	Positive
Figure 59	*EFCAB9*	F1 + R1	Testis	-	Positive
Figure 60	*MAS1*	F1 + R1	Brain (whole), Prostate, Bone marrow, Thymus, Uterus	-	Positive
Figure 61	*PSMA8*	F1 + R1	Testis, Brain (cerebellum), Spinal cord, Thymus, Uterus	HL-60	Positive
Figure 62	*SLC25A2*	F1 + R1	Testis, Liver, Bone marrow	-	Positive
Figure 63	*ZCCHC13*	F1 + R1	Testis, Spinal cord, Stomach	-	Positive
Figure 64	*ADAD1*	F1 + R1	Testis	-	Positive
Figure 65	*CATSPER1*	F1 + R1	Testis	-	Positive
Figure 66	*SNTG1*	F1 + R1a	Brain (cerebellum), Spinal cord, Spleen	-	Positive
Figure 67	*SNTG1*	F1 + R1b	Brain (cerebellum), Spinal cord, Spleen	-	Positive
Figure 68	*SOX30*	F1 + R1	Testis	-	Positive
Figure 69	*PTPN20A*	F1 + R1	Testis, Brain (cerebellum), Foetal brain	-	Positive

Appendix B: qRT-PCR

In Chapter 6.0, SYBR® Green-based real time RT-PCR was carried to assay *REC8* and *RAD21* expression in 1321N1 cells compared to NT2 cells, using commercial qRT-PCR primers (Qiagen). The relative expression of *Lamin A*, *GAPDH*, *REC8* and *RAD21* in NT2 cells and 1321N1 cells was calculated using the ΔCq method (Figure 2).

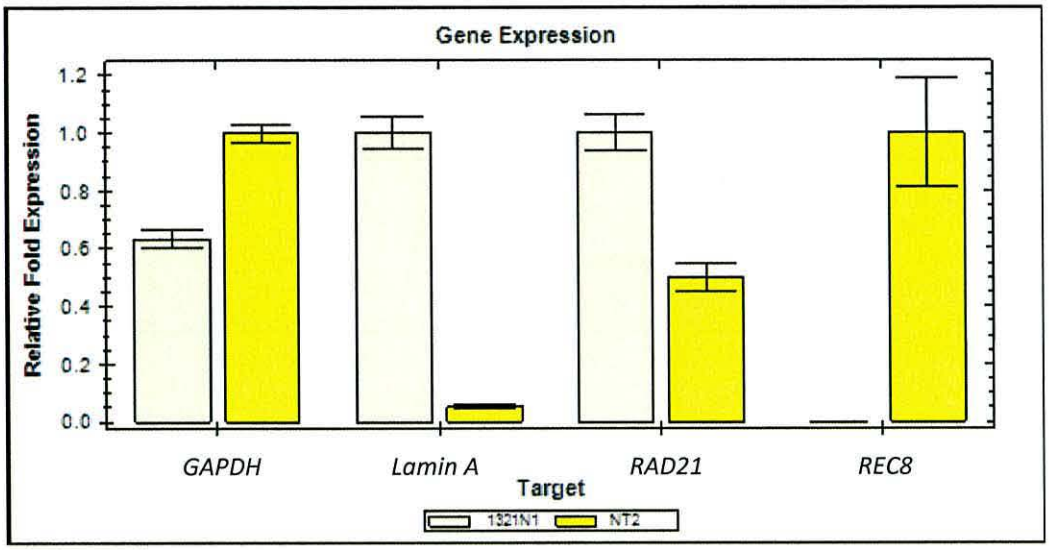

Figure 2. Relative qRT-PCR expression of *REC8* and RAD21 using NT2 and 1321N1 cells. Bar chart showing the relative fold gene expression results for *GAPDH*, *Lamin A*, *REC8* and *RAD21* in 1321N1 and NT2 cells. The relative gene expression was calculated using the ΔCq method. The data was analysed using the Bio-RAD CFX Manager. The error bars indicate the standard error for 3 repeats.

The *REC8* and *RAD21* qRT-PCR results were normalised to the qRT-PCR results for *Lamin A* and *GAPDH* using the ΔΔCq method (results shown in Chapter 6.0).

Melting curve analysis was carried out to establish if any non-specific amplicons were being produced by the primer assays (Figure 3).

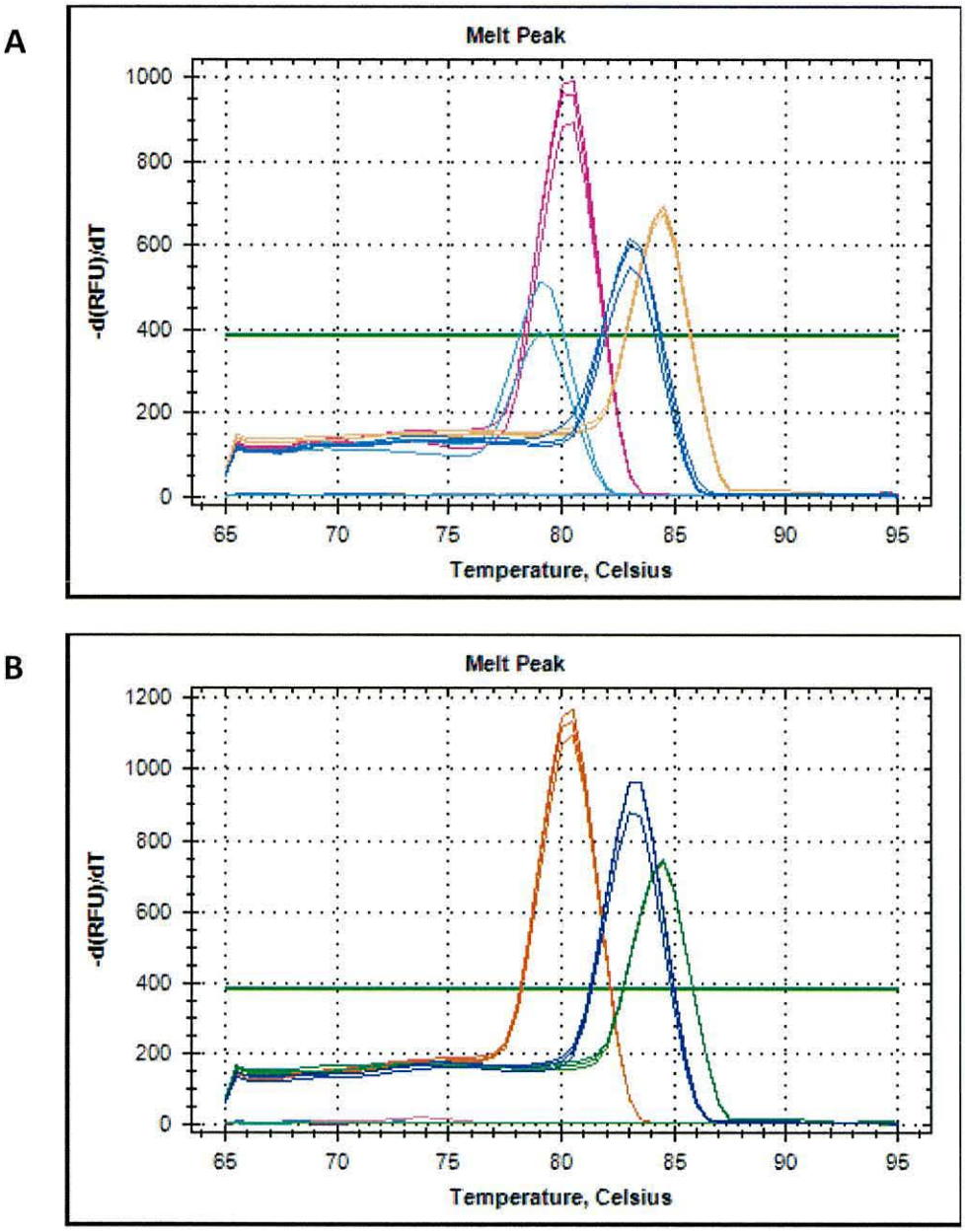

Figure 3. Melting curve analysis for qRT-PCR using NT2 and 1321N1 cDNA. A. Melting curve analysis using the NT2 cDNA. Three repeats are shown for the primer assay; *GAPDH* (orange), *LAMIN A* (dark blue), *REC8* (pale blue) and *RAD21* (pink). **B.** Melting curve analysis using the 1321N1 cDNA. Three repeats are shown for the primer assays; *GAPDH* (dark green), *LAMIN A* (dark blue), *REC8* (pale green) and *RAD21* (dark orange). The NTC have also been included, which show no amplifications, therefore suggesting that there was no genomic DNA contamination.

Appendix C: SEC standard protein elusion profiles

In Chapter 6.0, WCEs were prepared, for NT2 and NHDF cells, and subjected to SEC using the Superdex 200 10/300 GL column (GE Healthcare; 17-5175-01) which was calibrated using a gel filtration high molecular weight calibration kit (GE Healthcare; 28-4038-42). The standard proteins used to calibrate the SEC column were; Blue Dextran, Thyroglobulin, Ferritin, Aldolase, Conalbumin, Ovalbumin and Cytochrome C. The peak in which each standard protein was eluted was indicated in Figures 6.16 and 6.17. The SEC UV elution profiles are shown in Figures 4-10.

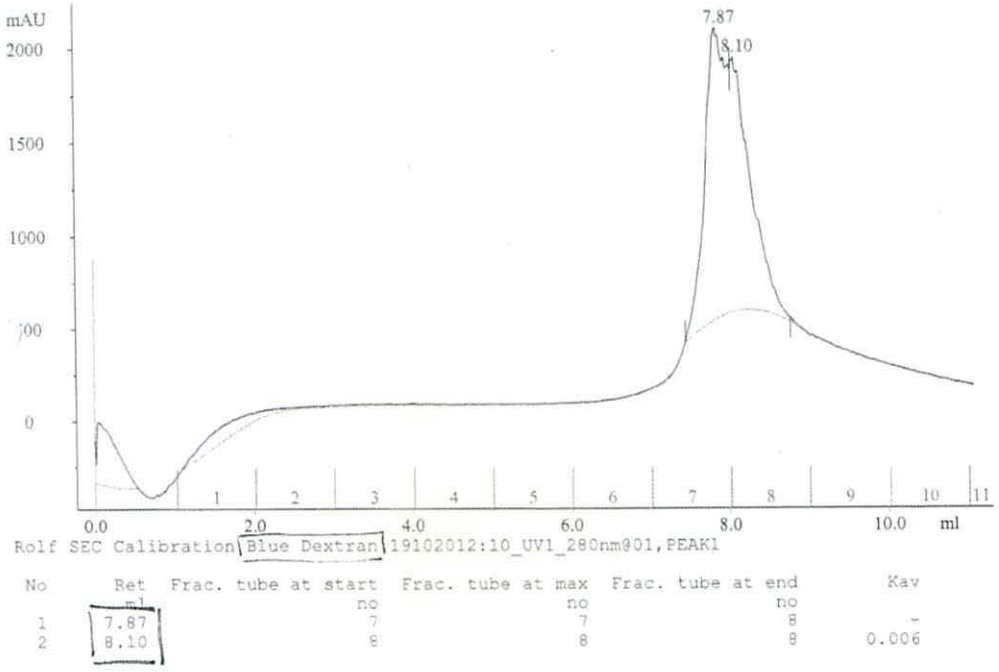

Figure 4. SEC calibration using Blue Dextran. The elution profile for Blue Dextran shows a peak in elution in fractions 7-8. The molecular weight of Blue Dextran is approximately 2000 kDa.

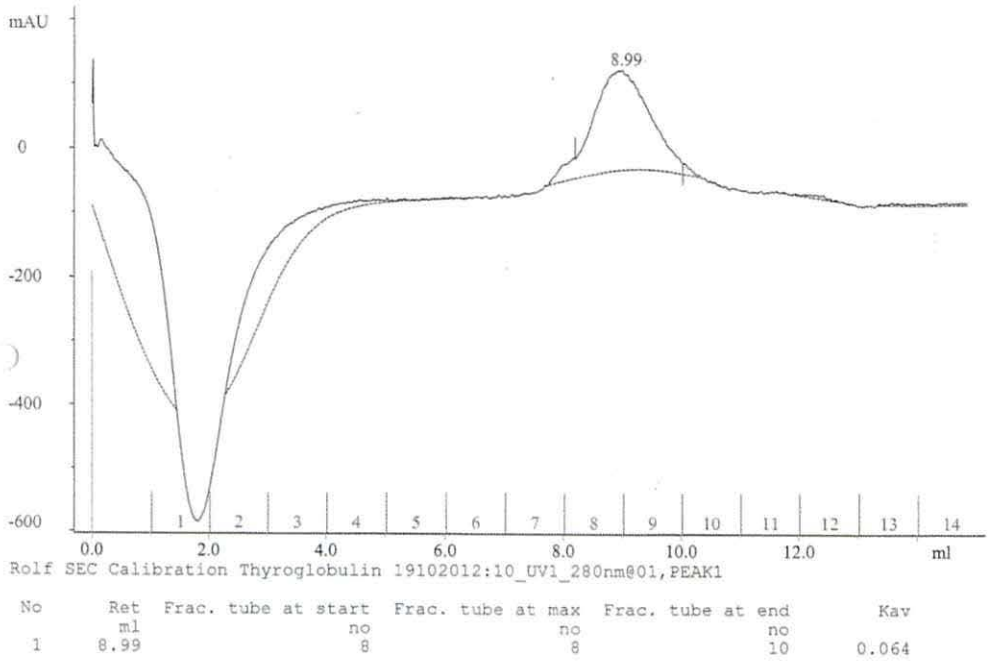

No	Ret ml	Frac. tube at start no	Frac. tube at max no	Frac. tube at end no	Kav
1	8.99	8	8	10	0.064

Figure 5. SEC calibration using Thyroglobulin. The elution profile for Thyroglobulin shows a peak in elution in fraction 8. The molecular weight of Thyroglobulin is 669 kDa.

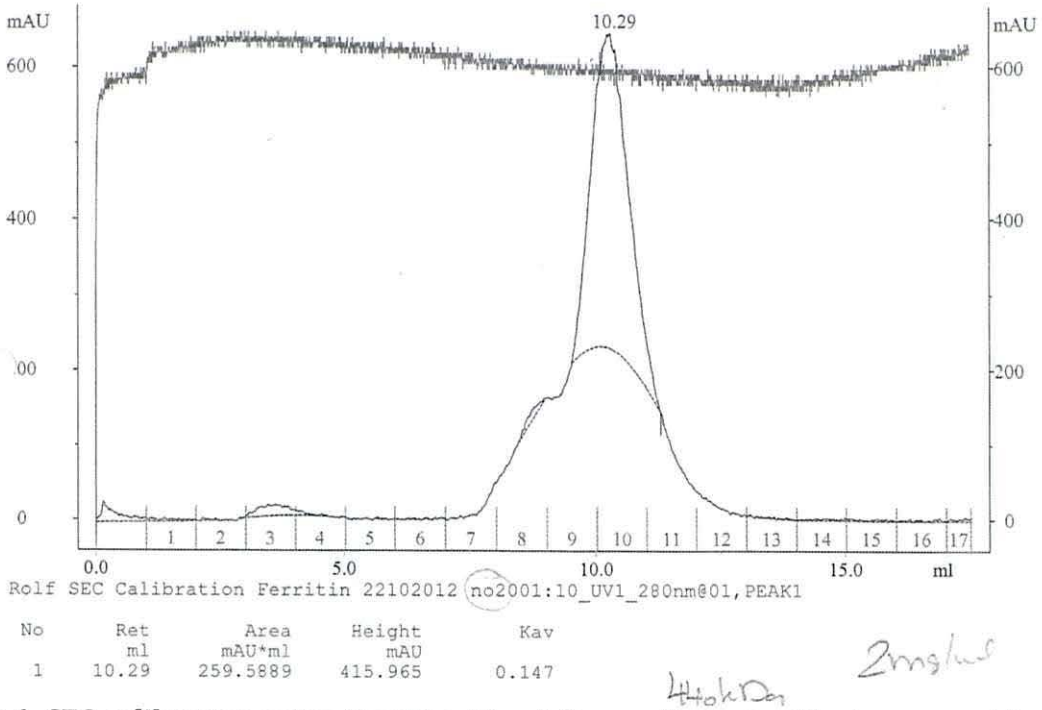

No	Ret ml	Area mAU*ml	Height mAU	Kav
1	10.29	259.5889	415.965	0.147

Figure 6. SEC calibration using Ferritin. The elution profile for Ferritin shows a peak in elution in fraction 10. The molecular weight of Ferritin is 440 kDa.

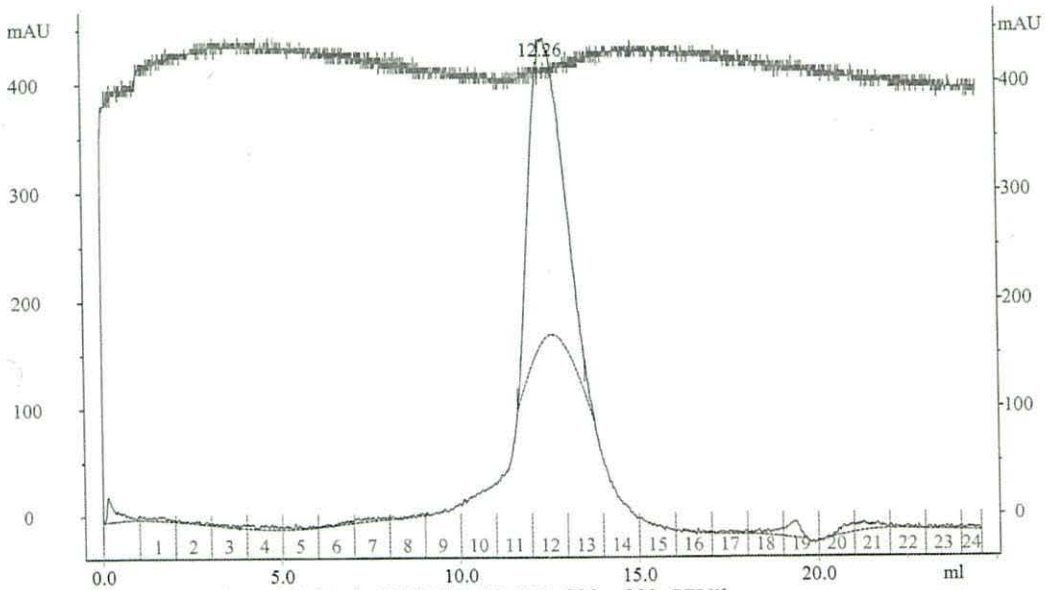

No	Ret ml	Area mAU*ml	Height mAU	Kav
1	12.26	90.8942	264.784	0.274
2	12.35	213.1442	279.354	0.280

158 kDa

Figure 7. SEC calibration using Aldolase. The elution profile for Aldolase shows a peak in elution in fraction 12. The molecular weight of Aldolase is 158 kDa.

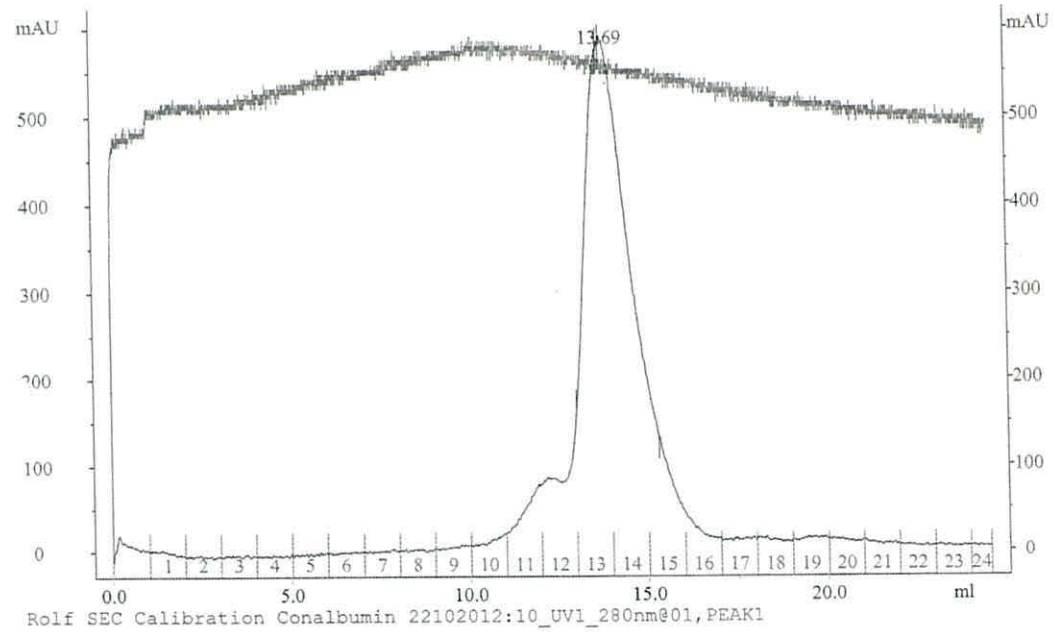

No	Ret ml	Peak start ml	Peak end ml	Area mAU*ml	Height mAU	Frac. tube at start no
1	13.69	13.04	13.70	142.2820	382.156	13
2	13.74	13.70	13.78	28.7923	390.423	13
3	13.82	13.78	15.33	276.4735	394.699	13

Figure 8. SEC calibration using Conalbumin. The elution profile for Conalbumin shows a peak in elution in fraction 13. The molecular weight of Conalbumin is 75 kDa.

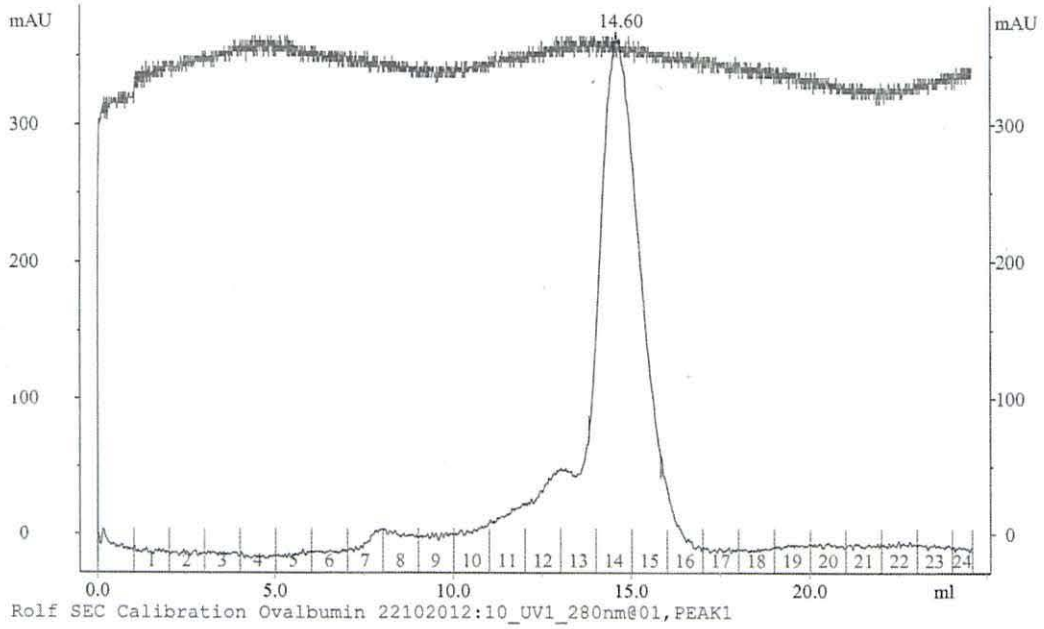

Figure 9. SEC calibration using Ovalbumin. The elution profile for Ovalbumin shows a peak in elution in fraction 14. The molecular weight of Ovalbumin is 44 kDa.

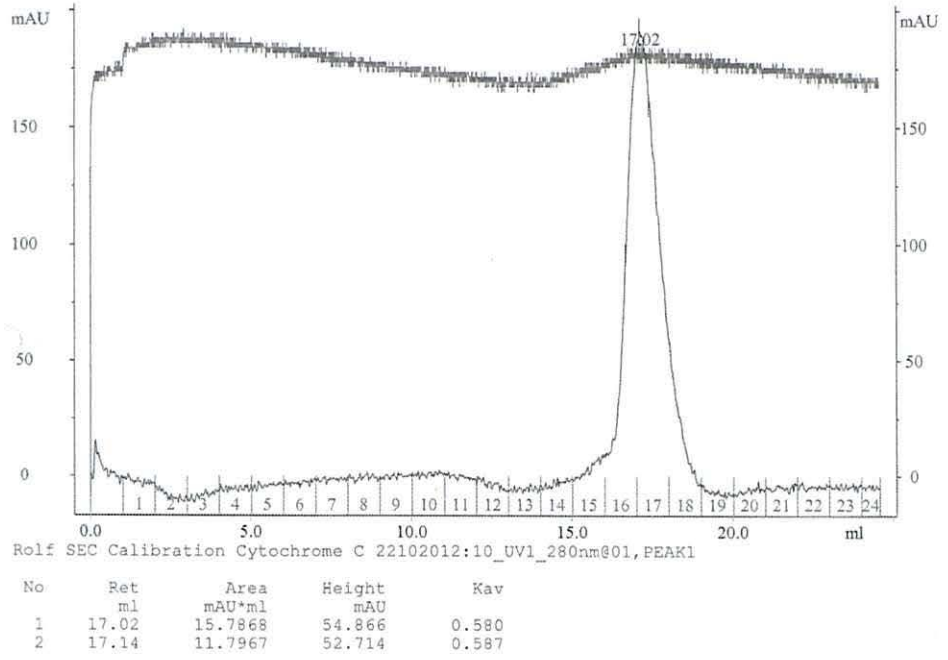

Figure 10. SEC calibration using Cytochrome C. The elution profile for Cytochrome C shows a peak in elution in fraction 17. The molecular weight of Cytochrome C is 13 kDa.